

THE UNIVERSITY OF MICHIGAN
COLLEGE OF ENGINEERING
Department of Meteorology and Oceanography

AN INVESTIGATION OF THE INFLUENCE OF WATER WAVES
ON THE ADJACENT AIRFLOW

Kenneth Laverne Davidson

Donald J. Portman, Project Director

ORA Project 08849

under contract with:

OFFICE OF NAVAL RESEARCH
DEPARTMENT OF THE NAVY
CONTRACT NO. N00014-67-A-0181-0005
WASHINGTON, D.C.

administered through:

OFFICE OF RESEARCH ADMINISTRATION ANN ARBOR

August 1970

OR 811

UMRØ638

This report was also a dissertation submitted in partial fulfillment of the requirements for the degree of Doctor of Philosophy in The University of Michigan, 1970.

A B S T R A C T

AN INVESTIGATION OF THE INFLUENCE OF WATER WAVES ON THE ADJACENT AIRFLOW

by
Kenneth Laverne Davidson

Chairman: Donald J. Portman

An observational study was made during August, September and October 1968 to investigate the influence of water waves on the adjacent airflow. Simultaneous measurements of wind and temperature fluctuations and waves were made from a tower on Lake Michigan. 11 periods were analyzed, and 8 included simultaneous measurements of velocity and temperature fluctuations at two levels above the mean water level. Pairs of levels (in meters) were; 1.5 and 4.0 or 1.5 and 15. or 1.0 and 2.0.

Hot-wire anemometers with X-probe sensors were used to obtain both the along-wind and vertical components of the fluctuating wind. High response resistance wires were used to measure temperature fluctuations and a capacitance gauge was used to measure the waves. Data were analyzed to obtain variance and covariance spectra over a frequency range from .01 to 15 Hz and are presented over a range from .03 to 10 Hz.

Velocity spectra show significant fluctuations in the airflow due to the waves. When the wind speed was much less than the phase speed of the dominant wave component, there is evidence of momentum transfer from the waves to the air. Cospectral results from one period clearly show upward transport of

momentum at the frequency of the wave spectrum peak. However, at the same frequency but at an upper level, enhanced downward transport of momentum occurs. Enhanced downward transport of momentum at frequencies near wave spectra peaks occurs in most cospectral results. When the wind speed was comparable to the wave speed, phase relationships between the wave-induced fluctuations and the wave are in agreement with those inherent in Miles' wave generation theory.

The universal nature of velocity spectra at high frequencies (10 Hz) does not appear to be influenced by the waves. At high frequencies, velocity spectra have slopes which are in agreement with Kolmogorov's power law relation. Smoothed spectra have maxima occurring at non-dimensional frequencies comparable to those reported by other investigators.

Stress estimates obtained from hot-wires exceed those obtained from wind profiles and are not constant with height. Relative intensities and the sign of skewness of velocity components appear to be related to the waves' influence. The non-dimensional divergence term in the turbulent kinetic energy balance equation is positive when the ratio of the measurement height to the wave length is less than .1 and when the wave speed is much greater than the wind speed.

The results lead to a conclusion that the waves influence the airflow to such an extent that the ocean surface cannot be considered a rigid boundary for purposes of analysis of the adjacent boundary layer.

ACKNOWLEDGEMENTS

The help and guidance of others have made this work possible. The author especially thanks Professor Donald J. Portman, the committee chairman, who has provided continuous guidance and encouragement during this study. For their careful review of the manuscript and useful suggestions, thanks go to Professors Walter Debler, Gerald Gill, Edward Monahan, and Mr. Floyd Elder. Thanks also to Professor Aksel C. Wiin-Nielsen, whose presence was a continuous source of inspiration during my years in the department.

The author is indebted to Messrs Edward Ryznar and Allen Davis for their large amount of time and effort spent in setting up the experiment on Lake Michigan and continued assistance throughout the study.

Messrs Floyd C. Elder and H.K. Soo provided assistance during the measurements and also bivariate and profile data which were essential during the interpretation of the data. The U.S. Army Engineering District, Lake Survey, provided supplemental wind and wave data and of no minor importance, the tower.

For assistance while preparing and analyzing data, the author thanks Mr. Eugene Mauch for the computer programming, and to Messrs Keith Heidorn, Chris Portman, Orren Walters, and Mrs. Karen Tingle for data abstraction and preparation of figures. Thanks also to Miss Jane Rod for her patience in typing the manuscript.

Thanks to fellow graduate students Frank Haurwitz, Jack Kaitala, Eduardo Michelena, and Michael Walter, whose moral sup-

port and helpful suggestions during the course of the work contributed to its success.

This research was supported by the Office of Naval Research, Contract No. N00014-67-A-0181-0005.

To my wife Joan, who has shared the loneliness and anxieties which accompanied this endeavor, and my children Erik, Anders and Marit a very grateful, thank you.

TABLE OF CONTENTS

	Page
LIST OF TABLES	viii
LIST OF FIGURES	ix
 Chapter	
1. INTRODUCTION	1
1.1 Purpose and Scope of Study	1
1.2 Limitations of Study	4
2. THEORETICAL AND OBSERVATIONAL BACKGROUND	6
2.1 Representative Equations and Definitions for Turbulent Airflow	6
2.1.1 Momentum and Turbulent Energy Equations	7
2.1.2 Spectral Representations of Fluctuating Quantities	11
2.2 Wind-Wave Coupling Theories	15
2.2.1 Relevant Aspects of Miles' Mechanism	16
2.2.1.1 Dynamics at the Critical Level	19
2.2.2 The Wave Driven Wind	24
2.3 Observational Investigations of Airflow Over Waves	28
2.3.1 Laboratory Studies	29
2.3.2 <u>In Situ</u> Studies	33
3. THE EXPERIMENT	40
3.1 Site and Tower	40
3.1.1 Location of Experiment	40
3.1.2 Description of Tower	43
3.1.3 Mounting Arrangements	45
3.2 Instrumentation	48
3.2.1 Velocity Measurements	48
3.2.1.1 Sensors and Electronics	48
3.2.1.2 Operational Considerations and Procedures	49
3.2.1.3 Relations Between Instantaneous Velocities and Hot-wire Outputs	50
3.2.1.4 Calibrations and Selection of Constants for Hot-wire Interpretations	54

TABLE OF CONTENTS (Continued)

	Page
3.2.1.5 Adjustment of Velocity Results by Axis Rotation	58
3.2.2 Temperature Measurements	60
3.2.3 Wave Measurements	62
3.3 Recording	68
4. DATA REDUCTION AND ANALYSES	71
4.1 General Considerations	71
4.2 Digitizing and Reconstructing Analog Signal (CDC 160-A)	71
4.2.1 Amplification and Reconstruction of Signal	72
4.2.2 Length (Sampling Interval) of Digitized Record, Low Pass Filter- ing and Sampling Rate	74
4.3 Digital Reduction and Processing (IBM 360/67)	77
4.3.1 Numerical Low Pass Filtering	80
4.3.2 Removal of Erroneous Data Points	83
4.3.3 Removing Trend and Mean and Com- puting 2nd, 3rd, and 4th moments	84
4.3.4 Application of Data Window and Performing the Fourier Transform	87
4.3.5 Computation of Spectral Values from Fourier Coefficients	89
4.3.6 Averaging Spectral Values over Local Harmonics	92
5. SUMMARY OF MEASUREMENTS AND DATA ANALYZED	95
6. PRESENTATION AND INTERPRETATION OF RESULTS	100
6.1 Introduction	100
6.2 Presentation of Spectral Results	100
6.2.1 Results from 19 August (Periods 1 and 2)	104
6.2.1.1 General Conditions	104
6.2.1.2 Spectral Results	107
6.2.2 Results from 24 September (Peri- ods 3 and 4)	118
6.2.2.1 General Conditions	118
6.2.2.2 Spectral Results	119
6.2.3 Results from 26 September (Peri- ods 5, 6, and 7)	131
6.2.3.1 General Conditions	131
6.2.3.2 Spectral Results (Peri- od 5)	135

TABLE OF CONTENTS (Continued)

	Page
6.2.3.3 Spectral Results (Periods 6 and 7)	142
6.2.4 Results from 27 September (Periods 8, 9, and 10)	151
6.2.4.1 General Conditions	151
6.2.4.2 Spectral Results	154
6.2.5 Results from 5 October (Period 11)	165
6.2.5.1 General Conditions	165
6.2.5.2 Spectral Results	168
6.3 General Interpretation of Spectral Results	175
6.3.1 Velocity Variance Results	176
6.3.2 Velocity Covariance Results	184
6.4 Presentation of Velocity Spectral Results in Universal Form	189
6.5 Turbulent Transports, Relative Intensities and Probability Distributions	200
6.6 Turbulent Energy Balance Computations	209
 7. CONCLUSIONS	 215
 APPENDIX A: DISCUSSION OF HOT WIRE RELATIONS AND CONSTANTS REQUIRED FOR INTERPRETATION	 219
A.1 Discussion of Hot-wire Relations	220
A.2 Constants and Calibrations for Hot-wire Interpretations	223
A.2.1 Empirical Constants m and n or $c = m/n$	224
A.2.2 Scaling Constant (K) and the Relative Response of Two Wires (K_1/K_2)	226
 APPENDIX B: DERIVATION OF EQUATIONS TO CORRECT SPECTRAL ESTIMATES BY AXIS ROTATION AND INFLUENCE OF ROTATION ON SPECTRAL RESULTS	 228
B.1 Derivation of Equations for Correcting Spectral Estimates by Rotation of Coordinate Axis	229
B.2 Influence of Rotation on Spectral Results	232
 APPENDIX C: SCHEMATICS OF BRIDGE-AMPLIFIER CIRCUITS USED WITH SENSORS	 240

TABLE OF CONTENTS (Concluded)

	Page
APPENDIX D: COMPUTER PROGRAM FOR AVERAGING OF SPECTRAL VALUES WITH BANDWIDTH INCREASING LOGARITHMICALLY WITH FREQUENCY	244
D.1 Determining the Averaging Intervals	245
D.2 Listing of Subroutine	245
APPENDIX E: TEMPERATURE SPECTRA AND \overline{wT} COSPECTRA	247
BIBLIOGRAPHY	254

LIST OF TABLES

Table	Page
3.1 Calibration and Relative Response Values Considered in Hot-Wire Interpretations.	57
4.1 Representative Sampling Errors ($\epsilon\%$)	75
4.2 Statistics Before and After Data Conditioning	86
4.3 Spectral Averaged (#AVG) and Representative Equivalent Degrees of Freedom (9-26, 1355 EST, Period 7)	94
5.1 Summary of 1968 Lake Michigan Measurements	96
5.2 General Conditions for Periods Analyzed	98
6.1 Phase and Coherence Values at Frequencies of Interest, During Periods 1-11	103
6.2 Amplitudes (u_0, w_0) and Normalized Amplitudes (U_n, W_n) at Dominant Wave Related Peaks	180
6.3 Percentage Increase in Stress (\overline{uw}) Within Bands With Wave Related Extrema	185
6.4 Composite Spectral Maxima and Lower Limits of $-2/3$ Slope Regions, (nz/\overline{U})	197
6.5 Ratios of ϕ_{ww}/ϕ_{uu} for Individual Levels	197
6.6 Estimates of Turbulent Transports, Drag Coefficients, z/L , Relative Intensities and C/u_*	201
6.7 Skewness and Kurtosis Results	208
6.8 Results From Energy Balance Computation Along With Wave Parameters	210

LIST OF FIGURES

Figure		Page
2.1	Schematics illustrating vortex force, $\rho \tilde{w}$, associated with a sinusoidal perturbation in shear flow at; (a) $z \neq z_c$, (b) $z = z_c$.	21
2.2	Streamlines of sinusoidal perturbation in a shear flow near $z = z_c$; (a) kinematic consequence, (b) consequence of dynamics of critical level.	23
2.3	Wind and wave strip chart records showing perturbations and net flow due to waves propagating into initially still air (after Harris, 1965).	25
2.4	Observational results showing isotachs which indicate a "supplemental maximum" of u momentum above wave troughs (after Yefimov and Sizov, 1969).	27
3.1	Location of U.S. Lake Survey Research Tower; (a) Lake Michigan, (b) tower site near Muskegon, Michigan.	41
3.2	Research tower; (a) as instrumented during experiment, (b) schematic showing underwater tripod support structure.	44
3.3	Sensor mounting arrangement on tower; (a) components and vertical array, "plumbline", (b) picture of sensors during measurement period.	46
3.4	Configuration and dimensions of X-probe sensor with assumed orientation to mean wind.	53
3.5	Portable wind tunnel and calibration accessories.	55
3.6	Picture of capacitance wave gauge and bridge-amplifier system.	63
3.7	Calibration results of wave gauge, immersion versus output (ma).	64
3.8	Influence of film on output from capacitance wave gauge and simplified circuit showing role of film.	67
3.9	Schematic of recording system components.	69

LIST OF FIGURES (continued)

Figure		Page
4.1	Flow chart of procedures in analog to digital processing.	73
4.2	Frequency response curve, $(A/A_0)^2$, and circuit employed in analog low-pass filtering.	76
4.3	Flow chart of digital processing procedures.	79
4.4	Comparison of response curves for several numerical filters (from, Powell, 1965).	81
4.5	Frequency response, $(A/A_0)^2$, curve and weight functions employed in numerical low-pass filter.	82
4.6	Representative occurrence of erroneous spikes from Brush recording of analog signal.	85
6.1	General conditions for 19 August, 1968.	105
6.2	General conditions for time encompassing Period 1.	106
6.3	Wave spectral estimates for Periods 1 and 2.	112
6.4	Velocity variance and covariance results for Period 1; (a) 1.5 meter level, (b) 4.0 meter level.	113
6.5	Velocity variance and covariance results for Period 2; (a) 1.5 meter level, (b) 15.0 meter level.	114
6.6	Phase and coherence spectra for Period 1; (a) 1.5 meter level, (b) 4.0 meter level.	115
6.7	Phase and coherence spectra for Period 2; (a) 1.5 meter level, (b) 15 meter level.	116
6.8	Composite schematic of phase relations between velocity components and waves at .2 Hz for Periods 1 and 2.	117
6.9	General conditions for 24 September, 1968.	119
6.10	General conditions for time encompassing Periods 3 and 4.	120
6.11	Wave spectral estimates for Periods 3 and 4.	125

LIST OF FIGURES (continued)

Figure		Page
6.12	Velocity variance and covariance results for Period 3; 1.5 meter level.	126
6.13	Velocity variance and covariance spectra for Period 4; (a) 1.5 meter level, (b) 4.0 meter level.	127
6.14	Phase and coherence spectra for Period 3; 1.5 meter level.	128
6.15	Phase and coherence spectra for Period 4; (a) 1.5 meter level, (b) 4.0 meter level.	129
6.16	Composite schematic of phase relations between velocity components and waves at .26 Hz for Periods 3 and 4.	130
6.17	General conditions for 26 September, 1968.	132
6.18	General conditions for time encompassing Period 5.	133
6.19	General conditions for time encompassing Periods 6 and 7.	134
6.20	Wave spectrum for Period 5.	138
6.21	Velocity variance and covariance spectra for Period 5; (a) 1.5 meter level, (b) 4.0 meter level.	139
6.22	Phase and coherence spectra for Period 5; (a) 1.5 meter level, (b) 4.0 meter level.	140
6.23	Schematic of phase relations between velocity components and waves at .26 Hz for Period 5.	141
6.24	Wave spectral estimates for Periods 6 and 7.	145
6.25	Velocity variance and covariance spectra for Period 6; 4.0 meter level.	146
6.26	Velocity variance and covariance spectra for Period 7; (a) 1.5 meter level, (b) 4.0 meter level.	147
6.27	Phase and coherence spectra for Period 6; 4.0 meter level.	148

LIST OF FIGURES (continued)

Figure	Page
6.28 Phase and coherence spectra for Period 7; (a) 1.5 meter level, (b) 4.0 meter level.	149
6.29 Composite schematic of phase relations between velocity components and waves at .26 Hz for Period 7.	150
6.30 General conditions for 27 September, 1968.	152
6.31 General conditions for time encompassing Periods 8, 9, and 10.	153
6.32 Wave spectral estimates for Periods 8, 9 and 10.	157
6.33 Velocity variance and covariance spectra for Period 8; (a) 1.0 meter level, (b) 2.0 meter level.	158
6.34 Velocity variance and covariance spectra for Period 9; (a) 1.0 meter level, (b) 2.0 meter level.	159
6.35 Velocity variance and covariance spectra for Period 10; 1.0 meter level.	160
6.36 Phase and coherence spectra for Period 8; (a) 1.0 meter level, (b) 2.0 meter level.	161
6.37 Phase and coherence spectra for Period 9; (a) 1.0 meter level, (b) 2.0 meter level.	162
6.38 Phase and coherence spectra for Period 10; 1.0 meter level.	163
6.39 Schematic of phase relations between velocity components and waves at .26 Hz for Period 9.	164
6.40 General conditions for 5 October, 1968.	166
6.41 General conditions for time encompassing Period 11.	167
6.42 Wave spectrum for Period 11.	171
6.43 Velocity variance and covariance spectra for Period 11; (a) 1.0 meter level, (b) 2.0 meter level.	172

LIST OF FIGURES (continued)

Figure		Page
6.44	Phase and coherence spectra for Period 11; (a) 1.0 meter level, (b) 2.0 meter level.	173
6.45	Schematic of phase relations between velocity components and waves at .26 Hz for Period 11.	174
6.46	Normalized velocity amplitudes (u_n, w_n) at dominant peaks associated with waves; influence versus z/λ_0 where λ_0 is wave length corresponding to frequency of peak.	181
6.47	Composite schematic of phase relations from case 2 periods; (a) phase relations between velocity components and waves, (b) streamlines determined from phase of w in ($\bar{U}-C$) frame of reference.	188
6.48	Smoothed and normalized velocity spectral results; Period 1.	190
6.49	Smoothed and normalized velocity spectral results; Periods 3 and 4.	191
6.50	Smoothed and normalized velocity spectral results; Period 5.	192
6.51	Smoothed and normalized velocity spectral results; Periods 6 and 7.	193
6.52	Smoothed and normalized velocity spectral results; Periods 8, 9 and 10.	194
6.53	Smoothed and normalized velocity spectral results; Period 11.	195
6.54	Comparison of reference velocity (cm/sec) obtained from profile, $u_*(p)$, estimates and hot-wire, $u_* = (-\overline{uw})^{\frac{1}{2}}$, estimates.	202
6.55	Relative intensities of velocity components (σ_u/u_* , σ_w/u_*) versus z/L .	205
6.56	Relative intensities of velocity components (σ_u/u_* , σ_w/u_*) versus C/u_* .	206
6.57	Normalized dissipation, ϕ_C , versus z/L and versus normalized production ($\phi - z/L$).	212

LISTS OF FIGURES (continued)

Figure		Page
6.58	Non-dimensional divergence, ϕ_D , as a function of $(z/\lambda_0) \cdot N$ where λ_0 would be representative of wave length corresponding to wave spectrum peak and N is a linear correction which is inversely proportional to wave height.	213
A.1	Flow geometry with respect to yawed hot-wire.	221
A.2	Calibration curves for hot-wires (Department of Meteorology and Oceanography Wind Tunnel).	225
A.3	Composite of several estimates of empirical constant c where lines were drawn to intercept $c = .90$ at $\Delta\phi = 0$.	225
B.1	Variance spectra $(\text{cm/sec})^2$ for 0° , 4° and 8° rotations; Period 5, 4.0 meter level.	234
B.2	Cospectra and cumulative cospectra $(\text{cm/sec})^2$ for 0° , 4° and 8° rotations; Period 5, 4.0 meter level.	235
B.3	Variance spectra $(\text{cm/sec})^2$ for 0° , 4° and 8° rotations; Period 8, 2.0 meter level.	236
B.4	Cospectra and cumulative cospectra $(\text{cm/sec})^2$ for 0° , 4° and 8° rotations; Period 8, 2.0 meter level.	237
B.5	Variance spectra $(\text{cm/sec})^2$ for 0° , 4° and 8° rotations; Period 11, 2.0 meter level.	238
B.6	Cospectra and cumulative cospectra $(\text{cm/sec})^2$ for 0° , 4° and 8° rotations; Period 11, 2.0 meter level.	239
C.1	Hot-wire anemometer bridge-amplifier (constant resistance); Miller, Model M-5.	241
C.2	Temperature system bridge-amplifier (constant current); Flow Corporation System, Series 900.	242
C.3	Typical capacitance bridge showing active oscillator and sensor (wave gauge).	243
E.1	Normalized temperature (t) spectra and \overline{wt} cospectra for Periods 1 and 2.	248
E.2	Normalized temperature (t) spectra and \overline{wt} cospectra for Periods 3 and 4.	249

LIST OF FIGURES (concluded)

Figure		Page
E.3	Normalized temperature (t) spectra and \overline{wt} cospectra for Period 5.	250
E.4	Normalized temperature (t) spectra and \overline{wt} cospectra for Periods 6 and 7.	251
E.5	Normalized temperature (t) spectra and \overline{wt} cospectra for Period 8.	252
E.6	Normalized temperature (t) spectra and \overline{wt} cospectra for Period 11.	253

1. INTRODUCTION

1.1 PURPOSE AND SCOPE OF STUDY

The link between the atmosphere and a major portion of the earth's surface is dependent on the turbulent transport processes in the layer of air adjacent to natural water waves. Distinctive features of this layer are caused by the mobility of the surface and the continuous transfer of energy, kinetic as well as thermal, through the interface. The processes are of practical concern to a wind-wave investigator for whom the airflow is a source of energy for wave generation, and the processes control the transfer of the energy into the waves. Meteorologists are concerned with turbulent processes in this region for the purpose of defining the boundary layer in terms of empirical relations for momentum, and sensible and latent heat transfer. These empirical relations should involve readily measured quantities such as mean wind speed, air-water temperature differences and the general state of the sea.

The purpose of this study was to observe the turbulent airflow over natural water waves and to interpret the results in terms of the nature and extent of the influence of the waves on the turbulent airflow above them. Emphasis is placed on the waves' influence on the airflow rather than the response of the wave field to the airflow. A measure of the waves' influence would be whether the adjacent layer of air can be logically described by assumptions which appear to be

adequate, or at least tested, for a layer of fully developed turbulence over land.

A substantial amount of observational data exists for turbulent flow over ground and has resulted in empirical relations describing turbulent transports of momentum, heat and moisture. The conditions within the same region over natural waves, however, are largely unknown because of a lack of observations. Therefore, existing empirical relations used for this region are often the same as those applied to a rigid boundary. A comprehensive review of turbulent airflow over the ground is provided in a text on atmospheric turbulence by Lumley and Panofsky (1964). A central concept in analysis of turbulent flow over land is the assumption that the structure of turbulence is determined by the turbulent flow itself and the prevailing meteorological conditions (wind speeds and temperature) are described by "external parameters" which may appear within the empirical relations as scaling factors. These scaling factors actually represent the magnitudes of the turbulent transports.

The influence of waves on the adjacent airflow is primarily manifested in motions in the airflow that are induced by the waves themselves and are superimposed on the existing turbulent flow. Two analytical approaches to the role of the wave-induced motion in a turbulent shear flow served as guidelines for experimental design and for interpretation of results. Both theories are described in Section 2.2 but for the purposes of this introduction the important aspect of

both approaches is that wave-induced motions influence the dynamics of the airflow at levels above the wave crests.

One of the approaches, which has been amended by several persons since its initial formulation, is referred to as the Miles' Theorem (Miles, 1957). Miles' Theorem is a wave generation theory and is based on the removal of momentum from the airflow at the level above the surface where the phase velocity of the growing wave equals that of the wind speed. The dynamics at this level, which result in a deceleration of the mean flow, are due to the interaction between the wave induced perturbation and the shear flow. The second approach (Harris, 1966) predicts a net increase of the horizontal wind at a level above the surface due to momentum imparted into the airflow by the waves.

If characteristics of the airflow implied by either of these theories can be identified in observational data, a lower limit, in terms of a scaling height, could be established for a region not influenced by the underlying wave surface. Such a scaling height would be the same as defining an "external parameter" for wind and wave conditions. Therefore, assumptions used for fully developed turbulent flows over land could be employed for analyses of turbulent airflow over water.

The scope of the study is determined by data from simultaneous measurements of two components (u, w) of the fluctuating wind, and fluctuating temperature at two levels (fixed with respect to the mean water level) and of the water sur-

face. Results include variance spectra of all measured variables and covariance spectra between velocity components, between velocity components and the surface height and between velocity components and temperature fluctuations. In addition, results include flux estimates from integration of all cospectral results from covariance computations of the variables in the air.

Variance spectral results enable quantitative identification of the wave-induced contribution to the existing turbulent flow. Covariance spectral results extend the interpretation with respect to possible interaction between the wave-induced motion and the turbulent shear flow. Flux computations, from cospectra integrations, are used to estimate terms in the turbulent energy balance equation. Results of the estimates are examined to determine if assumptions used over land, in which certain terms are considered negligible, are valid over water.

1.2 LIMITATIONS OF STUDY

Numerous limitations will go unrecognized until more results and procedures become available. Those which are most obvious are listed here:

1. The turbulent airflow is three dimensional and only two components of the turbulent wind were measured.
2. Conditions are never steady enough in nature to define properly a mean value. This pertains especially to establishing a level where the mean wind speed is equal to the wave speed and in considering turbulent

energy balance.

3. Instrumentation errors and sampling fluctuation errors permit only qualitative estimates of properties of the airflow.

The scale and unknown characteristics of turbulence in the atmospheric boundary layer inhibit explanations of deviations of results from the approximations inherent in existing linear theories. Furthermore, the data and analyses procedures provided information on numerous properties of turbulent flow which will not be examined in this study.

2. THEORETICAL AND OBSERVATIONAL BACKGROUND

2.1 REPRESENTATIVE EQUATIONS AND DEFINITIONS FOR TURBULENT AIR-FLOW

The purpose of this section is to examine the role of fluctuating terms of turbulent airflow as they appear in the momentum and turbulent energy equations and to introduce notation and spectral relations that are used for analysis of turbulent airflow. All turbulent quantities are deviations from means determined from an average over time,

$$\overline{(\quad)} = \frac{1}{T} \int_0^T (\quad) dt.$$

For the purpose of expressing variables in the airflow, they will be separated into mean and turbulent quantities.

Velocity field: $\vec{U}(t) = (U, V, W; x, y, z)$

x is the direction defined by the mean wind and is assumed to be parallel to the surface

z is defined by gravity, which acts in negative z direction

y is defined by the convention of the right hand rule

$$U = \bar{U} + u$$

$$V = v; \bar{V} = 0$$

$$W = w; \bar{W} = 0$$

$$|\vec{U}|^2 = \bar{U}^2 + 2\bar{U}u + q^2; q^2 = u^2 + v^2 + w^2$$

Scalar fields:

$$\text{pressure } P = \bar{P} + p'$$

$$\text{density } \rho = \bar{\rho} + \rho'$$

$$\text{temperature } T = \bar{T} + T'$$

2.1.1 Momentum and Turbulent Energy Equations

For conditions that are horizontally homogeneous (averaged quantities are functions of z only), momentum and turbulent energy (E) equations for two-dimensional flow¹ appear in the following differential forms (Lumley and Panofsky, 1964, page 63 and page 72),

$$\rho \frac{\partial \bar{U}}{\partial t} = \frac{\partial}{\partial z} (-\rho \bar{u}w + \rho \gamma \frac{\partial \bar{U}}{\partial z}) \quad 2-1$$

$$\frac{\partial \bar{E}}{\partial t} = \underbrace{-\bar{u}w}_{\text{I}} \frac{\partial \bar{U}}{\partial z} + \underbrace{\frac{g}{T} \bar{w}T'}_{\text{II}} - \underbrace{\epsilon}_{\text{III}} - \underbrace{\frac{\partial}{\partial z} (\bar{w}q^2 + \frac{\bar{p}'}{\rho} w)}_{\text{IV}}, \quad 2-2$$

where $\epsilon = \gamma \cdot (\overline{u \nabla^2 u} + \overline{v \nabla^2 v} + \overline{w \nabla^2 w})$

γ = kinematic coefficient of viscosity.

The terms I-IV in Equation 2-2 represent for turbulent kinetic energy,

I and II production, mechanical and buoyant respectively

III dissipation, by viscosity

IV divergence, due to transport by turbulence ($\bar{w} \cdot q^2$) and pressure work ($\bar{w} \cdot \bar{p}'/\rho$)

Momentum flux (which will often be referred to as shear stress or simply stress), τ , and heat flux, H , are related to quantities (u, w, T') of the turbulent field as follows;

$\tau = -\rho \bar{u}w$ downward transport is positive

$H = \rho C_p \bar{w}T'$ upward transport is positive

¹Two dimensional flow is considered here because results represent observations of only two components, u and w .

C_p = specific heat at constant pressure .

If conditions are steady ($\frac{\partial \bar{U}}{\partial t} = 0$) and viscosity is neglected, Equation 2-1 implies that shear stress should be constant with height and equal to that at the surface. This expectation is used for analysis of turbulent flow over land and a characteristic velocity which serves as an "external parameter" and as a scaling factor for velocity is defined as;

$$u_* = (\tau/\rho)^{\frac{1}{2}} = (-\overline{uw})^{\frac{1}{2}}. \quad 2-3$$

Other "external parameters" are $H/\rho C_p$ ($=\overline{wT'}$) and g/\bar{T} .

Scales of length (L) and temperature (T_*) are formed from $\overline{wT'}$ and g/\bar{T} which appear in empirical relationships that define mean properties of the turbulent boundary layer. These scales are (Monin, 1962);

$$L = \frac{\bar{T} u_*^3}{kg \overline{wT'}} \quad (a)$$

(Monin-Obukhov length)

2-4

$$T_* = \frac{1}{k} \cdot \frac{\overline{wT'}}{u_*} \quad (b)$$

where k = von Karman's constant = .4 .

An example of an application would be to consider the scaling length L which is a measure of the hydrostatic stability conditions near the surface. The importance of buoyant forces on turbulent flow at any height z would be determined by the ratio of the height z to L. If $|z/L| \ll 1$, then the magnitude of production of turbulent energy by buoyant production

would be negligible compared to that resulting from the shear stress working against the mean wind gradient ($-\overline{uw} \frac{\partial \overline{U}}{\partial z}$). A mean property of the turbulent boundary layer would be the increase of mean wind speed (wind shear) with height. For conditions of neutral stability, the wind shear as a function of height is assumed to have the following functional relationship with the "external parameter" u_* ,

$$\frac{\partial \overline{U}}{\partial z} = u_* / kz, \quad 2-5$$

and the mechanical production of turbulent energy ($-\overline{uw} \frac{\partial \overline{U}}{\partial z}$), therefore, would be u_*^3 / kz .

Normalizing the turbulent energy equation (2-2) with the above expression for mechanical production in neutral conditions yields the following non-dimensional form,

$$\frac{kz}{u_*^3} \frac{\partial \overline{E}}{\partial t} = \frac{kz}{u_*} \frac{\partial \overline{U}}{\partial z} + \frac{z \cdot g}{T} \frac{\overline{wT'k}}{u_*^3} - \frac{\epsilon kz}{u_*^3} - \frac{kz}{u_*^3} \frac{\partial}{\partial z} \left[\left(q^2 + \frac{p'}{\rho} \right) w \right] \quad 2-6$$

This can be written as follows¹, with Equation 2-4(a) in the term for buoyant production,

$$\phi - z/L - \phi_E - \phi_D = \frac{kz}{u_*^3} \frac{\partial \overline{E}}{\partial t} \quad 2-7$$

= 0 if local turbulent kinetic energy is statistically steady

where

ϕ = normalized mechanical production

z/L = normalized buoyant production

¹Notation is that of Busch and Panofsky (1968)

ϕ_E = normalized viscous dissipation

ϕ_D = normalized divergence.

Equation 2-7 is the form of the turbulent energy equation used in interpretation of results. Busch and Panofsky (1968) examined results from several overland investigations and concluded that the divergence term ϕ_D is negligible for analysis purposes of turbulent airflow over land.

Stewart (1962) suggested, however, that the divergence term may not be negligible over waves because kinetic energy is transported, unattenuated, from a level above the surface through the interface. The divergence terms appear in the integral form of the total kinetic energy balance equation as part of the integrand of a surface integral. The two-dimensional form for the complete integrand would be

$$-\overline{uw} \cdot \bar{U} - \frac{(\overline{p'w} + \overline{q^2w})}{\rho} \quad 2-8$$

Since it appears within a surface integral, the terms represent work by the vertical transport of total kinetic energy. For energy being transferred, unattenuated, into the waves, Expression 2-8 would be a component equation (=0). If the assumption that \overline{uw} is constant is used and that \bar{U} goes to zero at the surface, the other two terms have to compensate. They appear in the turbulent energy balance equation in the divergence term.

2.1.2 Spectral Representations of Fluctuating Quantities

As a point of departure from the preceding section, herein fluctuating quantities, both in the air and the water surface, are considered in terms of spectral representations. Several empirical relations exist for the spectral distribution of the measured variables and these also will be introduced.

Spectral densities, $\phi_{ij}(n)$, represent the contribution to the variance of a single variable, or covariance of two variables, from the frequency interval Δn centered at frequency n . With u as the fluctuating variable, this can be expressed as

$$\overline{u_i u_j} = \int_0^{\infty} \phi_{ij}(n) dn \quad 2-9$$

where $i = j$ for variance spectra

$i \neq j$ for covariance spectra.

For measurements at a fixed point, a wide range of frequencies is possible and it is convenient to use a $\ln(n)$ ¹ scale rather than a linear n scale. This representation also provides more detail on variations at low frequencies which are expected to exhibit physically significant differences between neighboring frequencies.

$\ln \phi_{ij}(n)$ vs. $\ln(n)$ plots provide detail in estimating variations at high frequencies and also advantages for examining power law distributions of spectral estimates.

¹ \ln refers to the logarithm of the value to the base e or natural logarithm, where $e = 2.71828\dots$

Another representation is $n \cdot \phi_{ij}(n)$ vs. $\ln(n)$ which leads to the area under the curve $n \cdot \phi_{ij}(n)$ being proportional to energy in an interval Δn since, from 2-9, $n \cdot \phi_{ij}(n) d \ln(n) = \phi_{ij}(n) dn$.

In order to relate time variations at a fixed point to spatial variations, the Taylor hypothesis may be used (Hinze, 1959, page 40). It relates variations in time to spatial variations through the relation between time and space derivatives

$$\frac{\partial}{\partial t} = -\bar{U} \frac{\partial}{\partial x} . \quad 2-10$$

There are several requirements for this assumption, and one which applies near the surface is that $K \cdot z \gg 1$ where K is the wave number or counterpart of frequency for spatial variation. K is defined as

$$K = \frac{2\pi n}{\bar{U}} . \quad 2-11$$

Therefore, relations which apply to all discussions of spectral representations are,

- i) $K = \frac{2\pi n}{\bar{U}}$, if Taylor hypothesis holds,
- ii) $n\phi_{ij}(n) = K\phi_{ij}(K)$, since K and n are proportional to each other
- iii) $\overline{u_i u_j} = \int_0^{\infty} \phi_{ij}(n) dn = \int_0^{\infty} n\phi_{ij}(n) d \ln(n) .$

Two power law relations for spectral distributions considered in the present study are a $-5/3$ relation for velocity spectra and a -5 relation for wave spectra.

The $-5/3$ Kolmogorov power law relation applies to the "inertial subrange" region of velocity spectra. In this region, no significant production or dissipation of energy takes place and the spectral shape should be determined by the cascade of energy, in wave number space, to smaller scales where viscous dissipation occurs. Kolmogorov's (Hinze, 1959, page 189; Lumley and Panofsky, 1964, page 84) hypothesis which is referred to as the "third" was determined by dimensional arguments to be;

$$\phi_{uu}(K) = d \epsilon^{2/3} K^{-5/3} \quad 2-12$$

where $d = \text{constant} = .48$ (Pond et al. 1963)

$\epsilon = \text{dissipation rate per unit mass.}$

From i) and ii) above this can be written,

$$n \cdot \phi_{uu}(n) = d \epsilon^{2/3} (2\pi)^{-2/3} \left(\frac{n}{U}\right)^{-2/3}. \quad 2-13$$

Dividing by u_*^2 and multiplying the right hand side by $\left(\frac{kz}{kz}\right)^{2/3} = 1$, where $k = .4$, von Karman's constant, gives

$$\frac{n \cdot \phi_{uu}(n)}{u_*^2} = \frac{.48}{(2\pi k)^{2/3}} \left(\frac{kz \epsilon}{u_*^3}\right)^{2/3} \cdot \left(\frac{zn}{U}\right)^{-2/3} \quad 2-14$$

or

$$\frac{n \cdot \phi_{uu}(n)}{u_*^2} = .26 \phi_\epsilon^{2/3} \left(\frac{z \cdot n}{U}\right)^{-2/3}. \quad 2-15$$

By definition, Equation 2-15, $\phi_\epsilon = (kz \epsilon / u_*^3)$.

Phillips (1958) formulated a power law relationship for the equilibrium region of the water wave spectrum. Equilibrium in this case means that wave components in this spectral region have attained "saturation" with respect to the forcing wind and will not grow. The relation was formulated by considering the stability of the water surface and assuming that breaking or white-capping would occur before growth for wave components in this spectral region. On dimensional grounds, the following expression was proposed by Phillips, (Phillips, 1966, page 111)

$$\phi_{nn}(n) = \beta g^2 n^{-5} \quad n_0 > n > n_r \quad 2-16$$

where n = frequency

n_r = frequency characteristic of capillary waves

n_0 = wave spectrum peak.

Phillips suggests that only those frequencies below n_0 , where n_0 would be the lower limit of a -5 slope region on a $\ln \phi_{nn}(n)$ vs. $\ln(n)$ plot, would grow.

2.2 WIND-WAVE COUPLING THEORIES

The theories discussed in this section are different not only by the fact that one (Miles') was formulated for the purpose of wave growth prediction and the other ("wave driven" wind) for the purpose of examining the possible influence of momentum imparted from the wave to the airflow but also by the amount of attention received by each since the initial formulations.

Modern wave growth prediction theories, because of their need in practical marine technology and because of a previous lack of realistic theories, have been the focus of several theoretical and experimental studies since the initial formulations (Miles, 1957, 1959; Phillips, 1957). Two complementary theories which form the framework for modern wave prediction models are those by Miles (1957) and Phillips (1957). Phillips' model is not coupled in the sense that the energy transfer to the wave is not dependent on the wave-induced perturbations in the airflow and applies to early stages of wave growth. Since properties of the airflow induced by existing waves are the concern of this study, aspects of the airflow as related to Miles' mechanism¹ are considered.

The "wave driven" wind theory, however, has not received

¹Miles' theory has been amended by many persons since its initial formulation but the coupled system approach is referred to as the Miles' mechanism.

as much attention as the wave prediction theories. Reasons for this could be that oceanic wind profiles (Roll, 1965) have been shown by numerous investigations to be near logarithmic which would be in direct conflict with a theory which predicts an increase in horizontal motion in the air due to the waves. Also, the most recent comprehensive books on processes at the air-sea interface (Kinsman, 1965; Phillips, 1966) were published prior to the study of Harris (1966). However, the possibility that the cospectra ($-\overline{uw}$) of momentum flux could reverse sign at frequencies of wave spectra peaks during a decaying or equilibrium sea is intuitively expected.

2.2.1 Relevant Aspects of Miles' Mechanism

Since Miles (1957) first introduced the role of the wave-induced perturbation as a factor in wave-generation, numerous analytical studies have appeared. These include several extensions by Miles himself (Miles, 1959, 1960, 1965, 1967).

The accuracy of the theory as a wave growth predictor was critically evaluated by Miles (1967). His evaluation was that existing data (laboratory and in situ) indicated that the theory underestimates wave growth. In situ data had the greater disagreement with the theoretical prediction ($\times 10$). This rather bleak critique of the theory as a wave predictor does not discount consideration of those properties in the airflow that are inherent in the theory.

Fortunately, related properties in the airflow received considerable analytical attention during the decade following the first formulation. Therefore, a substantial background

appears in the literature on the consequence of a sinusoidal perturbation on shear flow when the perturbation is induced by a wave which in turn receives energy from the air.

The central concept of the Miles' mechanism is the existence of a "critical level" defined as the height above water where the wind speed is equal to the phase speed of the wave. This level should be considered, in fact, of finite depth and is referred to as the matched layer, Phillips (1966, page 92). It is from this layer that momentum is removed from the mean shear flow to be transported to the wave.

Phillips (1966, page 87 ff.) related the wave induced stress to the momentum transport to the waves by considering one wave component moving with phase speed, C , and expressed the velocity and pressure field in terms of the mean, wave induced, and fluctuating components. If the fixed coordinate system is replaced by one moving with the speed of the selected wave, the instantaneous wind components may be written as

$$\begin{aligned} U &= \bar{U}(z) - C + \tilde{U}(x, z) + u'(x, y, z, t) \\ W &= \tilde{W}(x, z) + w'(x, y, z, t) \\ V &= v'(x, y, z, t) \end{aligned} \quad 2-17$$

where \tilde{U} and \tilde{W} = components stationary with respect to wave, and

u' and w' = turbulent velocity components.

Gravity acts in the negative z -direction, and the y -axis is parallel to the wave crest. Wave-induced perturbations are separated from the turbulent fluctuations by averaging in the

y-direction. An average in the y-direction will be denoted as $\langle \rangle$. Also, wave induced perturbations become stationary and sinusoidal in a frame of reference moving at speed C.

If one substitutes these expressions into the equation of motions,

$$\frac{\partial \bar{u}}{\partial t} + \bar{u} \cdot \nabla \bar{u} = - \frac{1}{\rho} \nabla P + \gamma \nabla^2 \bar{u} + \bar{G}, \quad 2-18$$

where \bar{G} = gravitational force, and averages in the y-direction, the component equation in the x-direction becomes,

$$\begin{aligned} (\bar{U}-C) \frac{\partial \bar{u}}{\partial x} + \bar{w} \frac{\partial \bar{u}}{\partial z} + \frac{\partial (\bar{u}^2)}{\partial x} + \frac{\partial (\bar{u}\bar{w})}{\partial z} \\ + \frac{\partial \langle u'^2 \rangle}{\partial x} + \frac{\partial \langle u'w' \rangle}{\partial z} = - \frac{1}{\rho} \left(\frac{\partial \bar{P}}{\partial x} + \frac{\partial \tilde{P}}{\partial x} \right), \quad 2-19 \end{aligned}$$

$$\text{where } \gamma \nabla_{x,z} (\bar{U} + \bar{u}) = 0$$

$$\langle P \rangle = \bar{P} + \tilde{P}.$$

By averaging in the x-direction and by assuming y averaged terms to be independent of x, the expression for a shear flow becomes,

$$\frac{\partial}{\partial z} (\overline{\bar{u}\bar{w}} + \langle u'w' \rangle) = 0.0, \quad 2-20$$

where $\overline{\bar{u}\bar{w}}$ is the wave-induced stress.

Furthermore, the mean flux of momentum to the wave is the correlation between the pressure and the wave slope,

$$F = \overline{\langle \tilde{P}_o \rangle \langle \frac{\partial \tilde{\eta}}{\partial x} \rangle} = -\overline{\langle \tilde{\eta} \rangle \langle \frac{\partial \tilde{P}}{\partial x} \rangle}_o \quad 2-21$$

where η = water surface elevation.

Subscript o refers to pressure at the surface and the x-wise independence on y averaged quantities is employed to obtain the right hand term.

Phillips shows (loc cit, page 94) that

$$F = -\rho \left[\overline{\langle \tilde{U}\tilde{W} \rangle}_o + \overline{\langle u'^2 \rangle \frac{\partial \langle \tilde{\eta} \rangle}{\partial x}} - \overline{\langle \tilde{\eta} \rangle \frac{\partial \langle u'w' \rangle}{\partial z}} \right]_o \quad 2-22$$

Equation 2-22 shows that the wave induced stress is the only contribution to the momentum flux to the wave in a linear theory in which products of turbulent quantities are assumed negligible. A non-zero value for the wave-induced stress is a consequence of the dynamics at the critical level.

2.2.1.1 Dynamics at the Critical Level

Lighthill (1962) provided a physical interpretation of the linear theory in which the existence of a sinusoidal perturbation at the critical level resulted in an average negative vortex force. For two-dimensional flow, the local change of momentum can be expressed in terms of the vortex force $(\Omega_y \cdot \tilde{W})$, which has a direction defined by the right hand rule with cyclic order being $(\Omega_y, \tilde{W}, \Omega_y \cdot \tilde{W})$, (see insert Figure 2.1), and total pressure (Kinsman, 1965, page 566-567). This relation

is

$$\rho \frac{\partial \bar{U}}{\partial t} = \overline{\rho \Omega_y \tilde{W}} - \frac{\partial \bar{P}_t}{\partial x} \quad 2-23$$

where Ω_y = component of vorticity parallel to wave front
or normal to mean flow

\tilde{W} = wave induced vertical velocity

$$P_t = \frac{1}{2} \rho (u^2 + w^2) + P$$

$$\frac{\partial \bar{P}_t}{\partial x} = 0, \text{ averaged over a wave length.}$$

Away from the critical level, the streamlines are sinusoidal with vorticity perturbations in phase with the displacement (Figure 2.1 (a)). Therefore, the vorticity variation along the streamline is 90° out of phase with the vertical component and $\overline{\Omega_y \tilde{W}} = 0$, where the overbar indicates an average over a wave length. At the critical level air moving downward carries less vorticity than that moving upward as a result of the decrease in profile curvature with height. Therefore, the vortex force in this region varies around a negative mean, $\overline{\Omega_y \tilde{W}} < 0$. The latter is shown, schematically in Figure 2.1 (b).

X-wise independence of wave-induced quantities leads to the following relation between the vortex force and the divergence of the wave-induced stress, (Phillips, 1966, page 95),

$$\overline{\rho \Omega_y \tilde{W}} = \rho \frac{\partial}{\partial z} \overline{(\tilde{U} \tilde{W})}. \quad 2-24$$

This leads to an expression for the non-zero wave induced stress due to the fact that the vortex force is non-zero at the critical level,

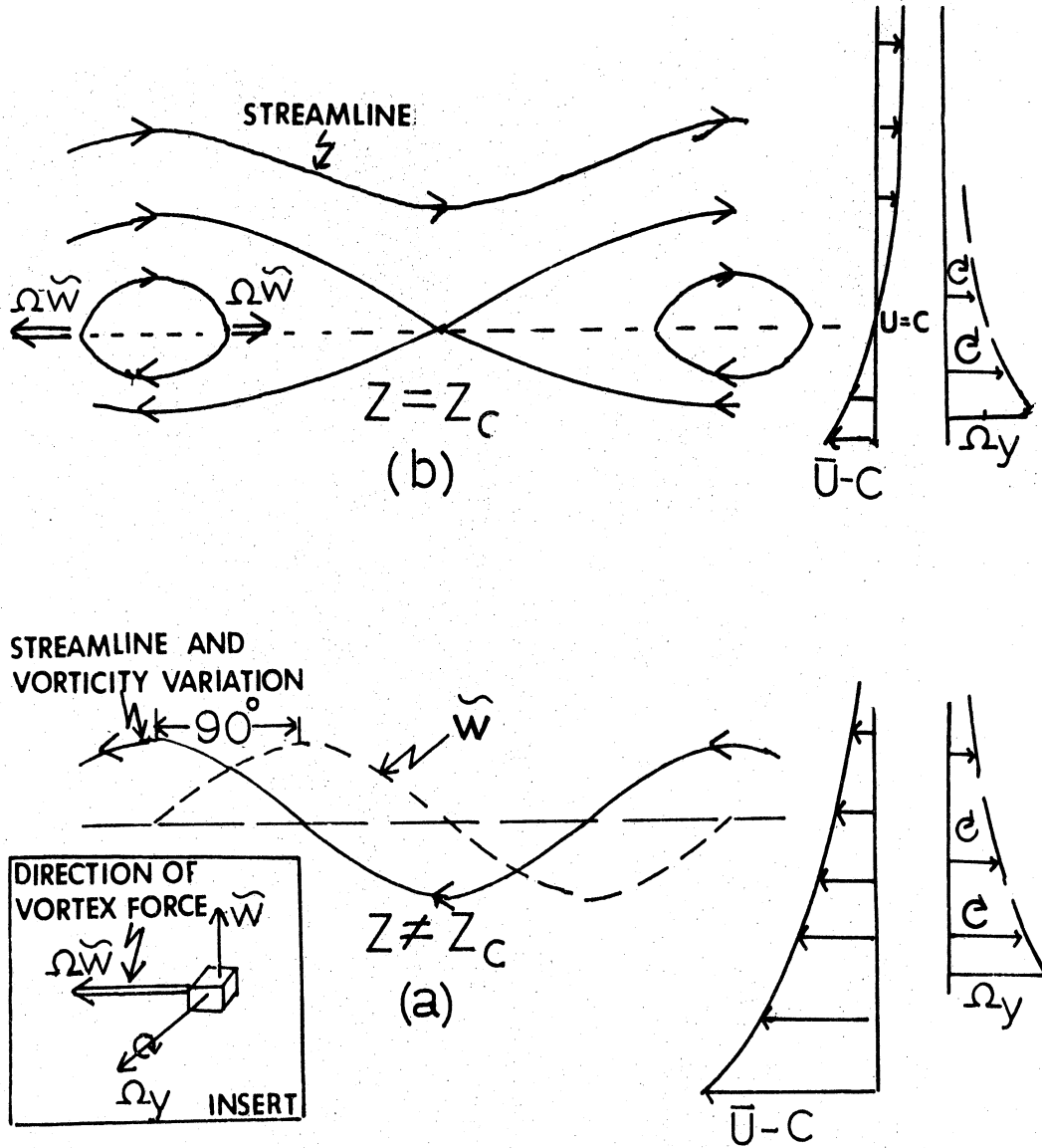


Figure 2.1: Schematics illustrating vortex force, $\Omega_y \tilde{w}$, associated with a sinusoidal perturbation in shear flow at; (a) $z \neq z_c$, (b) $z = z_c$.

$$-\overline{\rho \tilde{U} \tilde{W}} = \rho \int_z^{\infty} \overline{\Omega_y \tilde{W}} dz. \quad 2-25$$

The kinematic consequence of a sinusoidal perturbation in shear flow would be that reflected by the cat's eye pattern in Figure 2.2 (a). The streamlines below the critical level are pure sinusoids in which \tilde{U} and \tilde{W} are 90° out phase hence $\overline{\tilde{U} \tilde{W}} = 0$. The flow as shown in Figure 2.2 (b) appears in Phillips' (1966) text and reflects the non-zero wave induced stress by the shift in streamlines. The shift in streamlines indicates that the \tilde{W} component shifts from ahead of the crest near the surface to behind the crest in the matched layer. Kinsman (1965, page 571) shows that a non-zero wave induced stress would imply a shift of \tilde{W} with height. Phase relations between velocity components and the surface wave are, therefore, considered in the interpretations.

Lighthill (1962, page 396) also states that the velocity field induced by the vorticity perturbations at the critical level has a maximum horizontal velocity over the upwind node of the wave.

"...the horizontal components of velocity, and hence also pressures, have maxima over the nodes. In particular, at the surface, a component of pressure lagging 90° behind the surface elevation results..."

The pressure in phase with the wave slope as shown by Phillips is related to the momentum flux to the waves.

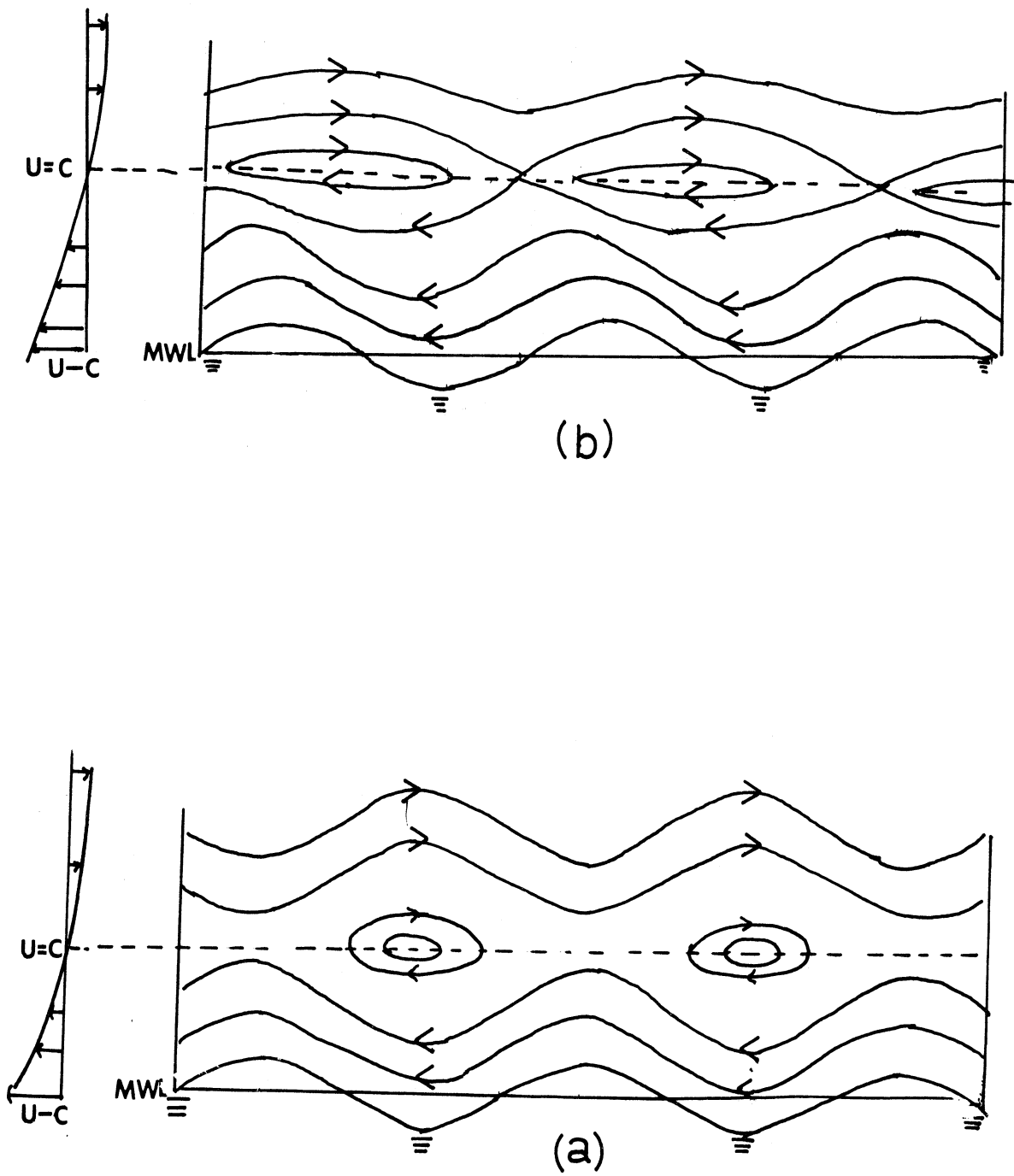


Figure 2.2: Streamlines of sinusoidal perturbation in a shear flow near $z = z_c$; (a) kinematic consequence, (b) consequence of dynamics of critical level.

2.2.2 The Wave Driven Wind

The possible role of waves as a source as well as a sink for momentum in the overlying airflow was considered by Harris (1965, 1966). He estimated the net contribution to the mean wind speed by considering second order terms in the wave amplitude in the solution of the equations of motion for a two-dimensional, inviscid airflow with a vertical shear in the mean wind. The boundary condition was a gravity wave propagating at the interface between two fluids of different density. The upper being the airflow and the lower being the water. The counterpart of Harris' results, mass transport in the water, was formulated by Stokes (1847).

The investigation also included a laboratory experiment in which smoke was used as a tracer over progressive waves. Harris observed that the smoke, in initially still air, moved in the direction of wave propagation. This represented an analysis in the Lagrangian sense of the resulting mass transport. The smoke was observed to move faster than any water surface currents observed by small pieces of paper. The latter observation suggested that viscous effects were not the reasons for the observed transport in the air. The net transport was also observed in the Eulerian sense by hot-wire anemometer measurements.

Results from the hot-wire measurements (Harris, 1965) are shown in Figure 2.3 along with the wave trace. Harris observed a phase difference between fluctuations in the airflow and the water surface as predicted by the linear theory of gravity

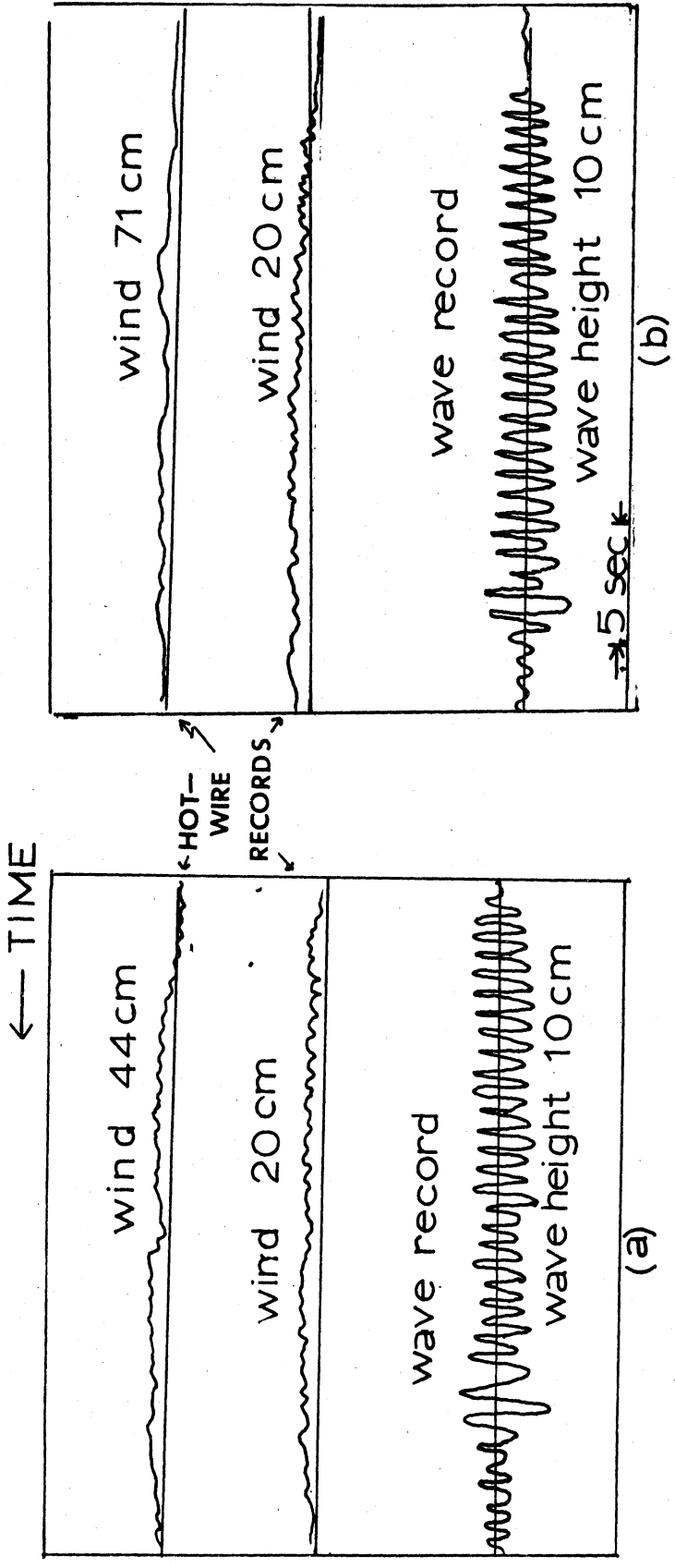


Figure 2.3: Wind and wave strip chart records showing perturbations and net flow due to waves propagating into initially still air (after Harris, 1965).

waves propagating at an interface between a lighter and denser fluid. A discussion of this occurrence is included in most texts on hydrodynamics (e.g. Lamb, 1932, page 370).

Although the problem considered by Harris was to determine the non-periodic result of momentum imparted to airflow by the waves, the initial periodic disturbance is of primary interest in this study. Figure 2.4 (Yefimov and Sizov, 1969) show results obtained using a vertical array of cup anemometers. The lines represent isotachs or lines of equal velocity whereas the lines in Figures 2.1 and 2.2 represented streamlines. The critical level, as defined by the dominant wave and wind conditions for the observation represented by Figure 2.4, was well above the highest level of measurement. In the first approximation, the isotachs for this case should be represented by the streamlines below the critical level in Figure 2.2 since waves of this length would simply bend or distort the mean shear flow. The closed isotachs were interpreted in this case as being due to momentum being imparted to the airflow by the waves.

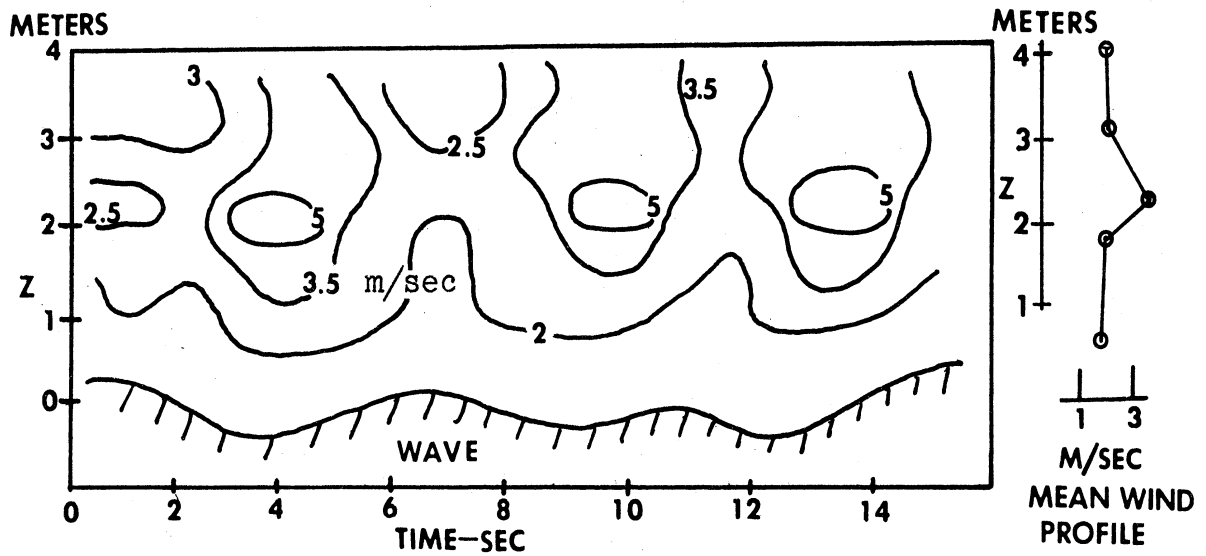


Figure 2.4: Observational results showing isotachs which indicate a "supplemental maximum" of u momentum above wave troughs (after Yefimov and Sizov, 1969)

2.3 OBSERVATIONAL INVESTIGATIONS OF AIRFLOW OVER WAVES

Properties of turbulent airflow over waves have been examined both in laboratory wind-wave tunnels and on lakes and oceans. In general, those in laboratory settings preceded the more difficult in situ investigations. Most investigations also included wind profile measurements because Miles' expression for momentum transferred to the waves is dependent on the curvature of the profile near the matched layer. The discussion which follows describes only those results which pertain to the observed wave induced fluctuations in the airflow.

In a review paper on the mechanics of the air-sea interface, Stewart (1967) emphasized the deficiency of direct measurements of turbulence over natural water waves. Such an unsatisfactory state for observational background was, of course, in direct contrast to the advance in analytical studies in the preceding decade.

A deficiency of in situ data is due, in a large part, to difficulties in making turbulence measurements close to the surface. Turbulence measurements require sensitive instrumentation which is not suited for the hostile environment at the air-sea interface. Furthermore, accessible locations normally have interfering shorelines or limited fetch conditions and platforms over open seas are expensive to construct and maintain.

2.3.1 Laboratory Studies

Conditions of a laboratory experiment can be well suited for examining wind-wave coupling for comparison with the analytical considerations. Advantages over in situ measurements are that steady conditions can be maintained both in the wind field and the wave field. In particular, a wave field consisting of one harmonic can be generated and the wave-induced perturbation isolated from the "background" turbulence which is generally low. Laboratory studies considered are those in which measurements were made both above and below the critical level. These include investigations by Karaki and Hsu (1968), Stewart (1968) and Shemdin (1969). Results of interest are those which describe:

1. The vertical extent of the waves' influence in the airflow;
2. The magnitude of the vertical and horizontal components associated with the wave-induced perturbation;
3. The phase of the velocity components with respect to the wave; and
4. The magnitude and sign of the wave-induced stress where magnitude is considered relative to the turbulent stress.

The above studies do not, individually, provide information on all four results listed above.

Karaki and Hsu (1968) made measurements with a hot-wire anemometer in which the sensor (tungsten wires of .00015 in. diameter arranged in a x-array) was fixed relative to the mean

water level but was relocated at several heights during the observations. The critical level during the measurements was near 4.5 inches above the waves with heights ranging from .5 to 1.5 inches. The influence of the waves on the airflow was observed to be limited to a region close to the waves. For all wave heights, the amplitudes of the wave induced u and w components (\tilde{U}, \tilde{W}) decreased and increased respectively with height. The magnitude of u decreased rapidly within the region of high shear close to the surface. The increase of w with height was not that assumed in theory, i.e. decrease proportional to $\exp(-Kz)$.

Close to the surface, the phase difference between u and the wave was near 180° , maximum in u occurred near the wave trough, and the maximum in u shifted approximately linearly with height toward the upwind node of the wave. Near the surface, the maximum in w was over the downwind slope of the wave and shifted significantly near the critical level, having nearly the same phase as u in the matched layer.

The variation of the wave-induced stress with height was oscillatory being negative below the critical level, near zero in the matched layer, and positive above. Close to the surface the wave induced stress was about 40% of the turbulent stress but the authors warn that the results have to be considered qualitatively in view of large uncertainty in the data. The results were influenced by the high level of background turbulence even though a low turbulence wind-wave tunnel was used.

R. H. Stewart (1968) measured two components of the wave induced perturbation using a fixed sensor (hot-wire anemometer) positioned at several levels. Wave induced perturbations in the velocity fields were determined from harmonic analysis and were compared with those from numerical solutions of several formulations of the linear theory. The observed amplitudes were found to agree with those obtained from the numerical solutions but the phase relations between u and w , except for a case when the critical level was effectively at infinity¹, did not.

Stewart compared the observed wave induced velocity components with those predicted by Miles' first approximation, simple bending of streamlines resulting in irrotational flow. He found that estimates agreed near the critical level but the observed amplitudes were less by a factor of 2, both above and below the critical level.

Phase analysis indicated that below the critical level u had a maximum over the trough of the wave and the maximum shifted toward the upwind node with height. The maximum in w was over the downwind side of the wave (near the node) and shifted back toward the crest with height. When the critical level was effectively at infinity, u was a maximum over the trough and w was a maximum over the downwind node of the wave at all measurement levels.

¹The terminology "effectively at infinity", in reference to the critical level, is used throughout this study to mean that the dynamics at the critical level should not influence the observed properties of the flow.

An oscillatory (change of sign) appearance of the wave induced stress with height was also observed by Stewart and one of his conclusions was that the momentum transport to the wave could not be estimated by extrapolating a wave-induced stress to the surface. He also concluded that application of his results to in situ conditions would be difficult because of the idealized conditions which could be maintained in the wave-wind tunnel. The scale of turbulence observed in natural regimes and the continuous spectrum of natural waves were the primary reasons cited for caution in applying the results to oceanic conditions.

Shemdim (1969) obtained velocity measurements with sensors which followed the water surface. Velocity was measured with total head and static pressure sensors during conditions when the wind speed was less and also greater than the wave speed. The primary results from his investigation contributing to the purpose of the present study were phase relationships between the horizontal components and the wave and descriptions of streamlines in the flow including the region in the trough.

Phase results from Shemdim's measurements (.5 inches above crests of waves with heights of 4.4 inches) indicated that the component of the wind in the direction of the wave propagation was a maximum over the trough when the level of measurement was below the critical level. The maximum shifts toward the upwind node of the wave with increasing wind speed. Increasing the wind speed is a lowering of the critical level.

Streamlines for a case when the critical level was well above the crest did not reflect pure bending of streamlines but rather indicated high pressure on the downwind slope and low pressure on the upwind slope (deformation). Shemdin concluded from this that momentum can be transferred from the waves to a shear flow when the mean wind is in the same direction as wave propagation.

A summary of these investigations would be that the amplitude of the perturbations in the airflow are in question even in wind-wave tunnels where the turbulence level is low and the perturbation should be readily isolated. The phase shifts with height of u and w in all three studies were in agreement in the sense that the maximum in u shifts from the region of the wave trough toward the upwind node and that the maximum in w shifts from a position over the downwind node back toward the crest.

2.3.2 In Situ Studies

A summary of results of most investigations up to 1967 was provided by Stewart (1967) in the same review paper in which he described the deficiency of direct turbulence measurements over natural waves. He concluded, on the basis of velocity spectra, that natural waves do not influence the airflow to any measurable extent. For the purpose of his summary, he used results obtained by Smith (1967) at the University of British Columbia overwater platform which sits on a tidal flat. Smith's results were representative of many investigations performed at that site as stated by Stewart (loc cit

page 52);

"Within our own program at the University of British Columbia we have a very large number of spectra obtained in the air over waves and in no case do we find a sharply defined wave peak."

Published results included in this group would be those by Pond et al. (1966), and Weiler and Burling (1967).

Results of recent investigations, however, have revealed maxima in velocity spectra coincident with those in the wave spectra. These include results reported by Seesholtz (1968), Byshev and Kutznetnov (1969), Yefimov and Sizov (1969), Volkov (1969) and Elder et al. (1970). Observations from these investigations were made with a variety of sensors and at several locations. Some results reported by Yefimov and Sizov (1969) appeared in Figure 2.4 page 27 Section 2.2.2. Results obtained by the investigations listed above are described in the next paragraphs.

Seesholtz (1968) conducted a series of measurements on a stable buoy near Buzzards Bay, Massachusetts. The location had prevailing swell from the southerly direction but a local sea breeze generated local wave conditions for most of the measurements.

Using cup anemometers, Seesholtz observed evidence of a wave-induced perturbation in the airflow. Anemometers were fixed relative to mean water level and also arranged on a wave following mast. Those on the wave following mast were spaced to be 30, 50 and 70 cm above the instantaneous water surface and the fixed anemometers at 1, 2, 3, and 4 meters above mean water level.

Using a wave following and a fixed sensor array, Seesholtz was able to observe that the maximum fluctuation related to the waves occurred about 1 meter above the surface of the trough. The occurrence was observed irrespective of the position of the critical level defined by wave spectra peaks. Furthermore, phase results between the velocity and waves were similar from the fixed and wave following anemometers. The phase relation was that the u component was a maximum over the trough. The latter was expected for the fixed anemometer but Seesholtz was surprised that it was observed with the wave following anemometers.

Byshev and Kuznetsov (1969) made measurements in the Pacific Ocean under conditions of swell and weak swell with wind waves. For conditions of swell (2-3 meters), the wave speed for spectra peaks exceeded the wind speed and the wind direction was in the same direction of the swell propagation.

The sensors were cup-shaped "induction" anemometers.¹ Two were attached to a wave following mast so they would be 64 and 250 cm above the instantaneous surface. In addition, two anemometers were positioned 225 and 305 cm above mean water level on a mast that was stable with respect to wave motion.

Their results were interpreted for the purpose of distinguishing between bending and deformation of the airflow streamlines. The wave following sensors were assumed to measure only deformation, and the fluctuations in the airflow were

¹A more complete description was not given.

thereby separated into that portion attributed to streamline bending and that to deformation. During times when the wave speed was considerably greater than the wind speed, approximately 30% of the fluctuations in the horizontal component was observed to be due to streamline bending. The component measured by the wave following sensor had a maximum over the trough, and that by the fixed sensor slightly ahead of the trough.

Yefimov and Sizov (1969) made measurements in the trade-wind zone of the Atlantic Ocean under conditions of mixed swell. (Swell propagating from at least two directions.) During most of their observations the wave speed associated with the predominant swell exceeded the wind speed. The sensors were attached to a buoy which was nearly steady with respect to the mean water level (for 2 meter waves of 40 meter length, vertical movement of the buoy did not exceed 5-7 cm). Four propeller anemometers were positioned from 1.5 to 4.5 meters above mean water level and another was attached to a wave following float.

The results contained information only on the u component and agreed with those observed by Seesholtz. The maximum in the u component occurred over the trough of the wave for both the floating and fixed anemometers. Furthermore, the spectral density in the u velocity component at the frequency of the wave spectrum peak varied with height. The maximum occurred near 2.5 meters above mean water level.

They observed very little phase shift between the fluct-

uations at different levels which included the floating as well as the fixed anemometers.

Volkov (1969)¹ observed both the u and w components of the fluctuating wind along with temperature fluctuations. The measurements were made in the Mediterranean Sea under various wind and sea conditions. A sonic² anemometer fixed at two meters above mean water level provided results which indicated the influence of the waves in both the u and w velocity component spectra.

Phase relation information was not reported but considerable attention was directed toward the relative intensity of each component ($\sigma u/u_*$, $\sigma w/u_*$) in relation to the ratio of the wave speed to the friction velocity, C/u_* . Over ground, similarity theories predict that the relative intensities should be a function only of hydrostatic conditions (Monin, 1962). Volkov found that the relative intensities increased with increasing values of the ratio C/u_* . The latter observation indicates that a significant portion of the turbulent kinetic energy ($\frac{1}{2}u_i^2$, $i = u, w$) in the wind field is due to the waves. He also observed that the estimates of stress (\overline{uw}) using measured values of u and w generally exceeded those ob-

¹Kitaygorodskiy (1969) also reported on these results.

²In the sonic anemometer, the elapsed time for a sound pulse to go from a transmitter over a fixed distance to the receiver is measured. Fluctuations in this time period are linearly proportional to the instantaneous wind speed between the two points.

tained from considering the wind profiles. This indicates that a portion of the turbulent transport of horizontal momentum near the waves is not involved in maintaining the wind speed (or mean wind profile) near the surface.

Elder et al. (1970) reported results obtained from measurements obtained at the same site as those in the present study. Results include those for one period in which measurements were made 2 meters above the mean water level with a bi-vane anemometer. This sensor provides data for velocity spectra of all three components (u,v,w) of the airflow. The critical level, defined by the speed of the waves whose frequency was at the spectrum peak, was well above the measurement level ($C = 7.4$ mps, $\bar{U} = 3.3$ mps at 2 meters). The wave field was described as being diminishing.

Both v and w showed spectral peaks coincident with the wave spectrum peak but u did not. The latter result indicates that the cross-wind component may be of importance. Phase relationships were such that the w component led the wave by 55° and both u and v led the wave by 130° . The difference between u and w of about 75° was interpreted as being descriptive of nearly irrotational flow in a sense opposite to that in the water.

A summary of results from these investigations would be;
1) Consistent observations of the wave induced peaks in the velocity spectra indicate that the region close to the waves is disturbed considerably by the presence of the waves, 2)
Consistent observations of maxima in the u component with wave

following sensors and phase agreement between the wave following and fixed sensors indicate that simple streamline bending does not describe the airflow over the waves.

All these are different from the present study because they lack results on spectral distributions of the stress ($\overline{-uw}$) and simultaneous measurements at two levels of more than one component of the wind field.

3. THE EXPERIMENT

3.1 SITE AND TOWER

3.1.1 Location of Experiment

All measurements in this experiment were obtained on Lake Michigan from a fixed U.S. Lake Survey Research tower located in 15 meters of water 1.6 km from shore near Muskegon, Michigan (Figure 3.1). Programs to study air-sea interaction processes have been in progress at the University of Michigan using this site for the field measurements since 1963. Initially, instrumentation was deployed to measure and record mean profiles of wind speed, temperature and humidity on a nearly continuous basis. Descriptions of results and efforts of early experiments have been reported by Elder and Portman (1963), Elder (1965) and Elder (1966). Because of the success at the site in observing representative meteorological and wave conditions, experiments were expanded to include measurements of turbulent properties of the air-flow and have continued each summer except 1966. The tower was, in fact, reinstalled in 1965 after a complete collapse during a severe storm on 24 September 1964.

Weather and wave conditions restrict field measurements to periods from June through October. Severe fall storms and surface ice require that the tower be removed before the end of November and it is usually not installed again before the end of May. Weather conditions over Lake Michigan, however, during summer and early fall combined with the location of

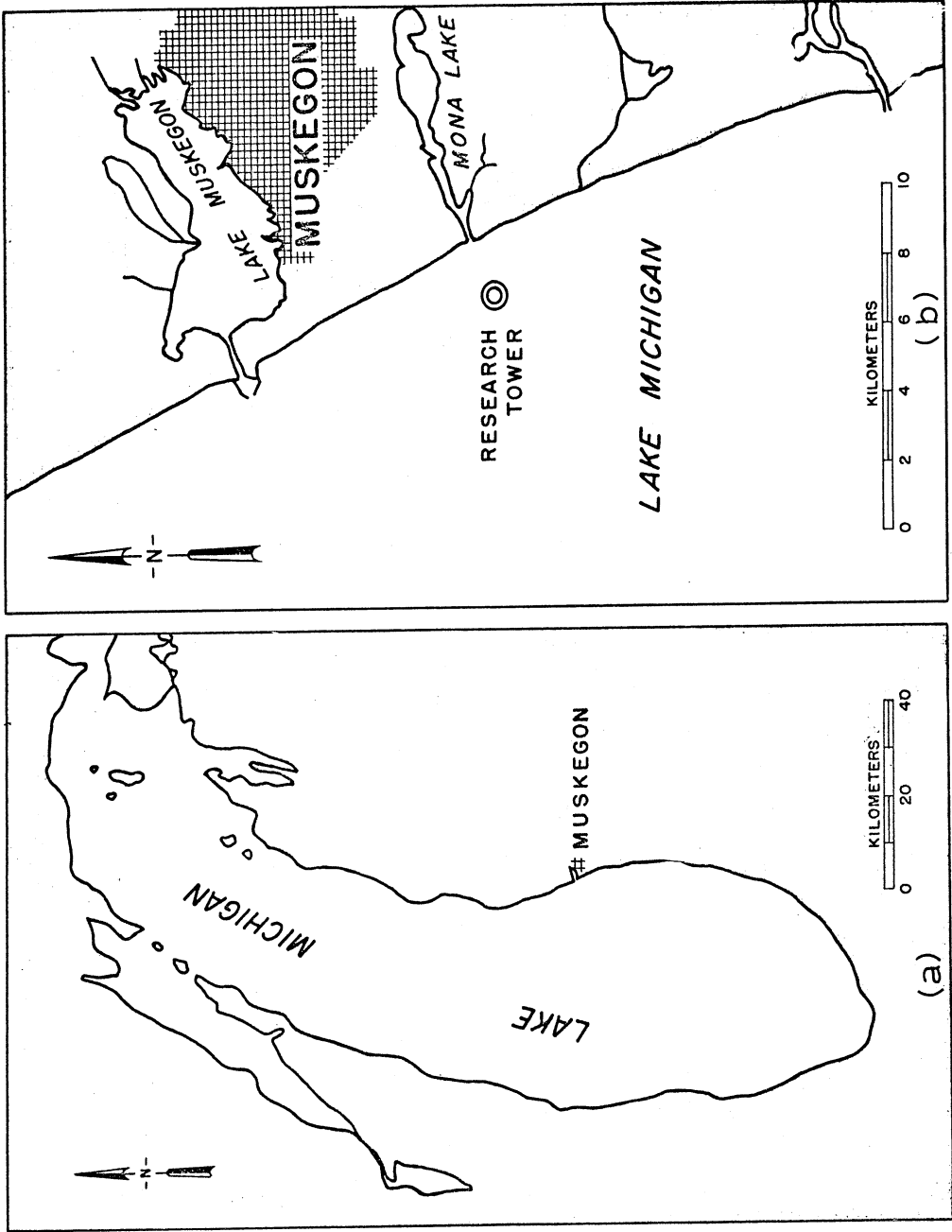


Figure 3.1: Location of U.S. Lake Survey Research Tower; (a) Lake Michigan, (b) tower site near Muskegon, Michigan.

the tower are factors which make this a good facility for studies of air-sea interaction processes. Open water fetches at the location vary from 80 to 300 miles from the south clockwise through northwest directions.

Oriented transverse to the normal west to east movement of weather systems, steady wind conditions with respect to direction and speed normally exist for periods of 12 to 24 hours. Large changes in hydrostatic stability occur, generally, with the advent of a different air mass. The lake is not so large, however, for the presence of separate weather systems and hence swell propagating from different directions. This simplifies the conditions for studying wind-wave coupling since the local wave field is often related to the wind field over the entire lake.

The gradually sloping bottom features and lengths (25-35 meters) of predominant waves diminish the influence of bottom effects on the observed wave field. Also, the lake is surrounded by first order weather stations¹ which enables acquisition of complementary meteorological information to plan experiments and to describe general meteorological conditions during measurement periods.

The reasons for selecting this site (Figure 3.1(b)) were the proximity to the Mona Lake channel and the uncomplicated bottom and shoreline features. The channel is normally deep enough so that a small boat can be used to go back and forth to the tower from a protected dock. A cottage on the channel served as a source for electrical power, supplied by submarine

¹These provide hourly weather observations for teletype transmission.

cable to the tower, and as a base for calibrations and sensor repair.

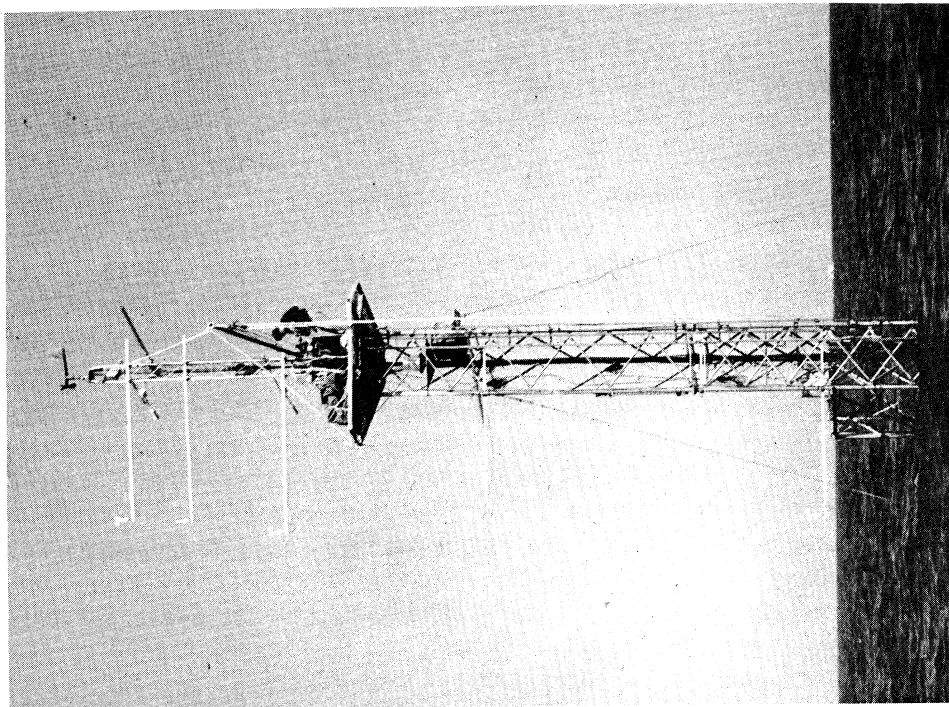
3.1.2 Description of Tower

Figure 3.2 shows the general construction of the research tower and its instrumentation during the experiment. Design and construction were accomplished by the U.S. Corps of Engineers which has also maintained it and associated power cables from shore each season. The structure was designed both to achieve stability and to minimize disturbance to the airflow and water motions.

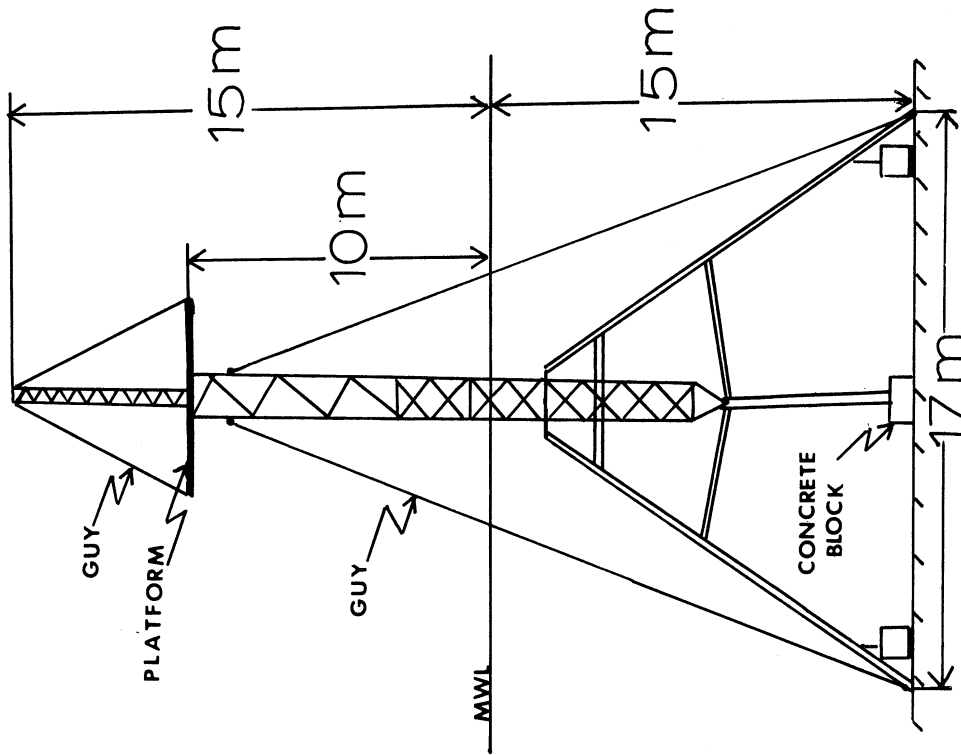
The main above water member of the tower extends 10 meters above mean water level and consists of a triangular truss of braced construction 1.25 meters on a side. A platform at the 10 meter level supports recorders and sensor electronics. Extending 5 meters above the platform is a smaller triangular mast. This arrangement enabled profile and turbulent measurements up to 15 meters above mean water level.

Stability is achieved by supporting the tower on the lake bottom by a tripod which is secured by a concrete anchor at each leg. The tower is also guyed in order to withstand extreme wind and wave conditions such as those which caused a similar one, without guys, to collapse in 1964.

The triangular truss and underwater support result in a minimum of interference to the air or water flow. However, the platform at the 10 meter level and associated recorders and electronics could influence the air flow so sensors were



(a)



(b)

Figure 3.2: Research tower; (a) as instrumented during experiment, (b) schematic showing underwater tripod support structure.

not mounted near this level. All cables and mounting arms were selected and secured in a way to keep the tower as open as possible.

3.1.3 Mounting Arrangement

Figure 3.3(a) consists of drawings which show features of the sensor mounting arrangement. These features include provisions for directing the sensors into the mean wind and for alignment of all sensors in the vertical (plumb line arrangement) above the same point (the wave gauge). A plumb line arrangement of sensors enabled determination of phase relations between waves and turbulent components in the air.

Velocity and temperature sensors and the wave gauge were mounted so they extended westward 2.5 times the width of the tower's side. Experiments which indicate that a 2.5 extension is sufficient for a tower of this type were made by Gill et al. (1967) in a wind tunnel and by Holub (1970) in a natural turbulent regime. Extension arms consisted of 5 cm rectangular tubing and were sturdy enough to avoid motion due to the airflow or waves.

A vertical pipe extended from below the water to two meters above the water so sensors could be positioned at any height from the wave crest to 2 meters. Figure 3.3(b) is a photograph of the sensors mounted on the vertical pipe above the mean water level. A wind vane such as that shown was used at all levels to monitor the direction of the mean wind with respect to the sensors. It is essential, for example, that the mean wind direction be in the same plane as the two

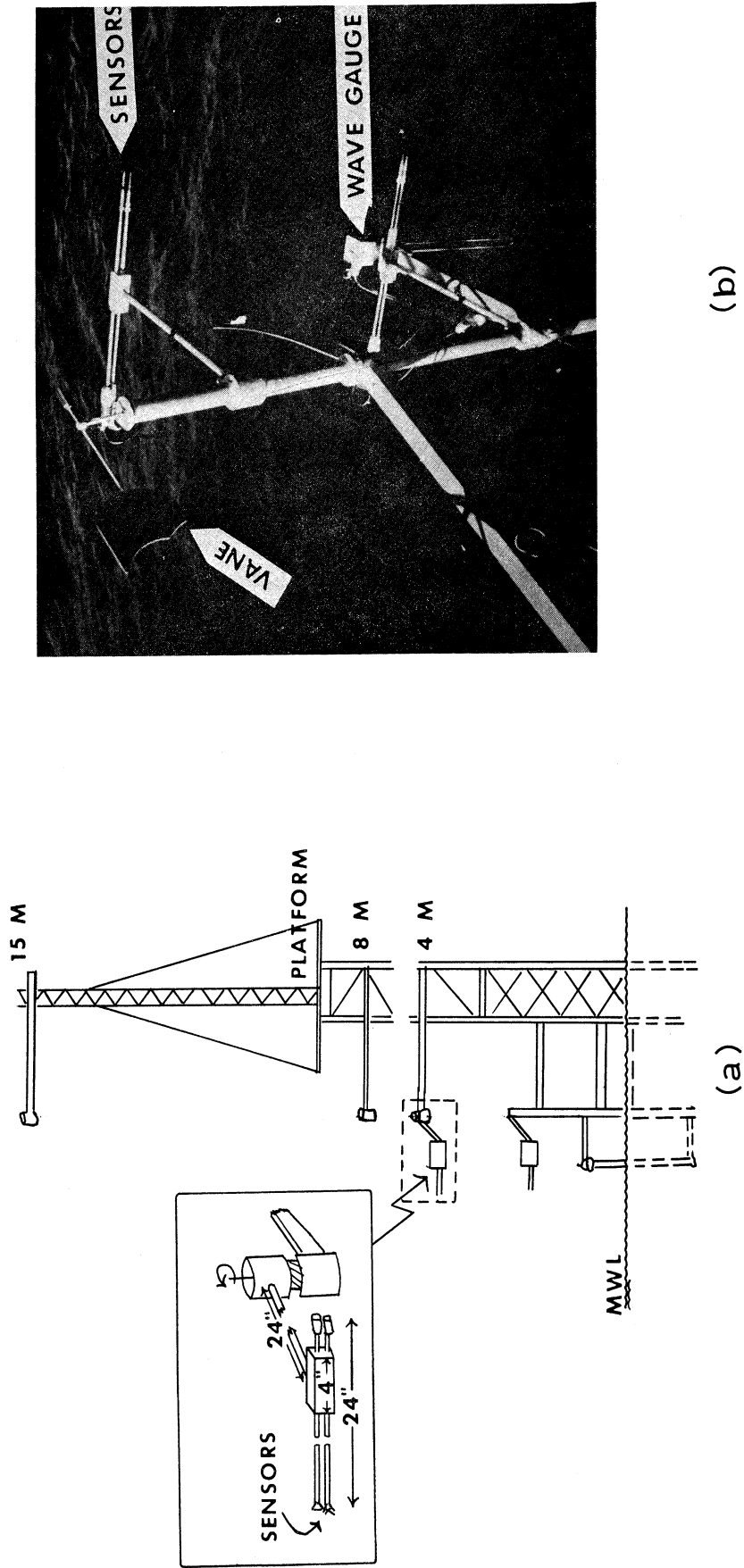


Figure 3.3: Sensor mounting arrangement on tower; (a) components and vertical array, "plumbline", (b) picture of sensors during measurement period.

wires of an X-probe array for proper interpretation of the hot-wire signals.¹ A discussion on the errors introduced if this is not the case was given by Weiler (1966). The vane shows that in this picture, the supporting arms and probes are properly oriented for the given wind direction because the vane shaft is parallel with the horizontal arm supporting the hot wires and temperature sensor. Shown in Figure 3.3(b), directly below the hot wires, is the wave gauge.

Above the two meter level, arms were located at the 4, 8 and 15 meter levels. During a set-up or change of levels, only the sensors and the mounting holder were moved. This procedure avoided the possibility of accidentally changing the level of the arms, which had been leveled quite accurately during the initial stages.

¹ Discussion of X-probe sensors and the signal interpretation appears in section 3.2.1.2.

3.2 INSTRUMENTATION

3.2.1 Velocity Measurements

3.2.1.1 Sensors and Electronics

Turbulent velocity measurements in this study were made exclusively with a constant-temperature hot-wire anemometer¹ system using two wires in an X-configuration as sensors (X-probes²). Each wire or filament of the probe forms one arm of a Wheatstone bridge in the system which also included a power supply and high gain differential feedback amplifier. A diagram of the bridge circuit appears in Appendix C, Figure C.1, and a drawing of the sensor appears in Figure 3.4, page 53.

By means of careful impedance matching, it is possible to obtain, with this unit, a stable and sensitive electronic circuit. During the course of the experiment, however, amplifiers would occasionally go into oscillation and several hours were spent trying to find pairs of transistors whose characteristics were "matched" well enough to operate successfully in the sensitive circuit. Fortunately, the transistor supply and investigator's perseverance overcame the difficulties in order to have operational hot-wire electronics when favorable experimental conditions existed.

¹Model M-5 Hot-Wire Amplifier Units; Kovaszny, Miller and Vasudeva (1963).

²Flow Corporation Model HWP-X-W12X-L24 (X-TYPE).

Probes were obtained commercially and consisted of two tungsten filaments mounted at right angles with a spacing of .03 inches at their intersection. Filaments were .19 inch long including a copper plated end and .00015 inch in diameter. The unplated section was .080 inch long and had a nominal resistance of from 12 to 15 ohms. The combined sensor bridge-amplifier circuit has a frequency response above 2,000 Hz.

3.2.1.2 Operational Considerations and Procedures

The sensitivity of a hot-wire to both flow direction and magnitude allows the use of two wires arranged in a X-array (90° to each other) to measure simultaneously two components of the wind. Properties of the air flow of special interest in this experiment were the covariance between the vertical velocity component (w) and the along-wind component (u) and also the covariance between the vertical velocity and temperature. These describe momentum and heat transport to or from the surface.

Although hot-wire anemometers have advantages of high frequency response and small sensor size, considerable effort is necessary to insure proper interpretation of the hot-wire signals from the two wires. Hot-wire results may be subject to several errors including those caused by 1) conductive heat losses to wire supports, 2) sensitivity (signal versus wind speed) change due to resistance change and contamination of the wire, 3) misalignments of the probe, 4) inherent inadequacies of empirical relations used to convert signal to vel-

ocity units, 5) deviation of assumed directional (cosine) response, and 6) ambient temperature fluctuations. The possibility of potential errors from any or all those listed above are difficult to avoid during measurements on an over water platform. Available working space, set-up time and the high turbulent level of the airflow, for example, prohibit calibrations on the platform.

Several methods had to be employed in parallel to examine and select the most probable constants for interpretation of the hot-wire signals. These methods included 1) wind tunnel calibrations before and, if possible, after measurement periods, 2) in situ calibrations based on simultaneous cup and propeller anemometer measurements, 3) determining relative response of the two wires on each X-probe. Relations used to convert hot-wire signals to velocity components, calibration procedures and comparative methods employed to determine constants in these relations are discussed in the sections 3.2.1.3 and 3.2.1.4

3.2.1.3 Relations between Instantaneous Velocities and Hot-Wire Outputs

Empirical relations describing relative sensitivity and response characteristics for hot-wires have been reported by various investigations¹. In general, early advances were refinements of concepts of heat loss relations for a small cylinder in an air stream as first formulated by King (1914).

¹Appendix A, Section A.1 contains additional discussions of interpreting hot-wire signals.

King's equation is:

$$(E^2 - E_0^2)^2 = K U \sin\phi, \quad 3-1$$

where E and E_0 are voltages across the wire at the velocity U and at zero velocity respectively; K is a scaling factor and ϕ is the inclination of the wire to the total instantaneous wind U . An important feature of the functional relationship in Equation 3-1 is that the hot-wire response (E) is not linear with respect to the wind speed, U .

Recent investigations on hot-wires by Webster (1962), Champagne, et al. (1967) and Sandborn (1967) have been directed towards improving the understanding of the directional sensitivity and the influence of the non-linear response in practical turbulence measurements. All of these investigations showed deviations from a perfect cosine response which is implied in Equation 3-1. Sandborn (1967), however, showed that voltage-velocity relations can be used in a differential form if the turbulent intensity level, $(\overline{u^2})^{1/2}/\overline{U}$, is below 30 to 40%.

Because turbulence levels in this experiment were below the 30% limit defined by Sandborn, hot-wire signals were not linearized during conversion to velocity units. The following expression, Equation 3-2, is the linear (differential) expression for the relation between fluctuations in signal and velocity components for a yawed hot-wire,

$$e = K (u + c \cdot w \cdot \cot\phi) \quad 3-2$$

where e is measured fluctuating voltage,

K is a constant that depends on wire response to wind (a scaling factor),

c is a constant which corrects for deviations from cosine response

u and w are components of fluctuating wind

ϕ is the angle between the wire and mean wind.

With an X-probe arrangement, two simultaneous equations (one for each of the two wires) of the form of 3-2 can be used to solve for u and w . If the X-array is in the plane of the mean wind, \bar{U} , and both wires are 45° to the horizontal then u would be the along-wind component and w the vertical component. A schematic showing the probe orientation and the velocity components appears in Figure 3.4 and expressions for u and w are given in the following equations:

$$u = \frac{(e_1 K_2 \cot \phi_2 + e_2 K_1 \cot \phi_1)}{K_1 K_2 (\cot \phi_1 + \cot \phi_2)} \quad 3-3$$

$$w = \frac{(e_1 K_2 - e_2 K_1)}{K_1 K_2 (\cot \phi_1 + \cot \phi_2) c} \quad , \quad 3-4$$

where the terms e_i , K_i , ϕ_i , ($i = 1, 2$; for wires 1 and 2), and c are defined with Equation 3-2.

With the assumption that $\phi_1 = \phi_2 = 45^\circ$, Equations 3-3 and 3-4 are rewritten as follows, and were the forms used for analyses during this experiment,

$$u = \frac{1}{K_2 \cdot 2} \left(\frac{e_1 K_2}{K_1} + e_2 \right) = c1 \left(e_1 \cdot \frac{K_2}{K_1} + e_2 \right) \quad 3-5$$

$$w = \frac{1}{K_2 \cdot 2c} \left(e_1 \frac{K_2}{K_1} - e_2 \right) = \frac{c1}{c} \left(e_1 \cdot \frac{K_2}{K_1} - e_2 \right) \quad , \quad 3-6$$

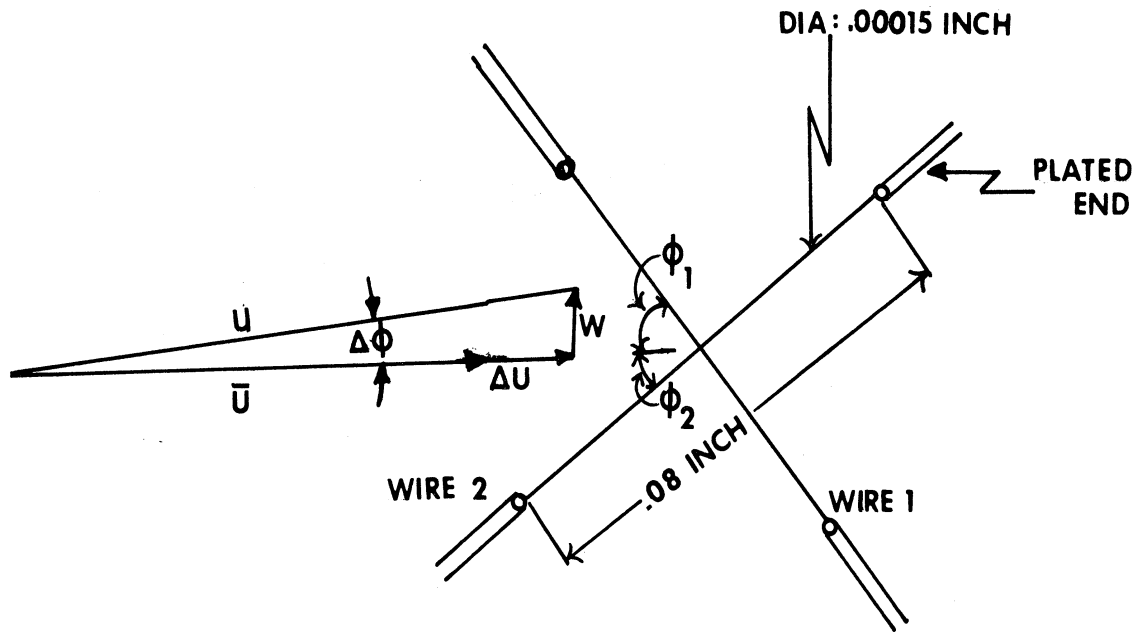


Figure 3.4: Configuration and dimensions of X-probe sensor with assumed orientation to mean wind.

where $C_1 = \frac{1}{K_2 \cdot 2}$

$$K_1 = \frac{\partial E_1}{\partial U} \text{ for wind tunnel calibration}^1$$

$$= \frac{E_1^2 - E_0^2}{4 \cdot U \cdot E_1} \text{ for in situ calibrations}^1.$$

3.2.1.4 Calibrations and Selection of Constants for Hot-Wire Interpretations

Constants which had to be determined through in situ or wind tunnel calibrations appear in Equations 3-5 and 3-6 and are:

- i) c = directional sensitivity which depends primarily on wire geometry
- ii) $\frac{K_2}{K_1}$ = relative response of hot-wires
- iii) C_1 = scaling factor to convert voltage to velocity units.

Calibrations, using a portable wind tunnel (Figure 3.5), were performed before and, if possible, after each day's operation on the tower. (Breakage during use was a common occurrence.) In addition to estimates of the constants (c , K_2/K_1 , C_1), calibrations served to:

- i) Evaluate angle between wires on each probe. This was performed by rotating the probe in an airflow and determining angular relations from observed minima and maxima voltages for each wire. If the angle between the wires was greater than $\pm 2^\circ$ from the preferred 90° relation, the wires were replaced.

¹Appendix A, section A.1, contains additional discussions on the two possible expressions for K_1 .

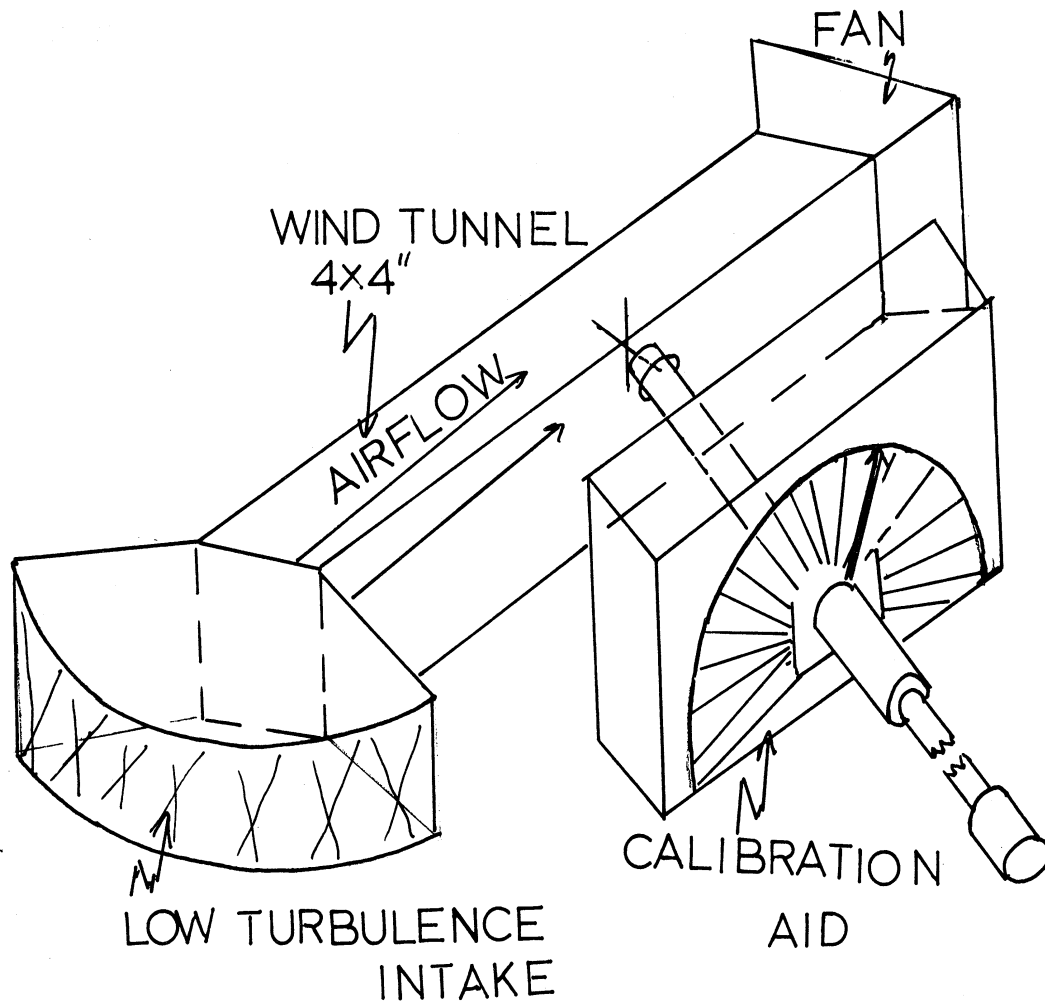


Figure 3.5: Portable wind tunnel and calibration accessories.

- ii) Evaluate performance of hot-wire amplifier units with respect to drift and noise level. This was necessary because the units were being operated in a relatively hostile environment while on the tower. For example, during initial stages of the experiment, a potentiometer which controlled the over-heat ratio of the wires was observed to cause a drift in the signal and was replaced.
- iii) Orient X-array relative to a mounting block so that when mounted on tower arms each wire would be 45° to the mean water level (hopefully).

For all processing, a value of .90 was selected for the constant c . The selection was made on the basis of results reported by other investigators whose techniques for determining its value were more refined than those in this experiment. Furthermore, estimates obtained during calibrations indicated that .90 was a reasonable choice¹. Because sensors were restrung with wire from the same spool and because c is primarily a function of wire geometry, selecting a single value for c seemed to be a reasonable decision.

Table 3.1 lists values which lead to selections of the constants K_2/K_1 (given as K_1/K_2 in the table) and C_1 . The selection procedure was first to select the most probable value (denoted $r(\text{sel})$) for K_1/K_2 by considering; 1) wind tunnel and 2) in situ estimates of K_1 's and 3), estimates of

¹A composite of results from several calibrations appears in Appendix A, Figure A.3.

Table 3.1. Calibration and Relative Response Values Considered in Hot-Wire Interpretations.

PRD	DATE	TIME*	a LEV	b PRB	c HW	Calibrations				Relative Response				K ₁ /K ₂ r(sel)	rot
						wind tunnel		In Situ		Computations		$\Delta E_1/\Delta E_2$			
						K ₁	K ₁ /K ₂	K ₁	K ₁ /K ₂	1	2	3	4		
1	8-19	1226	1.5	D	1	7.46	1.00	6.77	1.05	.92	.89	.56	**	1.0	0
					2	7.45		6.42							
			4.0	B	1	8.62	1.10	4.33	1.57	.94	.95	.89	1.01	1.0	0
					2	7.75		2.83							
2	8-19	1407	1.5	D	1	7.46	1.00	5.92	1.04	1.06	.86	.92	**	.9	0
					2	7.45		5.67							
			15.0	F	1	6.86	.92	3.36	.90	.87	.87	**	1.13	1.0	0
					2	7.46		3.74							
3	9-24	1724	1.5	C	1	4.86	1.05	7.67	.82	.94	.97	.93	1.08	1.0	0
4	9-24	1755	1.5	C	1	4.86	1.05	7.56	.80	.97	1.01	1.00	1.00	1.0	0
					2	4.61		9.51							
			4.0	B	1	4.17	1.49	9.59	1.26	.80	.92	.86	**	1.0	0
					2	2.80		7.61							
5	9-26	1100	1.5	B	1	3.82	1.45	7.66	1.25	.92	.83	.85	**	.9	0
					2	2.64		6.12							
			4.0	A	1	4.17	1.26	2.67	.79	1.08	1.07	1.08	1.08	1.1	8°
					2	3.33		3.40							
6	9-26	1324	4.0	B	1	3.58	1.49	4.98	1.05	.82	.94	.74	**	.9	0
					2	2.41		4.74							
7	9-26	1355	1.5	A	1	4.09	1.25	**	—	1.19	**	1.18	1.18	1.2	0
					2	3.29									
			4.0	B	1	3.58	1.50	5.94	1.08	.90	.81	.79	.89	.8	0
					2	2.41		5.52							
8	9-27	1120	1.5	F	1	3.92	1.29	16.10	3.64	1.33	1.26	1.34	1.40	1.3	0
					2	3.03		4.4							
			4.0	C	1	4.53	1.10	8.61	2.04	1.34	1.42	1.35	1.23	1.3	8°
					2	4.09		4.21							
9	9-27	1140	1.0	F	1	3.93	1.29	13.82	3.68	1.24	1.27	1.23	1.38	1.3	0
					2	3.03		3.74							
			2.0	C	1	4.53	1.11	8.99	2.06	1.28	1.09	.97	**	1.1	8°
					2	4.09		4.37							
10	9-27	1200	1.0	F	1	3.92	1.29	1.36	2.72	1.32	1.27	1.36	1.20	1.3	0
11	10-5	1650	1.0	A	1	4.03	1.02	2.81	.82	1.10	1.14	1.35	1.55	1.3	0
					2	3.97		3.44							
			2.0	C	1	4.53	1.11	8.53	1.57	1.11	.92	1.16	.92	1.0	8°
					2	4.09		5.42							

*Starting time for 18 minute period

** Erroneous values

a: measurement level (meters)

b: probe

c: wire on probe

the relative response¹ obtained by an independent in situ method. Values from Method 3) were given the most weight in selecting K_1/K_2 but agreement between any of the 3 methods was also a criterion.

Selection of C1 values amounted to selecting an in situ value of K_1 for at least one of the wires. Only one K_1 value was necessary at this stage since K_1/K_2 had already been selected and $C1 = 1/(2 \cdot K_2)$ could be determined from the ratio. An in situ estimate was preferred over a wind tunnel estimate because later tests indicated that exact flow rates in the portable wind tunnel were not known. The reasons for this are still unknown.

Once a K_1/K_2 selection was made, validity of individual in situ K_1 estimates could be assessed. For example, if the selected K_1/K_2 value differed considerably from the in situ K_1/K_2 value, it was sometimes easy to identify the wire which had an anomolous K_1 . This was the case for the 1.0 meter level during observation periods 8-10. Agreement between K_1 for individual wires between sequential periods was also a useful guide in the selection procedure. During periods 7 (1.5 meters) and 10 (1.0 meters), K_2 's from the previous periods were used.

3.2.1.5 Adjustment of Velocity Results by Axis Rotation

¹Appendix A, Section A.2.2 describes the background and method for in situ determination of the relative response ($\Delta E_1/\Delta E_2$)

Cospectral results for four periods had positive values within frequency bands in which one normally expects negative values in boundary layer flow. The bands were at low frequencies (.02 to .05 Hz) and, in some cases, in a broad band from 1 to 10 Hz. These results were judged to be caused by either incorrect calibration constants or probe misalignment, or both. Sampling fluctuations and wave influences were rejected as causes because of both the frequency range and the character of the anomalies. Positive values due to sampling fluctuations should occur at frequencies near .01 Hz and those due to the wave influences should occur from .1 to 1. Hz.

With the assumption that the positive cospectral estimates were caused by either incorrect calibration constants or probe misalignment, the effect was reduced with a transformation to a new coordinate system, rotated from the original system. Spectral results before and after the adjustments appear in Appendix B, Section B.2, for three of the four periods. The results shown therein indicate that the adjustments influenced the total stress considerably but not the variance spectra or the cospectral features near the frequencies of the wave spectrum peaks.

Rotations were performed on initial spectral estimates rather than on the values of velocity components. Relations for the rotation are obtained by considering the complex coefficients which lead to the spectral estimates¹ and are given by Equations 3-7 through 3-14. The primed and unprimed terms are the new and old estimates respectively.

¹Appendix B contains a discussion of the derivations of Equations 3-7 through 3-14.

$$\phi'_{uu}(n) = \phi_{uu}(n)\cos^2\theta + \phi_{ww}(n)\sin^2\theta + \phi_{uw}(n)\sin 2\theta \quad 3-7$$

$$\phi'_{ww}(n) = \phi_{ww}(n)\cos^2\theta + \phi_{uu}(n)\sin^2\theta - \phi_{uw}(n)\sin 2\theta \quad 3-8$$

$$\phi'_{uw}(n) = \left[\phi_{ww}(n) - \phi_{uu}(n) \right] \cdot \frac{\sin 2\theta}{2} + \phi_{uw}(n) \cdot \cos 2\theta \quad 3-9$$

$$\phi^{*'}_{uw}(n) = \phi^*_{uw}(n) \quad 3-10$$

$$\phi'_{us}(n) = \phi_{us}(n) \cdot \cos\theta + \phi_{ws}(n) \cdot \sin\theta \quad 3-11$$

$$\phi^{*'}_{us}(n) = \phi^*_{us}(n) \cdot \cos\theta + \phi^*_{ws}(n) \cdot \sin\theta \quad 3-12$$

$$\phi'_{ws}(n) = \phi_{ws}(n) \cdot \cos\theta - \phi_{us}(n) \cdot \sin\theta \quad 3-13$$

$$\phi^{*'}_{ws}(n) = \phi^*_{ws}(n) \cdot \cos\theta - \phi^*_{us}(n) \cdot \sin\theta \quad 3-14$$

where

ϕ^*_{ij} represents quadrature spectra,

θ angle of rotation, and

s represents a scalar quantity (temperature or wave height).

3.2.2 Temperature Measurements

Frequency response and accuracy requirements for temperature measurement are similar to those for velocity measurement. Existing systems for temperature measurement, however, do not have as desirable frequency response characteristics as those for velocity. Comparisons of the present results with those of Miyake et al. (1970) indicate that reasonable estimates were obtained for spectral distributions of temperature variance and covariance between temperature fluctuations and the

vertical velocity¹.

A resistance thermometer² was used to measure temperature fluctuations. The sensor, in this case a 30 ohm, .00015 inch tungsten wire, .16 in. long, is part of a constant-current circuit and with a small filament current (about 2 ma) serves as a resistance thermometer. A block diagram of the bridge circuit appears in Appendix C, Figure C.2. The frequency response of the system is determined by the thermal inertia of the wire itself and its resistance (i.e. wire length) cannot be reduced much below that used or the output is too small and within the noise region for the system.

The bridge unbalance caused by a temperature, and hence a sensor resistance change, was amplified 2500 times for the output signal. With this amplification a tungsten sensor of 30 ohms resistance would ideally have 125 mv output for a 1°C change which is a sufficient signal to record with suitable preamplification. Laboratory tests, with a controlled temperature environment and simulated temperature changes (by varying probe resistance), indicated that the system had enough resolution to measure temperature to .05°C.

Spectral descriptions of temperature fluctuations were restricted to frequencies below 20 Hz by system noise and

¹Spectral results of temperature fluctuations and cospectra of \overline{wT} appear in Appendix E.

²Flow Corporation 900 series.

sensitivity. Even with these limitations, interpretation over an important range of frequencies was possible since sensible heat flux is associated with frequencies below 10 Hz.

The probe was mounted 1 inch above the velocity probe with the wire normal to the mean wind. The spacing between the velocity and temperature sensors was determined by wind tunnel tests and insured that the temperature sensor would not be influenced by heat lost from the hot-wires.

3.2.3 Wave Measurements

Elevation of the water surface at a point directly below the velocity and temperature sensors was measured with a capacitance gauge system. Both the bridge and sensor which comprised the system were obtained commercially¹.

The bridge (capacitance to current transducer) was completely contained in a 10x14x6 inch enclosure which is shown in Figure 3.6. The bridge-amplifier output was 0 to 1 ma independent of load resistance up to 500 ohms. By adjusting a span control, outputs of 0 to 1 ma were obtained for no and total immersion respectively of a 60 inch sensor. Tests of the output versus immersion were performed in the laboratory and at the measurement site regularly and a linear relationship was found for intermediate immersions. Figure 3.7 shows representative curves.

The sensor (Figure 3.6) which was the capacitance arm of the bridge, consisted of a teflon (which served as the dielec-

¹C. F. Warrick Co., Berkley Michigan, Series C5-A.

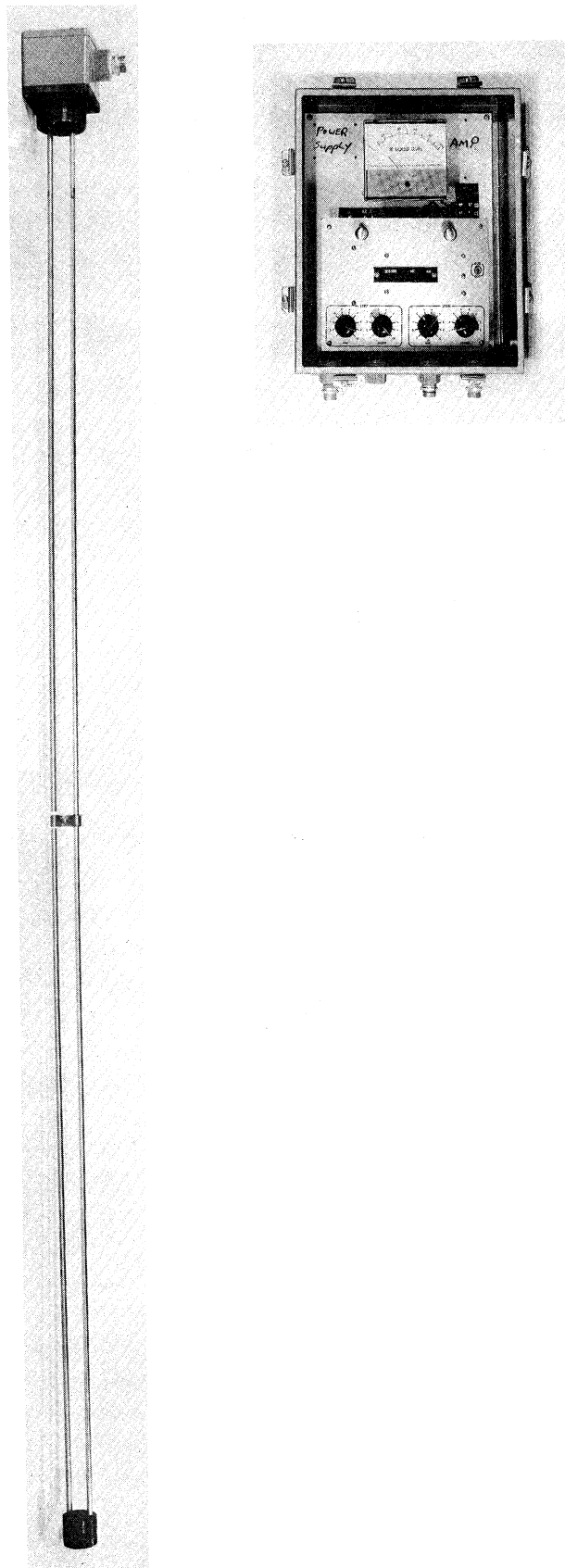


Figure 3.6: Picture of capacitance wave gauge and bridge-amplifier system.

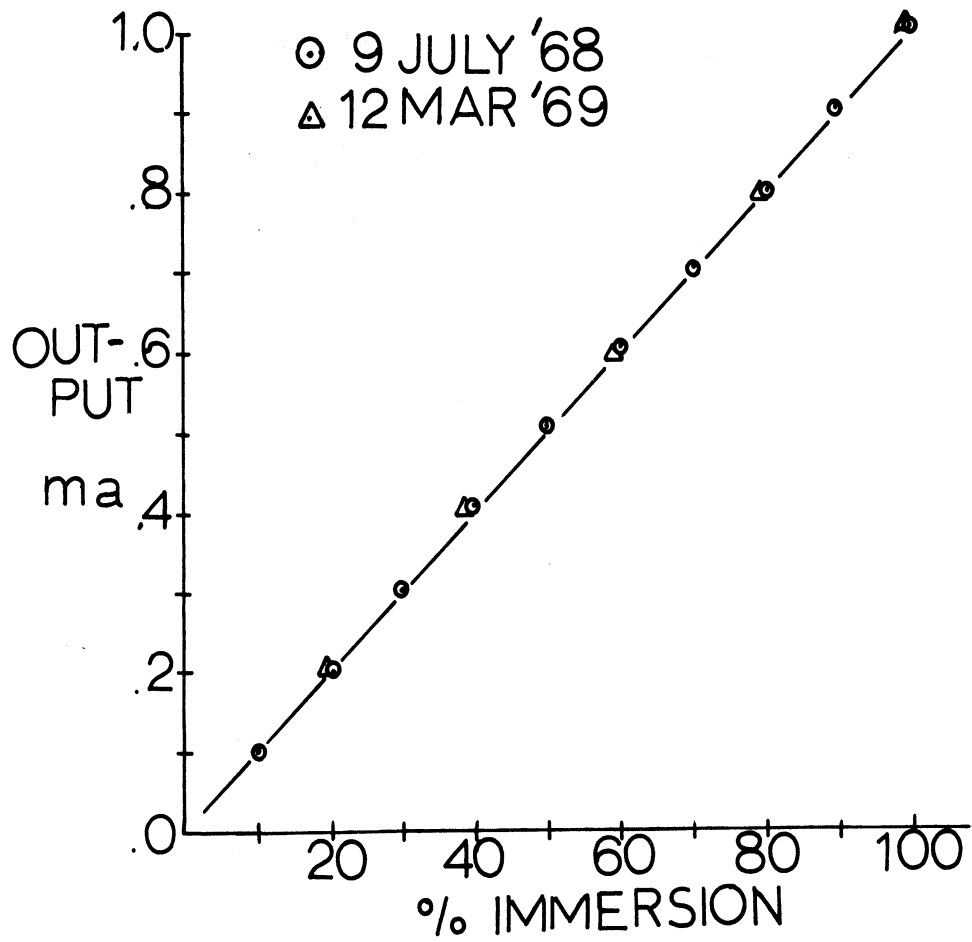


Figure 3.7: Calibration results of wave gauge, immersion versus output (ma).

tric) coated stainless steel rod .25 inch in diameter and 60 inches long. The length was selected on the basis of anticipated wave conditions and also resolution. A similar but non-insulated rod positioned one inch away served as the ground or other side of the capacitor. Although it increased the size of the sensor, the additional rod was used (i.e. rather than the tower) because of algae on the tower structure.

Manufacturer's proprietary rights prevented acquisition of detailed knowledge of the performance of components in the bridge circuit. A simplified capacitance bridge circuit appears in Figure C.3, Appendix C, and shows an active oscillator as a primary component. The frequency and performance of the oscillator is relevant to the influence of slow runoff of water "film"¹ from the sensor.

Considerable assistance on interpreting the effects of the film and designing procedures to test its influence were given by Dr. R. E. Davis², Scripps Institute of Oceanography. He contributed a simplified circuit diagram, Figure 3.8, to show the influence of the film, and the following relations for the impedance (Z) between the sensor and ground. The impedance (Z) is the measurement of the immersion and is given by;

$$Z = \frac{1}{i\omega C + \frac{1}{R + \frac{1}{i\omega C_f}}} \quad 3-15$$

¹"film" refers to water on the probe above the actual water level

²personal communication

$$= \frac{1}{\frac{1\omega C + 1\omega C_f}{\omega R C_f + 1}}$$

where ω is frequency of active oscillator

C, R, C_f are defined in Figure 3.8

$$i = (-1)^{\frac{1}{2}}.$$

If $R \cdot \omega$ in Equation 3-15 is large enough, the measured impedance is essentially that of the submerged probe. The resistance, R , and hence the product $R \cdot \omega$ would be increased by reducing the film. Film reduction was promoted by using a non-adhesive dielectric (teflon) on the sensor and also by removing the sensor after each observation period to keep it clean.

Because the occurrence of film could not be avoided completely and ω was an unknown, laboratory tests were conducted with fresh and salt water with representative waves simulated by pulling the sensor in and out of a calibration tube. The results of these tests appear in Figure 3.8 and show that the system was satisfactory for the Lake Michigan experiment in which waves had periods from 3 to 5 seconds.

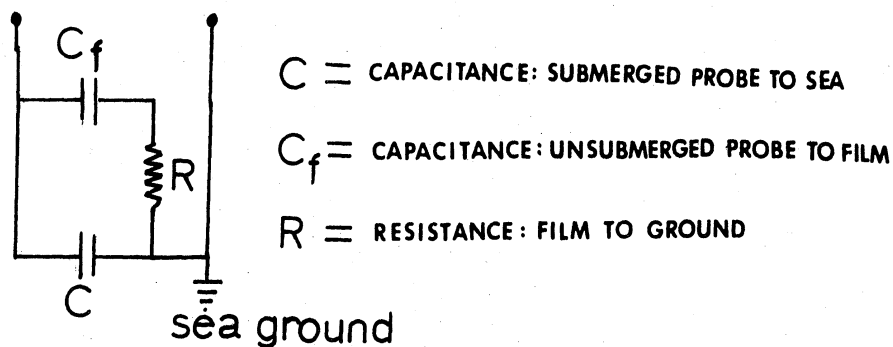
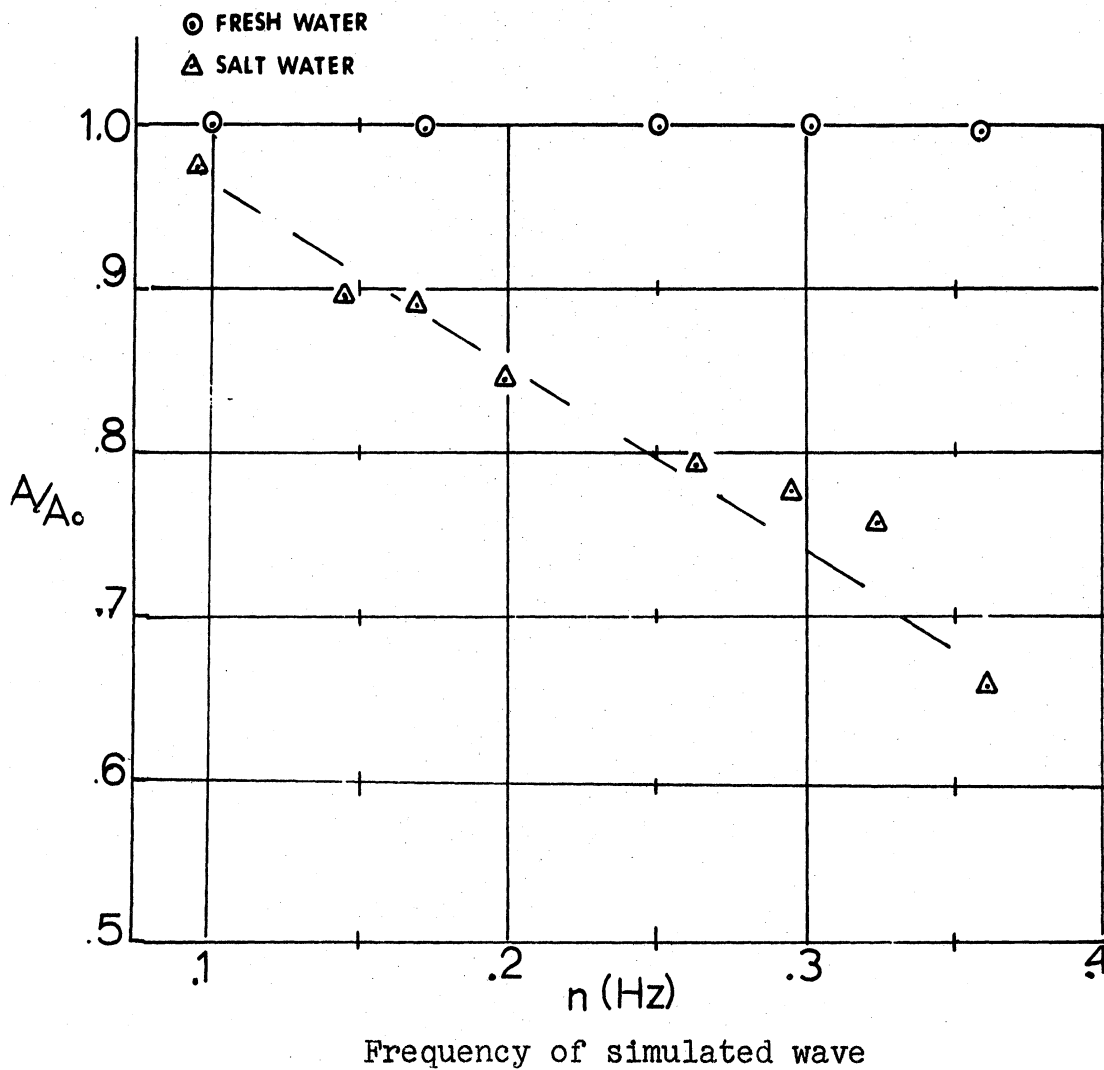


Figure 3.8: Influence of film on output from capacitance wave gauge and simplified circuit showing role of film; A = amplitude from wave gauge output, A_0 = actual amplitude

3.3 RECORDING

All data were recorded on magnetic tape in analog form by frequency modulation with a seven channel recorder¹. All recordings were obtained with a recording speed of 3 3/4 inches per second. At this recording speed the recorder had a frequency range from D.C. to 625 Hz.

A schematic diagram of the complete recording system (recorder and preamplifiers) appears in Figure 3.9. The D.C. amplifiers and zero-suppressor combination in series with the sensor electronics and recorder channels were necessary components to improve the signal to noise ratio of all inputs. Zero-suppression was required to allow a gain of 10 to be applied to the signals. The seven channels were allocated as follows² (if all sensors were operating);

Four hot-wires, two at each of two levels	4 channels
Two temperature sensors, one at each of two levels	2 channels
One wave gauge	1 channel

Calibration signals, were recorded on all channels at the beginning and end of each tape and at any point where record-

¹Ampex Model SP-300 with a .25 inch tape transport.

²Because of the number of data channels required there were no channels available for marking time by using, for example, a sine wave of known frequency. The latter provision would have been helpful to prevent possible aliasing at low frequencies from irregularities in the tape transport motor drive both during recording and play back procedures.

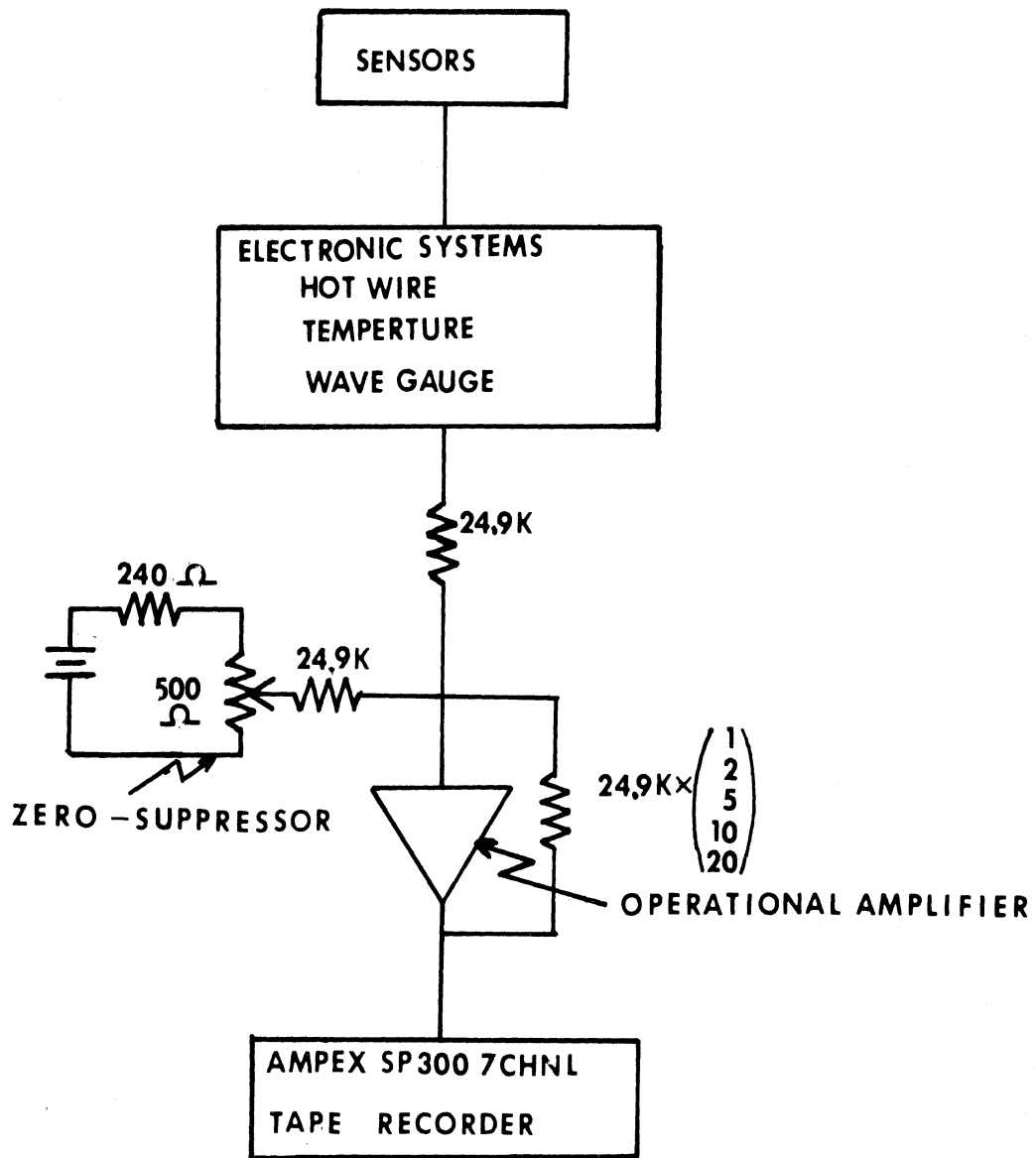


Figure 3.9: Schematic of recording system components.

ing was interrupted. These signals served as indicators of recorder drift as well as noise level and were used during digitizing procedures. Constant monitoring of amplified and pre-amplified signals was performed with a dual channel oscilloscope in order to evaluate the electronic outputs and to insure that the input signals would not exceed amplifier or recorder input limits.

4. DATA REDUCTION AND ANALYSES

4.1 GENERAL CONSIDERATIONS

Transforming time series representing measured variables into frequency space was the primary analysis procedure performed on the data. Emphasis on wind-wave coupling required cross spectrum analyses between different pairs of variables to obtain phase and coherence information. Therefore, all analog records that were observed simultaneously were processed in parallel (filtered, digitized, reduced and archived).

Procedures were developed in two parts in order to take best advantage of computer facilities available for the required tasks. The computer facilities were 1) a hybrid analog-digital CDC 160-A system and 2) an IBM 360/67 digital computer. The two parts are described in the following two subsections (4.2 and 4.3).

4.2 DIGITIZING AND RECONSTRUCTING¹ ANALOG SIGNAL (CDC 160-A)

A digital computer-analog system was employed and a description of the facility was given by Hewson and Brock (1967). The system was well suited for reconstructing, amplifying and digitizing analog signals with necessary low pass filtering. Components used during this stage of reduction were as follows

- i) Control Data Digital Computer, Model 160-A, with typewriter and punch paper tape input/output capability.
- ii) Three Applied Dynamics analog computers.

¹Reconstruct in this sense means to correct for gain and drift of recorder both in recording and reproducing stages.

- iii) An 8-channel Brush Strip Chart Recorder.
- iv) Control Data, Model 8000, analog to digital converter which has an output of 2000 divisions for a 100 volt input.
- v) Two 7-channel IBM compatible magnetic tape units.

Figure 4.1 depicts the tasks for which programs and procedures were prepared for this hybrid computer system. The following paragraphs described procedures which occurred while the recorder was reproducing the analog signal in real time (i.e. same speed as recorded). The procedures were:

- i) Amplify and reconstruct signal and also record on strip chart;
- ii) Low-pass filter analog signal with a terminal frequency (half-power point) of 150 Hz;
- iii) Digitize analog signal at 300 pt/sec using an external oscillator to control sampling interrupt;
- iv) Write output records on magnetic tape (1 each second); and
- v) Perform digital to analog operation and record back on strip-chart recorder in order to monitor successful completion of preceding procedures.

4.2.1 Amplification and Reconstruction of Signals

Because the recorded signals could range only from -2 to +2 volts and the analog-to-digital converter had a range from -100 to +100 volts, a gain of 50 was applied to all signals. The gain was achieved by using operational amplifiers with fixed feedback and input resistors which had accuracies within 1%.

Calibration signals recorded before, during and after measurement periods were used to adjust for gain and drift

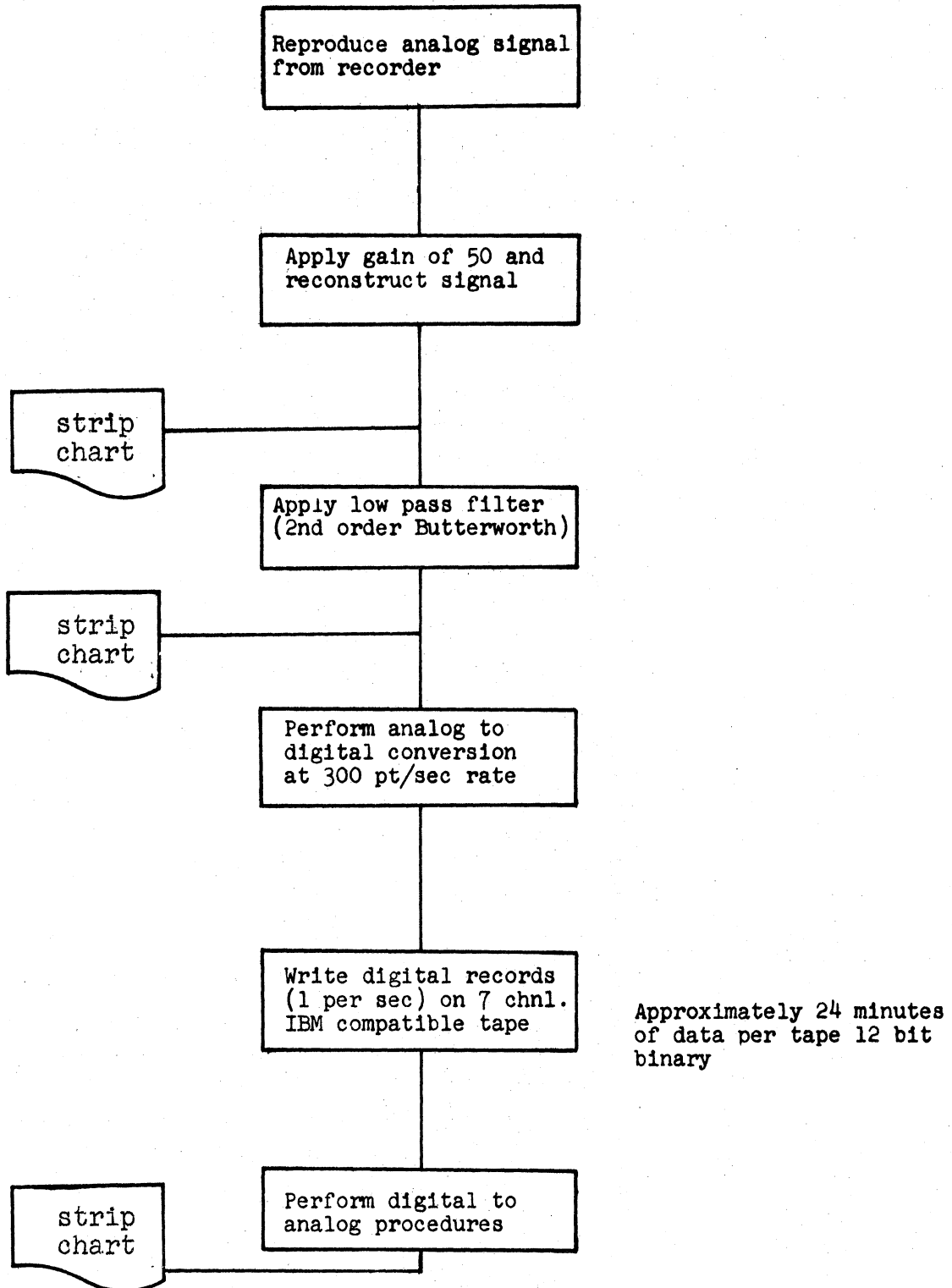


Figure 4.1: Flow chart of procedures in analog to digital processing.

errors in the recorder electronics. These signals were 1 and 2 volts and provided, from slope intercept relations between recorded and reproduced values, the coefficients a and b in the following expression:

$$V_c = aV_i + b \quad 4-1$$

where V_c = corrected signal

V_i = reproduced signal

a = correction for gain error

b = correction for drift error

4.2.2 Length (Sampling Interval) of digitized Record, Low Pass Filtering and Sampling Rate

Selection of the sampling interval was made on the bases of stationarity of conditions during observations ($\sim 20-30$ min) and requirements for convergence of spectral estimates. The requirements are described by Lumley and Panofsky (1964, pages 51-52) who provided a relation (Equation 4-2) to determine the induced error associated with a given band width and sampling interval. The error is called the "sampling fluctuation" error and occurs in digital processing because all functions (i.e. $u(t)$) are sampled discretely and truncated.

$$\epsilon^2 = \frac{2}{T_s \Delta n} \quad 4-2$$

where ϵ = induced error

Δn = bandwidth

$\Delta n = 1/T_s$ in harmonic analyses

$T_s =$ sampling interval.

In the next section (4.3), a method is described that increases the bandwidth by averaging over local spectral estimates. The resulting expression for Δn and ϵ^2 are

$$\Delta n = \#AVG/T_s \quad 4-3$$

$$\epsilon^2 = 2/\#AVG$$

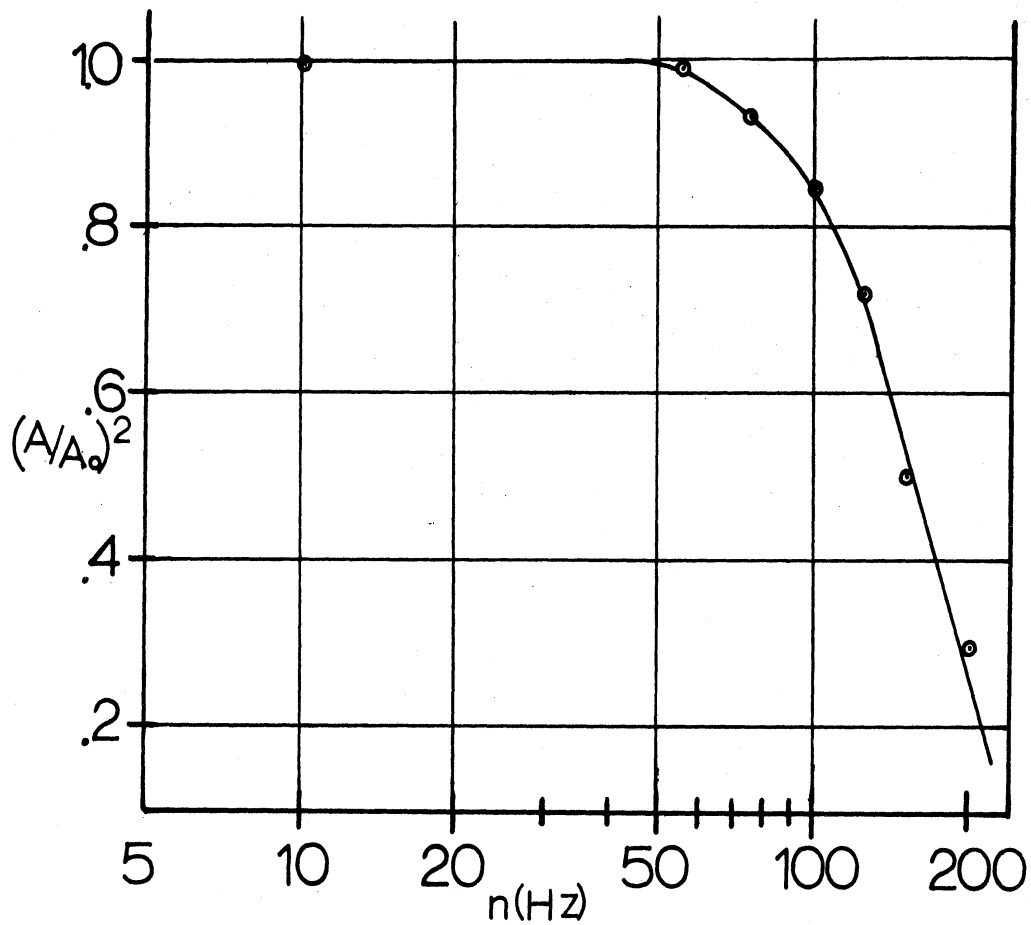
#AVG = number of spectral estimates averaged together.

Considering the stationarity of conditions and the sampling error defined by Equation 4-3, 18 minutes time series were selected for further processing. Sampling errors, ϵ , at several frequencies, as derived from Equation 4-3 and final #AVG values, are shown in Table 4.1.

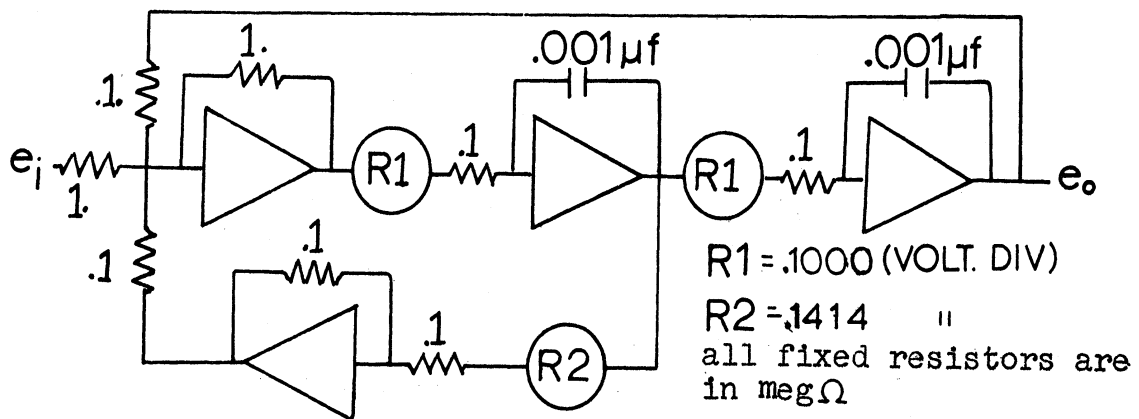
Table 4.1 Representative Sampling Errors ($\epsilon\%$)

Frequency (Hz)	$\epsilon\%$	#AVG
.05	59.	4
.10	37.	10
.25	25.	22
.50	18.	45
1.00	13.	86

Data from all channels were Low Pass Filtered through identical analog filters. Figure 4.2 shows the analog circuit, 2nd order Butterworth, and the energy response function. Checks of the response, before and after a digitizing operation,



ANALOG LOW-PASS FILTER (2nd order Butterworth)

Figure 4.2: Frequency response curve, $(A/A_0)^2$, and circuit employed in analog low-pass filtering.

were performed on all filters using a signal generator.

With a sampling rate of 300 pt/sec, the response function shown in Figure 4.2 insured that minimum energy existed above the Nyquist or aliasing frequency which was 150 Hz. The sampling rate (300 pt/sec) was higher than necessary for processing and analyses reported in this study. This was used, however, to obtain high frequency information for further analysis.

4.3 DIGITAL REDUCTION AND PROCESSING (IBM 360/67)

Digital computer and associated software requirements centered around fast and efficient transformation of time series, consisting of numerous data points, to frequency space. The transformation was achieved by harmonic analysis (direct approach) using the Fast Fourier Transform (FFT) algorithm developed by Cooley and Tukey (1965). It has received considerable attention in applied literature since that time. Papers on the algorithm and its use appear in the proceedings of a special conference held on the subject, Harris (1967).

Although harmonic analysis using the FFT algorithm enabled extensive analyses to be performed economically in this experiment, statistical confidence in initial spectral values is less than in the auto-correlation (statistical approach) method. Jenkins (1962) and Bartlett (1950) have shown that although the mean of a harmonic estimate, $F(n)$, converges to that of the auto-correlation estimate, $\phi(n)$, as the time interval goes to infinity, the variance of $F(n)$

estimates about $\phi(n)$ does not. This is apparent from Equation 4-2 in Section 4.2.2, page 74, which shows that the sampling error, ϵ , was independent of sampling time (T_s) since $\Delta n = 1/T_s$ in harmonic analysis.

Confidence in the "direct approach" and in the techniques required for the time series preparation have been gained through several recent works by other investigators, viz., Oort and Taylor (1969), Van Atta and Chen (1968), and Tukey (1967). In addition, averaging over local spectral values, discussed in Section 4.3.6, increased statistical confidence of final estimates.

A version of the Fast Fourier Transform algorithm was available in the University of Michigan Computing Center as a library subroutine. Therefore, most of the computer program development effort was directed toward selection and implementing of digital filtering, data editing and efficient data handling routines. Figure 4.3 shows the basic processing scheme. Procedures appearing in Figure 4.3 are:

- i) Convert CDC-160-A words (12 bit binary) to IBM 360/67 words (32 bit binary);
- ii) Low pass filter, with inverse transform filter, original 300 pt/sec records to 30 pt/sec records;
- iii) Convert input records to engineering units, cm/sec, °C, wave height, with primary effort on hot-wire signals;
- iv) Compute 1st through 4th moments and remove any data points which violate prescribed limits (e.g. $|u| > 4\sigma_u$);
- v) Remove mean and trend and recompute 1st through 4th moments;
- vi) Apply data window (cosine bell) and compute Fourier Coefficients and correct coefficients for decrease due to data window application;

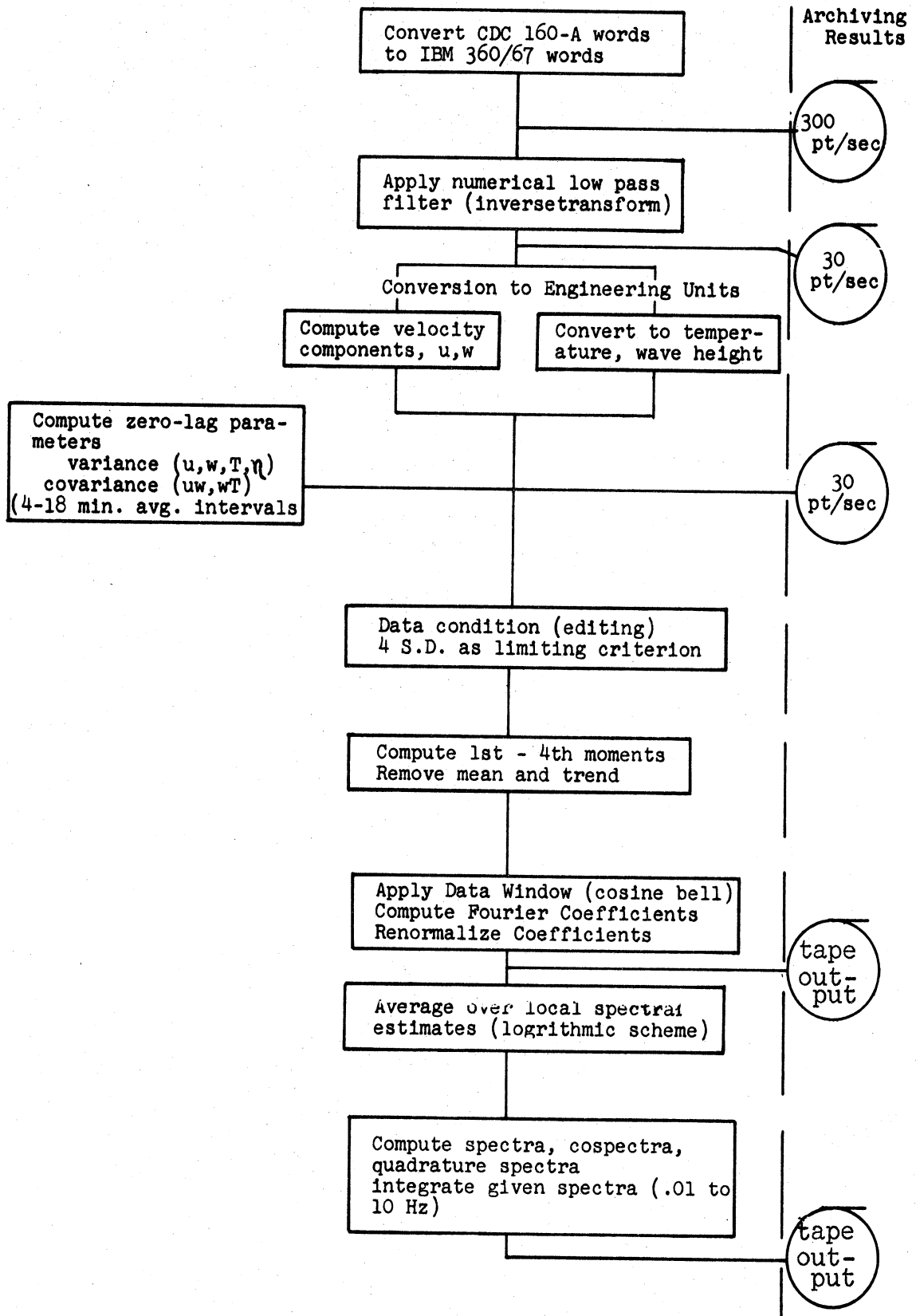


Figure 4.3: Flow chart of digital processing procedures.

- vii) Compute Variance and Covariance spectra;
- viii) Average of spectral values over local harmonics and compute confidence indicators (degrees of freedom, root mean square); and
- ix) Compute phase and coherence estimates from averaged estimates of cospectra and quadrature spectra.

4.3.1 Numerical Low-Pass Filtering

A numerical low-pass filter was applied to the original data to obtain records which had 30 points per second. Performing the additional filtering numerically rather than using analog procedures has several advantages including 1) high fidelity (digital calculations can be repeated identically), 2) problems of phase shift are diminished, 3) feedback problems inherent in analog circuits are eliminated, 4) precision is dependent on the number of weights and the selected filter, rather than being hardware bound, and 5) adjustment of final spectra can be readily made because the filter response functions are well defined.

There are several numerical filters being used and Figure 4.4 (Powell, 1965) shows a comparison of response curves for the most common ones. This figure indicates that the inverse transform is, perhaps, the most desirable filter with respect to cut-off sharpness and magnitudes of oscillations beyond the terminal frequency.

Figure 4.5 gives a response curve and expressions for an inverse transform filter. It is defined in frequency space by Equation i) and weight functions in time space are determined by transforming Equation i) to obtain Equation ii).

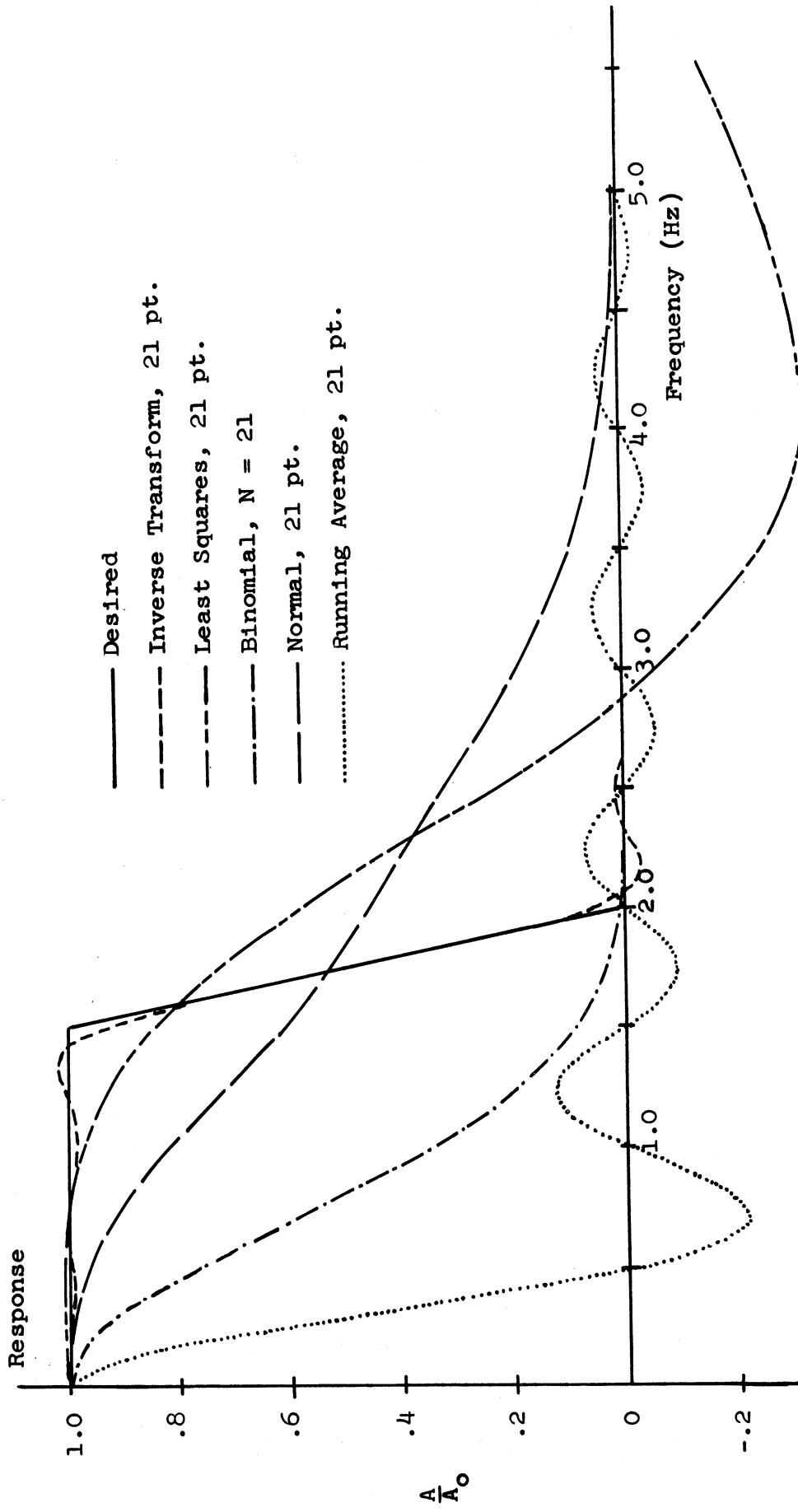
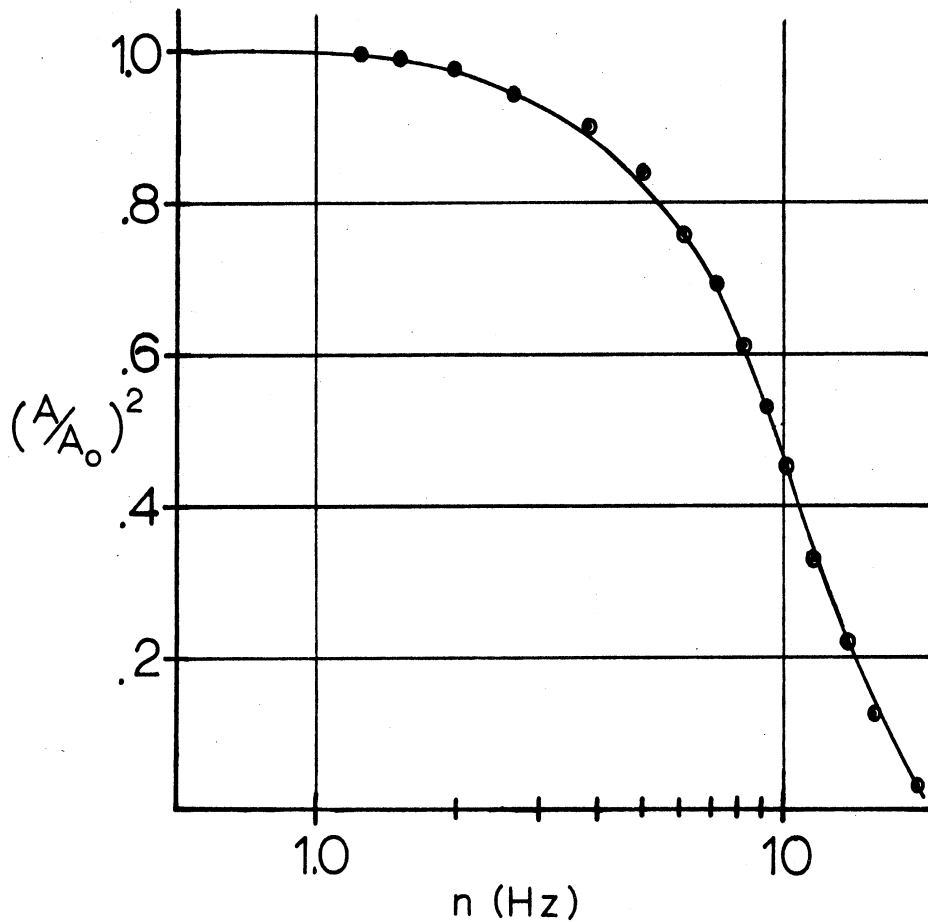


Figure 4.4: Comparison of response curves for several numerical filters (from, Powell, 1965).



$$i) H(\omega) = h_0 + 2\sum_{n=1}^{N/2} h_n \cos(n\Delta t\omega)$$

where ω = radian frequency;

Δt = time interval between data points

$$ii) h(n\Delta t) = \frac{\pi}{2n\Delta t} \left[\frac{\sin(\omega_t n\Delta t) + \sin(\omega_c n\Delta t)}{\pi^2 - (\omega_t - \omega_c)^2 (n\Delta t)^2} \right]$$

where: $\sum h_n = 1$ to insure no change in mean

N = number of weights (21)

ω_c = cut-off frequency ($\omega_c/2\pi = 10$ Hz)

ω_t = terminal frequency ($\omega_t/2\pi = 20$ Hz)

Figure 4.5: Frequency response, $(A/A_0)^2$, curve and weight functions employed in numerical low-pass filter.

The final shape of the filter is determined by selecting the number of weights (N), the cut-off frequency (ω_c) and the terminal frequency (ω_t). The sharpness of the filter depends on all three selections plus the spacing, Δt , of the points in the original time series. The inverse transform filter used in this study had 21 weights, cut-off and terminal frequencies of 10 and 20 Hz, respectively, which gave the response curve shown in Figure 4.5. All spectral estimates were corrected for any attenuation below 10 Hz.

4.3.2 Removal of Erroneous Data Points

Because data were recorded in analog form with inherent imperfection in both magnetic tape and electronic components, "drop-outs" and "spikes" appeared, occasionally, in data records. Therefore, an editing procedure was used to remove erroneous values that could influence the spectral estimates and, more importantly, the higher order moments such as skewness and kurtosis.

To remove erroneous values (editing), two passes through each time series were performed. In the first pass, first, second, third and fourth moments were computed. In the second pass, which was on a zero-mean time series, editing was performed by comparing each point with the initial estimates of the standard deviation. If the absolute value of any point exceeded four times the standard deviation it was replaced by an interpolated value. Since erroneous points normally occurred sequentially, or in groups, a forward search in the time series was performed to obtain a second point

within the required four standard deviation limit and this point was then used for the interpolation.

Figure 4.6 shows a strip chart record of erroneous data spikes within a record and Table 4.2 gives corresponding statistical parameters before and after the editing procedure. The number of spikes, each of which usually included several erroneous points, as well as the number of values corrected were counted by the editing routine. These numbers appear in Table 4.2. The table shows the influence of erroneous points on the kurtosis, an expected effect since its value is influenced by the end points of the probability distribution.

4.3.3 Removing Trend and Mean and Computing 2nd, 3rd and 4th Moments

Presence of scales of variation that are long compared to the length of record requires removing the trend so the residual time series can be treated as being stationary. Various procedures have been suggested for this purpose and are described in most books on time series analysis (Blackman and Tukey (1958, page 139), Panofsky and Brier (1965, page 135), Jenkins and Watts (1968, page 150)).

In this experiment, the trend and mean were removed by forming a best fit in a "least squares" sense to the original time series;

$$x(t) = A \cdot t + B \quad 4-4$$

and then subtracting, at each point or time, t , $x(t) = A \cdot t + B$ from the original value.

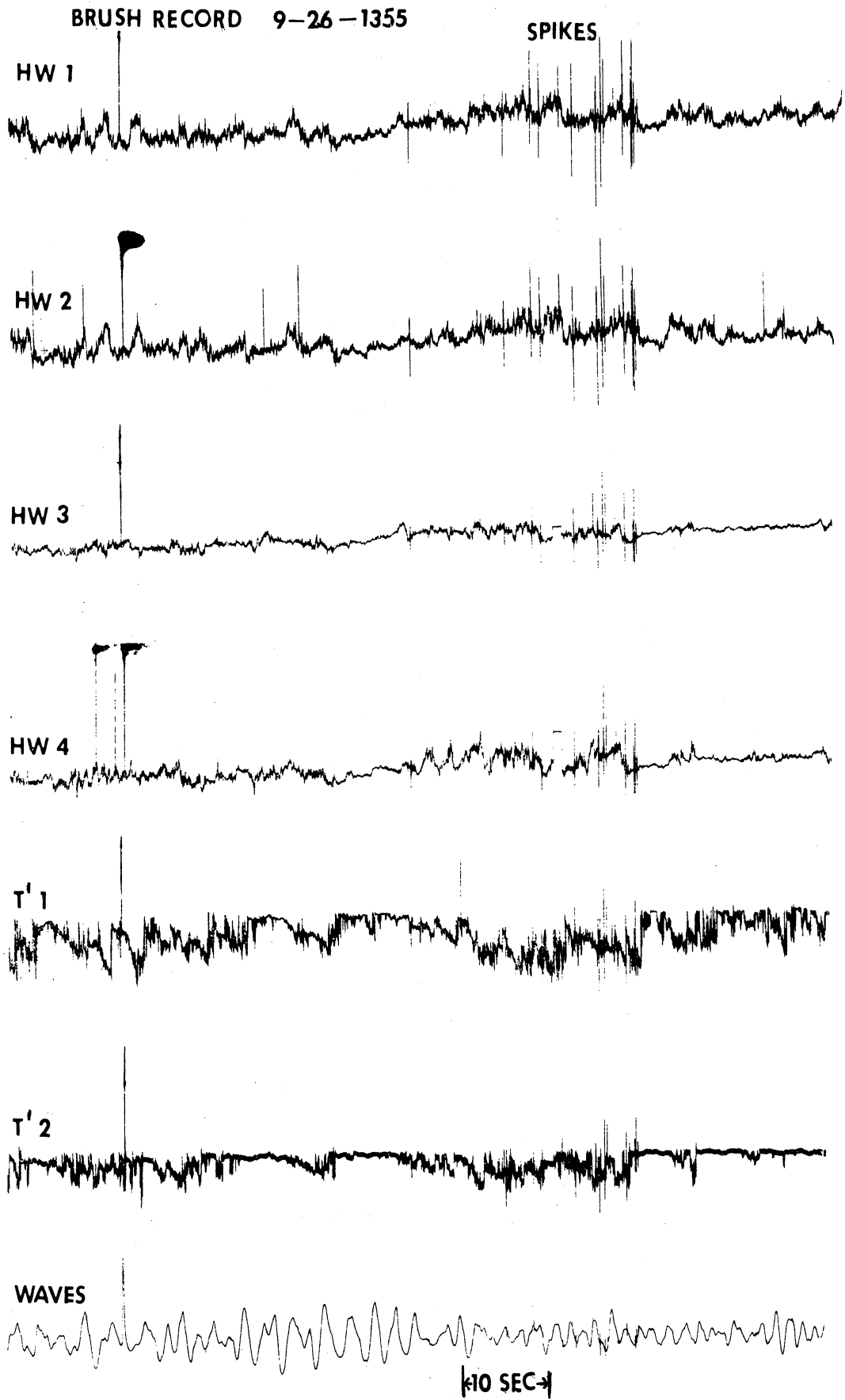


Figure 4.6: Representative occurrence of erroneous spikes from Brush recording of analog signal.

Table 4.2 Statistics before and after data conditioning: including spikes, points corrected, % of points corrected (input = 32,768 points) and normalizing correction (for cosine bell).

Period 9-26 Level (m)	Variable	Moments: conditioned-non conditioned				Skewness			3 + Kurtosis		Spikes and Points			Coeff. Norm. corr.
		Non- cond.	cond.	Non- cond.	cond.	Non- cond.	cond.	Non- cond.	cond.	Non- cond.	cond.	spikes	Points mod.	
1.5	u (cm/sec)	74.	67.	-.226	-.002	4.72	3.04	11	25	.008	1.37			
1.5	w (cm/sec)	35.	29.	-.645	.264	102.70	3.60	23	52	.016	1.40			
1.5	T(°C)	.315	.315	.399	.407	2.71	2.68	2	3	.001	1.38			
4.0	u (cm/sec)	73.	73.	-.003	-.003	3.01	2.98	1	2	.001	1.33			
4.0	w (cm/sec)	42.	40.	.576	.416	8.06	4.03	33	116	.035	1.28			
4.0	T(°C)	.230	.229	.681	.714	3.18	2.91	5	9	.001	1.34			
SFC	η (cm)	9.92	9.55	1.190	.203	15.67	3.14	10	28	.009	1.36			

Second, third and fourth moments, (variance, skewness and kurtosis) were computed for each time series after the mean and trend were removed. As indicators of properties of fluctuating variables, these statistics were computed and can be interpreted as follows (where u is used as the fluctuating variable).

- i) Variance, $\overline{u^2}$, is the average of the square of the deviation.
- ii) Skewness (S), $S = \overline{u^3}/(\overline{u^2})^{3/2}$, is a measure of the non-symmetry of the probability distribution. The sign of the skewness indicates if large deviations are predominantly negative or positive.
- iii) Kurtosis (K), $K = \overline{u^4}/(\overline{u^2})^2 - 3.$, is often used to indicate the intermittency ($\gamma = K_t/K$), where K_t would represent the kurtosis of a fully turbulent flow, of the fluctuations. The constant 3. represents the kurtosis value for a probability distribution which is Gaussian. Therefore, kurtosis values, as computed, would be zero if the probability distribution of the fluctuations was Gaussian.

4.3.4 Application of the Data Window and Performing the Fourier Transform

A data window is applied to a time series to diminish energy drainage between neighboring harmonics. The inverse transform of a data window would be a spectral window and a measure of the resolution of a selected data window would be the influence of a sinusoidal signal at frequency n on coefficients at other frequencies n_j . A suitable data window had to be selected for these data because their random nature insured the non-existence of genuinely periodic functions.

The data window selected was the "cosine bell", which corresponds to the Tukey Spectral Window (Blackman and Tukey, 1958, page 98). For numerical procedures, it is defined by

$$W(t) = \left[\text{SIN}(\pi(t+\Delta t) / (T+2\cdot\Delta t)) \right]^2, \quad 4-5$$

where $W(t)$ = weight which is applied to each term of original time series, $X(t) = W(t) \cdot X(t)$

Δt = time step between data values

T = length of record.

From Equation 4-5 it can be seen that the value of $W(t)$ vanishes at $t = -\Delta t$ and $t = T + \Delta t$ and has gradually increasing values up to the midpoint of the time series ($t = T/2$) where it equals 1.

Oort and Taylor (1969) described the resolution of the "cosine bell" window and showed that the influence of a sinusoid at frequency n on neighboring frequencies, n_j , tends to $\left[(n-n_j) / \Delta n \right]^{-3}$ for $(n-n_j) > 4\Delta n$. In this study, 20 harmonics were averaged together at frequencies corresponding to the observed wave frequencies so that energy drainage was of negligible concern in this important spectral region.

Time series were transformed into frequency space using a version of the Fast Fourier Transform (RHARM), Cooley and Tukey (1965), which is included in the IBM Scientific Subroutine Package. For the most efficient use of the algorithm, the time series should be a power of two so a time series of 32768 ($= 2^{15}$) points was selected. With 30 points per second records, the transformed series was 1092 seconds long.

The Fourier expansion of the real valued time series, $X(t)$, is as follows for the coefficients, a_n and b_n , obtained from the transform;

$$X(t) = \frac{1}{2} a_0 + \sum_{n=1}^{N/2-1} a_n \cos\left(\frac{2\pi n t}{N}\right) + b_n \sin\left(\frac{2\pi n t}{N}\right), \quad 4-6$$

where N = number of points in record

n = harmonic number.

Although the coefficients were obtained from a real valued transform, the complex coefficients are used for computations of spectral estimates¹. The complex coefficient ($A_j(n)$) is obtained from the relation;

$$A_j(n) = \frac{2}{N} \sum_{t=0}^N X(t) \exp \frac{-i \cdot 2\pi \cdot n \cdot t}{N} \quad 4-7$$

$$= a_n - i b_n,$$

where the coefficients a_n and b_n appear in the expansion of the real valued series $X(t)$ in Equation 4-6, $i = (-1)^{\frac{1}{2}}$, N = points in series and n = harmonic or frequency which has amplitudes a_n and b_n .

Because the data window (Equation 4-5) applies weights that are less than 1 to most of the values in the time series, coefficients were normalized so the integrated power spectrum equaled the variance obtained during the computations discussed in Section 4.3.3.

4.3.5 Computations of Spectral Values from Fourier Coefficients

¹Blackman and Tukey (1958, page 87) show that the spectral density function, which is the inverse transform of the autocovariance function, can be expressed directly in terms of the product of the complex Fourier coefficient and its conjugate. In their notation, $S(f)$ is the complex coefficient, and $S(-f)$ is the conjugate.

Spectral values $\phi_{jk}(n)$ are computed from complex Fourier coefficients (Equation 4-7) by forming the product of the complex coefficient ($A_j(n)$) with a conjugate ($A_k^*(n)$) where j and k could be the same or different. Spectral values were obtained as follows;

Spectrum density¹: $j = k$,

$$\phi_{jj}(n) = \frac{A_j(n) \cdot A_j^*(n)}{2\Delta n} = (a_n^2 + b_n^2) \frac{T}{2}, \quad 4-8$$

where $\Delta n = 1/T$,

Cross spectrum: $j \neq k$,

$$\begin{aligned} \phi_{jk}(n) &= \frac{A_j(n) \cdot A_k^*(n)}{2\Delta n} \\ &= \frac{T}{2} \left[(a_n c_n + b_n d_n) - i(b_n c_n - a_n d_n) \right]. \end{aligned} \quad 4-9$$

The real and imaginary parts of the cross spectrum are the cospectrum and quadrature spectrum respectively and are denoted as;

Cospectrum:

$$\phi_{jk}(n) = (a_n c_n + b_n d_n) \frac{T}{2} \quad (a)$$

Quadrature spectrum:

4-10

$$\phi_{jk}^*(n) = (b_n c_n - a_n d_n) \frac{T}{2} \quad (b).$$

Phase ($\theta_{jk}(n)$) and coherence ($\text{coh}_{jk}(n)$) values were computed from average values of variance and cross spectrum estimates. The averaging procedure is described in Section 4.3.6.

¹Variance spectra of a few wave records were obtained using a harmonic wave analyzer to check the digital procedures.

Phase spectrum values provide information of how much a sinusoid, at a given frequency, for one variable would lead or trail the corresponding sinusoid for the other variable in the cross spectrum analysis. Phase estimates ($\theta_{jk}(n)$) were obtained as follows: for $j \neq k$,

$$\theta_{jk}(n) = \arctan \frac{\overline{\phi_{jk}^*(n)}}{\overline{\phi_{jk}(n)}},$$

where $\overline{\phi_{jk}(n)}$ = cospectrum estimate (obtained from averaging over several band widths)

$\overline{\phi_{jk}^*(n)}$ = quadrature spectrum estimate (obtained from averaging over several band widths).

The coherence spectrum is the normalized cross spectrum and indicates the association or correlation, as a function of frequency, between the two variables in the cross-spectrum computation. Its value can range from 0 to 1, a value of 1 represents high correlation. One important use of coherence estimates is the evaluation of statistical errors in phase angle analysis (Panofsky and Brier, 1958, page 158).

Coherence estimates were computed as follows; for $j \neq k$,

$$\text{coh}_{jk}(n) = \frac{(\overline{\phi_{jk}^2(n)} + \overline{\phi_{jk}^{*2}(n)})}{\overline{\phi_{jj}(n)} \cdot \overline{\phi_{kk}(n)}}, \quad 4-11$$

where $\theta_{jk}(n)$ values are from coefficients as expressed in Equation 4-8 and 4-10 and ($\overline{\quad}$) indicates the use of averaged estimates.

4.3.6 Averaging Spectral Values over Local Harmonics

An harmonic analysis on a time series of 32768 points results in 16384 spectral values for each spectrum (variance and covariance). The bandwidth for each value is $1/T$ or, in the present study is 1092^{-1} Hz, which is a resolution of several orders of magnitude above that which was needed for analysis. In order to improve diagnostic values of spectral estimates (original estimates have considerable scatter) yet retain features which have physical significance, an averaging procedure was employed in which new values were obtained by averaging values from several neighboring harmonics i.e., original frequency bands¹.

Procedures in the present study follow those used by Oort and Taylor (1969) and are distinguished by a logarithmic increase, with frequency, of the number of spectral values averaged together². The averaged spectral values are

¹An other method which could be used to decrease the uncertainty due to sampling fluctuations would be to partition the time series into smaller segments (to obtain several time series) and perform ensemble averages across corresponding spectral values from each time series. Blackman and Tukey (1958, page 95), for example, suggest applying a number of short data windows to the longer time series for this procedure. Van Atta and Chen (1968), on the other hand, applied ensemble averaging to several observations obtained in a wind tunnel. Welch (1967) suggested segmenting an original time series by using a sliding data window, thus overlapping some points but considering each time series as contributing independent estimates for the ensemble averages.

²Appendix D provides additional information and the computer program implemented for the averaging procedure.

evenly spaced when plotted on a $\ln(n)$ scale.

During the averaging procedures, a statistic, used by Oort and Taylor (1969), was computed that indicates the variance of individual values around the average or final estimate. This statistic (DF) can be considered as the number of equivalent degrees of freedom (Blackman and Tukey, 1958, page 21-25). The DF values were computed from

$$DF = n \cdot (\bar{x})^2 / (\overline{x^2}), \quad 4-12$$

where x = original spectral value

n = number of spectral values averaged together.

Values of DF were used to interpret probability levels for phase relationships and also to select the averaging interval. Table 4.3 lists the number of values (#AVG) averaged together and representative DF values.

Table 4.3 Spectral Averaged (#AVG) and Representative Equivalent Degrees of Freedom (9-26, 1355 EST, Period 7)

n Hz	#AVG	Equivalent Degrees of Freedom (DF)						waves π
		u		w		uw		
		level (m) 1.5	level (m) 4.0	level (m) 1.5	level (m) 4.0	level (m) 1.5	level (m) 4.0	
.10	9	5	5	5	4	3	3	5
.11	9	6	5	5	6	3	2	3
.12	11	7	5	6	5	4	1	5
.13	11	6	6	7	7	1	1	8
.14	11	5	7	7	7	3	3	6
.15	13	7	8	5	5	5	5	8
.17	14	10	11	9	7	6	4	5
.18	15	10	8	9	7	4	1	8
.19	16	10	6	8	11	5	6	9
.21	17	9	10	11	10	4	6	8
.22	19	8	12	12	11	2	1	7
.24	20	11	11	10	12	4	9	10
.26	22	16	12	13	14	14	8	12
.28	24	13	14	14	14	4	2	15
.30	25	16	13	15	11	11	8	14
.33	28	19	14	18	17	8	10	16
.35	29	18	15	13	14	6	8	20
.38	32	14	20	15	16	3	2	21
.41	35	20	20	17	19	14	19	20
.45	37	23	26	17	20	12	11	19
.48	40	19	26	18	16	4	11	20
.52	44	24	26	18	24	14	9	24
.56	46	24	26	19	25	17	16	20

5. SUMMARY OF MEASUREMENTS AND DATA ANALYZED

Measurements were made during 14 periods on 10 different days from mid-August to mid-October, 1968. The periods and their durations were determined by equipment performance and weather conditions. Turbulence measurements were made primarily during times when complementary wind and temperature profile measurements were being made. Weather condition criteria were that the wind direction had to be from southwest through northwest which insured an overlake trajectory with no tower influence and that the wind had to be steady with respect to speed and direction for 20 to 30 minute periods.

Individual measurements periods along with coincident weather conditions are listed in Tabel 5.1. Under SUMMARY OF MEASUREMENTS it can be seen that simultaneous measurements of u , w and temperature fluctuations were made at two levels during 12 of the 14 periods. Measurement heights ranged from 1 to 15 meters above mean water level and emphasis was placed on the region close to the waves (1-4 meters).

A recorder malfunction on 22 August required its removal for repair and resulted in the three week period (23 August-13 September) in which observations were not made.

Since weather and wave conditions and system performance could not be fully anticipated, only part of the observations were considered for complete analyses procedures. Data from 13 September and 11 October were eliminated because of poor performance of a three filament hot-wire probe. Malfunction of profile equipment and light and variable winds caused data

Table 5.1 Summary of 1968 Lake Michigan Measurements*

Date	Time (EST)	Summary of Measurements Level (m)	Summary of Measurements Variable
7 Aug	1710-1830	1.4	u, w, T'
		8.0	u, w,
19 Aug	1135-1301	1.5	u, w, T'
		4.0	u, w, T'
		1.5	u, w, T'
22 Aug	1355-1512	1.5	u, w, T'
		4.0	u, w, T'
		8.0	u, w, T'
7 Aug	1621-1710	1.5	u, w, T'
		8.0	u, w, T'
13 Sept	1517-1644	1.5	u, v, w, T'
		1.5	u, w, T'
20 Sept	1721-1805	1.5	u, w, T'
		4.0	u, w, T'
24 Sept	1729-1815	1.5	u, w, T'
		4.0	u, w
26 Sept	1023-1157	1.5	u, w, T'
		4.0	u, w, T'
27 Sept	1121-1221	1.5	u, w, T'
		4.0	u, w, T'
5 Oct	1644-1730	1.0	u, w, T'
		2.0	u, w, T'
11 Oct	1110-1148	1.0	u, w, T'
		2.0	u, w, T'
11 Oct	1110-1148	1.5	u, v, w, T'
		1.5	u, v, w, T'

*waves were measured during all periods

from 7 August and 20 September to be eliminated. Recorder malfunction influenced most of the data from 22 August.

Within those periods selected for reduction and analysis, data for 20 minute intervals were digitized. Table 5.2 lists the periods. The numbers 1 through 11 will be used throughout further discussion to identify the periods. The table serves as reference for presentation of results in Chapter 6 and provides the following information to describe general conditions during each period:

- 1) An estimate of the reference velocity (u_*) from wind profile data. These estimates were made by employing the relation;

$$U = \frac{u_*}{k} \left[\ln(z) - \psi \right] + \frac{u_*}{k} \ln(z_0) \quad 5-1$$

u_* was obtained by regression analysis using U values at all available levels (z) and determining the parameter ψ , which accounts for momentum transfer by fluctuations of buoyant origin, by methods suggested by Paulson (1967, page 80). Paulson's study involved profiles over natural waves.

- 2) Mean wind speed at measurement levels.
- 3) Hydrostatic stability conditions, in terms of the Richardson number, $Ri = \frac{g}{T} \cdot \frac{\partial \bar{T}}{\partial z} / \left(\frac{\partial \bar{U}}{\partial z} \right)^2$, and the air-water temperature difference $(T^{\circ}C_{4m}) - (T^{\circ}C_{sfc})$ where $T^{\circ}(4m)$ is the 4 meter level air temperature and $T^{\circ}(sfc)$ the water surface temperature.
- 4) Wave heights, $H_{1/3}$, where $H_{1/3}$ = four times the

Table 5.2 General Conditions for Periods Analyzed

PRD	Date	Time	level meters	wind m/sec	u* (cm/sec)	R1	T ₀ (4m) - T(sfc)	H ₁ /3 cm	Wave Parameters				
									ρ ₀ Hz	λ(m)	C m/s	z _c meters	C u*
1	8-19	1226*	1.5 4.0	3.5 4.5	20.0	.08	1.2°C	103	.21	35	7.4	>15.	37
2	8-19	1407	1.5 15.0	4.0 4.7	24.0***	.08	1.5	107	.21	35	7.4	>15.	31
3	9-24	1724	1.5	6.0	19.9		-1.4	66	.26	23	6.0	< 1.5	23
4	9-24	1755	1.5 4.0	6.8 7.3	20.7	-.09	-.9	70	.26	23	6.0	< .5	25
5	9-26	1100	1.5 4.0	6.0 6.3	22.6	-.56	-5.0	48	.31 .26	16 23	5.0 6.0	< .5 ~ 1.5	22 27
6	9-26	1324	4.0	4.5	16.4	-.62	-5.8	39	.26	23	6.0	>15.	37
7	9-26	1355	1.5 4.0	4.7 5.1	16.7	-.56	-5.4	38	.26	23	6.0	>15.	35
8	9-27	1120	1.0 2.0	3.1 3.5	12.1	-.55	-3.2	42	.26	23	6.0	>15.	50
9	9-27	1140	1.0 2.0	3.5 3.8	12.2	-.71	-3.3	46	.26	23	6.0	>15.	50
10	9-27	1200	1.0	4.3	16.5	-.16	-3.3	44	.24	27	6.5	>15.	38
11	10-5	1650	1.0 2.0	4.5 5.1	22.0	.21	1.5	47	.33 .22	14 32	4.7 7.1	~ 1.5 ~12.	22 32

*starting time for 1097 second periods

***estimated from data 20 minutes later

standard deviation of water surface. Goodnight and Russell (1963), and Putz (1952) have shown that the value of $H_{1/3}$ is a good estimate of the average height (peak to trough) of the highest one-third waves in the record.

- 5) Frequency, n_o , of the peaks in the wave spectra and other frequencies at which wind-wave coupling, judged to be significant, occurred. The spectrum peak, n_o , appears first in the column.
- 6) Phase speed (C) and wave lengths (λ) corresponding to the frequencies listed. C and λ were determined from the dispersion relation for deep water waves which is considered valid if the wave length to water depth ratio (h/λ) is greater than 1/2. The expressions are;

$$C = g/(2\pi n); \text{ m/sec}$$

$$\lambda = C/n; \text{ meters}$$

where $g = 9.8 \text{ m/sec}^2$

$n = \text{frequency of wave.}$

- 7) The "critical level", z_c , determined from wave phase speed, C, and the wind data for the period. Since wind speeds were available only up to 15 meters, the notation >15 means that the critical level was above the highest level of measurement.
- 8) The ratio C/u_* where C corresponds to wave speed and u_* is the estimate of the reference velocity obtained from wind profiles (described in 1) above).

6. PRESENTATION AND INTERPRETATION OF RESULTS

6.1 INTRODUCTION

Results of the analysis of data from the 11 periods include variance and covariance spectra of turbulent quantities $(u, w, T')^1$ in the airflow and the water surface along with total variance and covariance values. Complementing these results are data describing mean wind, temperature and wave ($H_{1/3}$) conditions as listed in Table 5.2.

Spectral results are presented in Section 6.2 and interpreted in Section 6.3. Section 6.3 is necessary for general interpretations because observations were made under various wind and wave conditions. Presentations in Section 6.2 and interpretations in Section 6.3 emphasize the peaks in the velocity spectral results near frequencies corresponding to the wave spectra peaks.

Velocity spectral results are presented in Section 6.4 also but the emphasis is on the nature of the high frequency portion. Sections 6.5 and 6.6 contain discussions of total variance and covariance (integrated spectra) results as they relate to the intensities, $(\sigma_u/u_*, \sigma_w/u_*)$, and probability distributions of turbulence and contribute to turbulent transports and to the turbulent kinetic energy balance.

6.2 PRESENTATION OF SPECTRAL ANALYSIS RESULTS

This section consists of five subsections (6.2.1 to

¹Spectra of temperature fluctuations and cospectra of $\overline{wT'}$ appear in Appendix E and are not included in the presentation here.

6.2.5) one for each of five selected observation days (19 August, 24, 26, and 27 September and 5 October, 1968). Although some periods occurred sequentially in time, periods are considered as individual observations. Information on complementary data and conventions used in presenting spectral results are given in the following paragraphs.

i) General Conditions for Observation Days and Periods:

Wave and wind histories extending over the period of an observation day were obtained from a staff wave gauge¹ and an aerovane² (mounted 16 meters above mean water level) respectively. Both instruments provided continuous (24 hr/day) records which were averaged over 1 hour periods for use in this presentation. Information from these sources is referred to as hourly averages.

Mean wind and wave $H_{1/3}$ histories (6 minute averages) over shorter periods of time encompassing measurement periods were obtained from cup anemometers³ and the capacitance wave gauge (Section 3.2.3). The cup anemometers along with aspirated thermocouples also provided wind and temperature profile information which are presented for the periods of measurement (18 minute averages).

ii) Spectral Results:

Wave spectral densities (cm^2/Hz) appear in graphs of $\ln(\phi_{\eta\eta}(n))$ versus $\ln(n)$. A line representing a -5 slope

¹U.S. Lake Survey System

²Bendix Aerovane

³Elder and Soo (1969)

appears on each plot. The -5 power relation (Phillips, 1958) was described in Section 2.1.2, page 14.

Velocity spectral results appear in graphs of $n \cdot \phi_{jj}(n) \text{ (cm/sec)}^2$ vs. $\text{Ln}(n)$. This representation has the advantage that it is an energy conserving diagram. The scales for covariance spectra (cospectra and quadrature spectra) are 2 times that for the variance spectra.

Phase and coherence spectra appear together and are given for a band from .05 to 1 Hz which includes nearly all the observed wave energy. Phase and coherence estimates were computed between velocity components and between each velocity component and the waves. All three results appear on the same diagram with appropriate lines and symbols to identify them.

Bandwidths of individual spectral estimates are defined by a logarithmic increase with frequency as determined by 128 final estimates in the presented spectra¹. Sampling errors for representative frequencies associated with estimates appear in Table 4.1, page 75.

Schematics that show phase relationships between velocity components and the waves are presented. Phase angles for this purpose were selected by considering

- a) Trends of phase value near frequency being examined (if neighboring phase angle values had a

¹Appendix D and Section 4.3.6 include discussions of the averaging procedures and bandwidths associated with specific frequencies.

Table 6.1 Phase and coherence values at frequencies of interest, during Periods 1-11.

PRD	Date Time	Level	n(Hz)	Phase and coherence values**					
				uw		ηu		ηw	
				θ°	coh	θ°	coh	θ°	coh
1	8-19 1226	1.5	.21	290*	.04	143	.08	92*	.22
		4.0		206*	.10	207	.13	75*	.36
2	8-19 1407	1.5	.21	260*	.05	175	.19	93*	.82
		15.0		180*	.20	137	.08	56*	.12
3	9-24 1729	1.5	.26	188*	.30	223	.12	86*	.33
4	9-24 1755	1.5	.26	190*	.27	208*	.13	45	.03
		4.0		170*	.20	226*	.17	354	.04
5	9-26 1100	1.5	.26	154*	.21	133*	.09	212	.05
		4.0		171*	.34	150	.04	283*	.07
		1.5	.31	150	.09	215	.03	336	.05
		4.0		156	.17	94	.01	195	.01
6	9-26 1324	4.0	.20	162	.30	274	.02	80	.01
		4.0	.26	194	.26	179	.04	62	.01
7	9-26 1355	1.5	.26	188*	.38	189*	.33	38	.24
		4.0		172*	.21	168*	.11	6	.01
8	9-27 1120	1.0	.26	237	.50	191	.49	80	.74
		2.0		120	.15	194	.54	273	.61
9	9-27 1140	1.0	.26	237	.48	200*	.63	80*	.80
		2.0		140*	.10	198	.66	270*	.72
10	9-27 1200	1.0	.24	215	.46	200	.40	80	.69
11	10-5 1050	1.0	.26	176*	.39	175	.01	95*	.11
		2.0		160*	.14	170	.02	109*	.06
		1.0	.33	223	.12	156	.04	84	.12
		2.0		174	.08	167	.08	94	.06

** for phase interpretation of xy computation y leads x by θ°
 For phase and coherence spectrum

- = uw = w leads u by θ°
 Δ = ηu = u leads wave by θ°
 \odot = ηw = w leads wave by θ°

*values used in constructing phase composites.

consistent or preferred value, this was interpreted as having physical significance).

- b) Magnitudes of coherence estimates (high coherence increases the probability level of the phase angle for a given number of degrees of freedom).

Table 6.1 lists, for specific frequencies, phase angles between velocity components, u and w , and between the velocity components and the wave, η_u and η_w , and corresponding coherence estimates. Table 6.1 will be referenced during discussions of phase relation schematics.

6.2.1 Results from 19 August (Periods 1 and 2)

<u>Period</u>	<u>Time</u>	<u>Measurement Levels (meters)</u>
1	1226-1244	1.5 and 4.0
2	1407-1425	1.5 and 15.0

These periods are distinguished by having the highest waves observed during the total experiment. Isolated white caps appeared toward the end of Period 2 but were not observed during Period 1. Complementary profile data were not available during Period 2 but the observations are included because of the need for additional results during high wave conditions.

6.2.1.1 General conditions

Figure 6.1 shows the weather map for 0700 and hourly wind and wave histories for the day. A warm front passed over the southern portion of Lake Michigan during the early

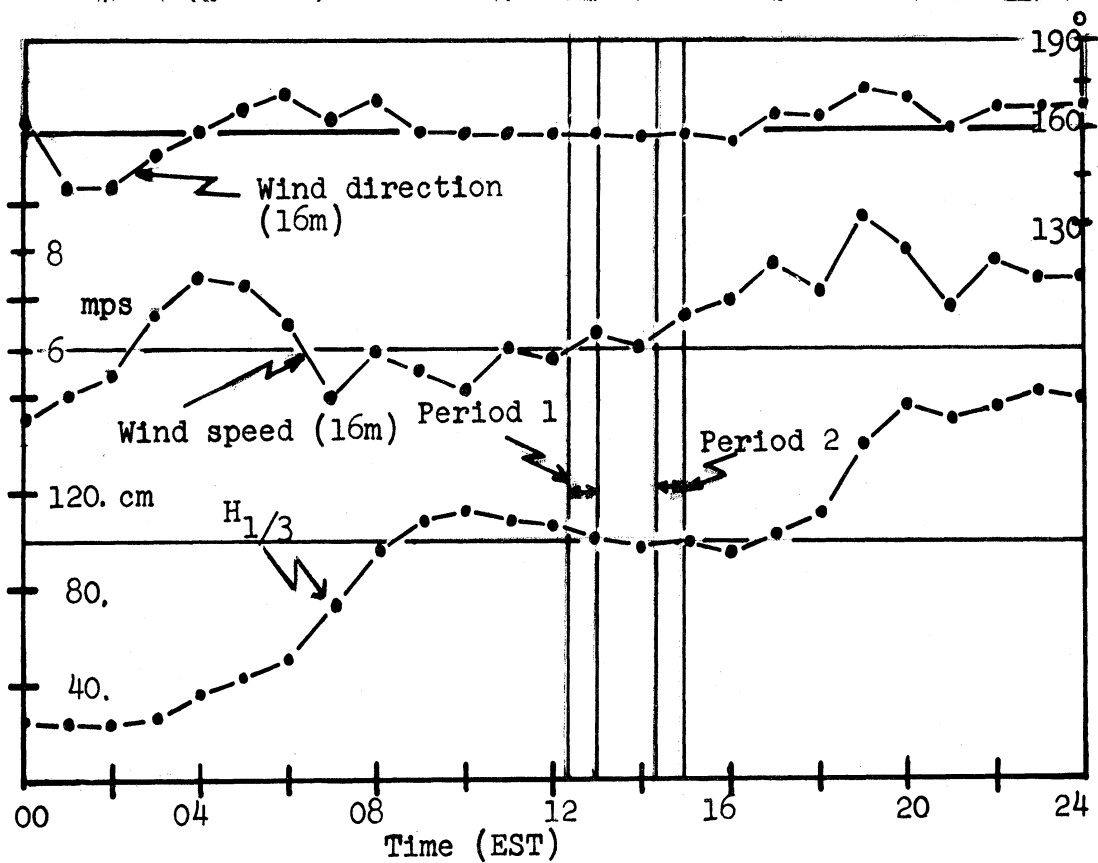
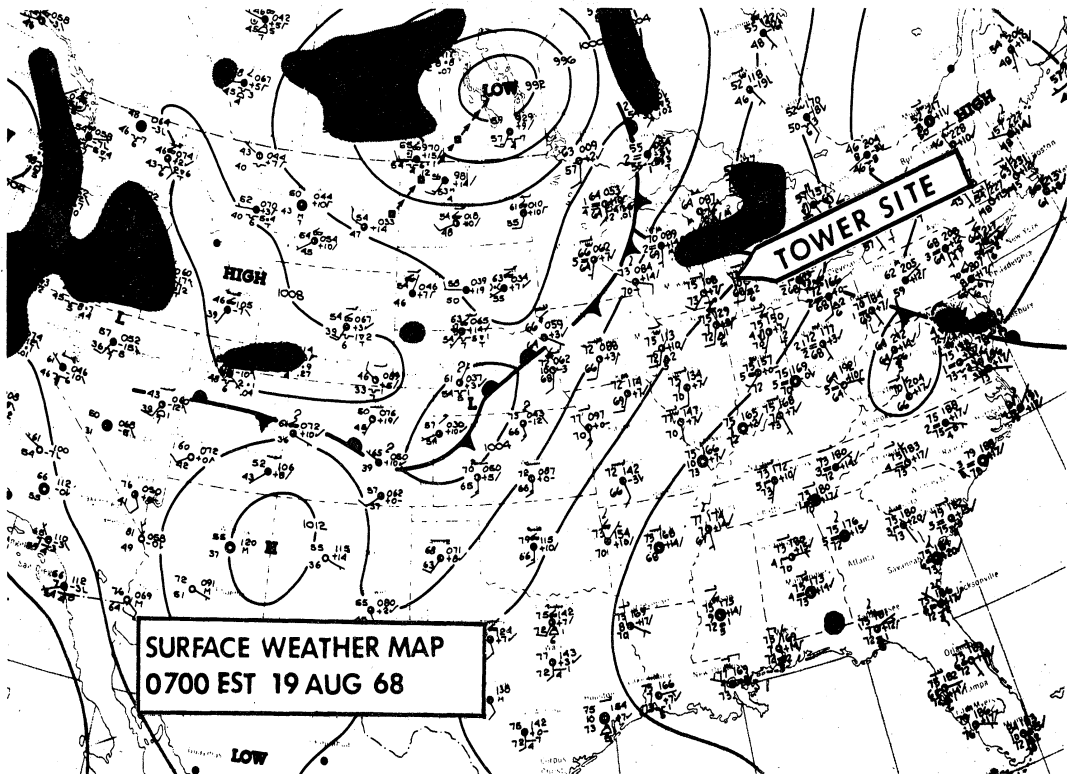


Figure 6.1: General conditions for 19 August, 1968.

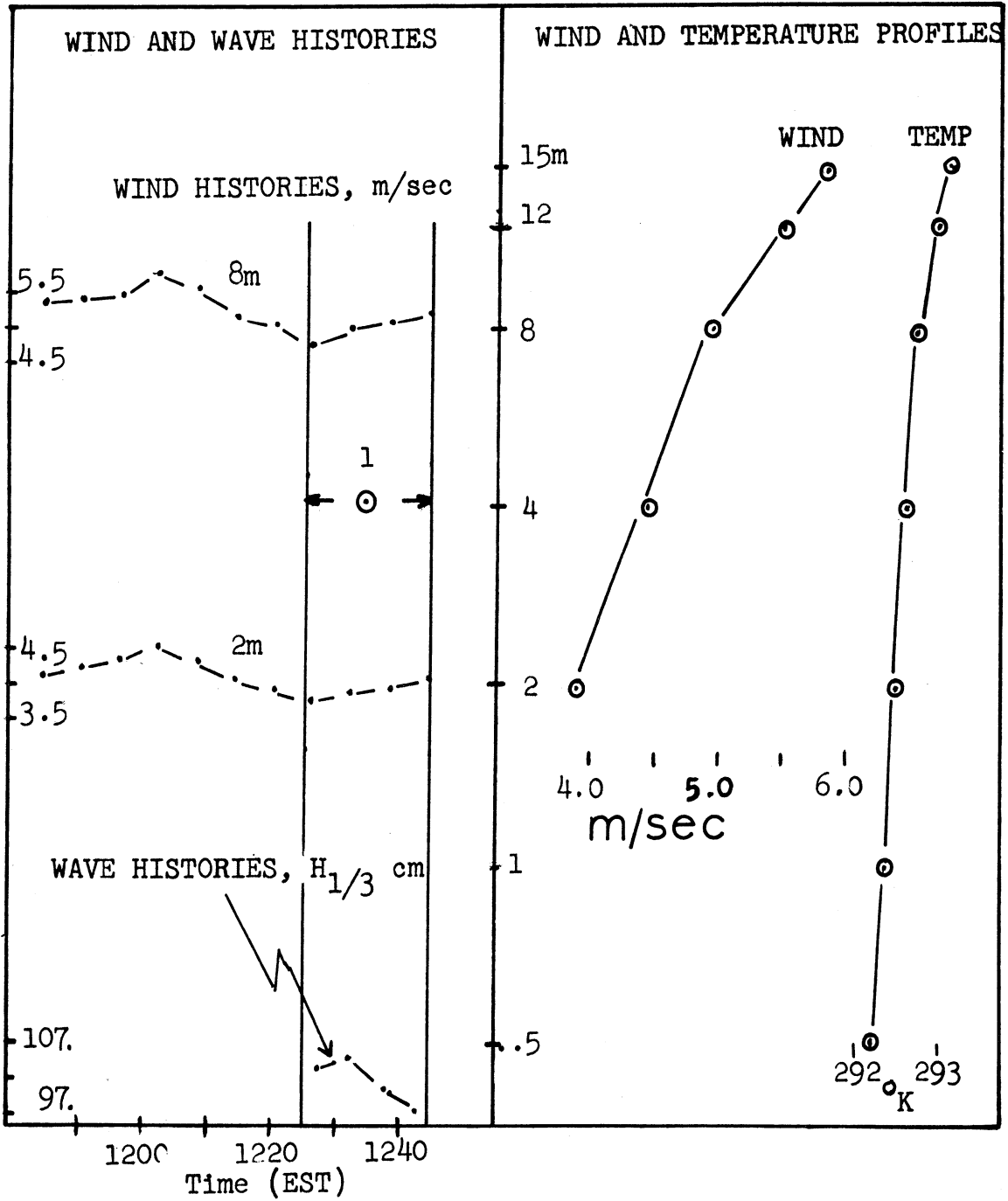


Figure 6.2: General conditions for time encompassing Period 1.

morning resulting in southerly winds and stable stratification during the observation periods. The temperature difference between 4 meters above mean water level and the surface was 1.2 to 1.5°C. There were scattered clouds from mid-morning to late afternoon. Wind (at the 16 meter level) and wave histories ($H_{1/3}$ cm, hourly averages) indicate that waves began to develop under the influence of the steady south wind which prevailed after the frontal passage. Although the wind speed increased throughout the day, the wave field appears to have attained equilibrium by mid-morning (0900) and remained so through both observation periods. The wind direction and wave propagation direction were observed to coincide during both periods.

Figure 6.2 shows wind, temperature and wave ($H_{1/3}$) conditions encompassing Period 1. Wind histories are given for both 2 and 8 meters. During Period 1, there was a slight increase of wind speed and the wave field appears to have been decreasing during the second half of the period. From Table 5.2, page 98, and the wind profiles, it can be seen that the critical level for the primary wave ($n_0 = .21$ Hz, $C = 7.5$ m/sec) was effectively at infinity. Therefore, dynamics of the matched layer should have no influence on the observed results.

6.2.1.2 Spectral Results (Periods 1 and 2)

Wave spectral data appear in Figure 6.3 and velocity variance and covariance spectra appear in Figure 6.4 (Period 1) and 6.5 (Period 2). Wave spectral data for the two per-

iods are similar even though a two hour interval separated the periods. An approximate -5 slope region occurs at frequencies above the spectral peak at .21 Hz with a deviation from a -5 relation across a band from .4 to .7 Hz. Deviations from a -5 power relation at frequencies above those of the spectral peaks occurred for a majority of the observed wave spectra. The deviations could correspond to shorter waves or could be due to the fact that primary waves are not pure sinusoids and harmonic analysis would generate secondary peaks at multiples of the primary harmonic.

Variance and covariance spectra (Figures 6.4 and 6.5) show prominent features in the range of frequencies corresponding to the wave frequencies¹ (.1 to 1 Hz). A significant feature in this band is the similarity between the lower (1.5 meter) level data and between the upper (4.0 and 15.0 meter) level data for the two periods. Specific features at lower and upper levels are discussed in the following two paragraphs. Results of interest appear near .2 Hz and .4 Hz, at both levels, and coincide, therefore, with the peaks and -5 slope deviations in the wave spectra (Figure 6.3). They also appear near .13 Hz, at upper levels, in correspondence with an abrupt rise on the "forward face"² of the wave spectra.

At the lower level (Figure 6.4a and 6.5a), extrema in spectral data occur in a narrow band centered near .2 Hz.

¹Hereafter this band may be referred to as the band enveloping the wave spectrum.

²The forward face of the wave spectrum consists of those frequencies lower than the spectrum peak.

Variance spectra for both u and w have maxima near this frequency and u also has a secondary maxima near .4 Hz. Covariance spectra, near .2 Hz, show relative maxima and minima in the cospectra and quadrature spectra respectively. The cospectra extrema, representing both upward (Period 1) and decreased downward (Period 2) momentum transfer indicate that the waves not only distort the streamlines in the air-flow but are, apparently, transferring momentum into the overlying air. Such transfer was reported by Harris (1965, 1966) who observed it in a wave tank experiment as noted in Section 2.2. Abrupt changes in the quadrature spectra near .2 Hz suggests that highly organized motion exists at this frequency.

At the upper levels (Figure 6.4b and 6.5b) extrema are associated with broader bands than for the lower levels. The broadening of the band is toward lower frequencies. Variance spectra for u and w have maxima or relative maxima near .2 and .13 Hz. Covariance spectra show a broad band (.13 to .3 Hz) of enhanced stress (minima) being about 100% above that in neighboring bands.

Figures 6.6 and 6.7 show phase and coherence spectra for both periods. For all levels and for both periods, phase relations in the neighborhood of .2 Hz are of primary interest. Phase relations between the wave and w appear to have preferred values in a band centered at .2 Hz. For example, the values are about 90° at the lower levels and slightly smaller values, about 60° , at the upper levels. Furthermore, at the 1.5 meter level phase relations between u and w show

a narrow but distinct band near .2 Hz with values about 290° for Period 1 and about 260° for Period 2.

Table 6.1, page 103, lists phase angles and coherence values at .21 Hz. Figure 6.8 shows a composite schematic (including both Periods 1 and 2) of selected phase relations between velocity components and the wave. For the purpose of this composite, the 1.5 meter level results from Period 2 were scaled at a higher level than those from 1.5 meters during Period 1 because higher wind speeds occurred during Period 2. The composite shows that nearly wave like motion, in a direction opposite to that of particle motion in the water, occurs close to the surface. The w component maximum shifts back toward the wave crest with height and, at the upper levels, the u component has a maximum ahead of the wave trough.

Spectral results and phase relationships for these periods may be summarized as follows;

- 1) Close to the waves (1.5 meters), near the frequency of the wave spectra peaks, there occurs nearly potential flow and also upward transport of u momentum due to the waves. These interpretations are based on the appearance of the co-spectra which were near zero or had positive values near .2 Hz. Phase relationships indicated that motion in the airflow was in the opposite sense of that in the water since u lead w by 90° in the air whereas in the water w leads u by 90° .

- 2) At higher levels (4.0 and 15.0 meters), in a frequency band defined by the corresponding wave spectra, broad bands of energy concentration appeared in both components but

particularly in the u component. Whereas, near the surface the wave-induced motion resulted in decreased stress, at the upper levels a band of enhanced stress was observed.

3) The maximum in the horizontal component (u), at the frequency of the dominant surface wave, occurred near the wave trough at the lower level and slightly ahead of the trough at upper levels.

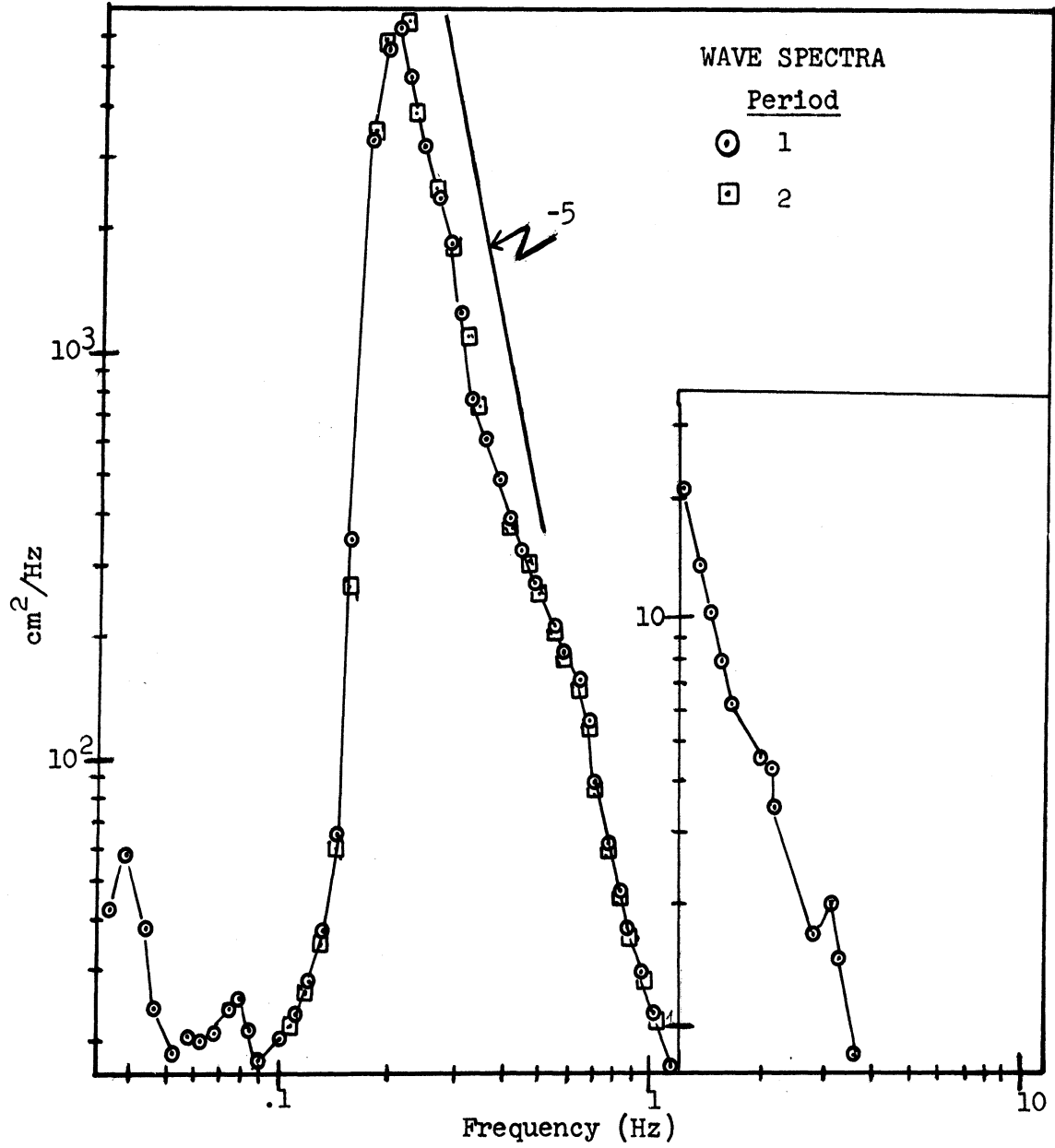


Figure 6.3: Wave spectral estimates for Periods 1 and 2.

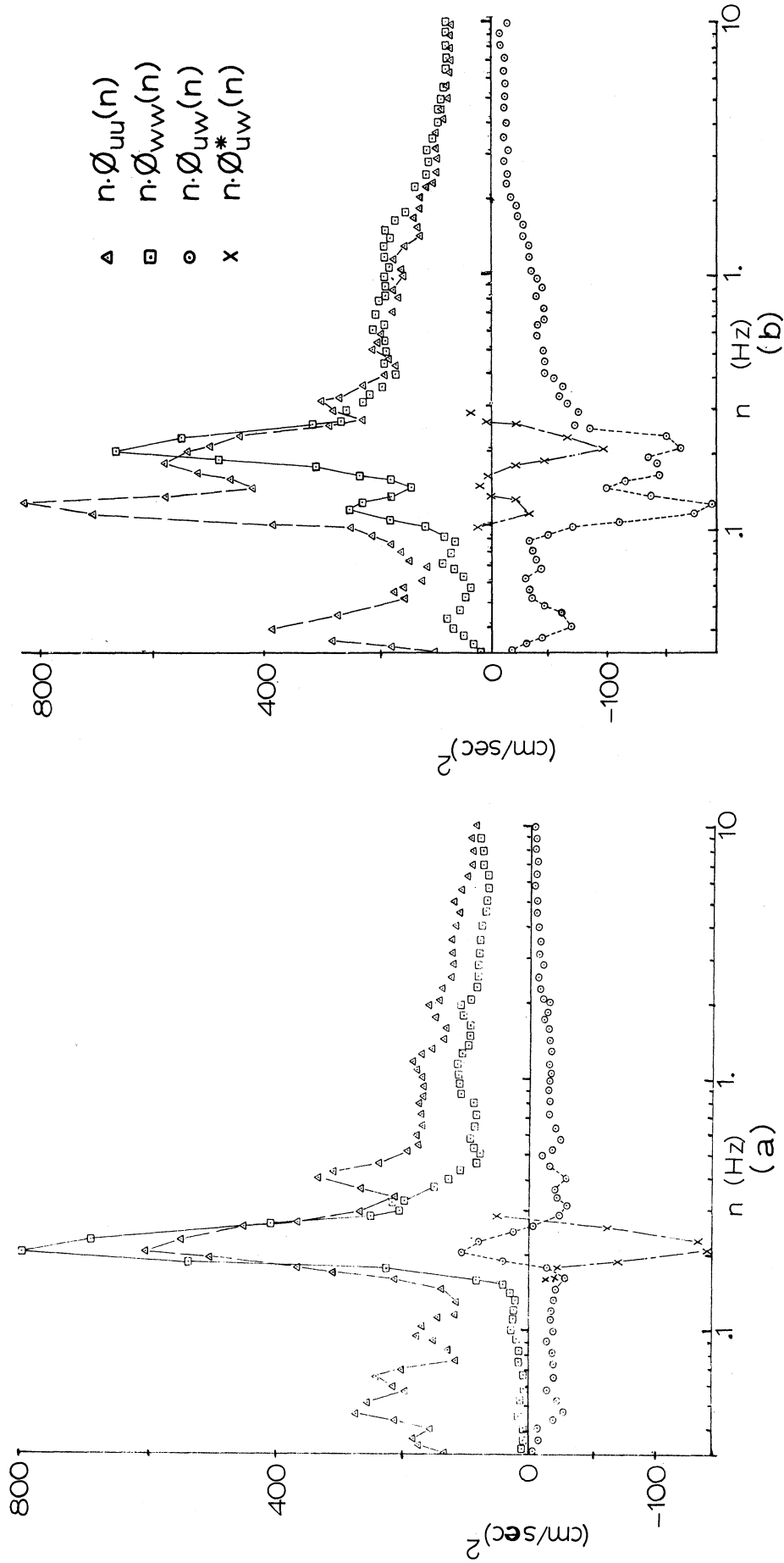


Figure 6.4: Velocity variance and covariance results for Period 1: (a) 1.5 meter level, (b) 4.0 meter level.

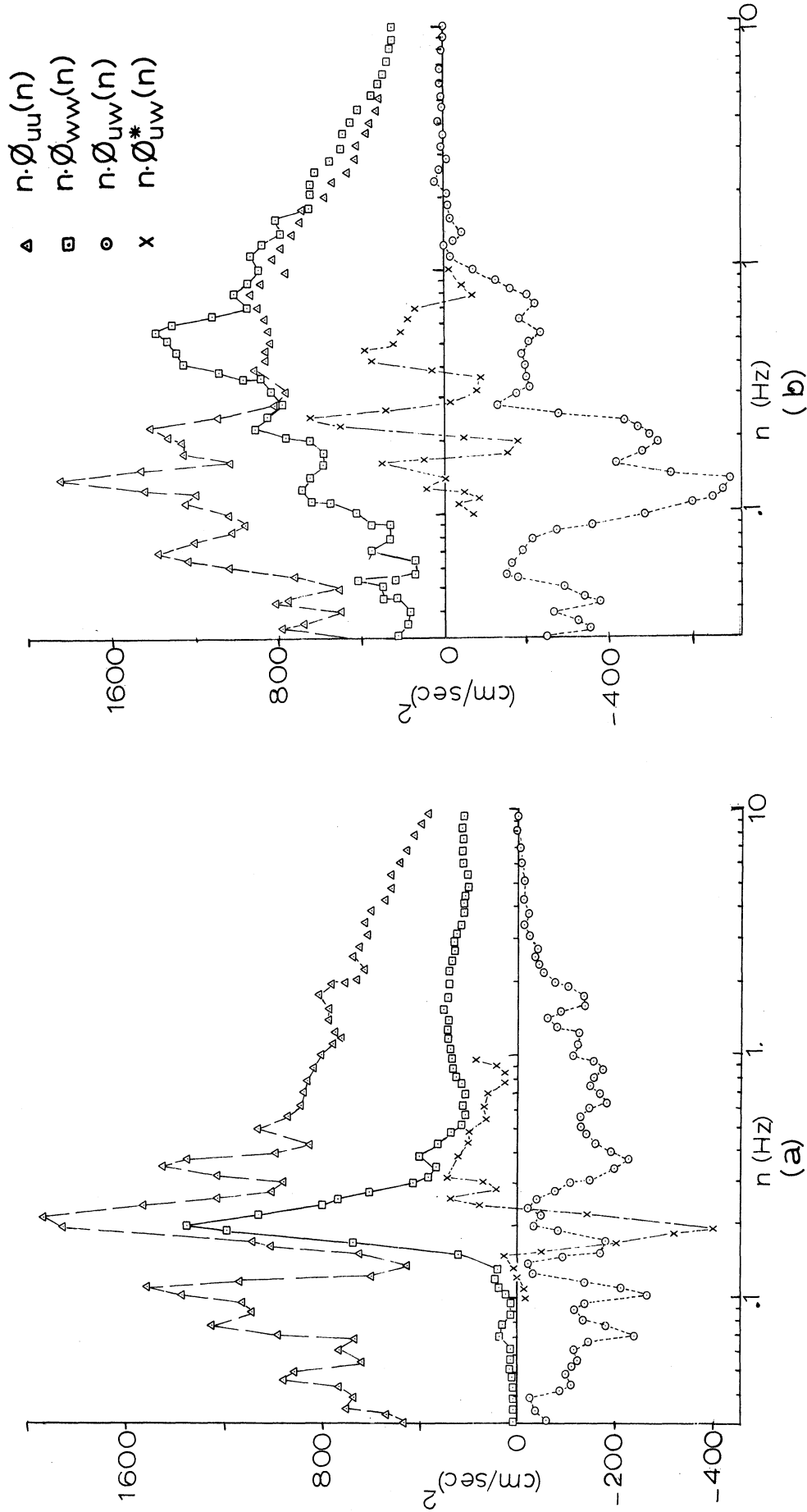
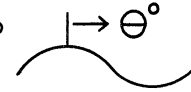


Figure 6.5: Velocity variance and covariance results for Period 2; (a) 15.0 meter level, (b) 15.0 meter level.

legend: \square - uw, \circ - η w, \triangle - η u; η = wave

phase : $\left\{ \begin{array}{l} \square \text{ w leads u} \\ \circ \text{ w leads wave} \\ \triangle \text{ u leads wave} \end{array} \right\}$ by θ° 

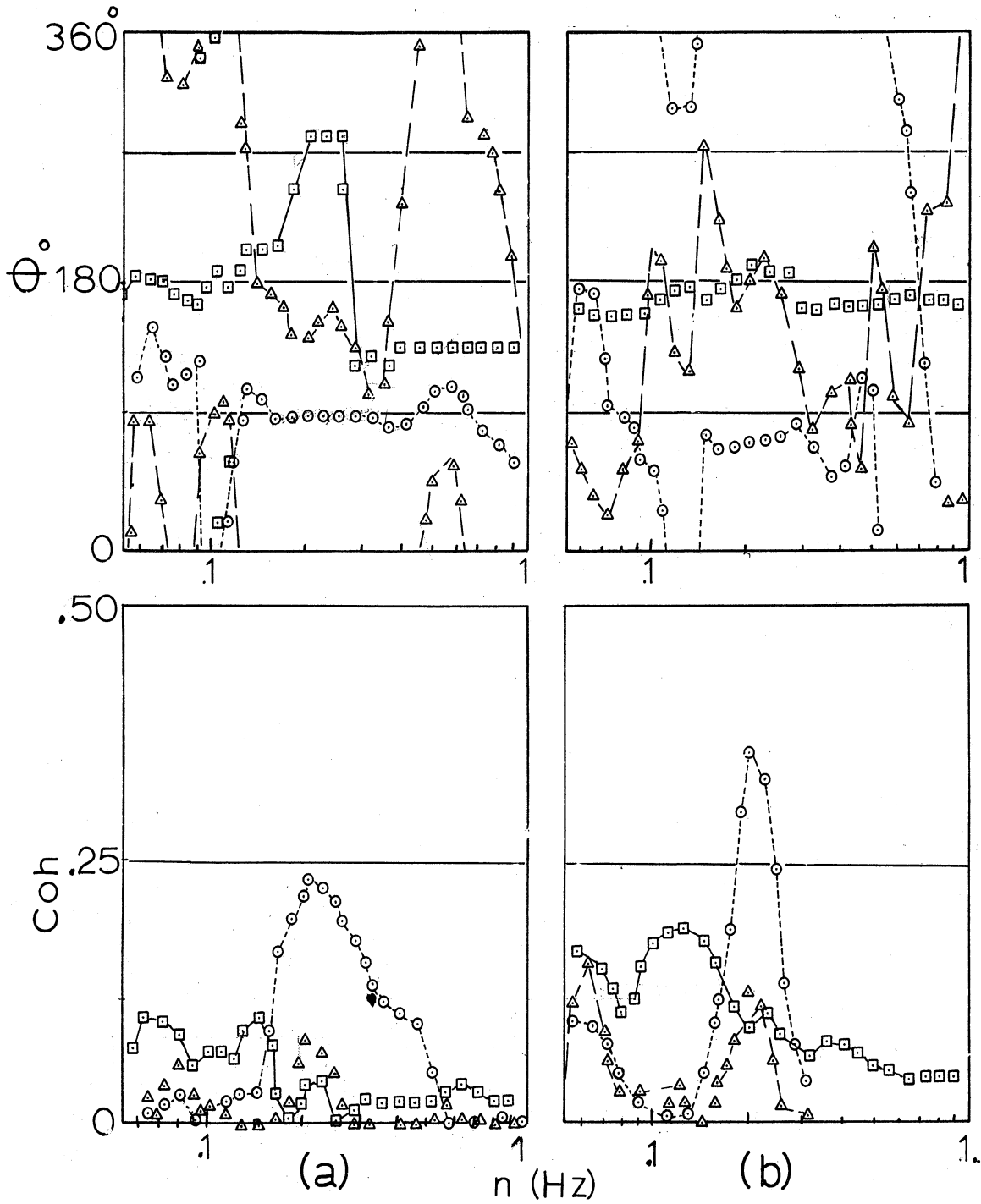
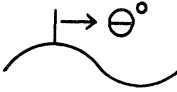


Figure 6.6: Phase and coherence spectra for Period 1; (a) 1.5 meter level, (b) 4.0 meter level.

legend: \square - uw, \circ - η w, Δ - η u; η = wave

phase : $\left\{ \begin{array}{l} \square \text{ w leads u} \\ \circ \text{ w leads wave} \\ \Delta \text{ u leads wave} \end{array} \right\}$ by θ° 

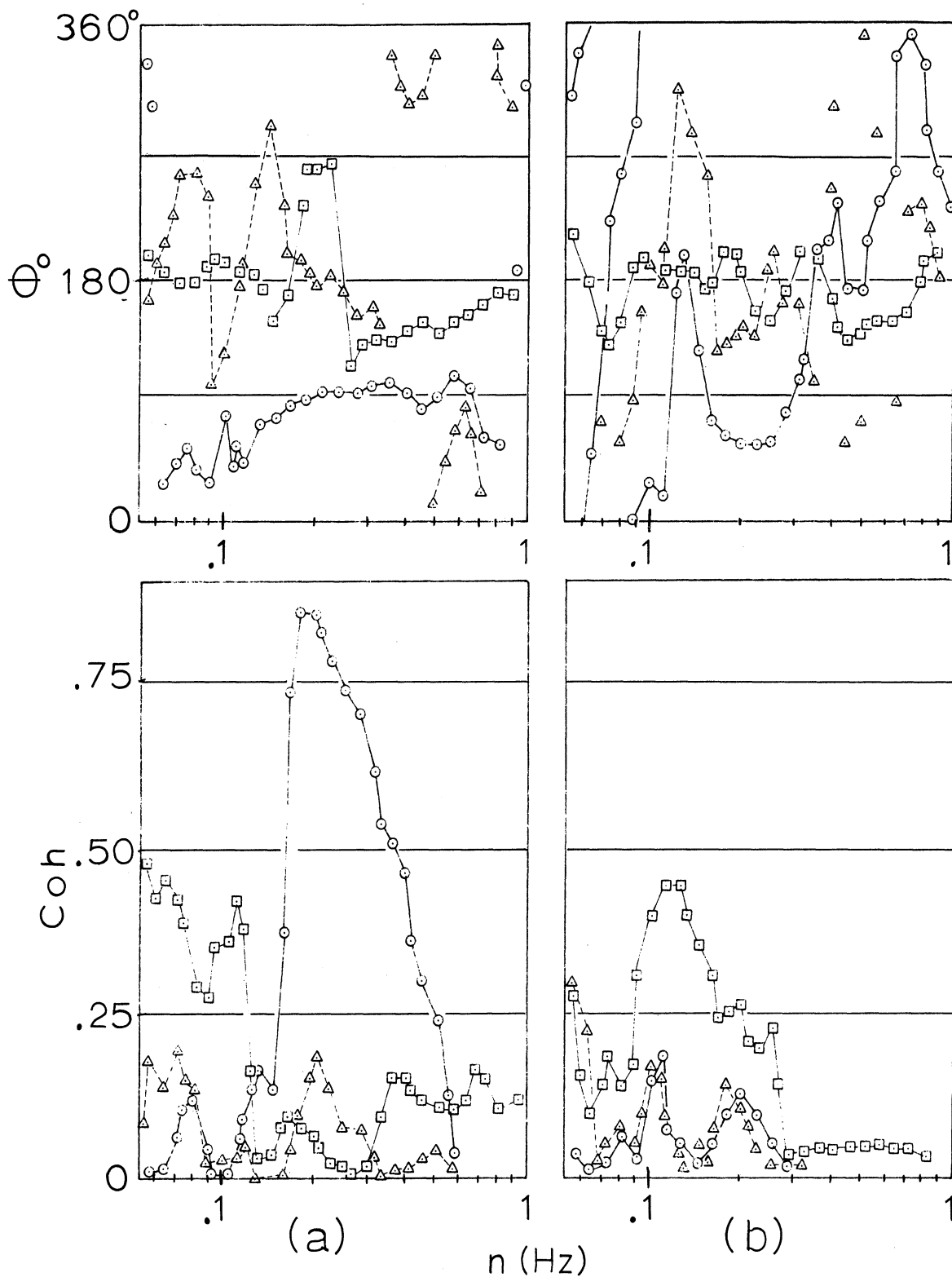


Figure 6.7: Phase and coherence spectra for Period 2; (a) 1.5 meter level, (b) 15 meter level.

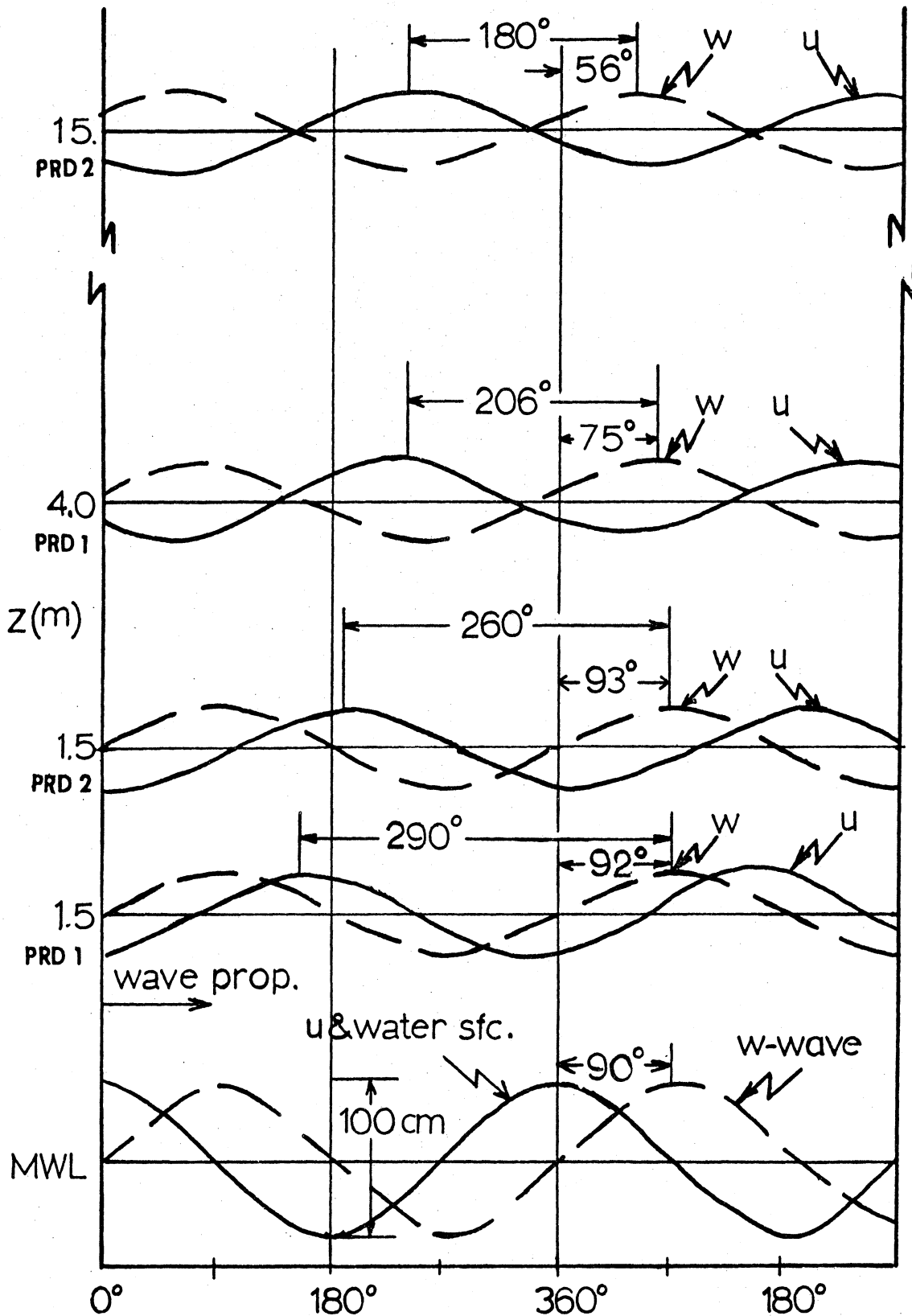


Figure 6.8: Composite schematic of phase relations between velocity components and waves at .2 Hz for Periods 1 and 2.

6.2.2 Results from 24 September (Periods 3 and 4)

<u>Period</u>	<u>Time</u>	<u>Measurement levels (meters)</u>
3	1729-1747	1.5
4	1755-1813	1.5 and 4.0

Periods 3 and 4 occurred nearly sequentially in time but are distinguishable by the occurrence of a higher wind speed during Period 4. These are the only observation periods during which wave generation was occurring. A few white caps were observed during each period.

6.2.2.1 General Conditions

Figure 6.9 shows a cold front, moving west to east with associated rain showers that passed the observation site around 0800. Winds increased following the frontal passage but resumed the same direction that prevailed before the frontal passage. The wave heights increased during the afternoon under the influence of the increasing winds. There were scattered clouds during the observation periods. The air temperature at 4 meters was 1°C less than the water temperature.

Figure 6.10 shows that an increase in both wind speed and wave heights occurred during both periods. The increase in mean winds between Period 3 and 4 is reflected in the wind profiles. Table 5.2, page 98, and the wind profiles in Figure 6.10 indicate that the critical levels, corresponding to the wave spectra peaks ($n_0 = .26 \text{ Hz}$, $C = 6 \text{ m/sec}$), were near or below the measurement levels during both periods. Relating measurement levels with respect to the critical level has to

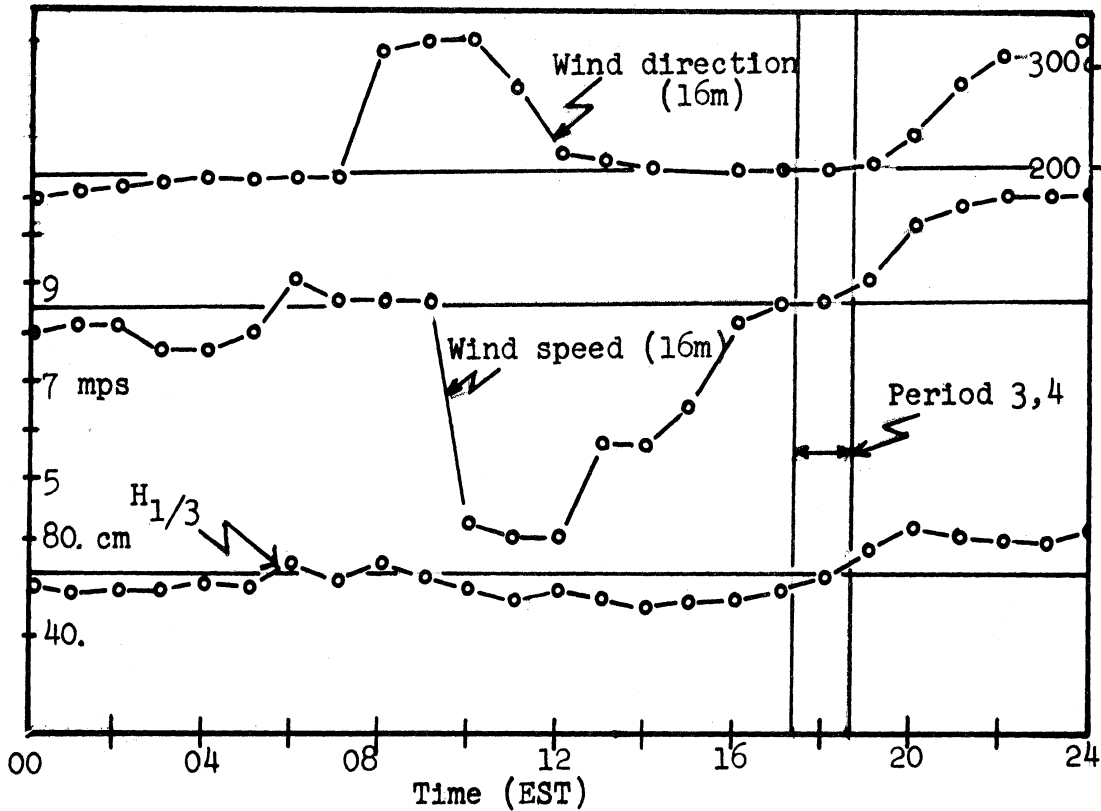
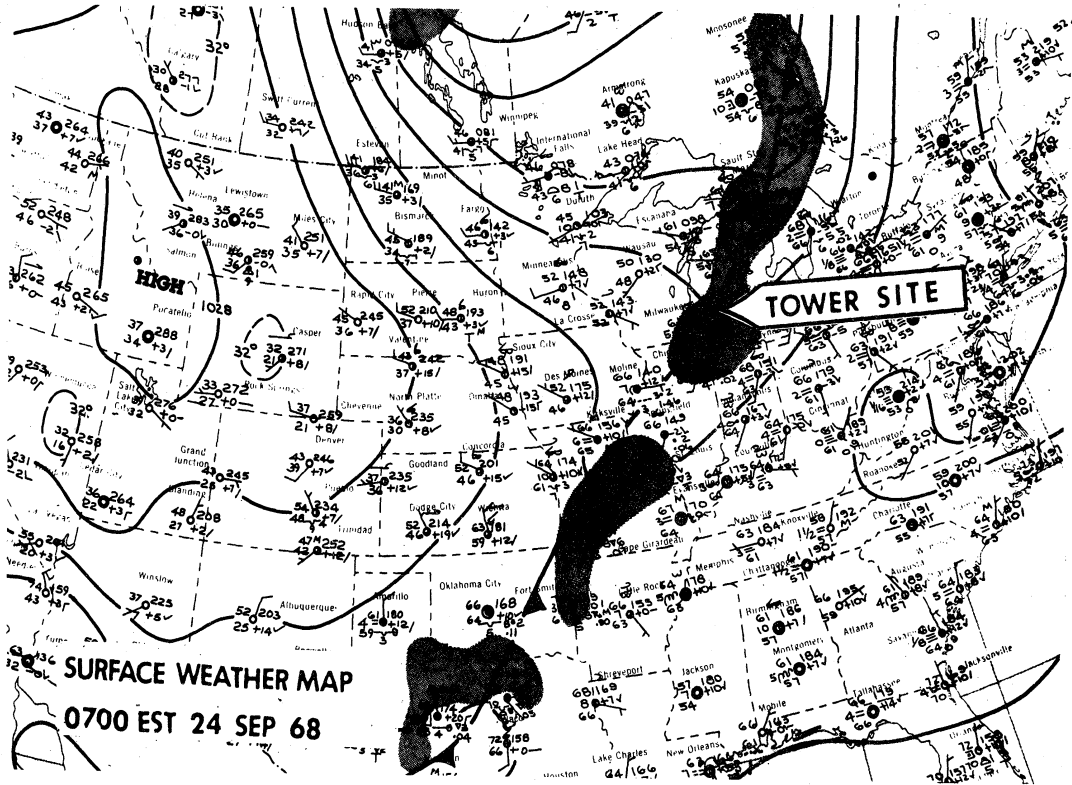


Figure 6.9: General conditions for 24 September, 1968.

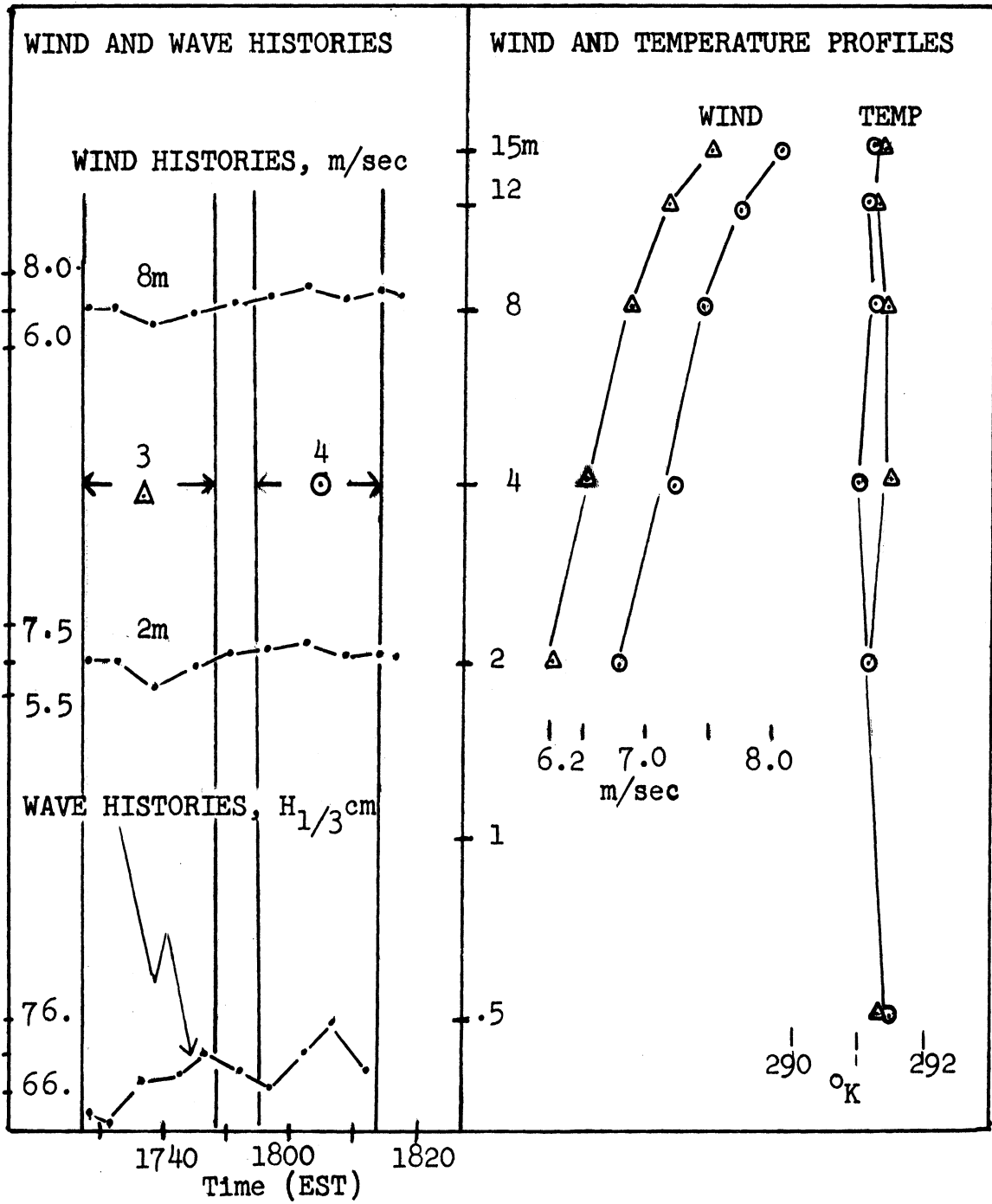


Figure 6.10: General conditions for time encompassing Periods 3 and 4.

be considered in view of the random nature of the wave field and also the changing wind speeds. The approximate height of the critical level is used, primarily, for comparison with other periods.

6.2.2.2 Spectral Results

Wave spectral data appear in Figure 6.11 and velocity variance and covariance spectra appear in Figures 6.12 (Period 3) and 6.13 (Period 4). Wave spectral data show no significant differences between the two periods. In both cases, the frequency of the peak ($\sim .26$ Hz) is the lower limit of a -5 slope region and a deviation from this power relation occurs near .4 Hz. The lower limit of another -5 slope region occurs at .5 Hz. Possible interpretations of such a deviation were given in the presentation of wave spectral data for Periods 1 and 2, page 108.

Variance and covariance spectra (Figure 6.12 and 6.13) show that the results for the lower level (1.5 meters) are similar for the two periods and that the upper and lower level during Period 4 differ with respect to the frequency of the extrema. Frequencies of interest in these results are near .26 Hz (wave spectra peaks), and .5 Hz (lower limit of -5 slope regions in wave spectra).

For the lower level (Figure 6.12 and 6.13a), near .26 Hz, variance spectra for both u and w have relative maxima and the cospectra have minima. Momentum transport toward the surface (represented by negative cospectra) is enhanced 100-150% above those in neighboring bands. At .5 Hz, for each period,

u has a relative maximum and, for Period 3, w has a relative minimum. At the upper level, (Figure 6.13b) variance spectra for both u and w have relative maxima near .26 Hz, that for the u component has a broader band than either of those at the lower level. The cospectrum at this level does not have the distinct minimum that appeared at the lower level but has a broad band of enhanced stress that extends to a minimum near .2 Hz. A broadening of the band associated with extrema was also observed at the upper levels during Periods 1 and 2.

Figure 6.14 (Period 3) and Figure 6.15 (Period 4) show phase and coherence spectra. Estimates near .26 Hz are of primary interest for all levels. For Period 3, both η_w and uw coherence estimates are large near .26 Hz, and w leads the wave by about 90° and leads u by about 190° . For Period 4, at both levels, phase relations between u and the wave appear to have preferred values near .26 Hz being about 210° at the lower level and about 230° at the upper level. The coherence estimates between u and w have relatively high values near .26 Hz with phase relations being about 190° at the lower level and about 170° at the upper level.

Table 6.1 page 103, lists phase angles used to form the phase relation composite for both periods shown in Figure 6.16. Results from 1.5 meters during period 3 were positioned below those for the same level during Period 4 by determining the level at which the mean wind during Period 3 would have occurred during Period 4. Since the critical level, z_c ,

was near 1.5 meters during Period 3, this could be considered a z/z_c vertical scale.

The significant feature in Figure 6.16 is the distinct difference between the results for the two 1.5 meter level data sets which had similar variance and covariance spectra. Phase relations for Period 3 ($z/z_c \approx 1$) are those expected near the critical level since u is a maximum over the upwind node of the wave. Between the 1.5 meter levels, u and w shift back towards the trough and crest respectively. They retain, essentially, the same phase with the wave for Period 4. Period 4 observations were made above the critical level corresponding to the wave spectrum peak.

Spectral features and phase relations for these periods may be summarized as follows;

1) At all levels, both u and w spectra have peaks corresponding to the wave spectrum peak. Cospectra at lower levels (1.5 meters) are similar in shape with enhanced stress at the wave spectrum peak. At the upper level, stress enhancement extends to lower frequencies, a characteristic also observed during a case (Periods 1 and 2) when the critical level is effectively at infinity.

2) The lower level (1.5 meter) results are different with respect to the phase relations between velocity components and the wave. For Period 3, when $z/z_c \approx 1$, phase relations exhibit features associated with the "matched layer", u being a maximum over the upwind node of the wave. For Period 4, when $z/z_c > 1$, the maximum in u occurred near the

trough and in w slightly ahead of the crest. The same phase relations occurred at both levels during Period 4.

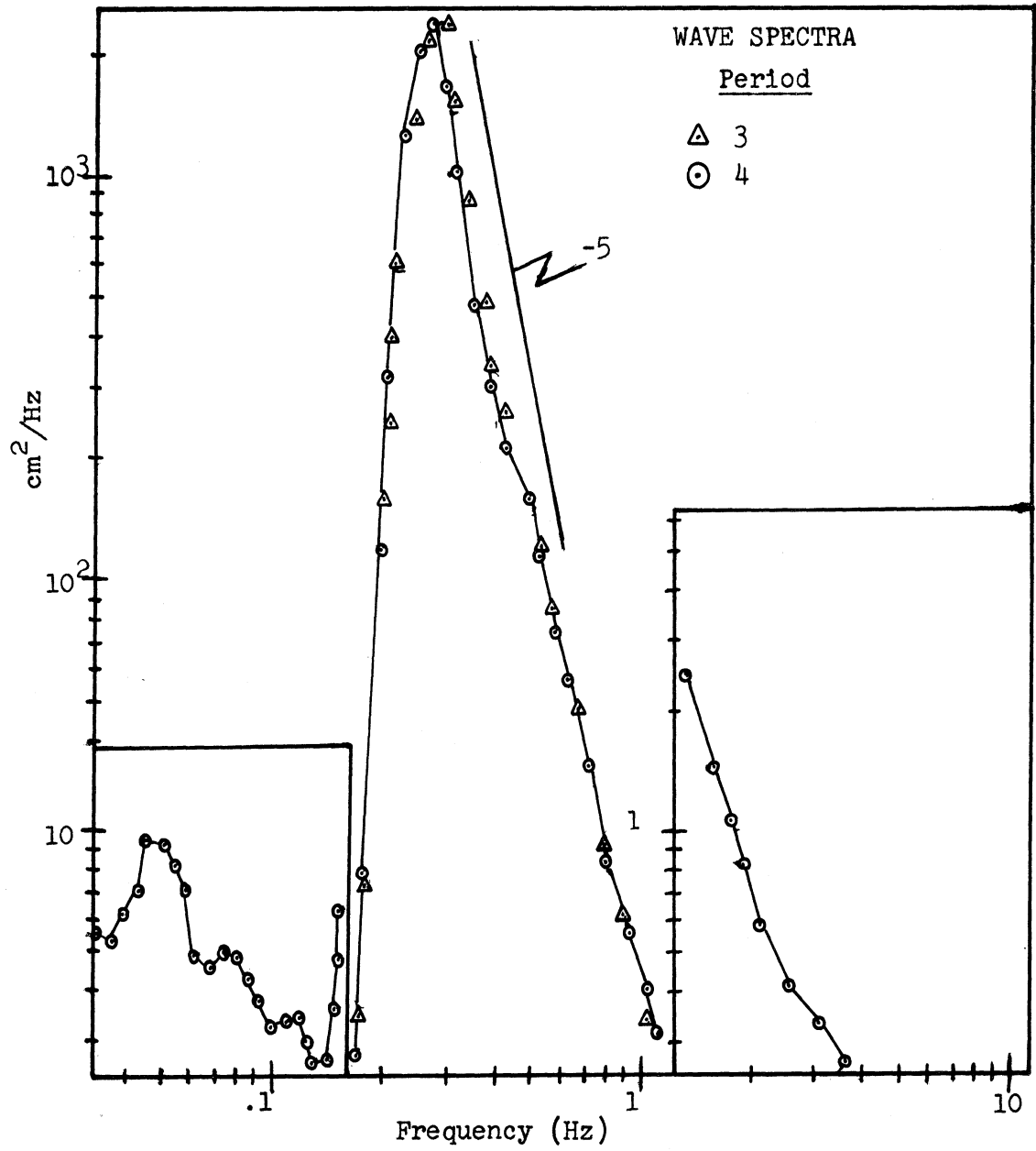


Figure 6.11: Wave spectral estimates for Periods 3 and 4.

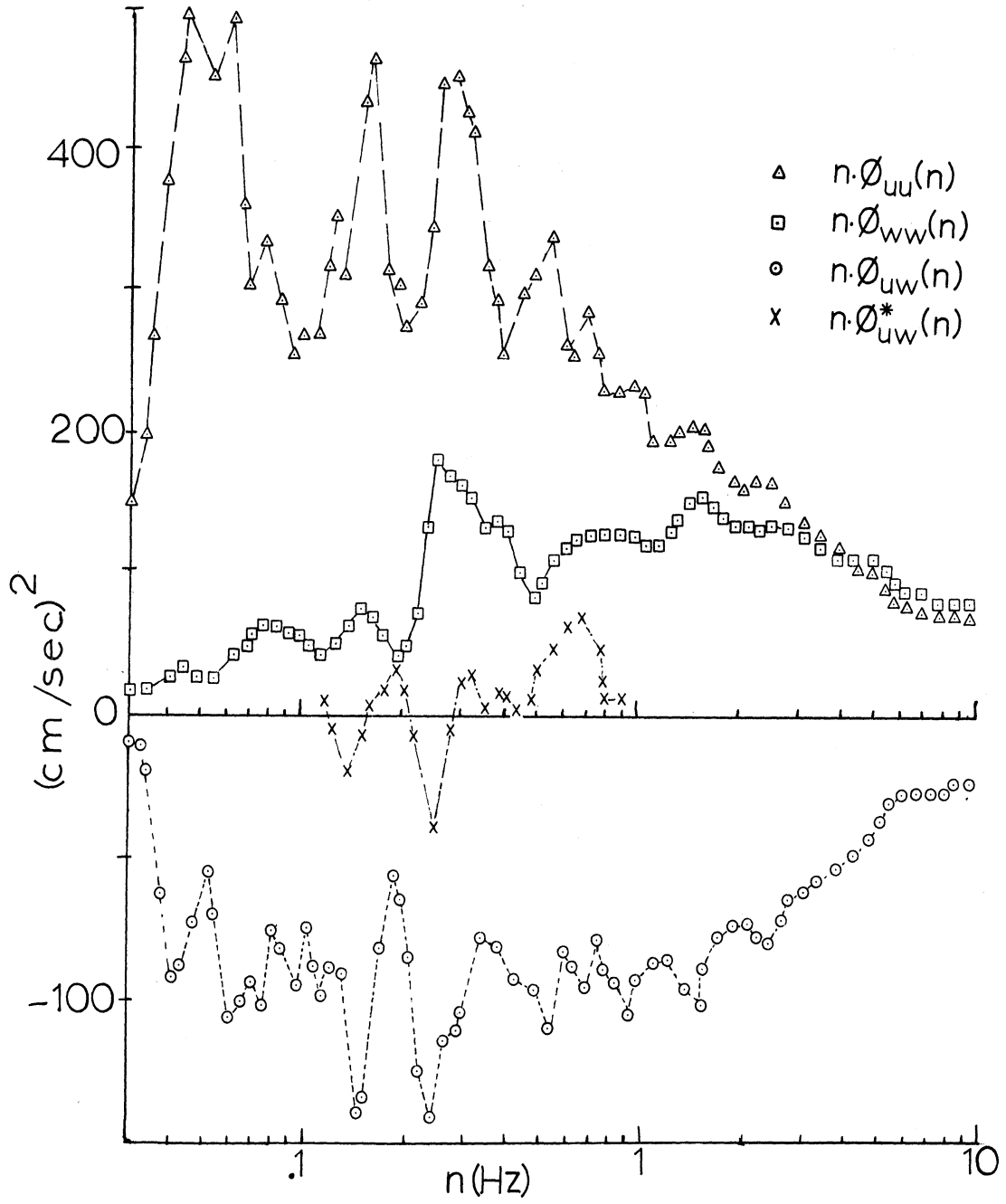


Figure 6.12: Velocity variance and covariance results for Period 3; 1.5 meter level.

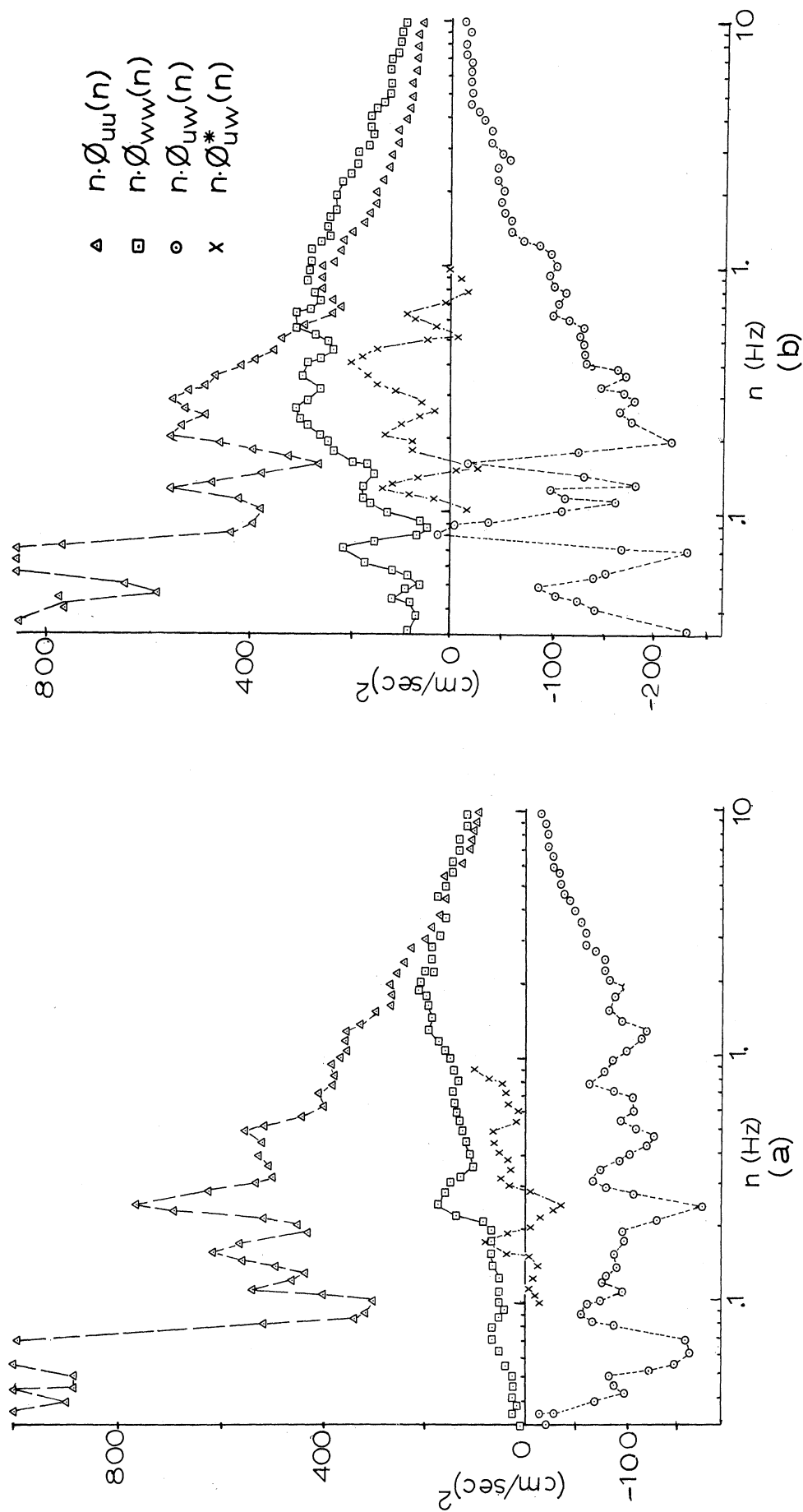
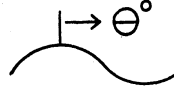


Figure 6.13: Velocity variance and covariance spectra for Period 4; (a) 1.5 meter level, (b) 4.0 meter level.

legend: \square - uw , \circ - ηw , \triangle - ηu ; η = wave

phase : $\left\{ \begin{array}{l} \square w \text{ leads } u \\ \circ w \text{ leads wave} \\ \triangle u \text{ leads wave} \end{array} \right\}$ by θ° 

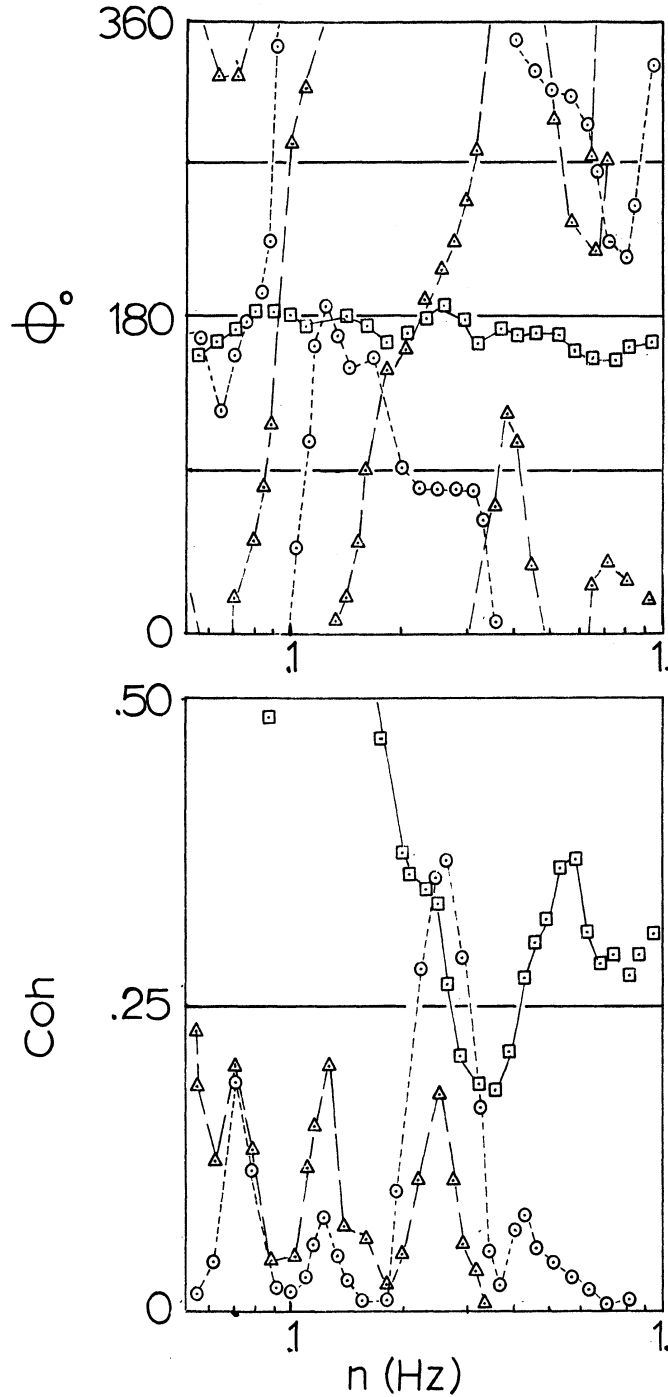
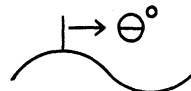


Figure 6.14: Phase and coherence spectra for Period 3; 1.5 meter level

legend: \square - uw, \circ - η w, Δ - η u; η = wave

phase : $\left\{ \begin{array}{l} \square \text{ w leads u} \\ \circ \text{ w leads wave} \\ \Delta \text{ u leads wave} \end{array} \right\}$ by θ° 

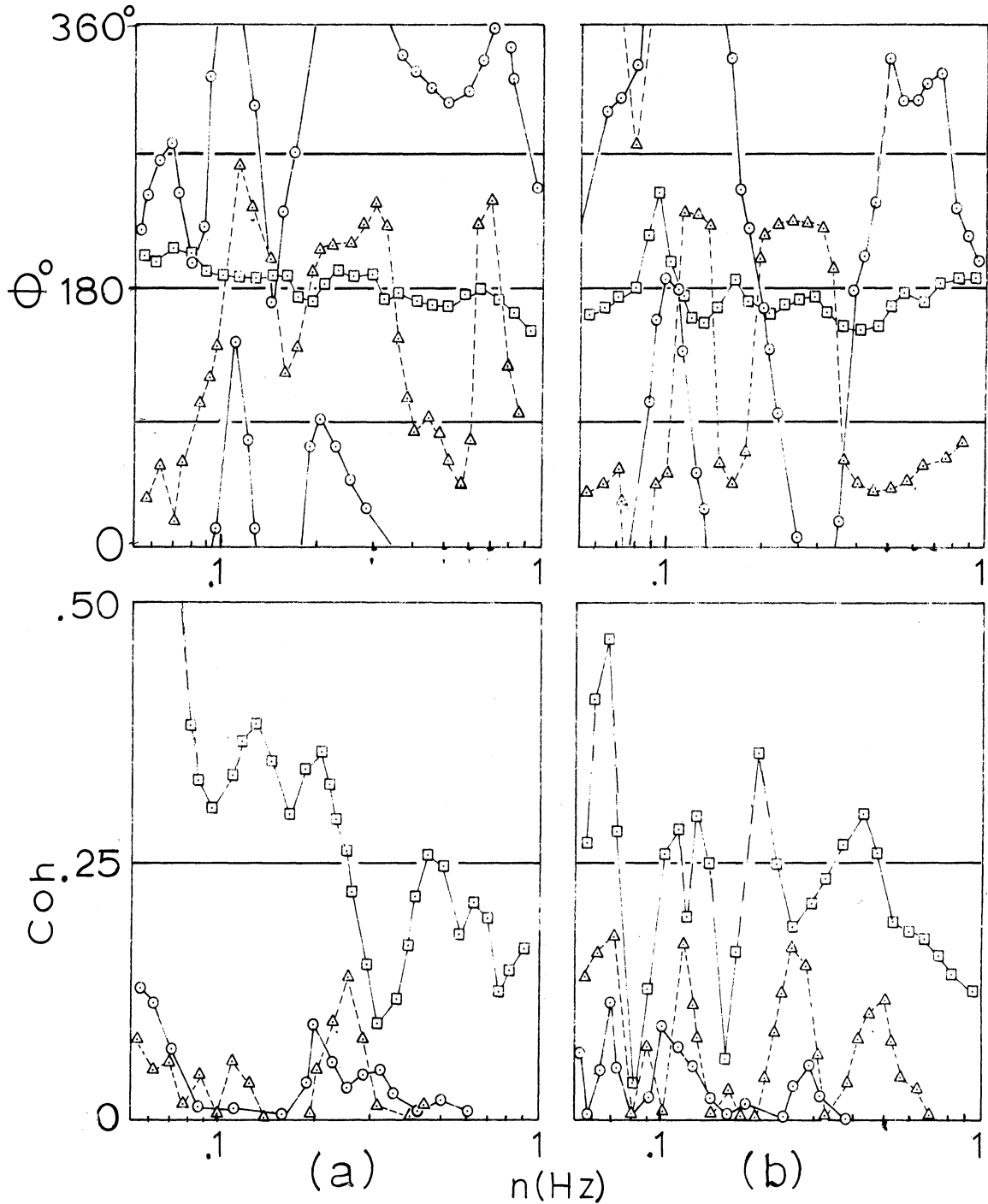


Figure 6.15: Phase and coherence spectra Period 4;
 (a) 1.5 meter level, (b) 4.0 meter level.

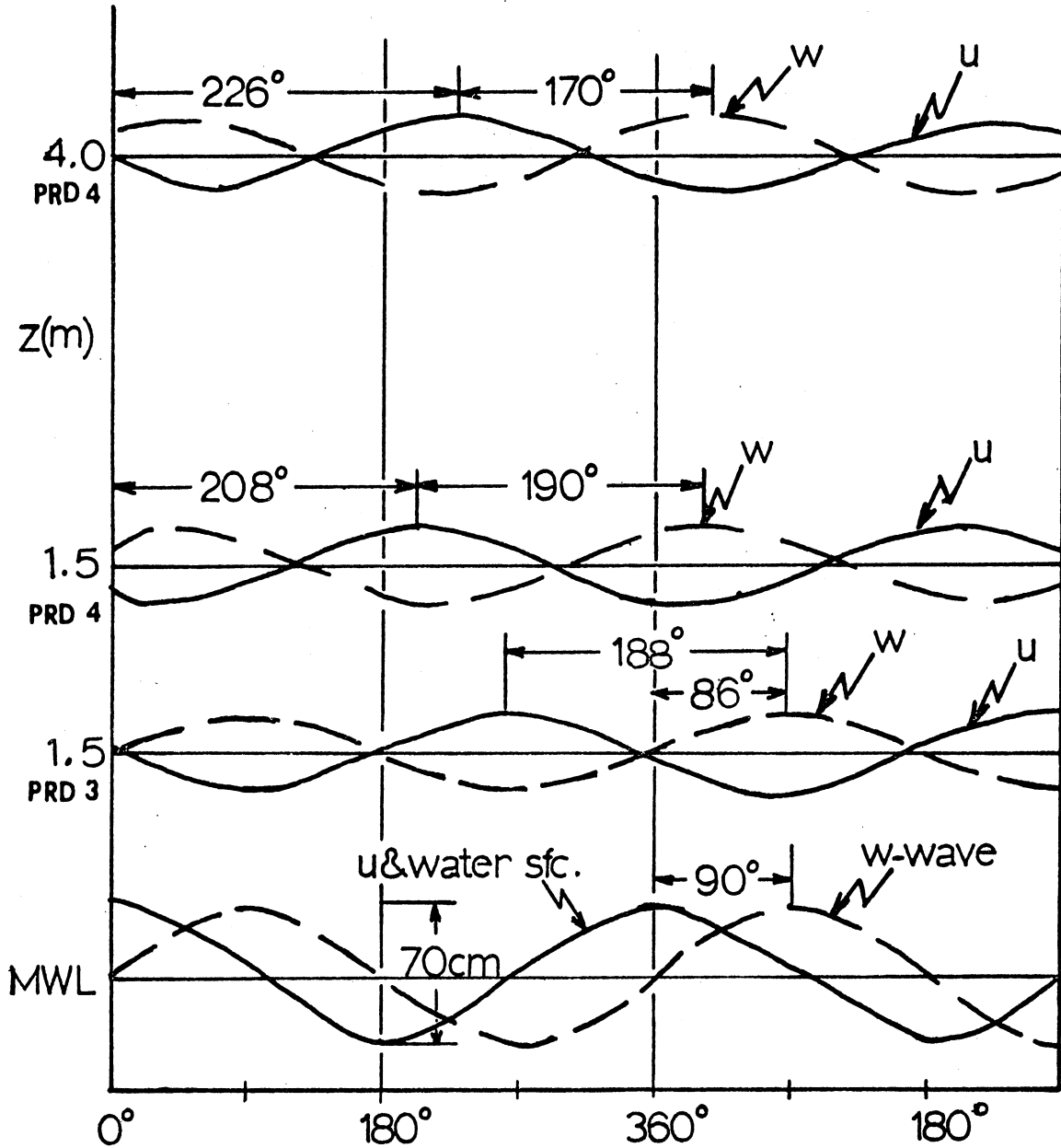


Figure 6.16: Composite schematic of phase relations between velocity components and waves at .26 Hz for Periods 3 and 4.

6.2.3 Results from 26 September (Periods 5, 6 and 7)

<u>Period</u>	<u>Time</u>	<u>Measurement level (meters)</u>
5	1100-1118	1.5 and 4.0
6	1324-1342	4.0
7	1355-1413	1.5 and 4.0

These periods are of special interest because they represent times when the critical level was near the level of measurement (Period 5) and when it was effectively at infinity (Periods 6 and 7). Wave heights were generally decreasing from the beginning of the first period to the end of the last, an interval of 5 hours. Wave spectra changed shape during this time by a shift of the spectral peak to a lower frequency.

Complementary wind, temperature and wave data are presented together (6.2.3.1) for purposes of comparison but spectral results are presented in two parts, one for Period 5 (6.2.3.2) and one for Periods 6 and 7 (6.2.3.3).

6.2.3.1 General conditions

Figure 6.17 shows that the weak pressure gradient over Lake Michigan resulted in diminishing winds during the day (7 m/sec at 1000 to 2 m/sec at 2000 EST). Moderate winds during Period 5 were due to the influence of the low pressure system located southwest of the lake. Hydrostatic conditions were unstable with the water temperature about 5°C higher than the air temperature at 4 meters.

Figure 6.18 (Period 5) and 6.19 (Periods 6 and 7) show

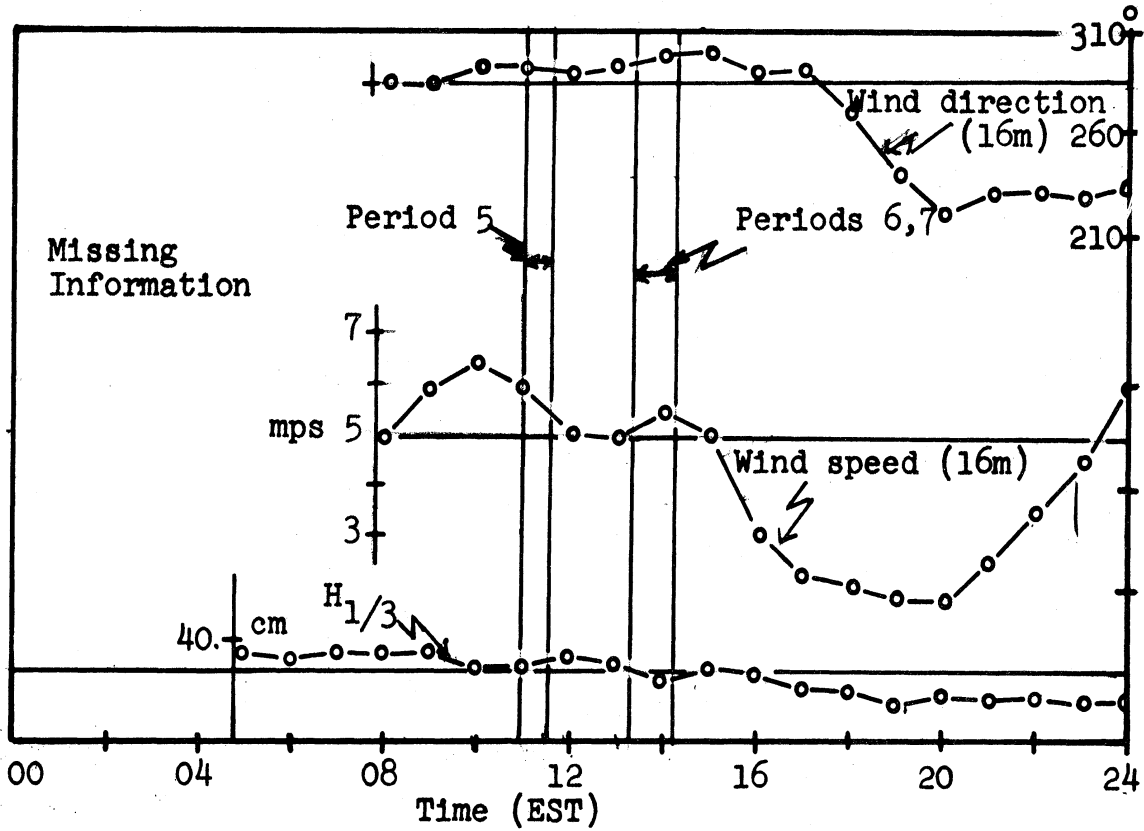
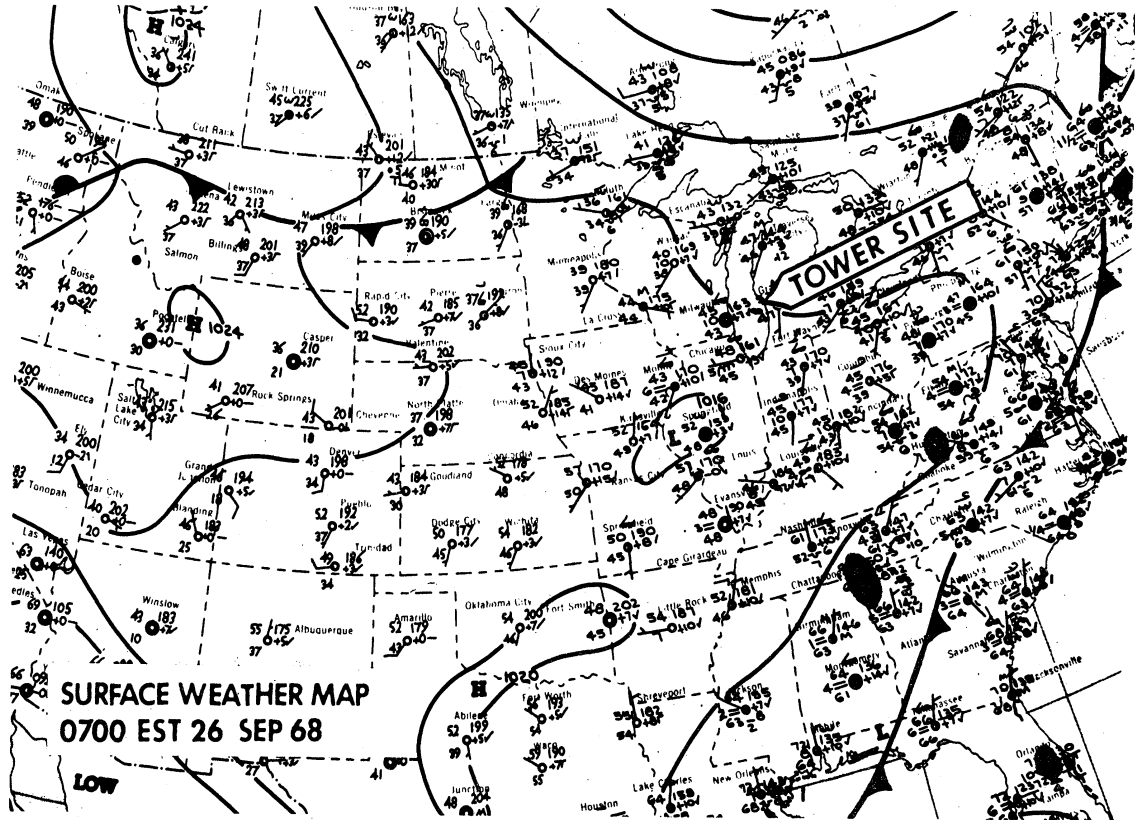


Figure 6.17: General conditions for 26 September, 1968.

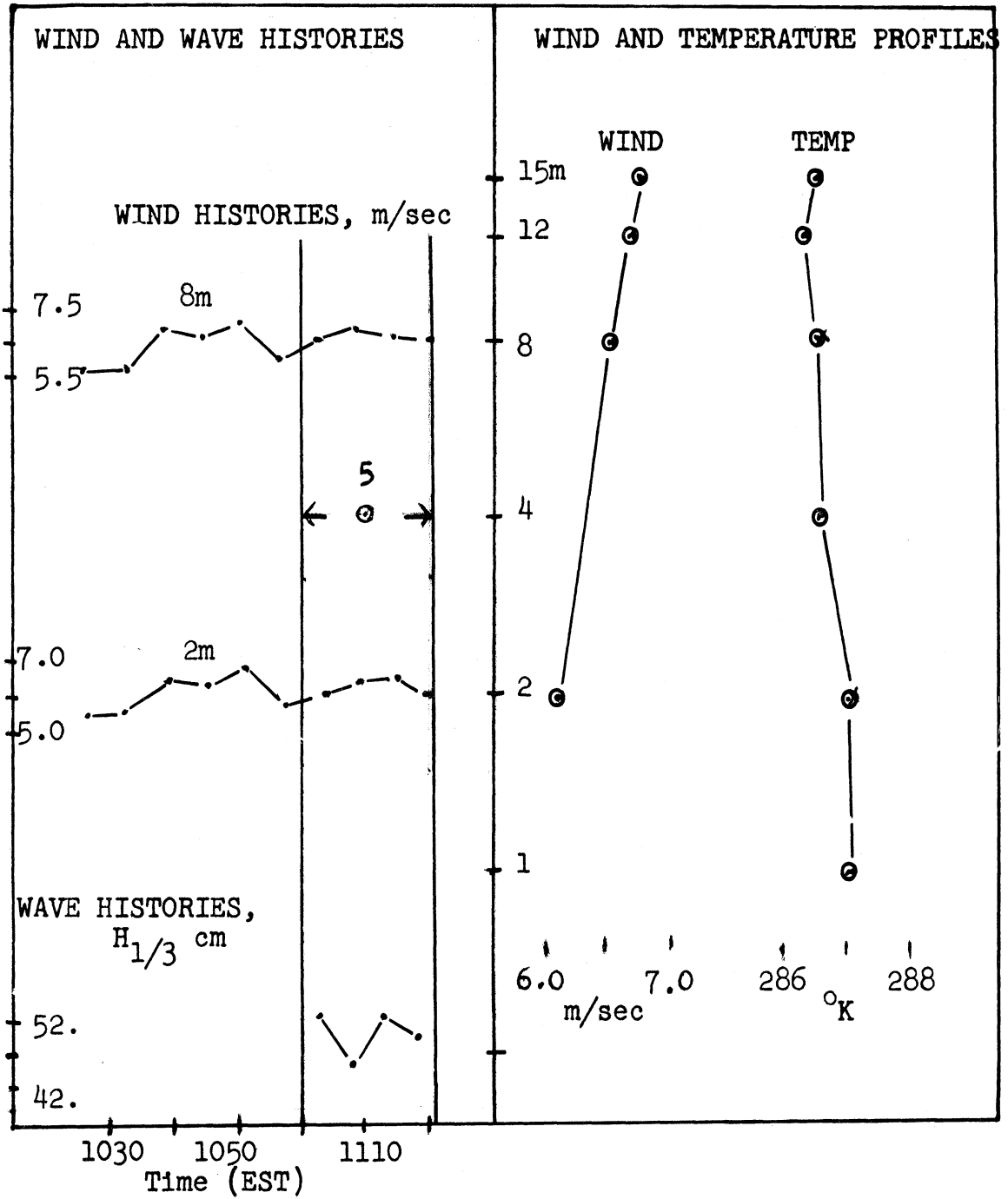


Figure 6.18: General conditions for time encompassing Period 5.

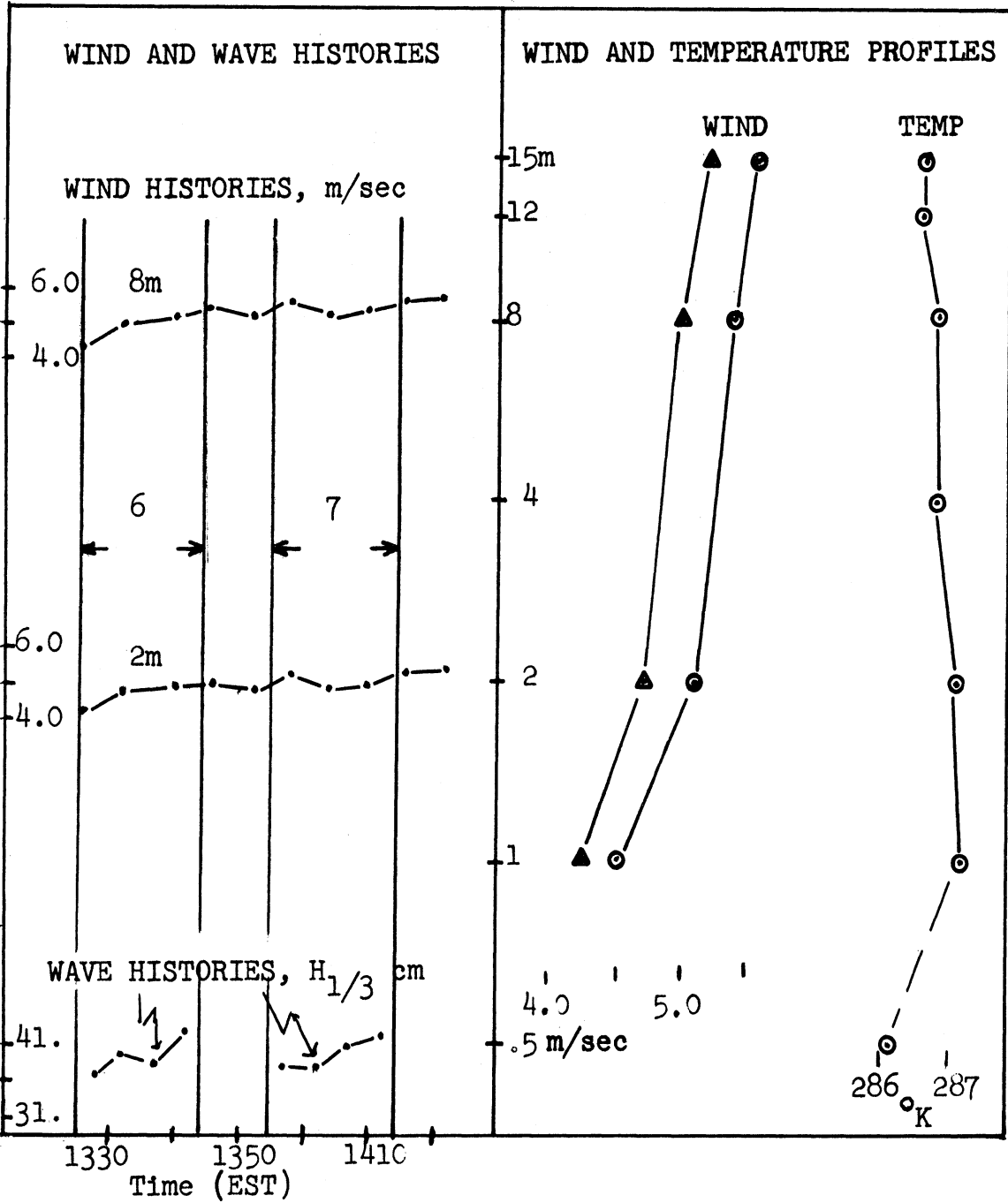


Figure 6.19: General conditions for time encompassing Periods 6 and 7.

that wind speeds were increasing during 6. Wave heights decreased during Period 5 and increased during Periods 6 and 7. Winds profiles show the difference in mean wind speeds between the morning (Period 5) and afternoon periods (6 and 7) and also the increase in mean wind between Periods 6 and 7. Temperature profiles show the unstable conditions which existed during all three periods. No white caps were observed during either of these periods.

6.2.3.2 Spectral Results (Period 5)

The wave spectrum in Figure 6.20 shows a peak near .3 Hz and a secondary peak near .26 Hz. The first peak is the lower limit of an approximate -5 slope region. The -5 slope relation has a deviation near .4 Hz.

The critical level for .3 Hz was below ($z/z_c > 5$) and that for .26 Hz near ($z/z_c \approx 1$) the 1.5 meter level. An 8° rotation was performed on initial spectral results for the 4.0 meter level but the spectral features described in the following paragraphs were not influenced by this adjustment¹.

Variance and covariance spectra (Figure 6.21) show that significant extrema occur near .26 Hz but not at .3 Hz. Variance spectra at the two levels exhibit similar features across the band corresponding to the wave spectra (.15 to 1 Hz) but cospectra for the two levels are different. Specific features are discussed in the following two paragraphs.

¹Appendix B, Section B.2 includes spectral results for this level for 0° , 4° and 8° rotations respectively.

Variance spectra, at both levels, show a narrow band of energy concentration in the u component near .26 Hz and relative maxima near .4 Hz. w spectra also have relative maxima near .26 Hz. At the lower level, there are distinct relative minima for both u and w near .3 Hz.

The 4.0 meter cospectrum has a distinct minimum at .26 Hz; it does not appear at 1.5 meters. At the lower level, however, a distinct maximum appears near .3 Hz which may be related to the variance spectra at this frequency. The cospectrum at the lower level shows a broad band of enhanced stress at frequencies above .4 Hz. This could be related to interaction between shorter waves and the wind field.

Figure 6.22 shows phase and coherence spectra for both levels. At the lower level, phase relations between u and the wave appear to attain preferred values near .26 Hz being about 135° . At the upper level, w and wave appear to attain a preferred value of 270° . Coherence estimates for uw have relative maxima near .26 Hz with phase relations between u and w being about 155° at the lower level and 170° at the upper level.

Figure 6.23 is a schematic which shows the phase relations between velocity components and the wave at .26 Hz. The values are those listed in Table 6.1. There is little shift with height of either component with respect to the wave. The position of the maxima over the downwind node in the w component agrees with that depicted by Phillips (1966, page 91, Figure 4.3) for the matched layer.

Spectral features and phase relationships for this period may be summarized as follows:

- 1) There is no evidence of wave induced motion at the wave spectrum peak (.31 Hz) for which $z/z_c > 5$. However, definite evidence of wind-wave coupling appeared at .26 Hz for which $z/z_c \approx 1$. The lower level (1.5) had a broad band of enhanced stress and the upper level (4.0) had a definite band of enhanced stress at .26 Hz.
- 2) Phase relations between the velocity components and the waves were similar at both levels and are what one would observe within the matched layer.

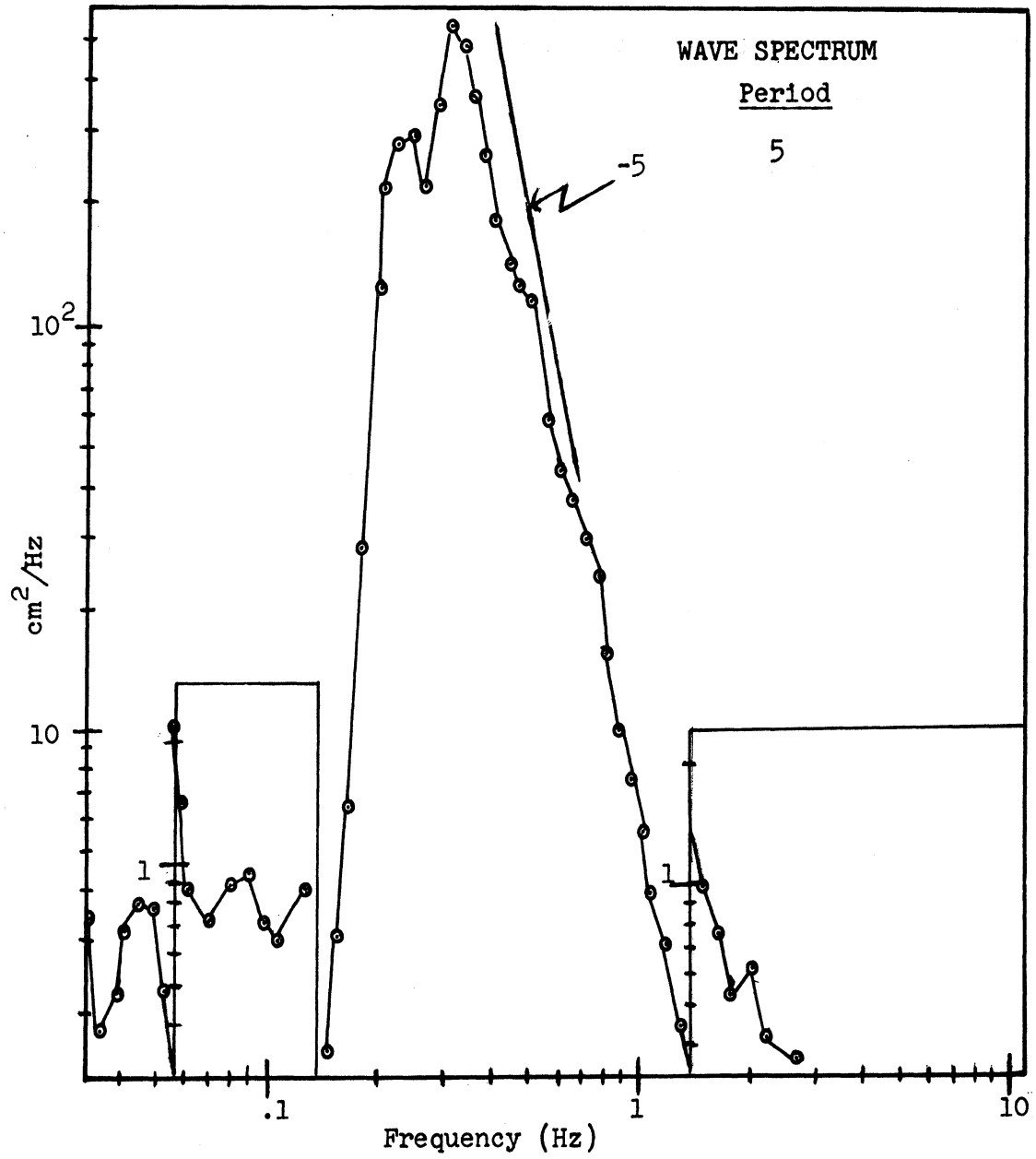


Figure 6.20: Wave spectrum for Period 5.

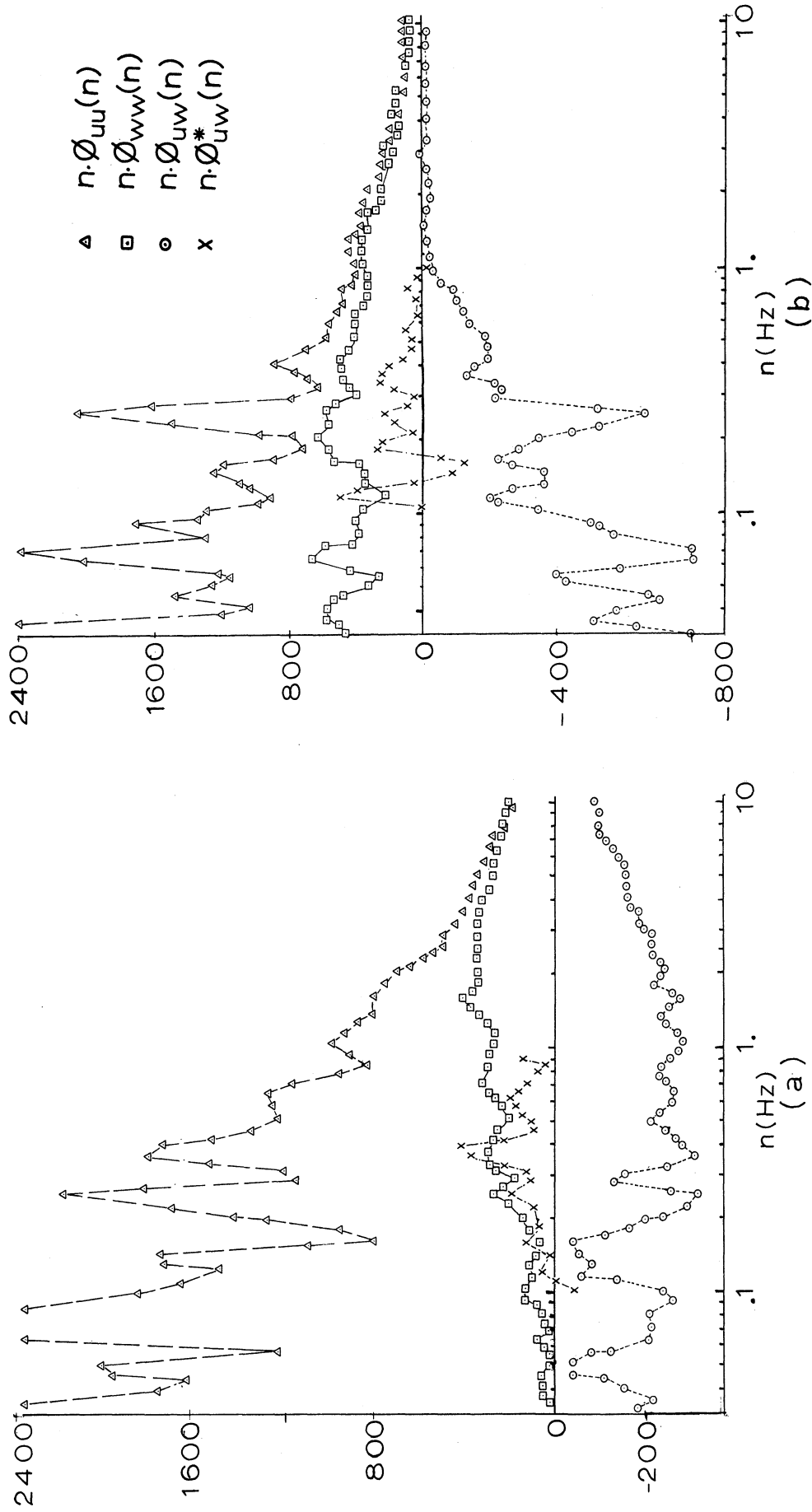
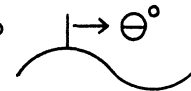


Figure 6.21: Velocity variance and covariance spectra for Period 5; (a) 1.5 meter level, (b) 4.0 meter level.

legend: \square - uw, \circ - η w, Δ - η u; η = wave

phase : $\left\{ \begin{array}{l} \square \text{ w leads u} \\ \circ \text{ w leads wave} \\ \Delta \text{ u leads wave} \end{array} \right\}$ by θ° 

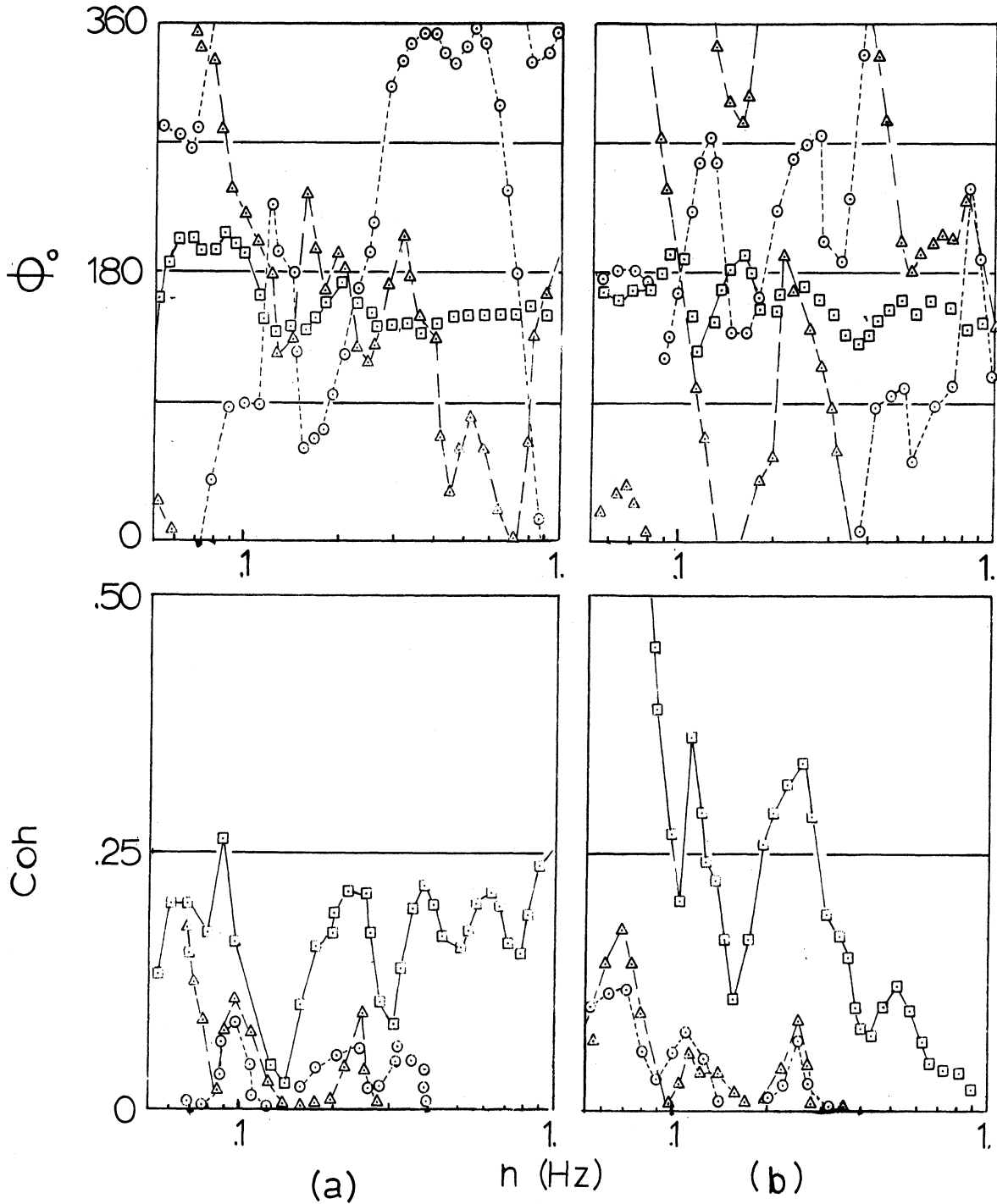


Figure 6.22: Phase and coherence spectra for Period 5; (a) 1.5 meter level, (b) 4.0 meter level.

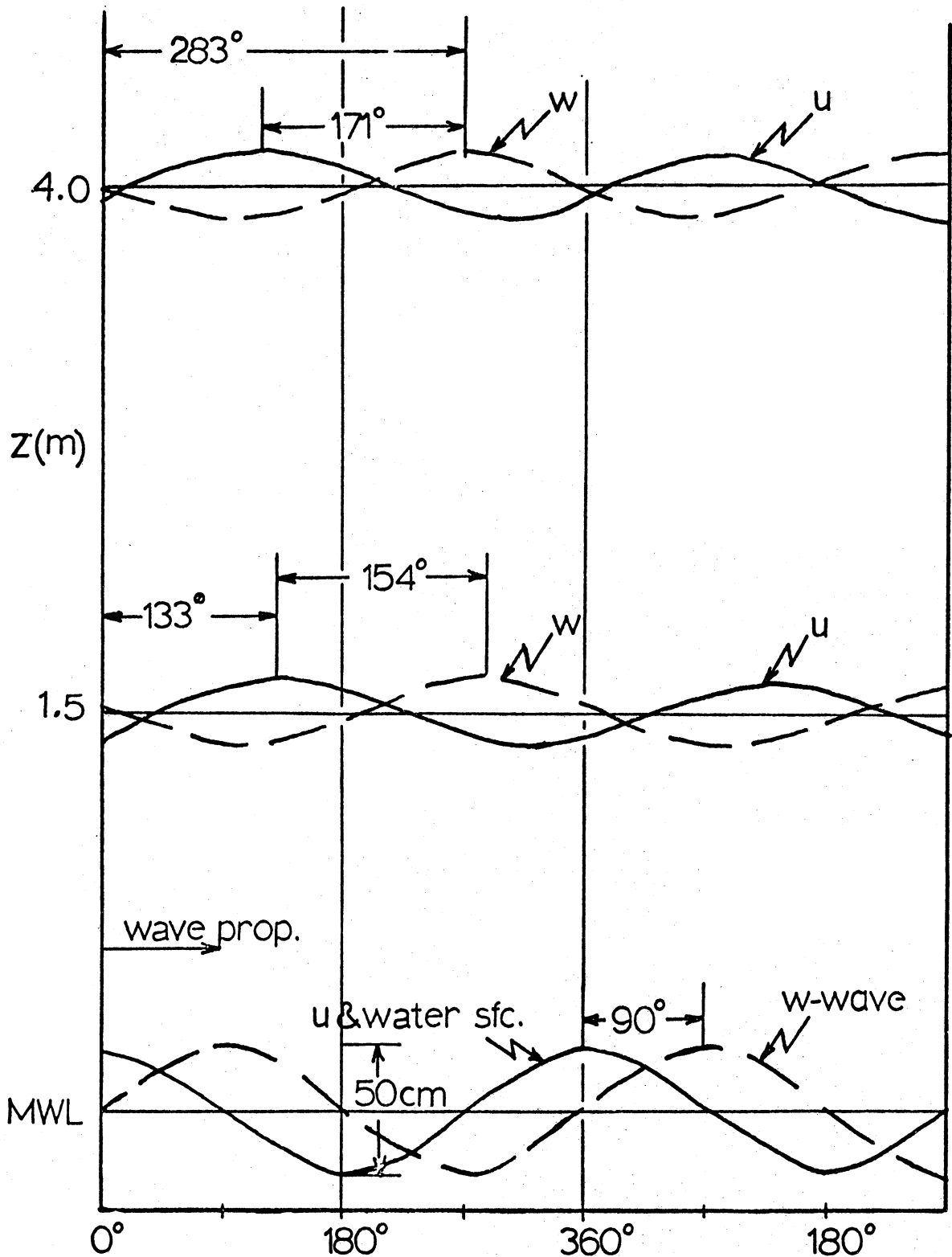


Figure 6.23: Schematic of phase relations between velocity components and waves at .26 Hz for Period 5.

6.2.3.3 Spectral Results (Periods 6 and 7)

Wave spectra appear in Figure 6.24 and velocity variance and covariance spectra appear in Figures 6.25 (Period 6) and 6.26 (Period 7). Wave spectra show that the primary peak occurs near .26 Hz which was the frequency of a secondary peak during Period 5. The occurrence of the peak at .26 Hz was probably due to a decrease of spectral values above that frequency since the amplitude at .26 Hz between Periods 5, 6 and 7 showed little change in magnitude. A spectral peak at the lower limit of a -5 slope region at about .4 Hz, decreased between Periods 6 and 7. The critical level for both periods, for the wave spectra peak (.26 Hz), was effectively at infinity.

Variance and covariance results (Figures 6.25 and 6.26) show a significant difference between two sequential measurements at 4.0 meters. Results from Period 7, however, show similarities between the two levels. This suggests that the mean wind speed is, indeed, important when considering the influence of waves on the airflow because wave spectra for the two periods were similar.

During Period 6 (Figure 6.25) variance spectra for both u and w show relative maxima near .2 Hz which is a frequency on the forward face of the wave spectrum. A secondary peak occurs in u near .4 Hz and w appears to have relative maxima coincident with the wave spectrum peak at .3 Hz and also near .5 Hz which coincides with a lower limit of a -5 slope region of the wave spectrum during Period 7. Cospectra show

relative minima near .2 Hz and also near .5 Hz.

During Period 7 (Figure 6.26), variance spectra for u have maxima near .26 Hz and relative maxima near .4 Hz. At the lower level, w has a maximum near .26 Hz. Covariance spectra for the two levels differ, having narrow and broad bands of minima at lower and upper levels respectively. At the upper (4.0 meter) level the band appears to extend across a corresponding band (.26-.5 Hz) in the wave spectrum (Figure 6.24) where the lower limit is defined by the spectral peak and the upper limit by a start of an approximate -5 slope region.

Figures 6.27 and 6.28 show phase and coherence spectra for Periods 6 and 7 respectively. Frequencies of primary interest are those where spectral results indicate wave influence on the airflow, viz. .2 Hz for Period 6 and .26 Hz for Period 7. For Period 6 (Figure 6.27), near 2. Hz, u leads the wave by about 270° and w leads the wave by about 80° . At both levels for Period 7 (Figure 6.28), phase relations appear to attain preferred values in the neighborhood of .26 Hz. u leads the wave by about 190° at the 1.5 meter level and by about 170° at the 4.0 meter level. w leads u by about 190° at the 1.5 meter level and by about 170° at the 4.0 meter level.

Figure 6.29 is a schematic showing phase relationships between the velocity components and the wave for Period 7. The frequency represented in the schematic is .26 Hz and values of angles used are given in Table 6.1, page 103.

Phase angles for Period 6 are given in Table 6.1 for .20 and .26 Hz but are not included in the schematic.

Spectral features and phase relationships for these periods may be summarized as follows;

- i) During Period 6, which had light winds, spectral data indicate that there may be wave-induced fluctuations at frequencies on the forward face of the wave spectrum, near .2 Hz. Only the w component shows any evidence of influence near the wave spectrum peak.
- ii) During Period 7, the upper level (4.0 meter) co-spectra had a broad band of enhanced stress which appeared to coincide with a distinct band in the wave spectrum. Both levels showed maxima in u spectra at the wave spectrum peak. There is evidence, at the lower level, of wave influence at .4 Hz a lower limit of a -5 slope region in the wave spectrum.
- iii) During Period 7, the maximum in the u component maintained a phase over the wave trough for both levels and w shifted from ahead to behind the crest with height.

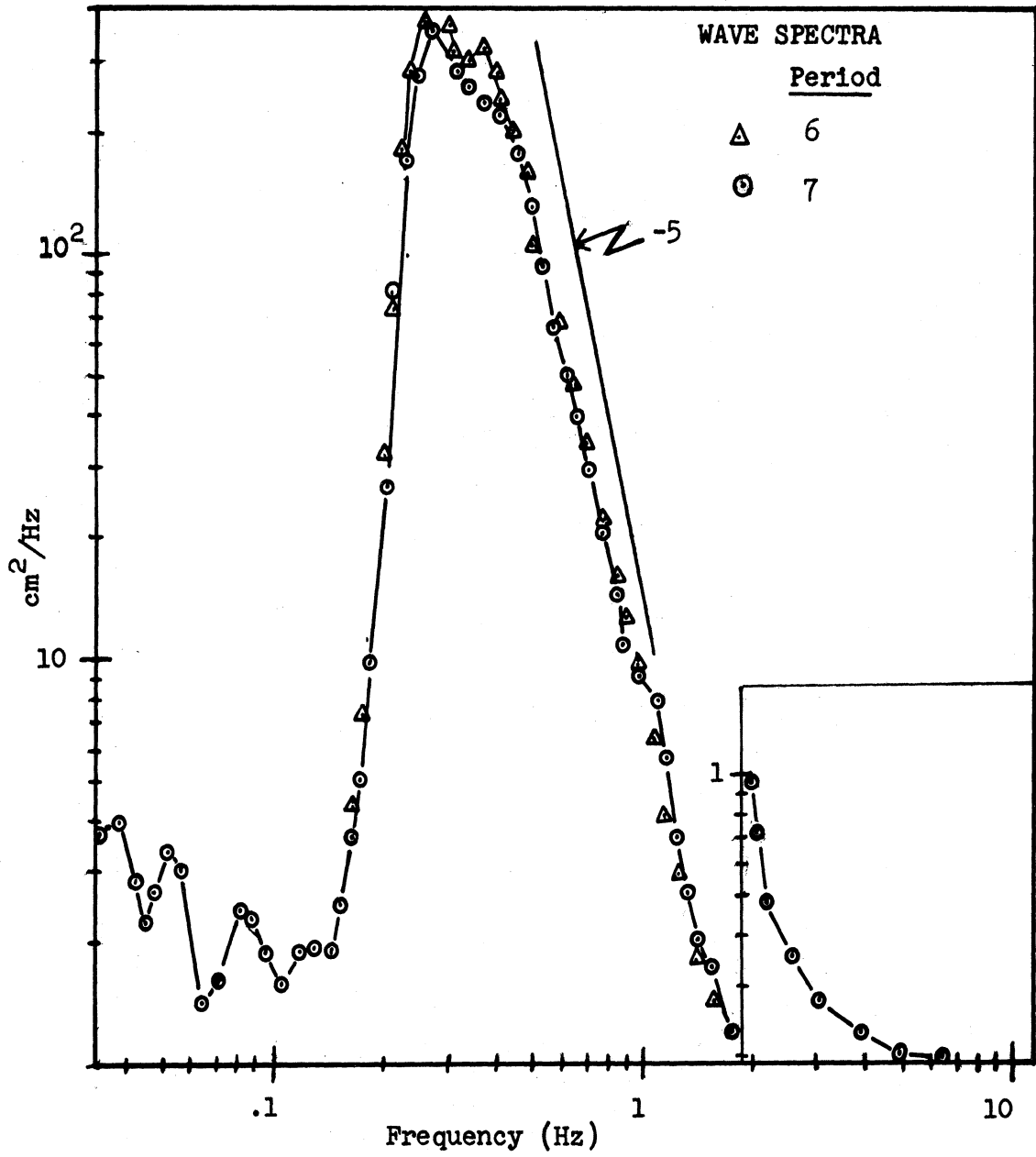


Figure 6.24: Wave spectral estimates for Periods 6 and 7.

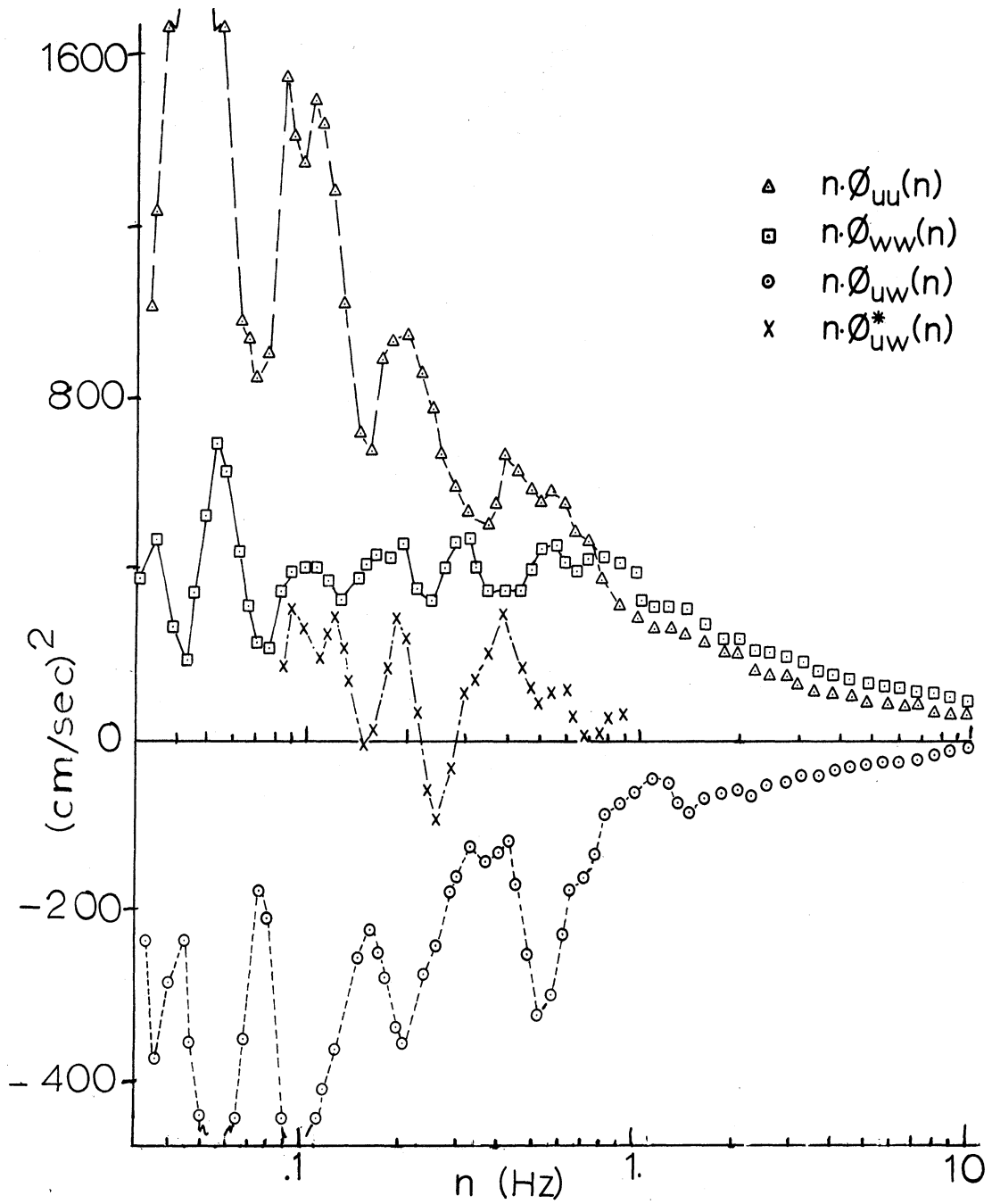


Figure 6.25: Velocity variance and covariance spectra for Period 6; 4.0 meter level.

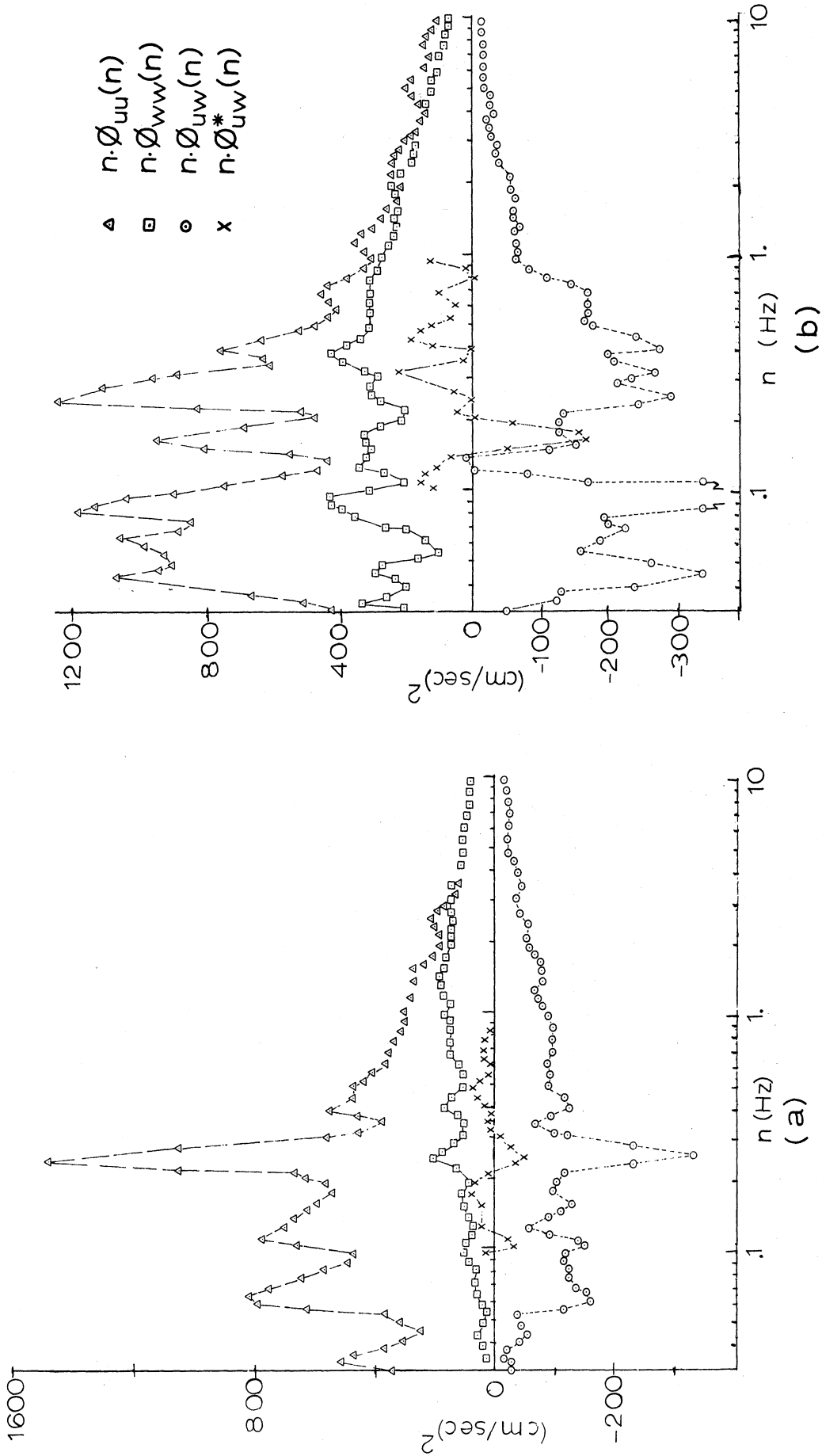
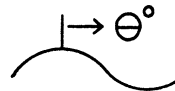


Figure 6.26: Velocity variance and covariance spectra for Period 7; (a) 1.5 meter level, (b) 4.0 meter level.

legend: \square - uw , \circ - ηw , \triangle - ηu ; η = wave

phase : $\left\{ \begin{array}{l} \square w \text{ leads } u \\ \circ w \text{ leads wave} \\ \triangle u \text{ leads wave} \end{array} \right\}$ by θ° 

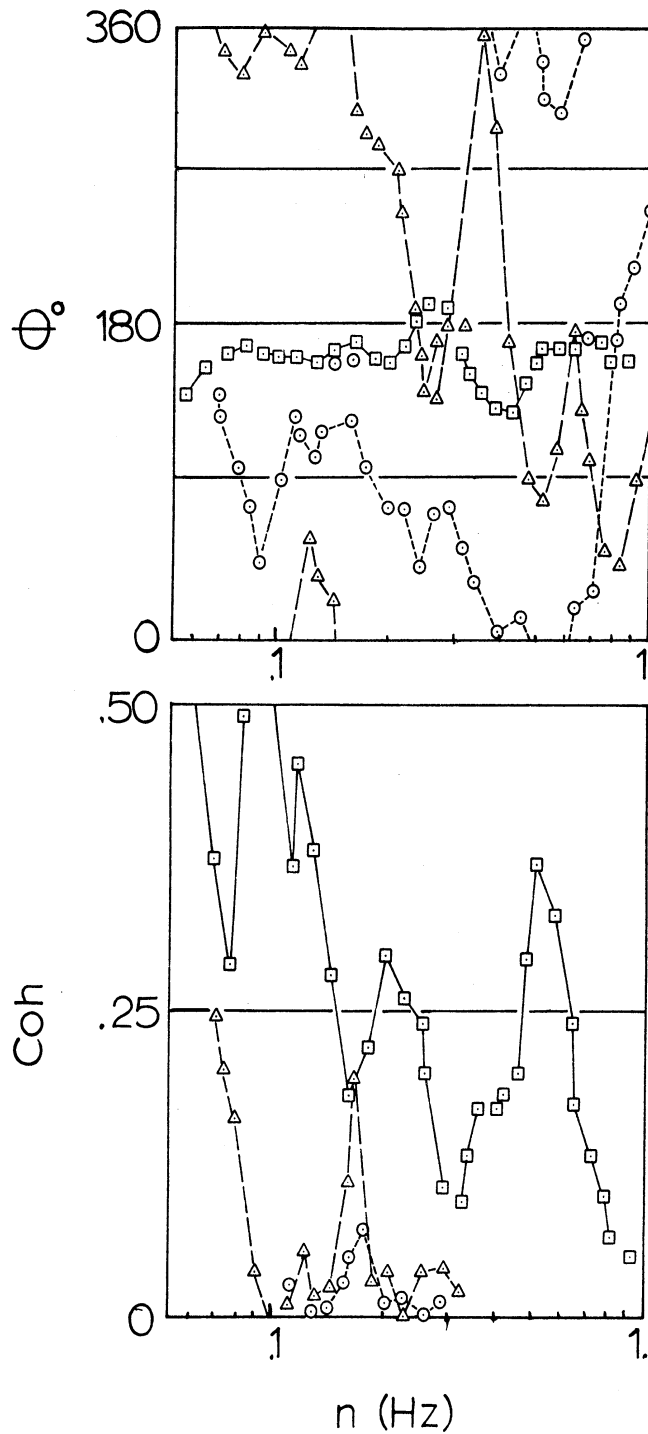
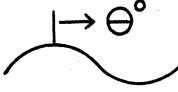


Figure 6.27: Phase and coherence spectra for Period 6; 4.0 meter level.

legend: \square - uw, \circ - η w, \triangle - η u; η = wave

phase : $\left\{ \begin{array}{l} \square \text{ w leads u} \\ \circ \text{ w leads wave} \\ \triangle \text{ u leads wave} \end{array} \right\}$ by θ° 

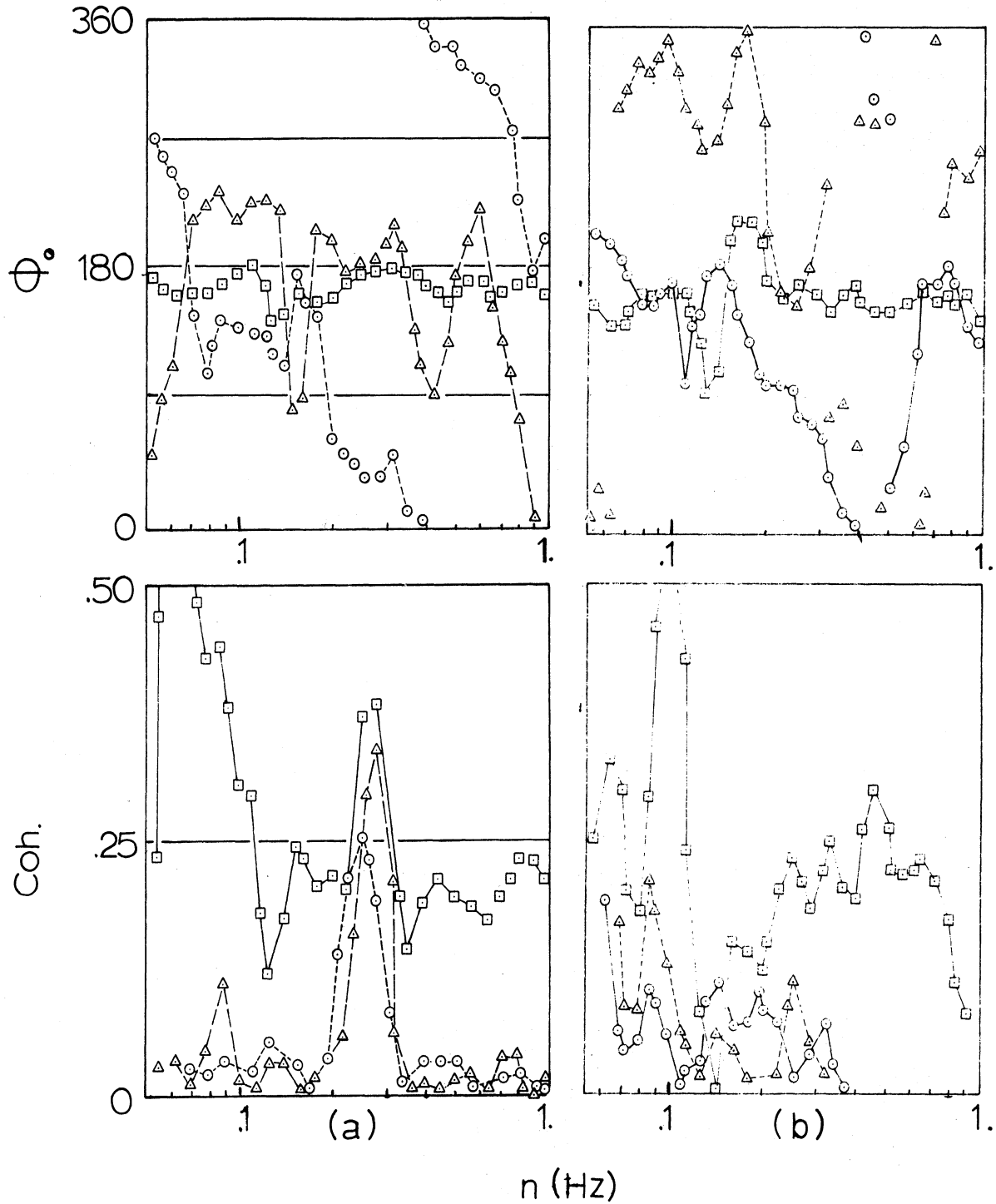


Figure 6.28: Phase and coherence spectra for Period 7; (a) 1.5 meter level, (b) 4.0 meter level.

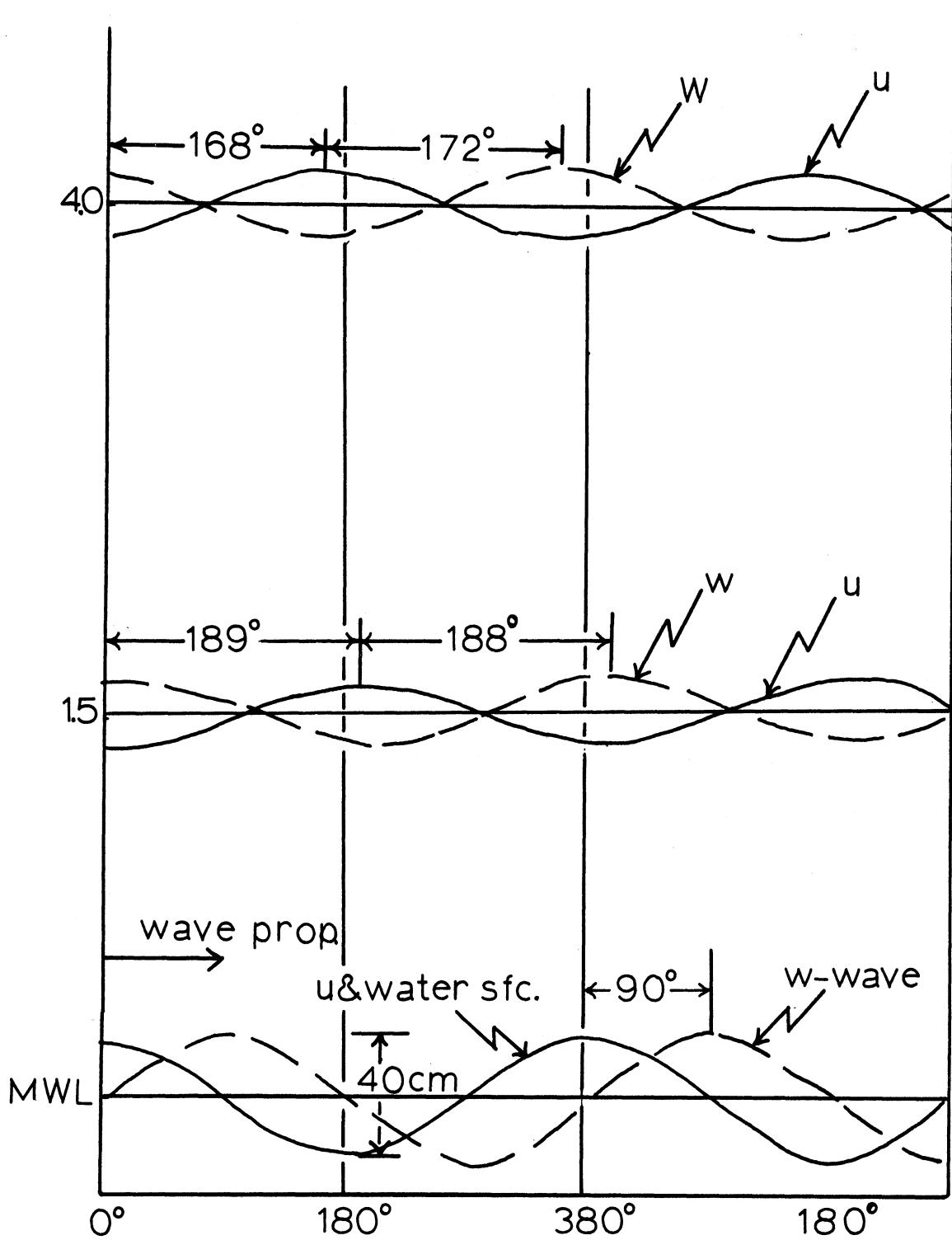


Figure 6.29: Composite schematic of phase relations between velocity components and waves at .26 Hz for Period 7.

6.2.4 Results from 27 September (Periods 8, 9 and 10)

<u>Period</u>	<u>Time EST</u>	<u>Measurement level (meters)</u>
8	1120-1138	1.0 and 2.0
9	1140-1158	1.0 and 2.0
10	1200-1218	1.0

These periods, which have data for levels 1 meter apart, are distinguished from others by significant phase shifts in the wave-induced w component.

6.2.4.1 General conditions

Figure 6.30 shows that moderate wind speeds occurred during the morning (0000-0600 EST) and generated a wave field which persisted through mid-morning. A decrease in wind and associated decrease in the wave heights occurred from 0800 to 1100. After 1100 EST, increasing wind speeds appeared to maintain the wave conditions at equilibrium throughout the afternoon. The water surface temperature was 3°C higher than the air temperature at 4.0 meters.

Figure 6.31 shows a general increase of wind speed through the periods with some variation in wave height. Wind profiles exhibit little curvature but there is evidence of a "kink" at 2.0 meters. The distinct change in temperature from 2.0 to 4.0 meters is attributed to an aspirating system, common for the lower three levels, that was not functioning properly. The temperature profile from 4 to 15 meters shows a nearly neutral hydrostatic condition. This was unexpected because of the large air-water temperature

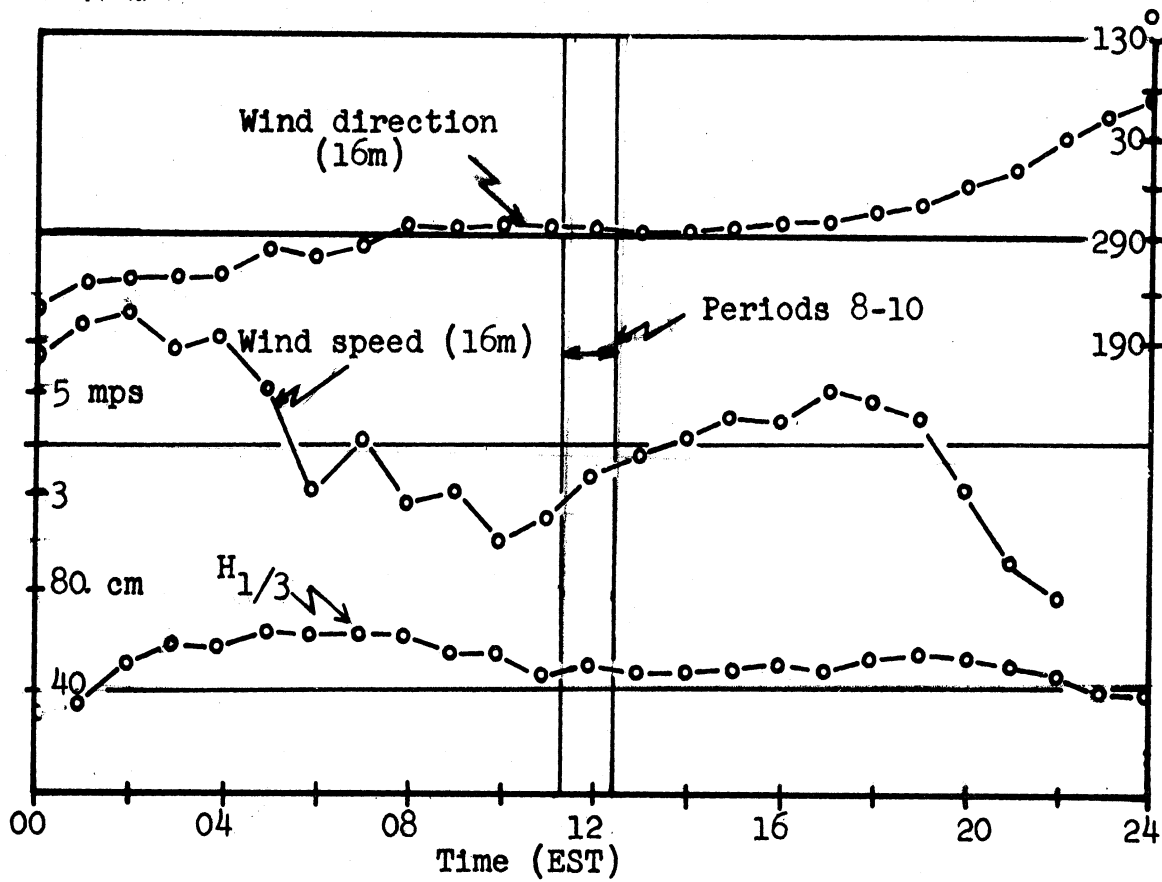
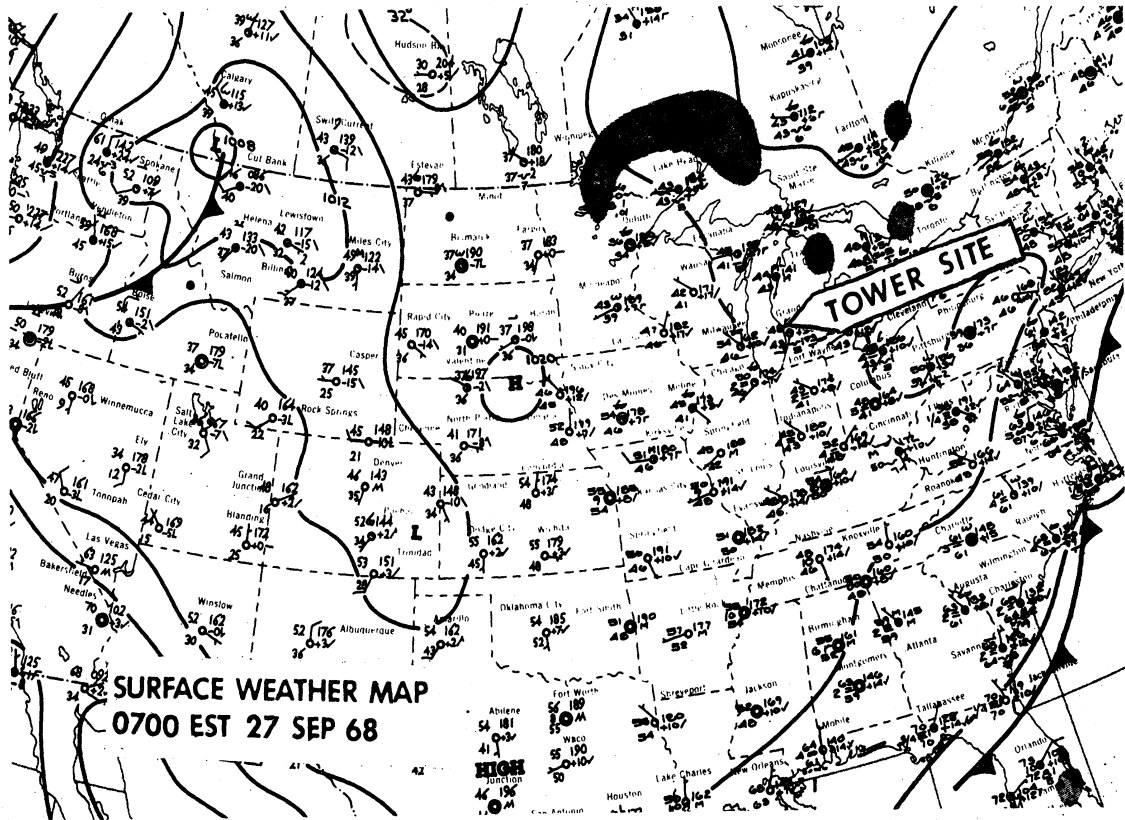


Figure 6.30: General conditions for 27 September, 1968.

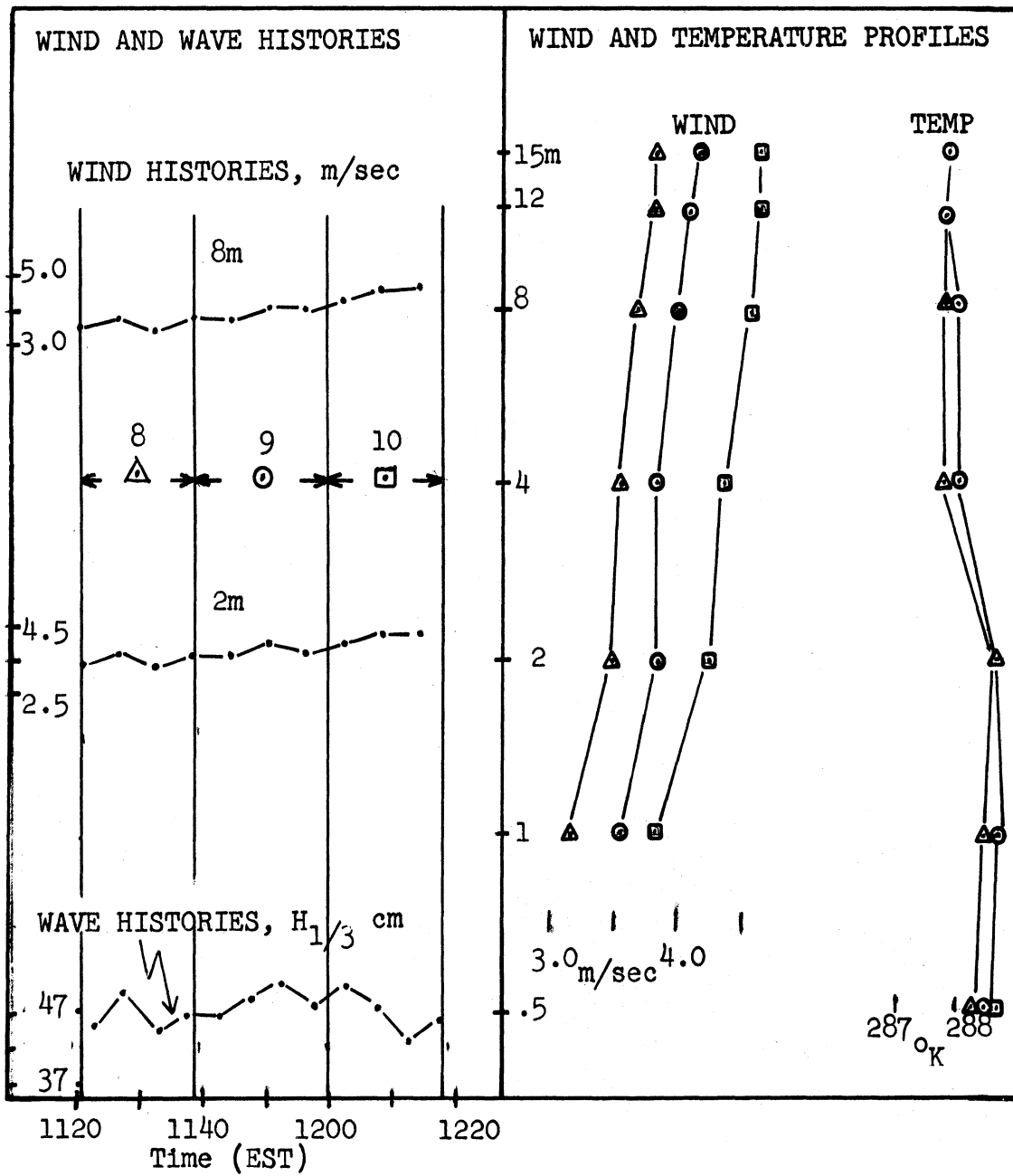


Figure 6.31: General conditions for times encompassing Periods 8, 9 and 10.

difference. Because of the light winds, the critical level for these periods was effectively at infinity.

6.2.4.2 Spectral Results

Wave spectra appear in Figure 6.32 and velocity variance and covariance results appear in Figures 6.33 (Period 8), 6.34 (Period 9) and 6.35 (Period 10). Wave spectra show that all periods have peaks near .26 Hz and that Periods 8 and 10 have deviations from an approximate -5 slope near .4 Hz. The abrupt rise of the forward face occurs near .15 Hz.

A significant feature of the covariance spectra (Figures 6.33 and 6.34) is that the quadrature spectra near .26 Hz changed sign between the two levels. The sign change occurs with distinct extrema and is associated with a phase shift of w , with respect to the wave, between the two levels. An 8° rotation was performed on the results for the 2 meter level but had no influence on the interpretations in this section¹.

Variance spectra, at all levels, show maxima in both u and w near .26 Hz. At the wave-induced peak, w has a distinct maximum at both levels which is less than u at the lower level and approximately the same as u at the upper levels. At the 2.0 meter level, u spectra have peaks of the same magnitude as that at .26 Hz, at frequencies corresponding with the forward faces of the wave spectra. Also during Period 8, u has a signifi-

¹Appendix B, Section B.2, includes spectral results for 2.0 meters in Period 8, for 0° , 4° and 8° rotations.

cant peak near .5 Hz which coincides with a deviation from an approximate -5 slope in wave spectrum during this period.

Cospectra at 1.0 meter have narrow bands of minima near .26 Hz, at 2.0 meters the corresponding bands are definitely broader. The broadening appears to be associated with similar features in the u spectra.

Figure 6.36, 6.37 and 6.38 show phase and coherence spectra for Period 8, 9 and 10 respectively. The following refers to the frequency band near .26 Hz. Phase spectra for 1.0 meter in all periods show that w and u lead the wave by about 80° and about 200° respectively and have high coherence values in this band. At the 2.0 meter level, w and u lead the wave by about 280° and about 170° respectively and the η_w computation has high coherence values.

Figure 6.37 is a schematic which shows the phase relationships between the velocity components and the waves at .26 Hz for Period 9 which is representative of the three periods. Values used in the composite appear in Table 6.1, page 103. This figure shows a significant shift of w over the 1 meter vertical distance.

Two significant points of these results are:

- 1) Variance spectra and cospectra show direct significant wave induced motion. There is distinct evidence of broadening of extrema within this band with height even though the levels were separated by only one meter.
- 2) Because w shifted phase, with respect to the wave,

so much between 1.0 and 2.0 meters, one questions if simple streamline bending is the characteristic feature of the waves' influence on the airflow.

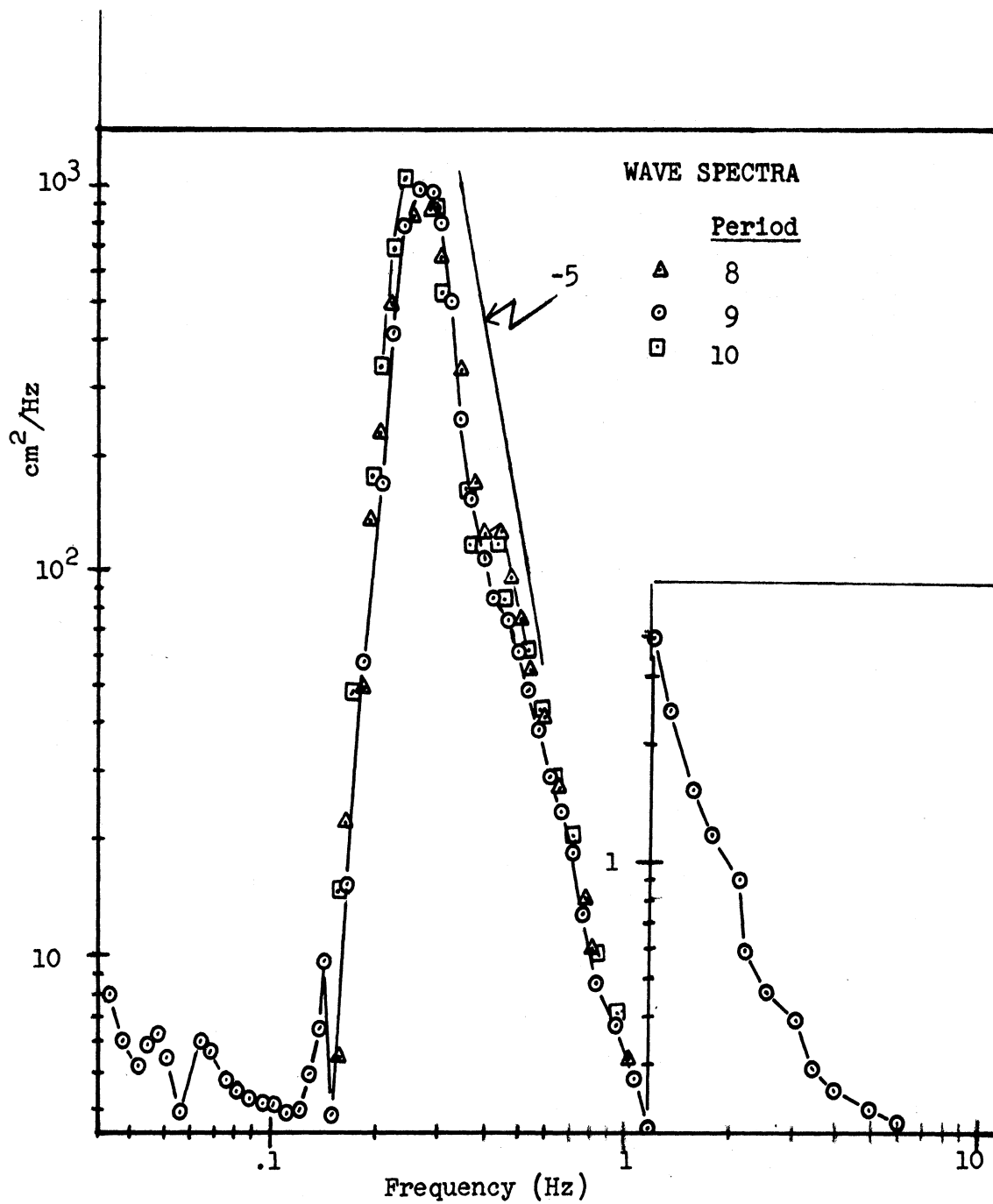


Figure 6.32: Wave spectral estimates for Periods 8, 9 and 10.

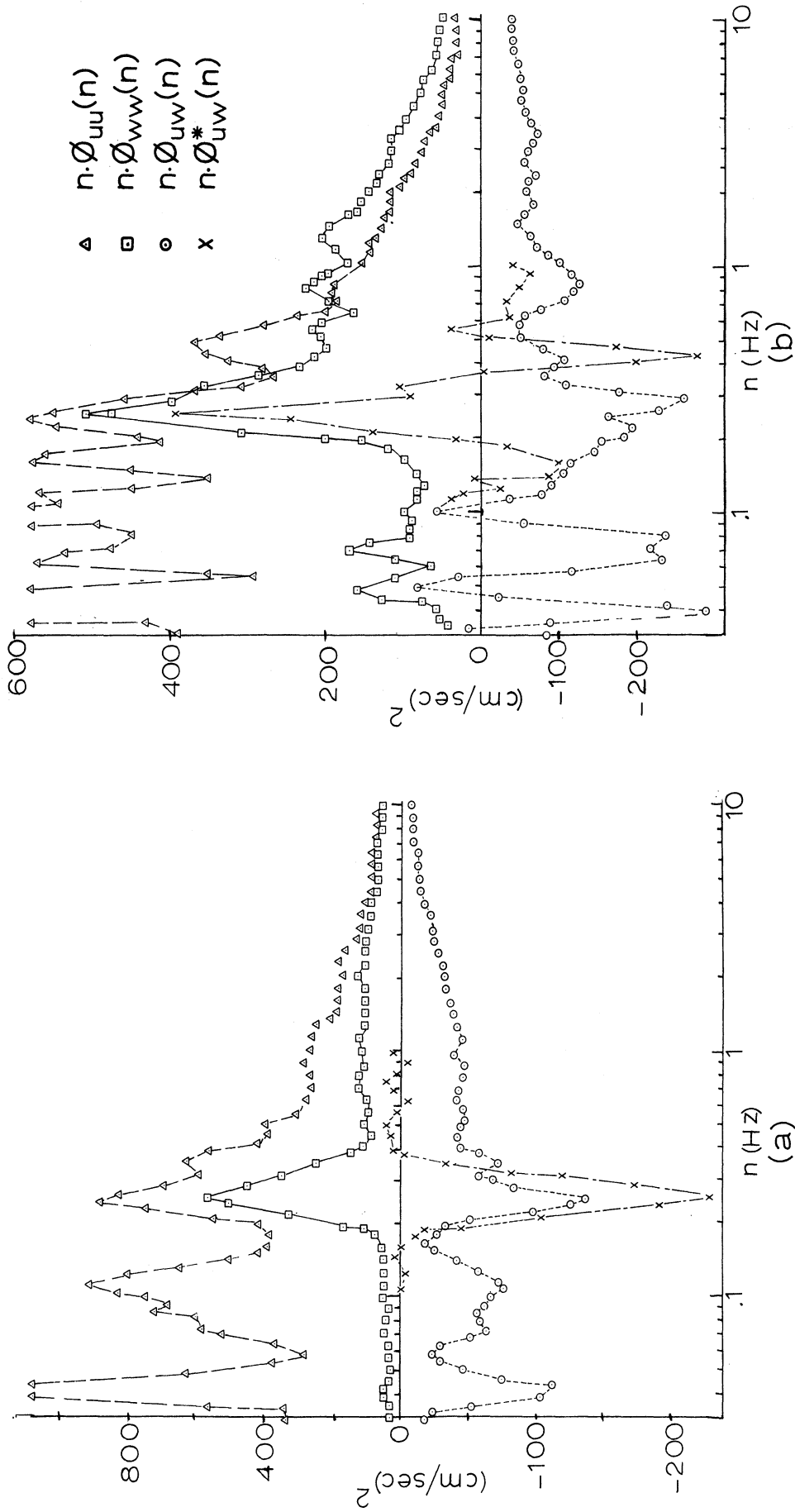


Figure 6.33: Velocity variance and covariance spectra for Period 8; (a) 1.0 meter level, (b) 2.0 meter level.

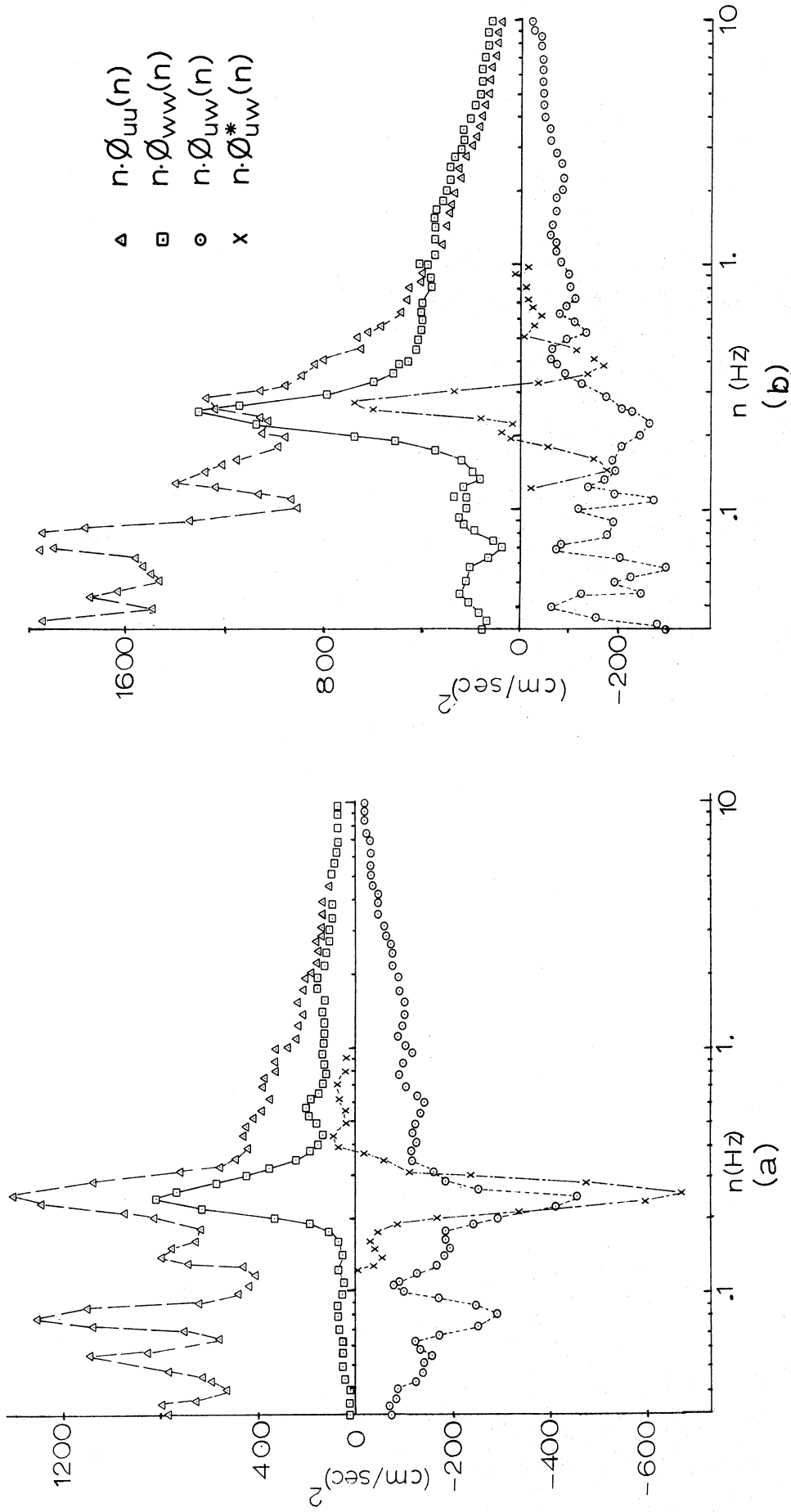


Figure 6.34: Velocity variance and covariance spectra for Period 9; (a) 1.0 meter level, (b) 2.0 meter level.

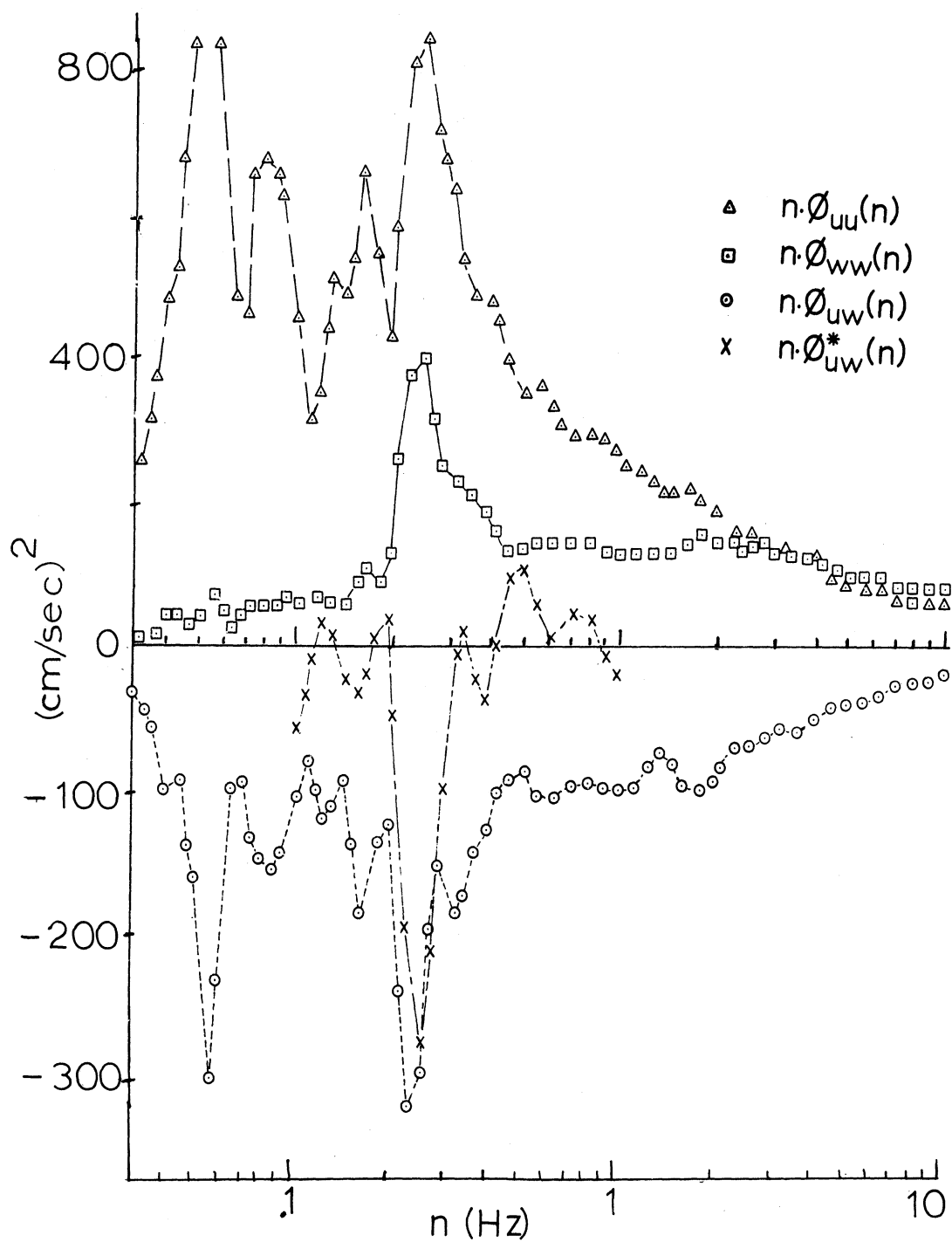
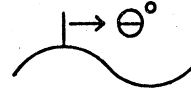


Figure 6.35: Velocity variance and covariance spectra for Period 10; 1.0 meter level.

legend: \square - uw, \circ - η w, \triangle - η u; η = wave

phase : $\left\{ \begin{array}{l} \square \text{ w leads u} \\ \circ \text{ w leads wave} \\ \triangle \text{ u leads wave} \end{array} \right\}$ by θ° 

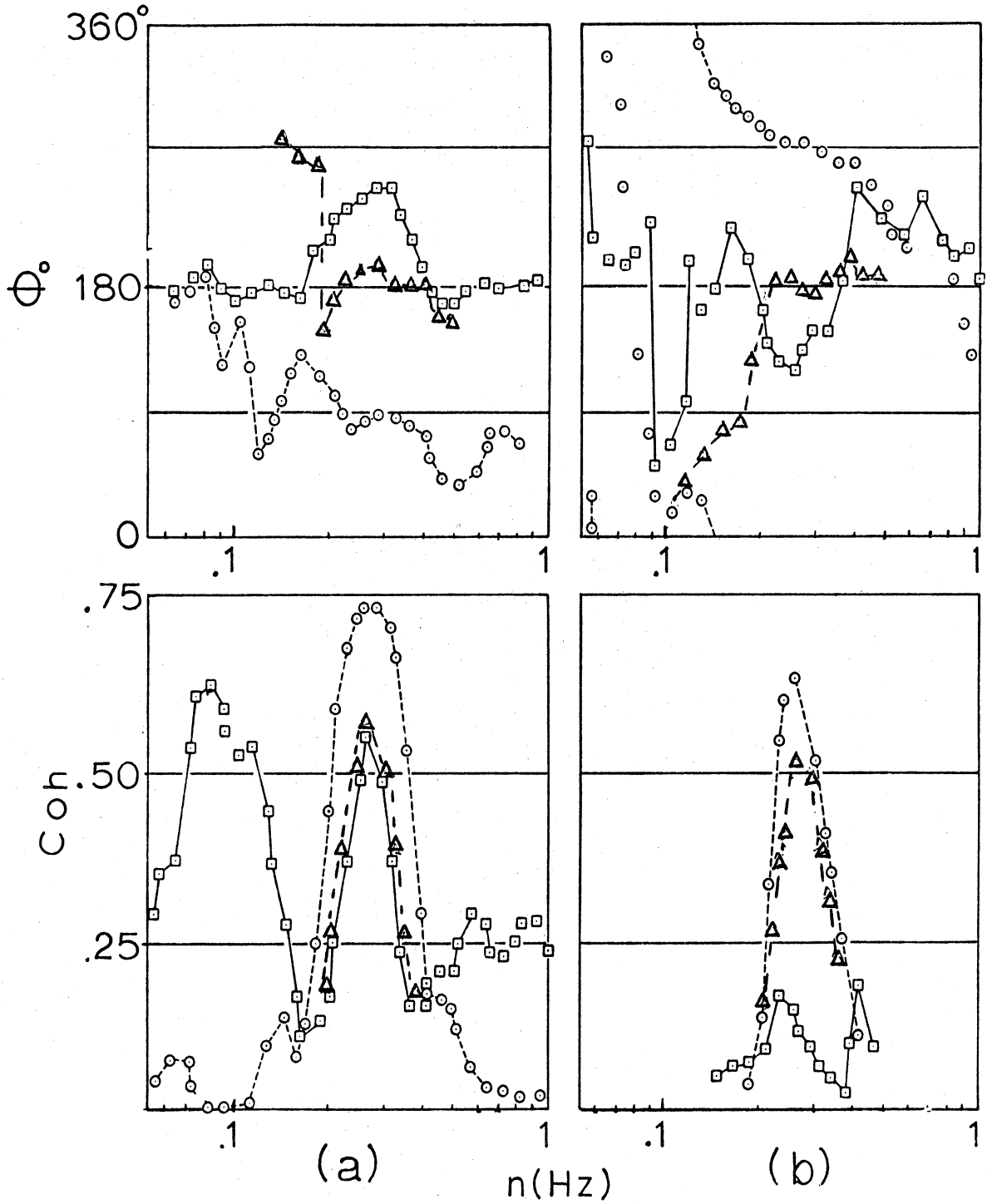
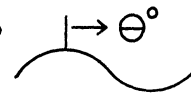


Figure 6.36: Phase and coherence spectra for Period 8; (a) 1.0 meter level, (b) 2.0 meter level.

legend: \square - uw , \circ - ηw , Δ - ηu ; η = wave

phase : $\left\{ \begin{array}{l} \square \text{ } w \text{ leads } u \\ \circ \text{ } w \text{ leads wave} \\ \Delta \text{ } u \text{ leads wave} \end{array} \right\}$ by θ° 

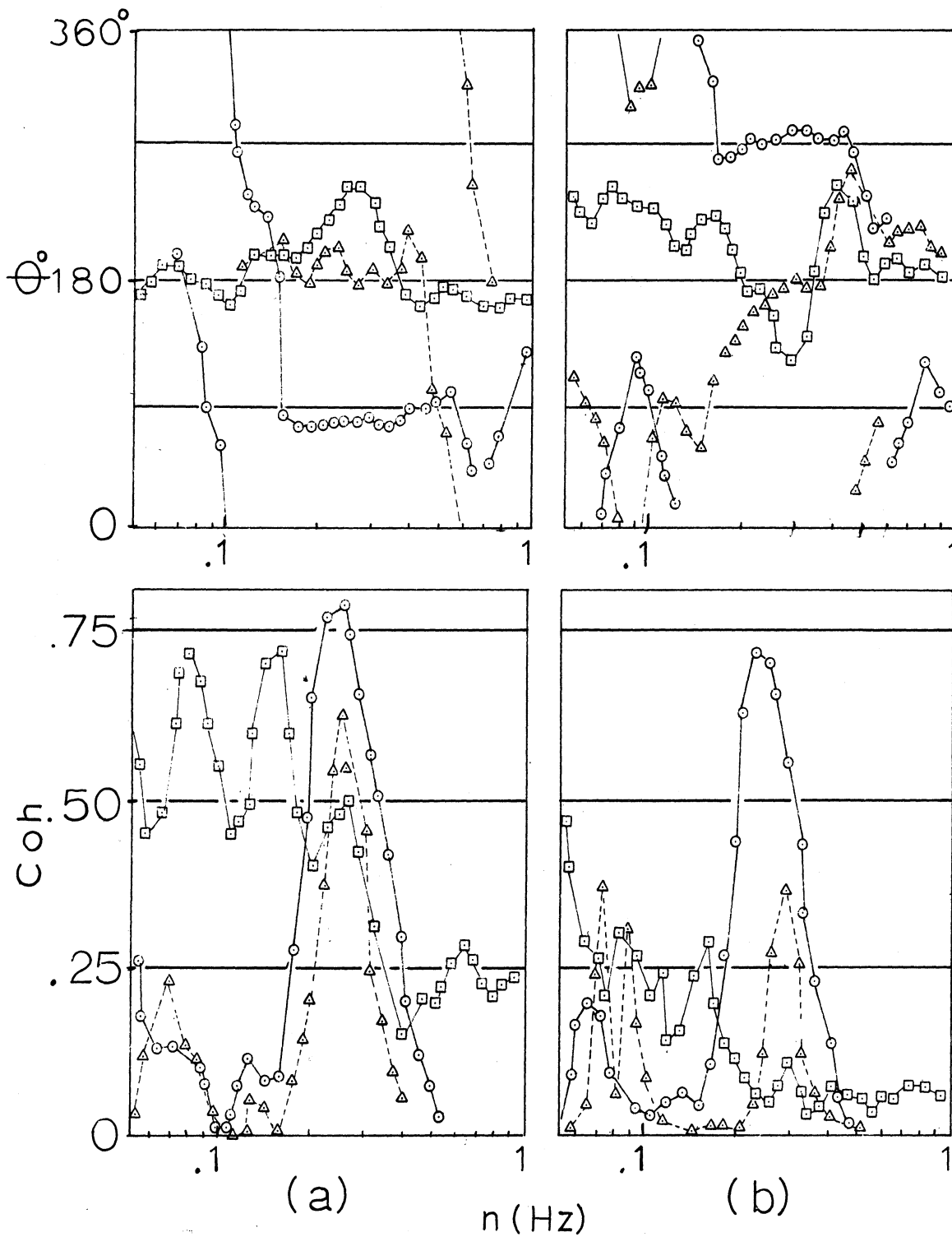
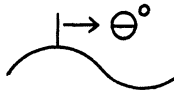


Figure 6.37: Phase and coherence spectra for Period 9; (a) 1.0 meter level, (b) 2.0 meter level.

legend: \square - uw , \circ - ηw , \triangle - ηu ; η = wave

phase : $\left\{ \begin{array}{l} \square w \text{ leads } u \\ \circ w \text{ leads wave} \\ \triangle u \text{ leads wave} \end{array} \right\}$ by θ° 

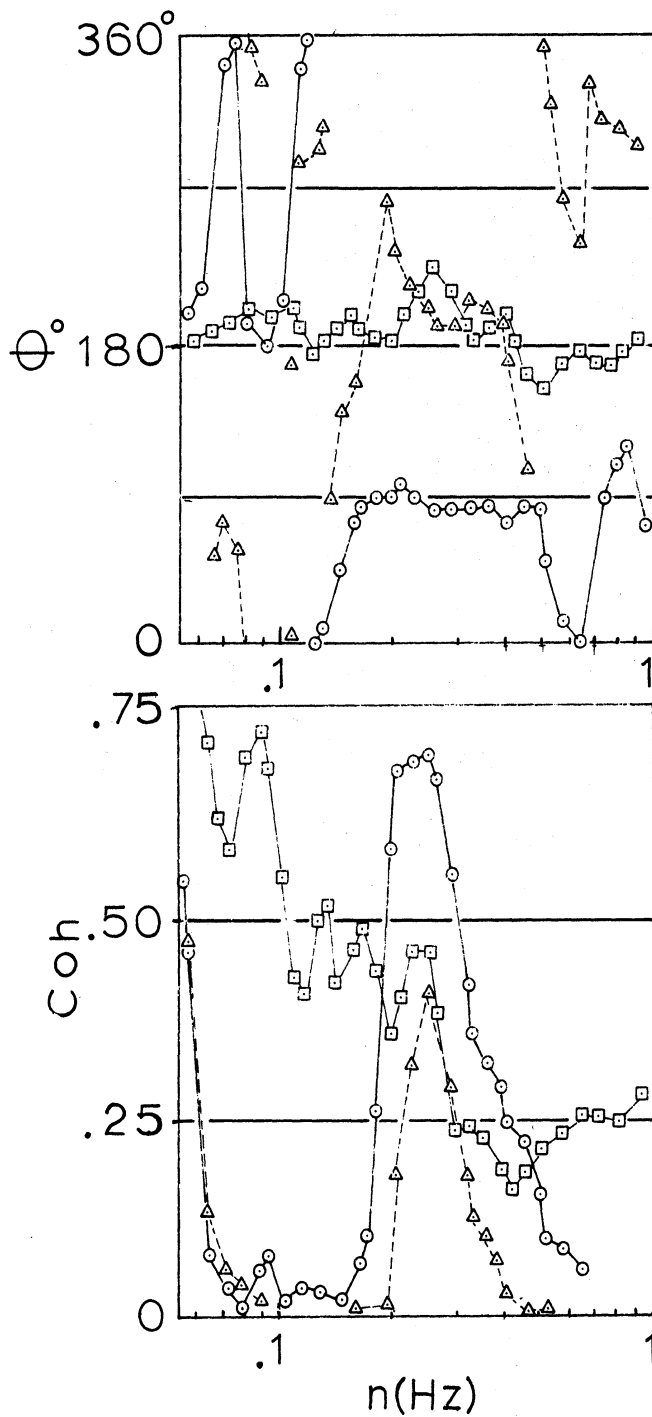


Figure 6.38: Phase and coherence spectra for Period 10; 1.0 meter level.

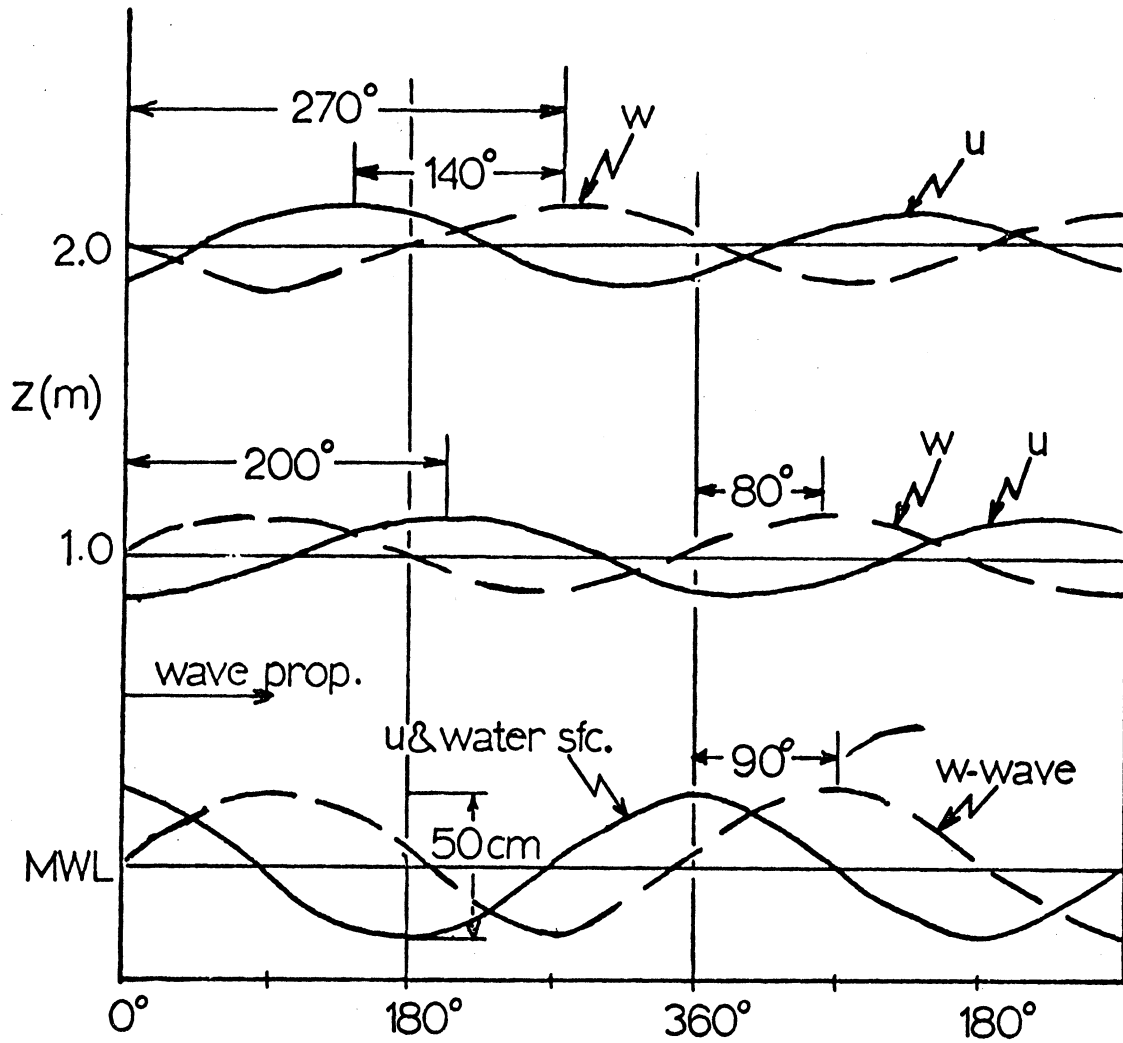


Figure 6.39: Schematic of phase relations between velocity components and waves at .26 Hz for Period 9.

6.2.5 Results for 5 October (Period 11)

<u>Period</u>	<u>Time EST</u>
11	1650-1708

Two interesting aspects associated with this period are:

- i) The critical level (z_c) associated with the wave spectrum peak (.33 Hz) was near 1.5 meters which was between the two measurement levels, and
- ii) The wave spectrum was similar to that which was observed during Period 5 (26 September, 1100), in which a wave component below the frequency of maximum amplitude appeared to be developing. The wave spectrum peak was at .33 Hz and the lower frequency was near .26 Hz.

6.2.5.1 General conditions

Figure 6.40 does not include wave histories because the staff gauge system was not working. The wind direction became southerly by 1200 and resulted in general stable conditions with the temperature at 4 meters being 1.5°C higher than the water surface temperature (Table 5.2). The sky was clear and white caps were not observed.

Figure 6.41 shows that the wind speed was steady during the observation period. The temperature profile shows the stable conditions which existed. The wind profile shows that a mean wind of 6 m/sec occurred near the 12 meter level. The latter result is important because the wave frequency which appeared to have significant velocity spectral results was

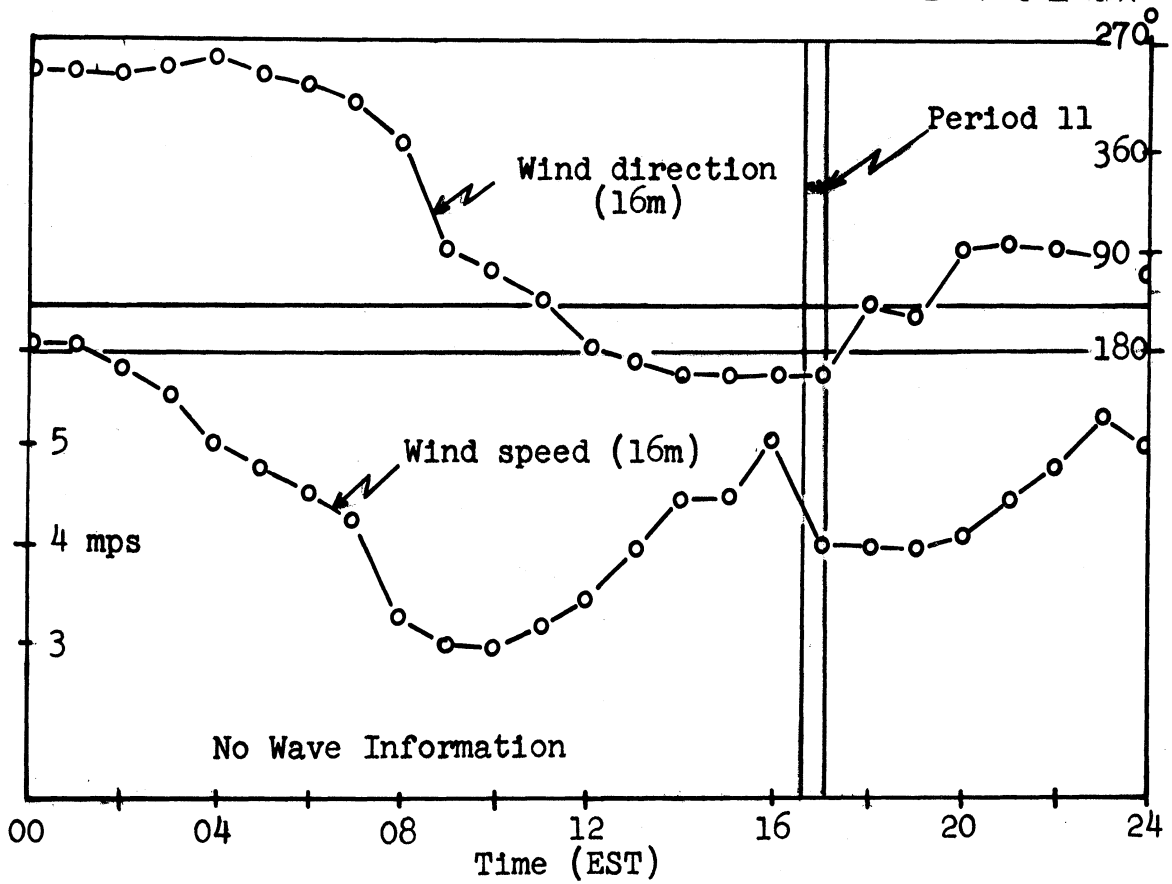
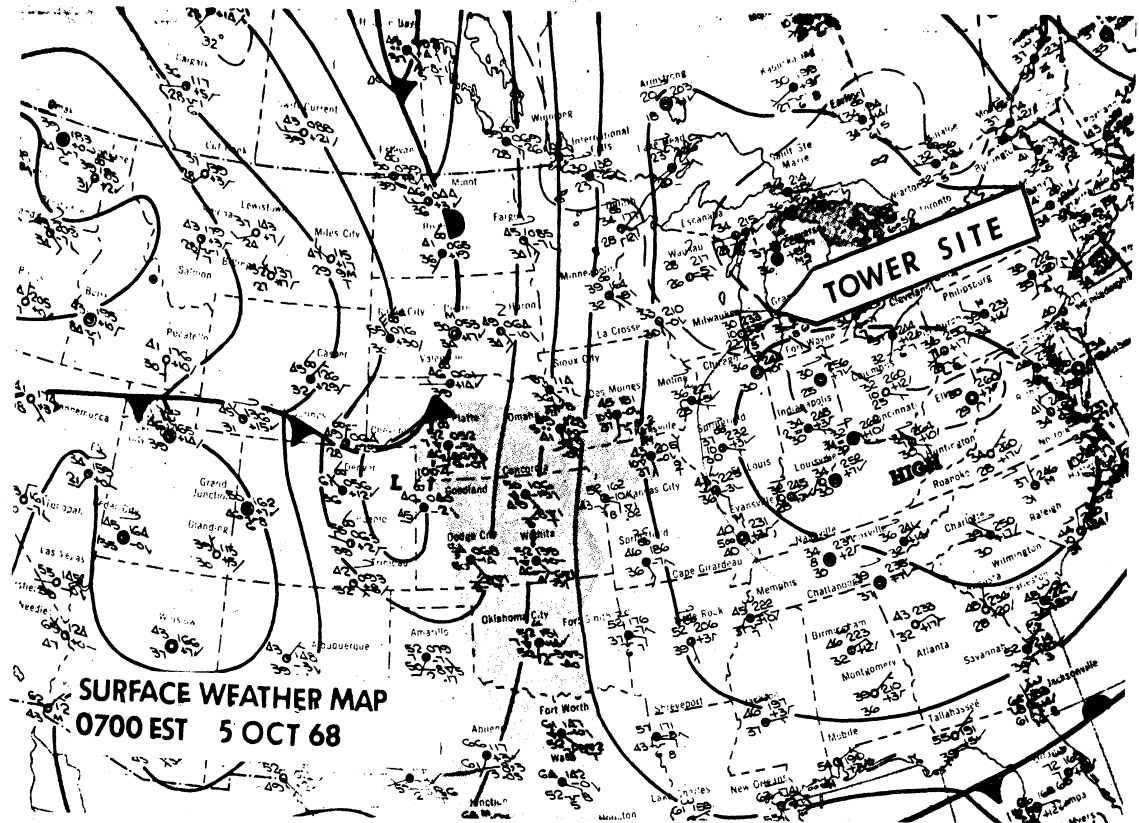


Figure 6.40: General conditions for 5 October, 1968.

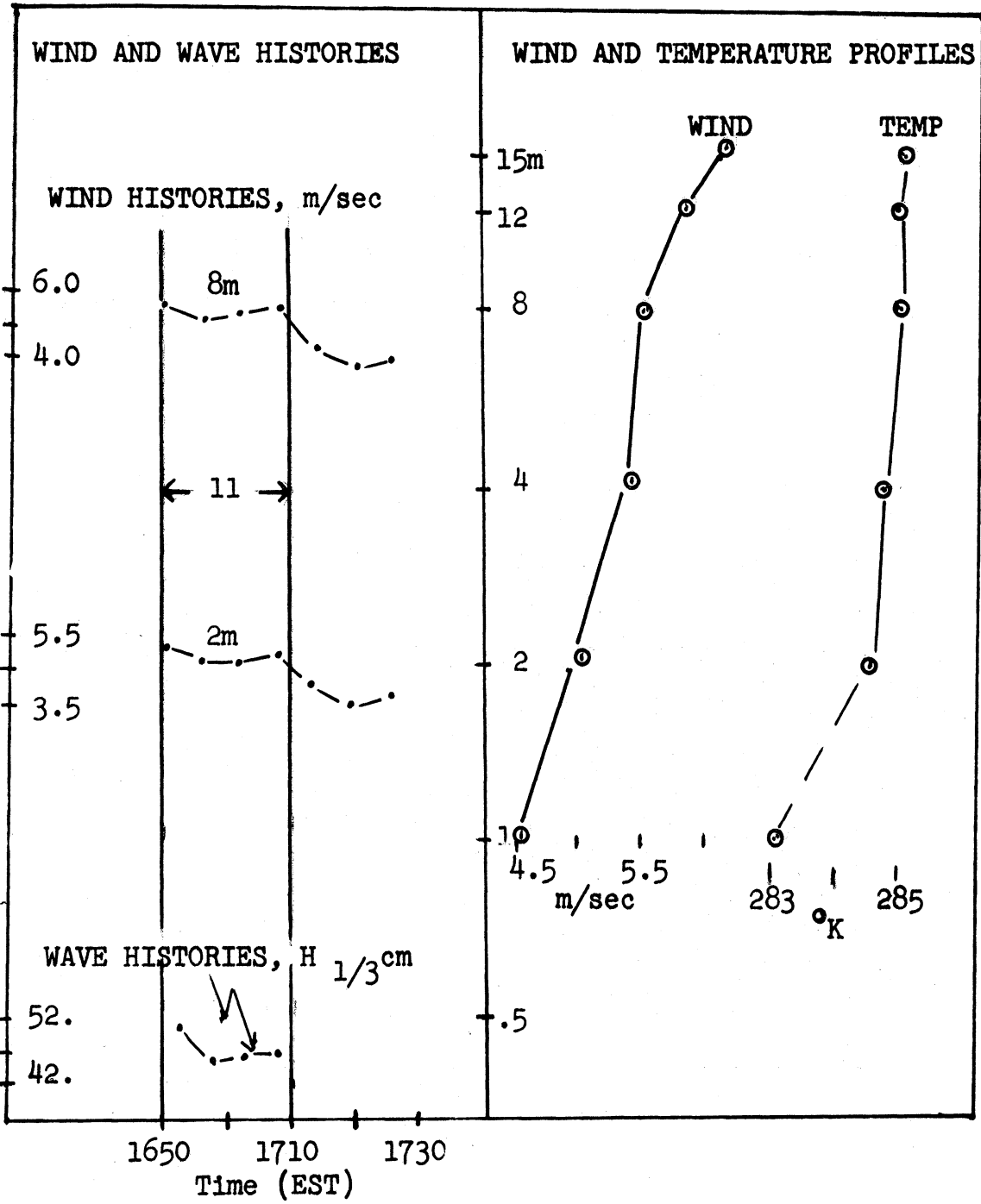


Figure 6.41: General conditions for time encompassing Period 11.

.26 Hz for which $C = 6$ m/sec.

6.2.5.2 Spectral Results

Figure 6.42 shows the wave spectrum for the period. The spectral peak (.33 Hz) is also the lower limit for an equilibrium range (-5 slope region). A secondary maximum appears at a frequency (.26 Hz) lower than that of the spectrum peak.

Figure 6.43 shows variance and covariance spectra. An 8° axis rotation¹ was performed on initial results from the 2.0 meter level to correct for large positive values in a low frequency band (.01-.04 Hz) of the cospectrum. The rotation, however, should have no influence on the spectral features described in this section.

Variance spectra show that both u and w at the lower level (Figure 6.43a) have relative maxima near .26 Hz. For the upper level (Figure 6.43b), variance spectra show that only w has a relative maximum at .33 Hz but it does not, however, have one at .26 Hz.

Covariance spectra for the lower level (Figure 6.43a) show that near .26 Hz the quadrature has relative maximum and cospectrum a relative minimum. For the upper level (Figure 6.43b), the cospectrum shape is significantly different from that observed 1 meter below. It has a relative minimum near .16 Hz which corresponds to a relative minimum in the quadrature spectrum. The quadrature spectrum, however, has a maximum near .26 Hz similar to the lower level.

¹Appendix B, Section B.2 includes spectral results for 2.0 meters for 0° , 4° and 8° rotations.

Figure 6.44 shows phase and coherence relationships for both levels. Phase spectra appear to have distinct preferred values in the neighborhood of .26 Hz. At the lower level (1.0 meter, Figure 6.44a) w leads the wave by 90° and leads u by about 180° . At the upper level, (2.0 meters, Figure 6.44b), w leads the wave by about 110° and leads u by about 160° .

Table 6.1 lists values at .26 Hz. Figure 6.45 is a schematic showing relationships between u and w and the waves at .26 Hz. It shows that, at both levels, the maximum in the horizontal component occurs over the upwind node and that the maximum in the w component occurs over the downwind node of the wave.

Spectral features and phase relationships described in the preceding paragraphs can be summarized as follows;

- 1) Near the frequency (.33) that corresponded to $z/z_c \approx 1$ and to the wave spectrum peak, relative maxima occur in variance spectra of both u and w at the lower level and only in w at the upper level. There are, however, no corresponding extrema in the cospectra at this frequency. Therefore, fluctuations near this frequency reflect primarily those due to pure vertical translation with evidence of strong attenuation with height.
- 2) Near a frequency (.26 Hz) which corresponds to $z/z_c < 1$ there are relative maxima in the u component variance spectra and there are relative minima in the uw co-

spectra. Phase relationships show that u component is a maximum over the upwind node of the wave. This means energy transfer to the waves.

- 3) The influence of stability on the attenuation of the wave indicated undulations was, perhaps, an important factor on the absence of a peak in the u spectra near .33 Hz. Booker and Bretherton (1967) have shown that internal gravity waves are attenuated by a factor $\exp \left[-2\pi(Ri - 1/4)^{\frac{1}{2}} \right]$ at the critical level if the Richardson number (Ri) is greater than .25. In this case, $Ri \approx .21$ so the attenuation as described by Booker and Bretherton could be applicable.

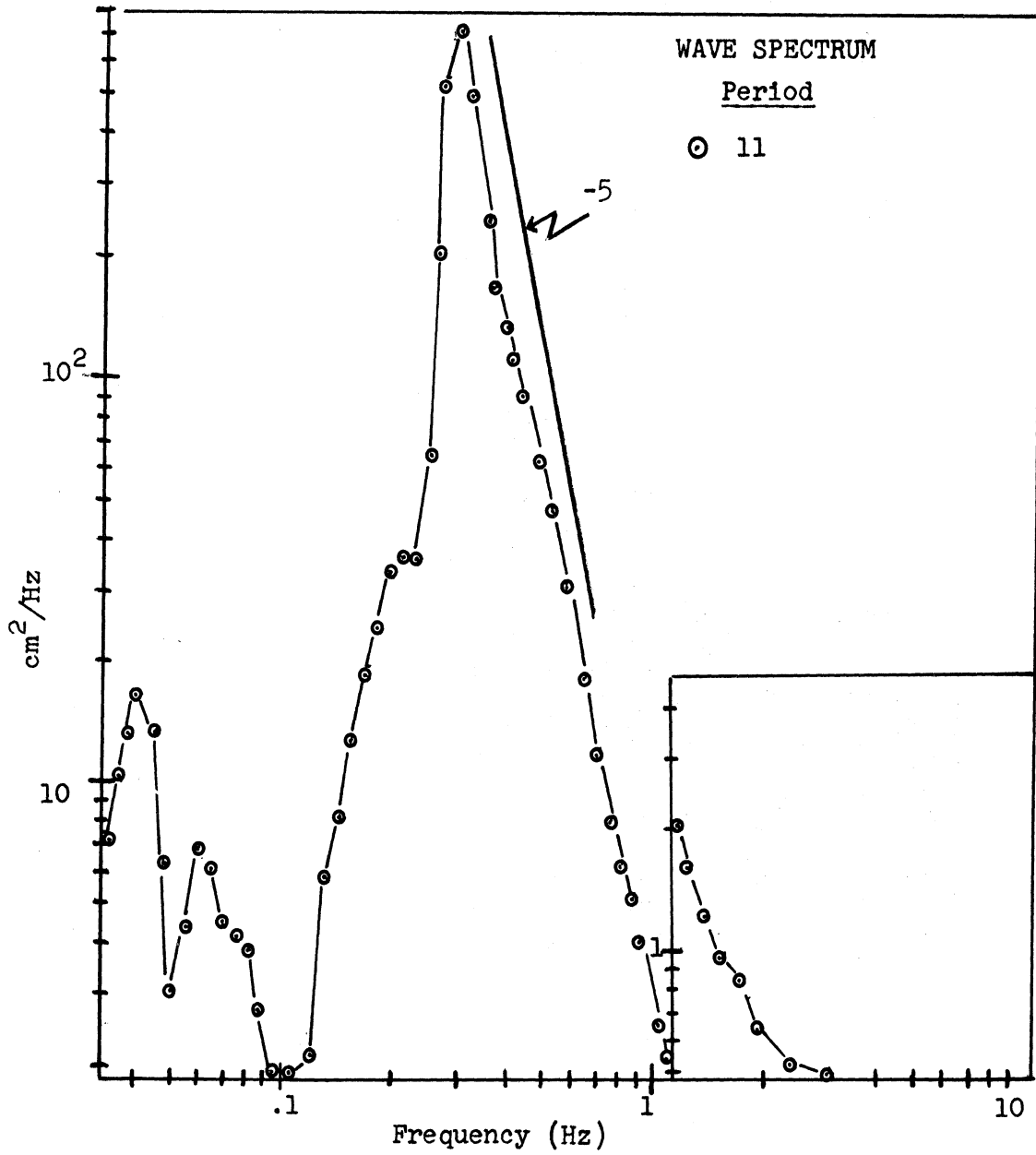


Figure 6.42: Wave spectrum for Period 11.

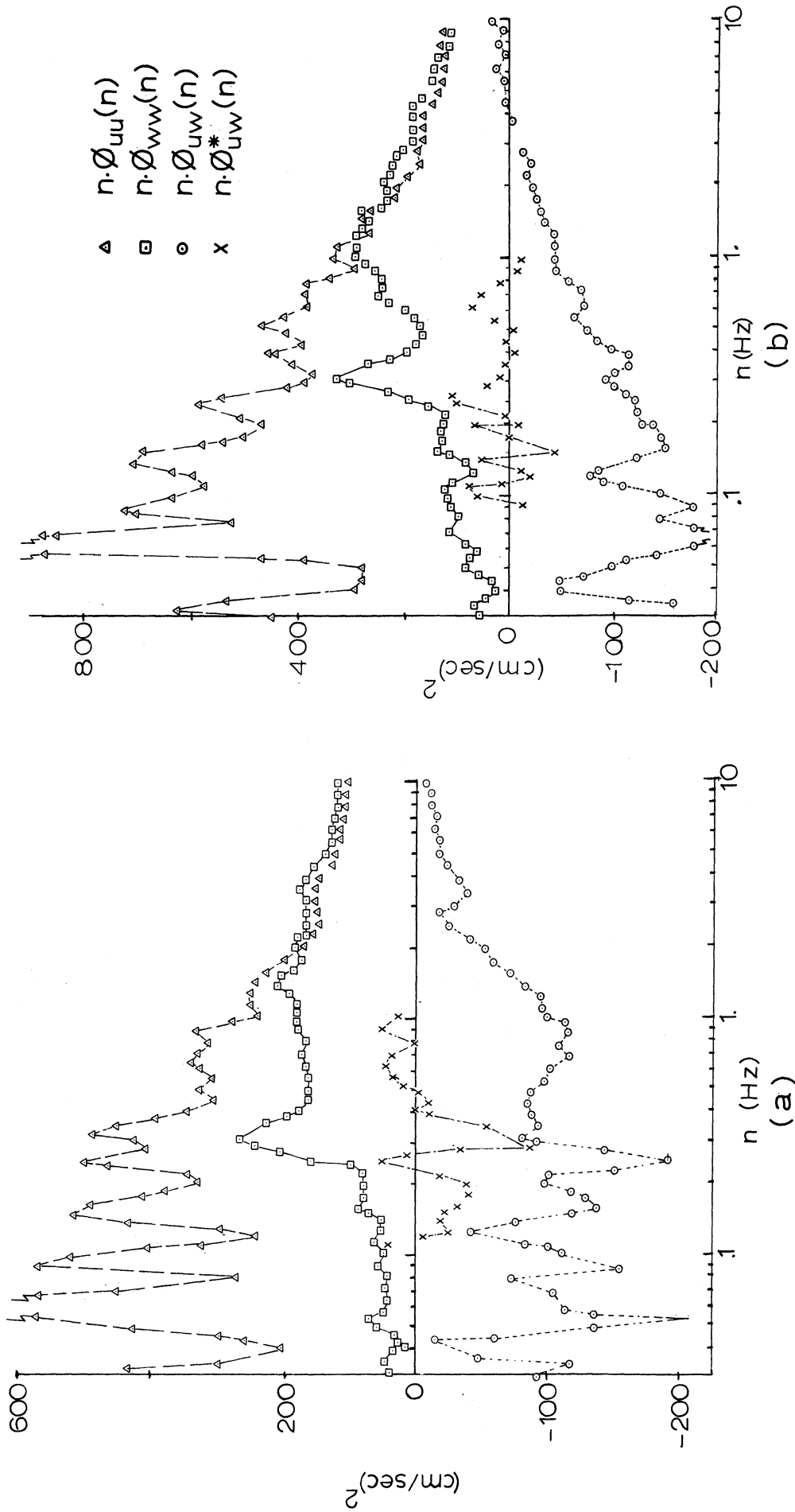
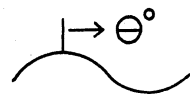


Figure 6.43: Velocity variance and covariance spectra for Period 11; (a) 1.0 meter level, (b) 2.0 meter level.

legend: \square - uw, \circ - η w, Δ - η u; η = wave

phase : $\left\{ \begin{array}{l} \square \text{ w leads u} \\ \circ \text{ w leads wave} \\ \Delta \text{ u leads wave} \end{array} \right\}$ by Θ° 

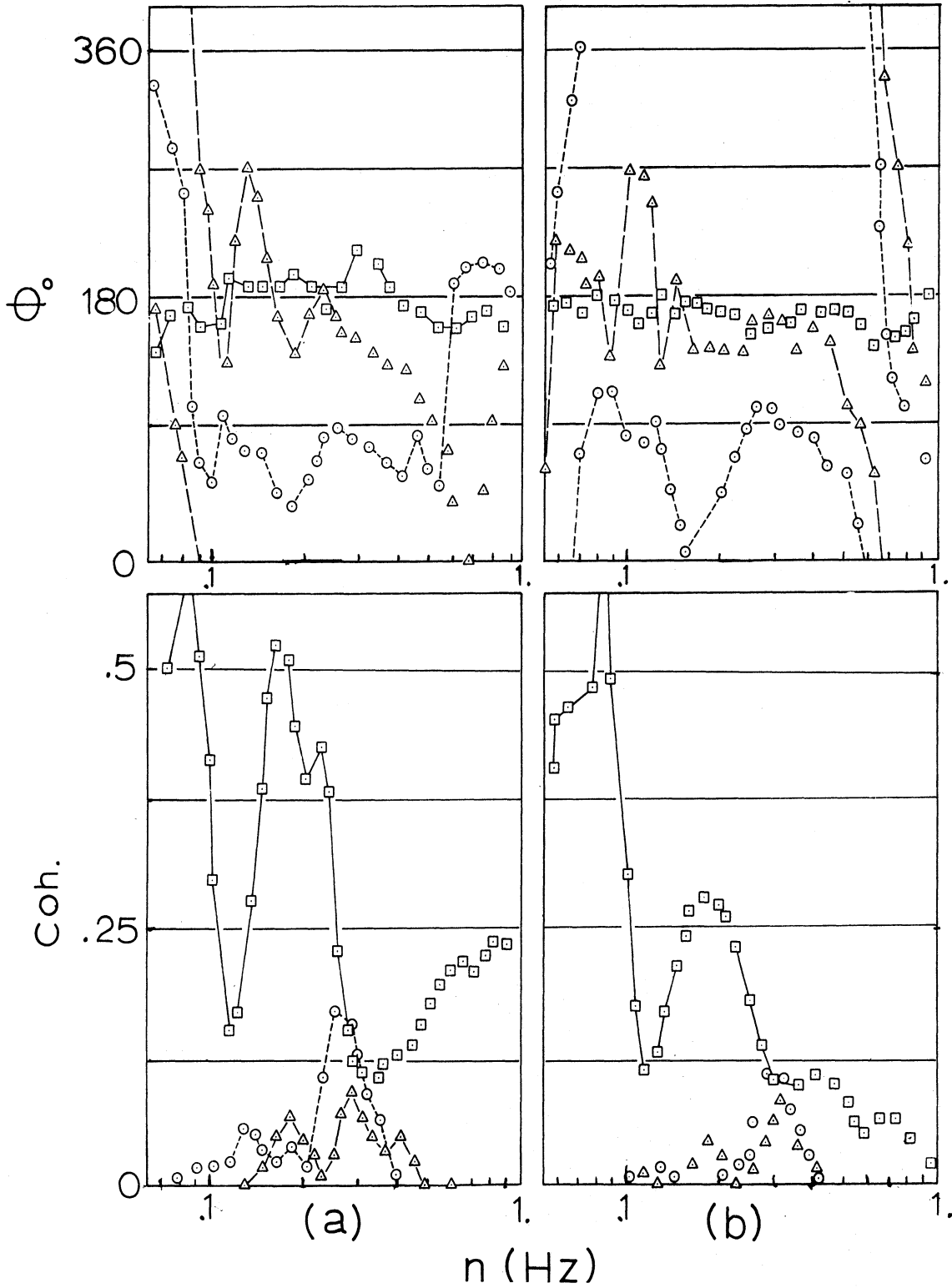


Figure 6.44: Phase and coherence spectra for Period 11; (a) 1.0 meter level, (b) 2.0 meter level.

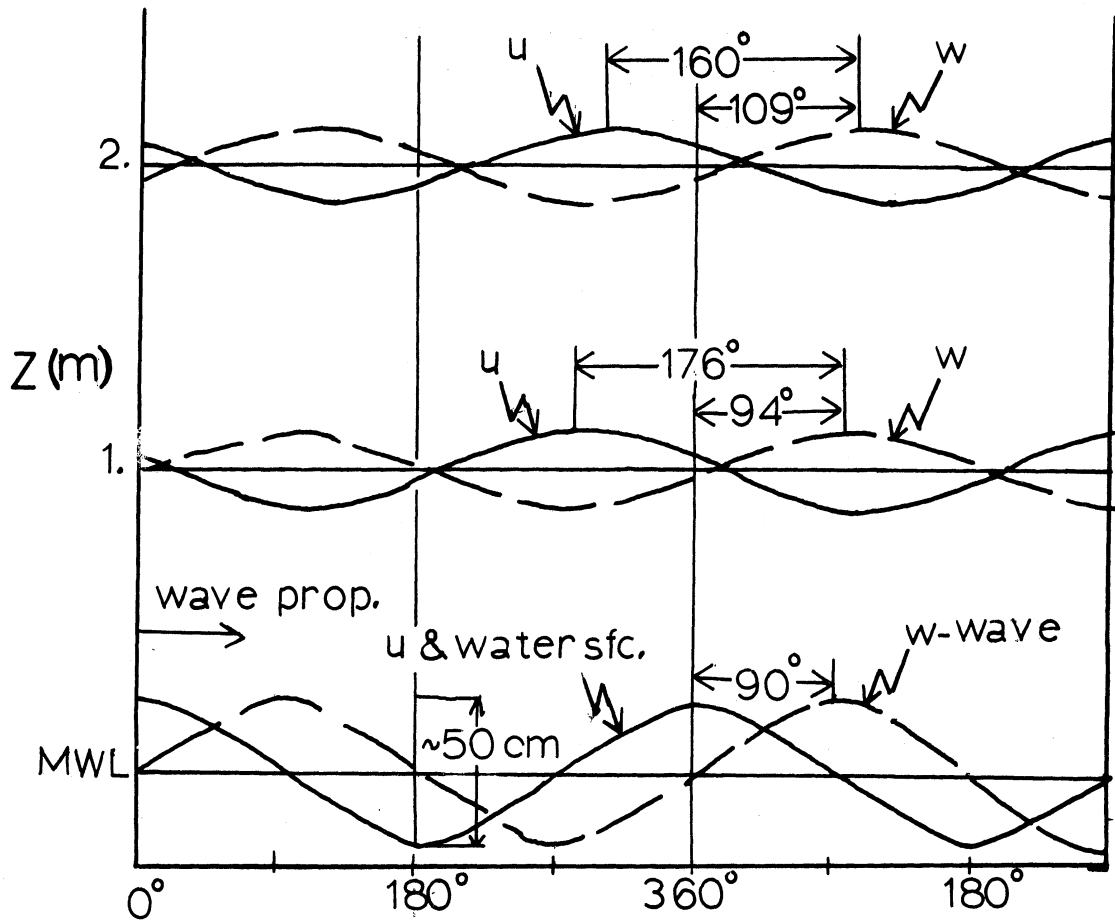


Figure 6.45: Schematic of phase relations between velocity components and waves at .26 Hz for Period 11.

6.3 GENERAL INTERPRETATIONS OF SPECTRAL RESULTS

Results presented in Sections 6.2.1 to 6.2.5 represent those from a coupled system ($u = u_t + \tilde{U}$) consisting of normal turbulent fluctuations (u_t) and those associated with the wave (\tilde{U}). The fact that low coherence values between velocity components and the waves were common is evidence of the relatively high level of "background" turbulence. Close examination of wind-wave coupling for a given period with respect to any existing analytical theory is, therefore, limited. Instead, properties of the airflow resulting from the waves presence are interpreted from composites that represent consistent occurrences of wave-induced spectral extrema and consistent phase relationships between velocity components and the surface waves.

In the following sections, the terms peak and secondary peak apply to features of variance spectra (velocity and wave) which previously were referred to as extrema (usually relative maxima). Cospectral minima and maxima are referred to as reduced and enhanced stress respectively. All references to properties of velocity components apply to their occurrence in frequency space. For example, a maximum u value would mean a spectral estimate of u rather than a real-time value.

Observation conditions are considered as belonging to one of two cases:

Case 1, times when the critical level, or matched layer, was effectively at infinity and, therefore, had no influence on observed spectral results. Periods in this cat-

egory are numbers 1, 2, 6, 7, 8, 9, and 10.

Case 2, times when the critical level was near the level of measurement. The critical level in this case is defined by the frequency of the wave which appeared to correspond to prominent features in velocity spectral results. Periods in this category are numbers 3, 4, 5, and 11.

Case 1 and Case 2 results are interpreted together within two subsections which describe separately, variance (6.3.1) and covariance (6.3.2) spectral results. Separating the spectral results in such a manner and presenting them in this order is useful because of their relative complexity and, perhaps tenableness. The first section (variance) presents the interpretation of the kinematics of the flow as influenced by the waves. The second section (covariance) uses the interpretations of flow kinematics in order to study those features which are responsible for observed stress extrema.

6.3.1 Velocity Variance Results

Peaks and higher frequency secondary peaks were observed for both Cases 1 and 2 and were generally at the same frequency as the corresponding wave spectra peaks. Other investigations which have revealed peaks associated with the waves were discussed in Section 2.3.2. Because measurements were obtained using a sensor at a fixed level above the mean water level, a first interpretation would be that the primary influence of the waves on the adjacent airflow is simple

bending of streamlines. However, Seesholtz (1968) and Yefimov and Sizov (1969) observed similar features with wave following sensors. An important result of these interpretations will be that simple bending of streamlines is not a complete description of the waves' influence on the kinematics of the airflow.

As a point of departure, the occurrence of coincident high frequency secondary peaks in velocity and wave spectra will be interpreted. These peaks, which occurred primarily in the u component, can be interpreted as indicating the occurrence of either of the two following conditions.

- i) Close similarity between the shapes of streamlines in the airflow and the water surface: Since harmonic analysis would generate harmonics at multiples of a primary water wave, which was distorted, secondary harmonics in the velocity field would imply that similar distortion was associated with its streamlines.
- ii) Wave induced fluctuations due to wave components shorter than that of the primary wave.

Because velocity and wave records were obtained and processed with the same kind of harmonic analysis, secondary peaks, at frequencies above primary surface wave frequency, which appeared during Period 1 and 2 (Figure 6.4 and 6.5, pages 113-114), 3 and 4 (1.5 meter level) Figure 6.12-6.13, page 126-127) and 6 (Figure 6.25, page 146) and 8 (2.0 meter, Figure 6.34, page 159) are explained by conditions i). Be-

cause of low coherence values and bandwidth increases at higher frequencies no attempt was made to invoke condition ii).

Dominant velocity peaks that could be associated with characteristics of the wave spectra were observed to be coincident either;

- a) with wave spectrum peaks,
- b) with frequencies of the forward faces of the wave spectra, or
- c) with secondary wave spectrum peaks having frequencies lower than primary peaks.

Velocity peaks associated with forward faces appeared either as individual peaks or as peaks caused by broadening of peaks at adjacent frequencies. The latter occurred at higher levels. Those associated with secondary wave peaks occurred without peaks at the wave spectrum peaks, e.g., Period 5 (Figure 6.21, page 139) and the u component at 2 meters for Period 11 (Figure 6.43, page 172).

Table 6.2 lists amplitudes of the velocity components (u_0 , w_0) at the peaks which were considered dominant and of wave origin. The periods are classified as being Case 1 or 2 and peaks as being of type a), b) or c). The amplitudes were examined to see if their magnitudes can be attributed to simple streamline bending. For this purpose, peaks associated with case 1 observations were normalized with potential flow expressions and a composite constructed in which the normalized values were plotted against z/λ_0 .

If streamline bending accounted for the observed magnitudes of the peaks, magnitudes of u_o and w_o would be related to wave height (H), convected frame velocity ($\bar{U}-C$) and wind shear ($\frac{\partial \bar{U}}{\partial z}$) as follows, (Stewart, 1967),

$$u_o = \left(K \cdot H \cdot (\bar{U}-C) - H \cdot \frac{\partial \bar{U}}{\partial z} \right) \cdot e^{-Kz} \quad 6-1$$

$$w_o = \left[K \cdot H \cdot (\bar{U}-C) \right] \cdot e^{-Kz} \quad 6-2$$

$$K = 2\pi/\lambda_o$$

where λ_o = wave length, wave component (n_o)

H = wave height obtained from $H_{1/3}$ values

\bar{U} = mean wind during period

C = wave speed for wave of frequency n_o .

Non-dimensional quantities (U_n and W_n) which are functions of z and λ_o only can be obtained by dividing the left-hand sides of equations 6-1 and 6-2 by the terms enclosed in [] and [] respectively,

$$U_n = u_o / \left(\quad \right) = \exp(-2\pi z / \lambda_o) \quad 6-3$$

$$W_n = w_o / \left[\quad \right] = \exp(-2\pi z / \lambda_o) \quad 6-4$$

U_n and W_n are magnitudes of the observed peaks "normalized" for different wave, wind speed and wind shear conditions.

Table 6.2 lists values of U_n and W_n for most periods classified as Case 1. Figure 6.46 shows plots of U_n and W_n versus $\ln(z/\lambda_o)$ where the straight solid line represents a functional relation appropriate for potential flow as shown

TABLE 6.2 Amplitudes (u_o, w_o) and Normalized Amplitudes (U_n, W_n) at Dominant Wave Related Peaks

Period	Level	Wave parameters $n(\text{Hz})$	Wave parameters z/λ_o	Case	Peak Type	u_o (cm/sec)	w_o	U_n	W_n
1	1.5	.21	.043	1	a	2.32	2.74	.36	.76
	4.0	.21	.111	1	a	2.75	2.90	.76	1.08
2	1.5	.21	.043	1	a	4.15	3.56	.66**	1.09**
	15.0	.21	.444	1	a	3.80	2.48	normalized	
3	1.5	.26	.065	2	a	1.80	1.10	values	
4	1.5	.26	.065	2	a	2.30	1.07	not	
	4.0	.26	.174	2	a	1.92	1.47	computed	
5	1.5	.26	.065	2	c	3.87	2.23		
	4.0	.26	.174	2	c	3.90	2.13		
6	4.0	.20	.095	1	b	3.20	2.08		
	4.0	.26	.174	1	a	*	*		
7	1.5	.26	.065	1	a	3.50	1.25	2.15	1.85
	4.0	.26	.174	1	a	2.90	1.47	5.16	3.14
8	1.0	.26	.043	1	a	2.50	2.00	.94	1.62
	2.0	.26	.086	1	a	2.04	1.93	1.31	1.20
9	1.0	.26	.043	1	a	3.04	2.34	1.21	1.30
	2.0	.26	.086	1	a	2.48	2.25	1.30	1.48
10	1.0	.24	.037	1	a	2.50	1.76	1.22	2.44
11	1.0	.26	.043	2	b	1.52	*		
	2.0	.26	.086	2	b	2.10	*		

*no apparent wave related peak

** DU

DU and (\bar{U} -C) approximated from closest pro-
DU file results ~20 minutes later

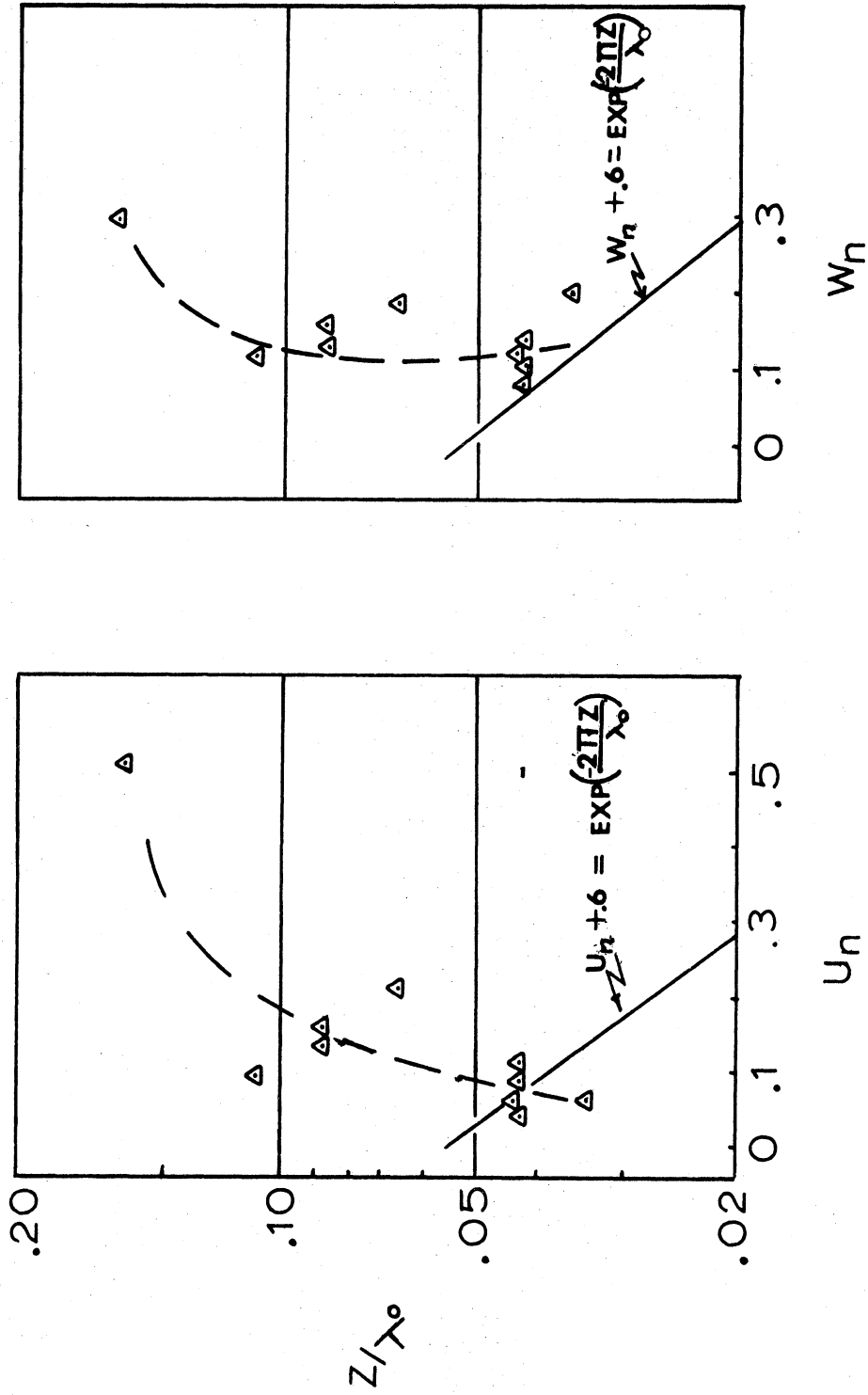


Figure 6.46: Normalized velocity amplitudes (U_n, W_n) at dominant peaks associated with waves' influence versus Z/λ_0 where λ_0 is wave length corresponding to frequency of peak.

by Equations 6-3 and 6-4. The dashed lines, drawn subjectively, show that neither U_n nor W_n have the height dependence predicted by simple streamline bending. U_n appears to increase with z/λ_0 and has, perhaps, a maximum above $z/\lambda_0 = .1$.

The occurrence of a maximum in spectral peak amplitudes at a level above the surface was observed by Yefimov and Sizov (1969) and was shown in this study in Figure 2.4, page 27. They interpreted this as being due to the waves imparting momentum to the air. The results from Period 1 at 1.5 meters provide the most convincing evidence for this interpretation since the cospectrum (Figure 6.4, page 113) represents transport of u momentum away from the surface at the frequency of the wave spectrum peak.

General features of velocity peaks of wave origin listed as a), b) and c) on page 178, are interpreted with the assumption that waves can impart momentum into the airflow.

- a) Peaks coincident with wave spectra peaks are due to bending of streamlines and are enhanced by momentum imparted by the waves. The latter occurrence appears to influence, primarily, peaks in u spectra at 4.0 meters and was quite evident for Period 7 (Figure 6.26, page 147) and Period 5 (Figure 6.21, page 139). If it were not for the addition from the wave imparted momentum, one might assume that peaks would not have been observed so consistently at the 4.0 meter level. Fluctuations in u due to bending of streamlines (potential flow) would be very small at this level

because of reduction of the wind shear (see Equation 6-1).

- b) Primary peaks on or broadening of peaks toward forward face frequencies of the wave spectra, where no apparent secondary peak occurred, could be related to vertical transport, by turbulence, of the wave imparted momentum. In support of this interpretation, one could consider the results observed by Harris (1965) in the wave tank experiment which were shown in Figure 2.3, page 25, of this study. The supporting feature in Figure 2.3 is that at upper levels fluctuations appear to have lower wave numbers than the forcing wave.
- c) The occurrence of peaks coincident with secondary peaks on forward faces of the wave spectra, when none occurred at the wave spectra peaks, prompts one to ask; Why should the airflow reflect streamline bending corresponding to an inferior wave harmonic? This feature was associated with Case 2 periods and occurred in Period 5 (Figure 6.21, page 139) and in the u spectra at 2.0 meters in Period 11 (Figure 6.43, page 172). Responsible conditions during these periods could have been the nearness of the critical level, large wind shear (Period 5) and/or stable stratification (Period 11). Although Period 5 results support the idea that the critical level being near the surface with associated large wind shear could result in no velocity spectral peak coincident with the wave

spectrum peak, there was an exception to this within other results. The exception occurred during Periods 3 and 4 (Figures 6.12 and 6.13, page 126 and 127) when wind conditions and z/z_c values were similar to those in Period 5. However, velocity peaks coincident with wave spectra peaks during Periods 3 and 4 could be attributed to the presence of larger waves which were 50% higher than those in Period 5.

6.3.2 Velocity Covariance Results

Occurrences of enhanced or decreased stress, in cospectral results, coincided with peaks in corresponding velocity spectra. Generally, coincident peaks occurred in both u and w spectra but those in the u spectra appeared to be the determining factor. Interpretations of variance spectral results in the previous section related the primary peaks in u and w spectra for both Cases 1 and 2 to streamline bending by waves with contributions, primarily in u spectra, from momentum imparted by the waves.

Table 6.3 lists the percentage increase in momentum flux within "peak" bands where the percentage increase was determined by considering what would represent normal stress estimates for the cospectra, i.e. $\% \text{ increase} = \left(\frac{\text{total} - \text{normal}}{\text{normal}} \right)$. "Normal" estimates were determined by interpolating a smooth cospectrum through the band of enhanced or decreased stress. Results in Table 6.3 indicate that stress enhancement (percentage increase) is not a distinguishing factor between Cases 1 and 2. Qualitatively, stress enhancements for Case 1 are

TABLE 6.3 Percentage Increase in Stress ($\bar{u\bar{w}}$) within Bands with Wave Related Extrema

Period	Level(m)	~ % increase	Case
1	1.5	-200	1
	4.0	150	1
2	1.5	- 80	1
	15.0	140	1
3	1.5	175	2
4	1.5	90	2
	4.0	120	2
5	1.5	0	2
	4.0	160	2
6	4.0	125	1
7	1.5	160	1
	4.0	110	1
8	1.0	130	1
	2.0	100	1
9	1.0	130	1
	2.0	100	1
10	1.0	110	1
11	1.0	110	2
	2.0	-	2

related to the wave imparted u momentum and for Case 2 to the dynamics of the matched layer.

For Case 1 conditions, Period 1 (Section 6.2.1.2, Figure 6.4) gives the strongest support for the idea that wave imparted momentum results in enhanced stress at upper levels. The general picture for Case 1 conditions is one in which the wave imparted u momentum is a maximum over the trough of the wave which is also a region where the wave-induced w component is negative. This relationship between u and w has the net result of enhancing stress at the frequency of the wave imparted u momentum.

A shift with height of the maximum in the w component from the downwind slope towards the crest was characteristic of Case 1 periods. (Figure 6.8, page 117, Figure 6.29, page 150, and Figure 6.39, page 164, are phase composites for Case 1 periods what show this general feature). It appears that the "supplemental maximum"¹ could be responsible for this. It is suggested that the reason for the large shift in the w component during Periods 8 and 9 (Figure 6.39) between the 1 and 2 meter levels was due to the "supplemental maximum", i.e. wave imparted momentum. Wind profiles for Periods 8 and 9 (Figure 6.31, page 153) show a kink at 2.0 meters, similar to that observed by Yefimov and Sizov.

¹Terminology introduced by Yefimov and Sizov (1969) for maximum in u due to wave imparted momentum. The "supplemental maximum" was observed to be associated with a "kink" in the wind profiles, Figure 2.4, page 27.

For Case 2 conditions, a composite of phase relationships between the velocity components and the waves gives support for the interpretation that the dynamics at the critical level are responsible for the stress enhancement at the wave spectra peaks. A discussion of the analytical interpretation for this case appeared in Section 2.2.1.1.

Figure 6.47 is the composite of phase relations selected from Case 2 periods. (In this figure the vertical scale is proportional to $\ln(z/z_c)$.) The positioning of the selected phase relation results relative to z/z_c was approximate because wind conditions were never steady enough to establish an exact critical level for a given observation period. Levels and periods represented in the composite were selected because they support the general interpretation. Those not included do not necessarily disagree or invalidate the interpretation.

Phase relations in Figure 6.47 show a shift of w with height and a maximum in the u component over the upwind node. These features agree with those associated with a wave-induced stress due to the dynamics at the critical level.

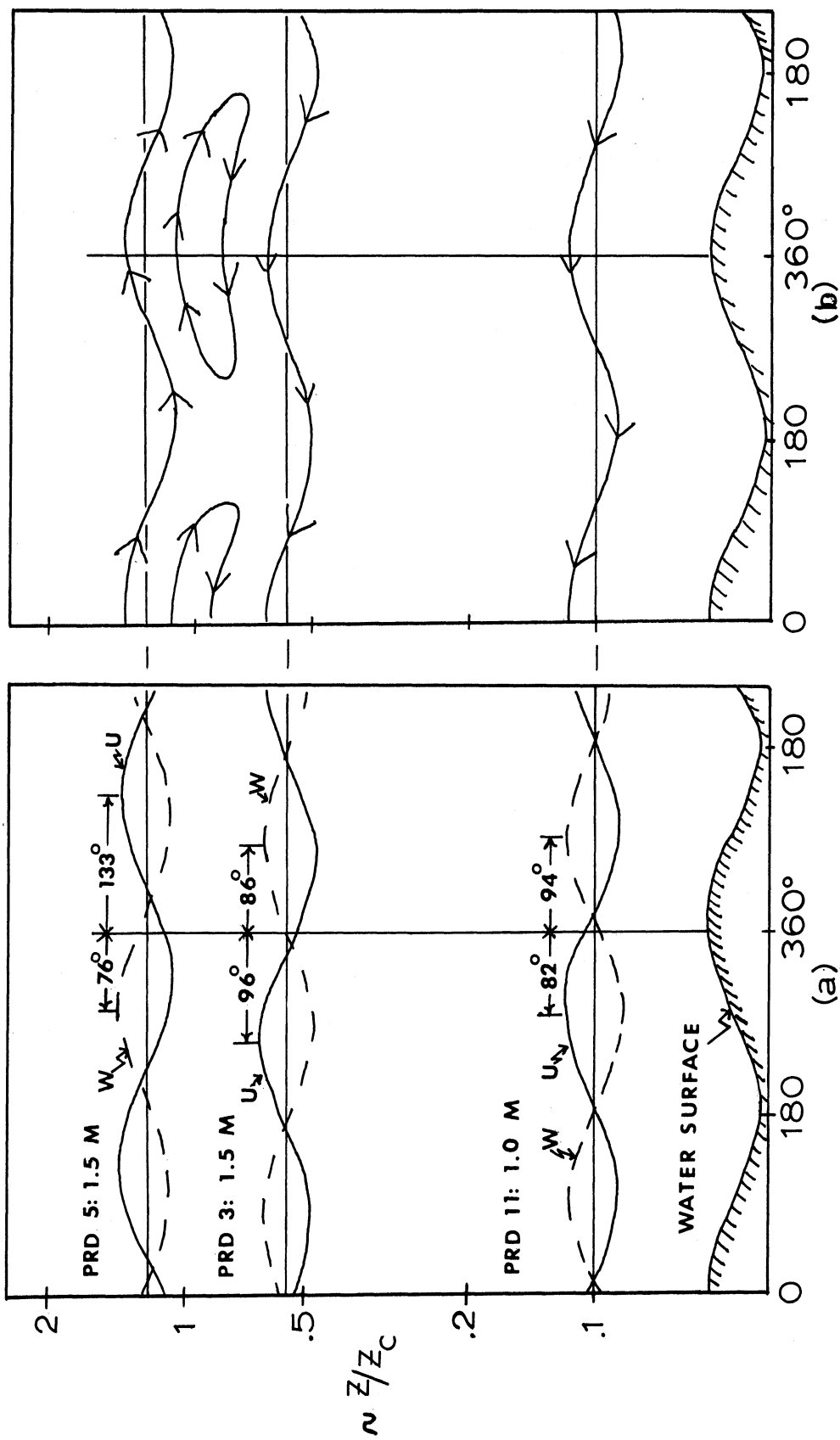


Figure 6.47: Composite schematic of phase relations from case 2 periods;
 (a) phase relations between velocity components and waves,
 (b) streamlines determined from phase of w in $(\bar{u}-c)$ frame of reference.

6.4 PRESENTATION OF VELOCITY SPECTRAL RESULTS IN UNIVERSAL FORM

This section presents the velocity spectral results in forms amenable for comparison with suggested universal forms for the spectra. These include power laws or slopes of the spectra at high frequencies. For this purpose, velocity results presented in Section 6.2 were smoothed using a 5 point binomial weighting function and grouped on composite diagrams. A composite diagram consists of the smoothed spectral results from the data obtained at all levels in adjacent time periods. Periods and corresponding figures are;

<u>Periods</u>	<u>Figure</u>
1	6.48
3 and 4	6.49
5	6.50
6 and 7	6.51
8, 9 and 10	6.52
11	6.53

Results are plotted as $\ln(n \cdot \phi_{ij} (n)/u_*^2)$ versus $\ln(\frac{nz}{\bar{U}})$. The normalized form for the variance spectrum $(n \cdot \phi_{ij} (n)/u_*^2)$ appeared in Section 2.1.2 Equation 2-15 as a function of the non-dimensional dissipation, ϕ_e , and (nz/\bar{U}) . nz/\bar{U} is referred to as the natural or non-dimensional frequency. Its use was suggested by Panofsky and McCormick (1960) to account for spectral variations due to differences in wind speed and height.

The universal nature of nz/\bar{U} as a frequency scale is in-

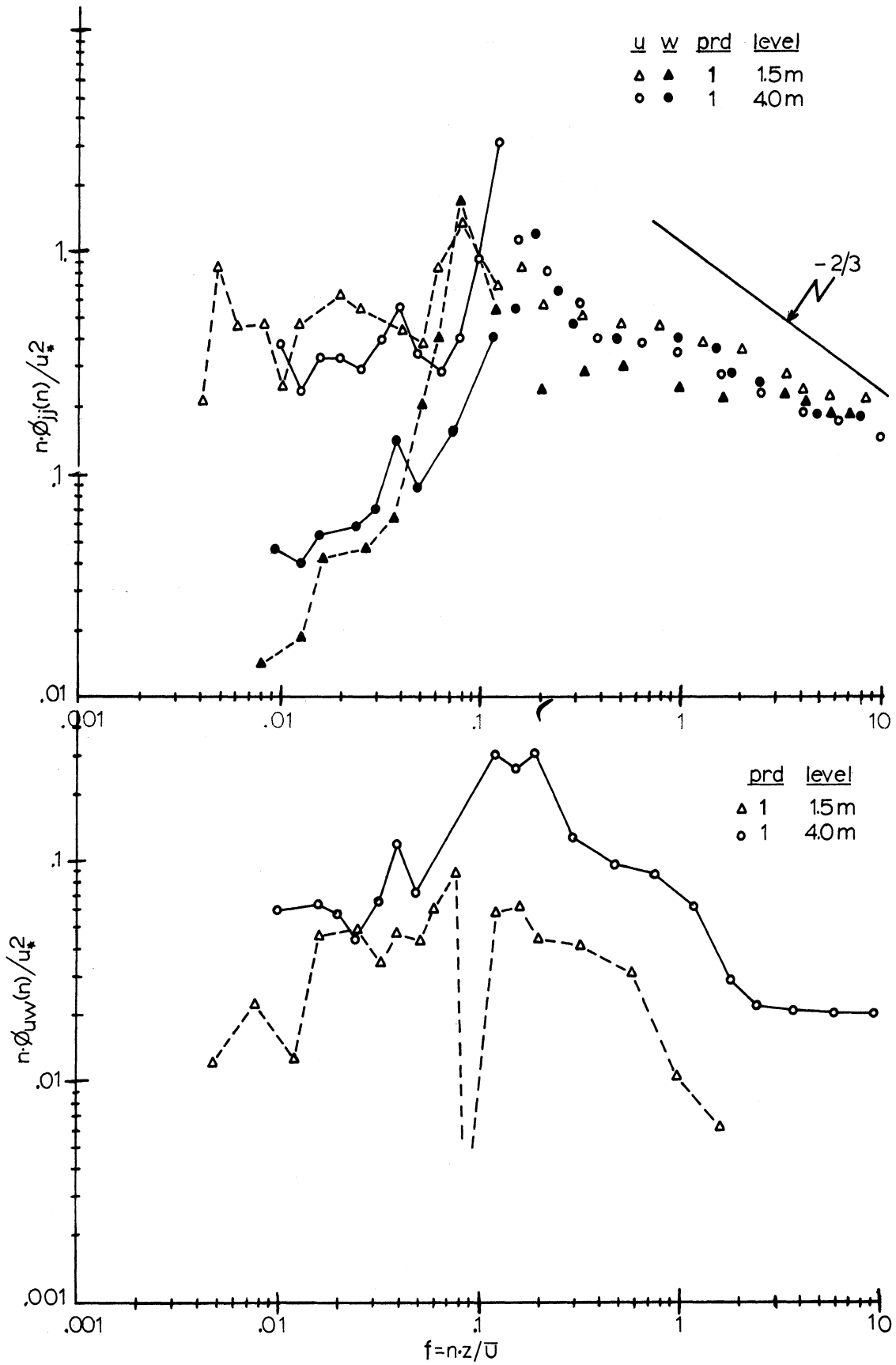


Figure 6.48: Smoothed and normalized velocity spectral results; Period 1.

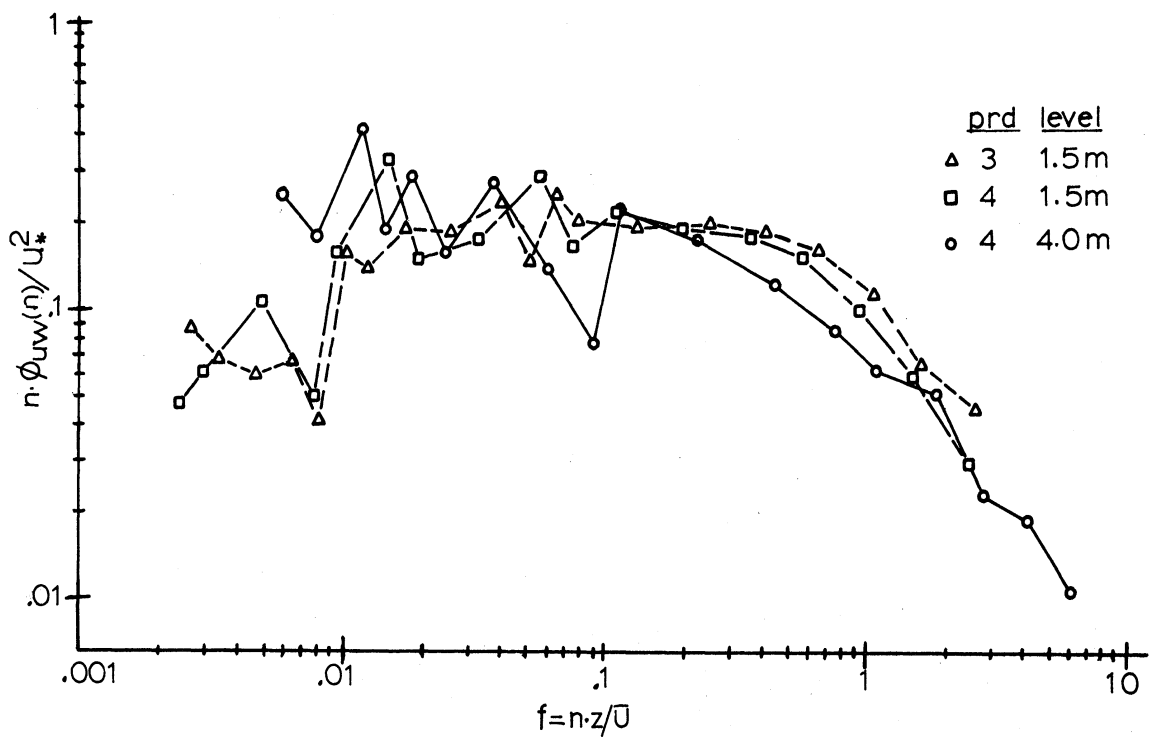
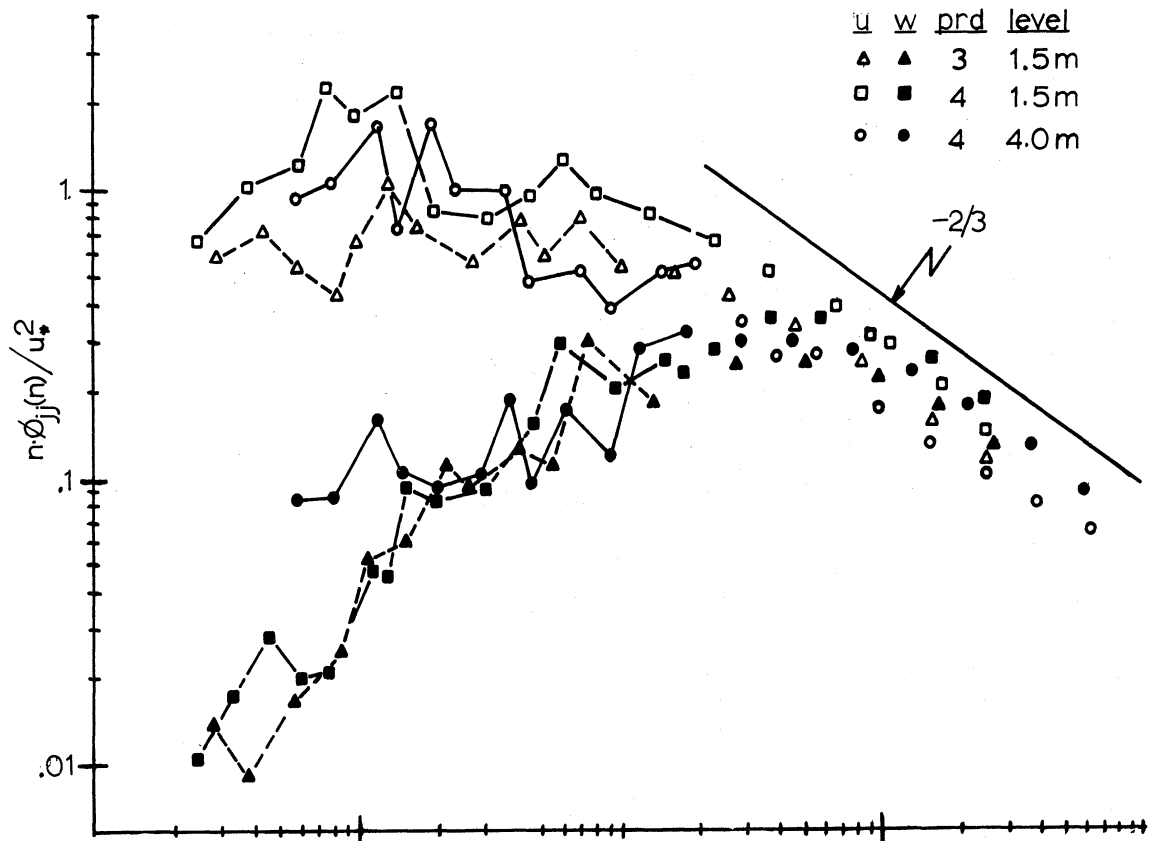


Figure 6.49: Smoothed and normalized velocity spectral results; Periods 3 and 4.

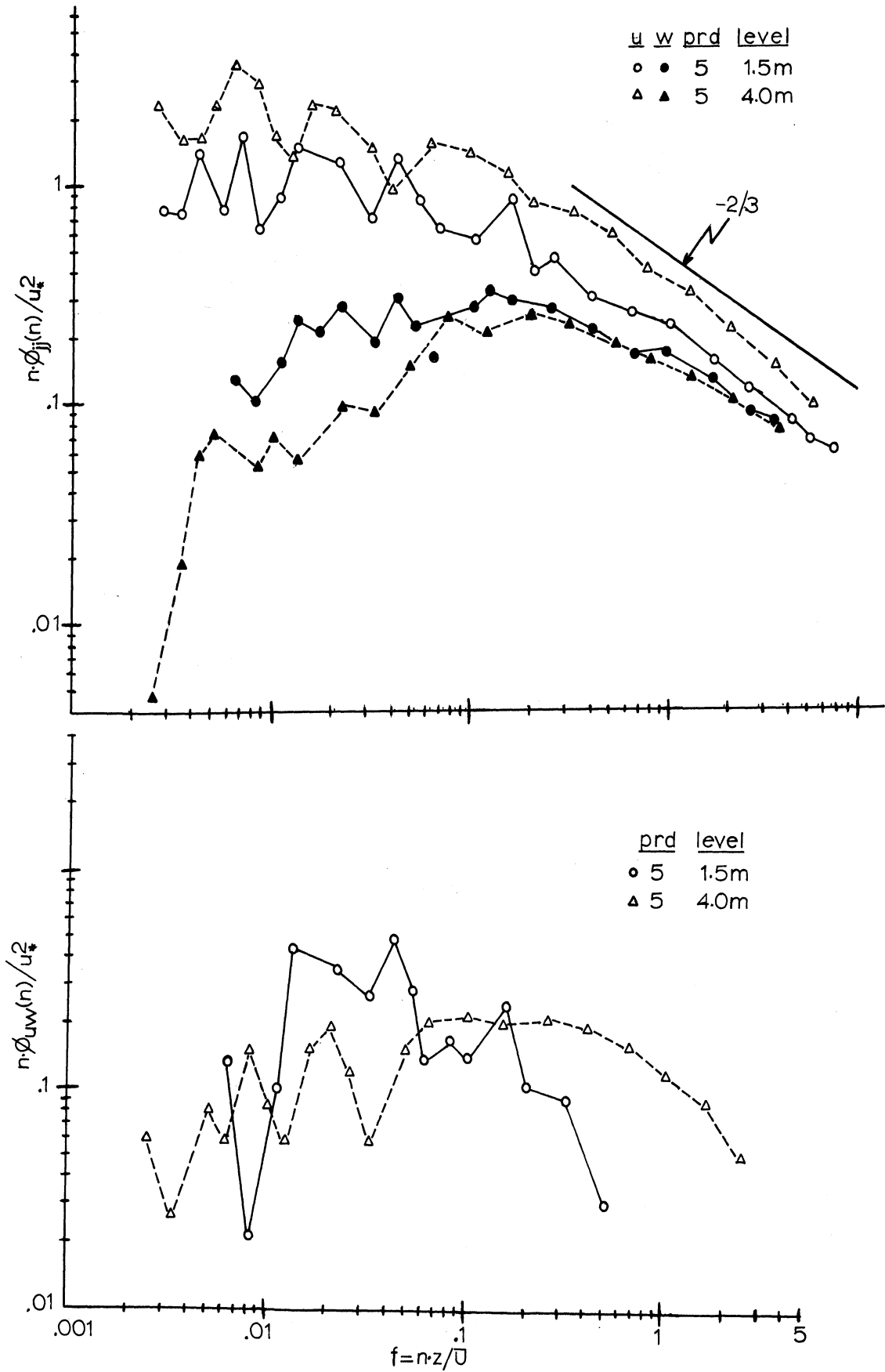


Figure 6.50: Smoothed and normalized velocity spectral results; Period 5.

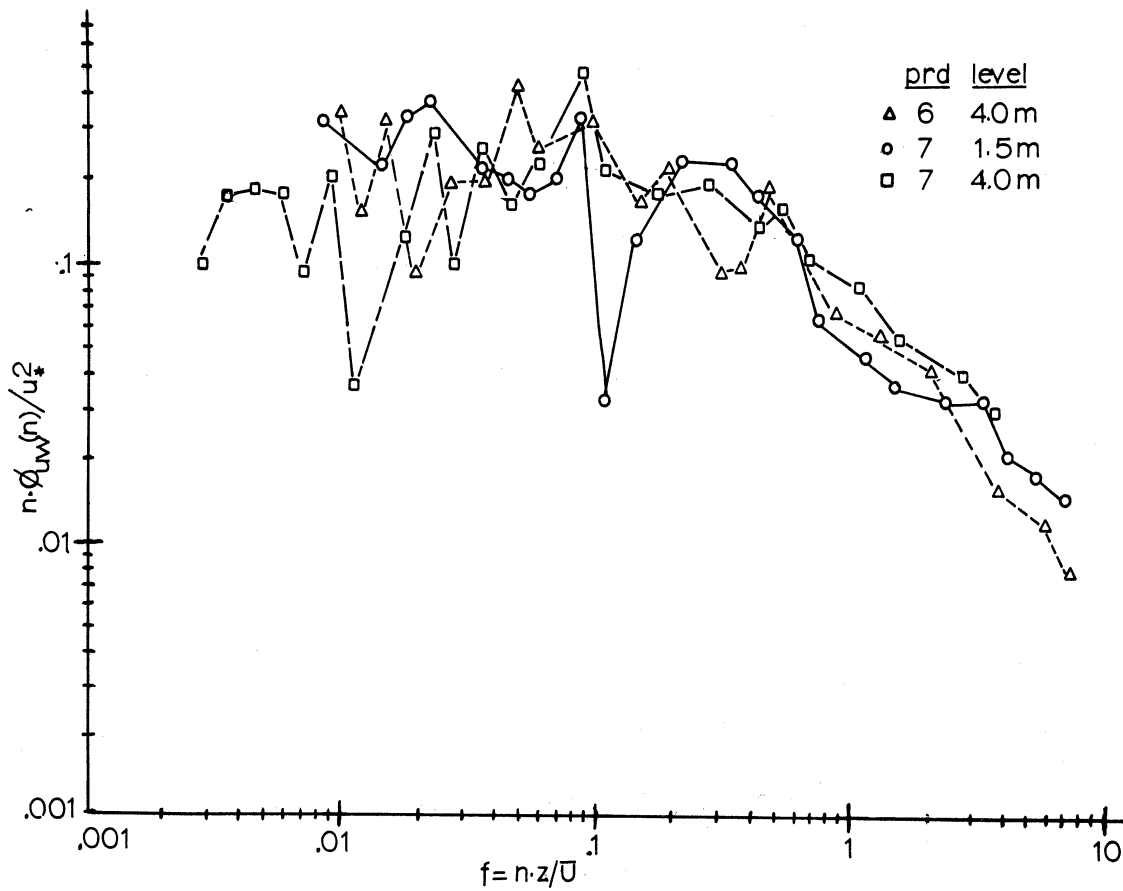
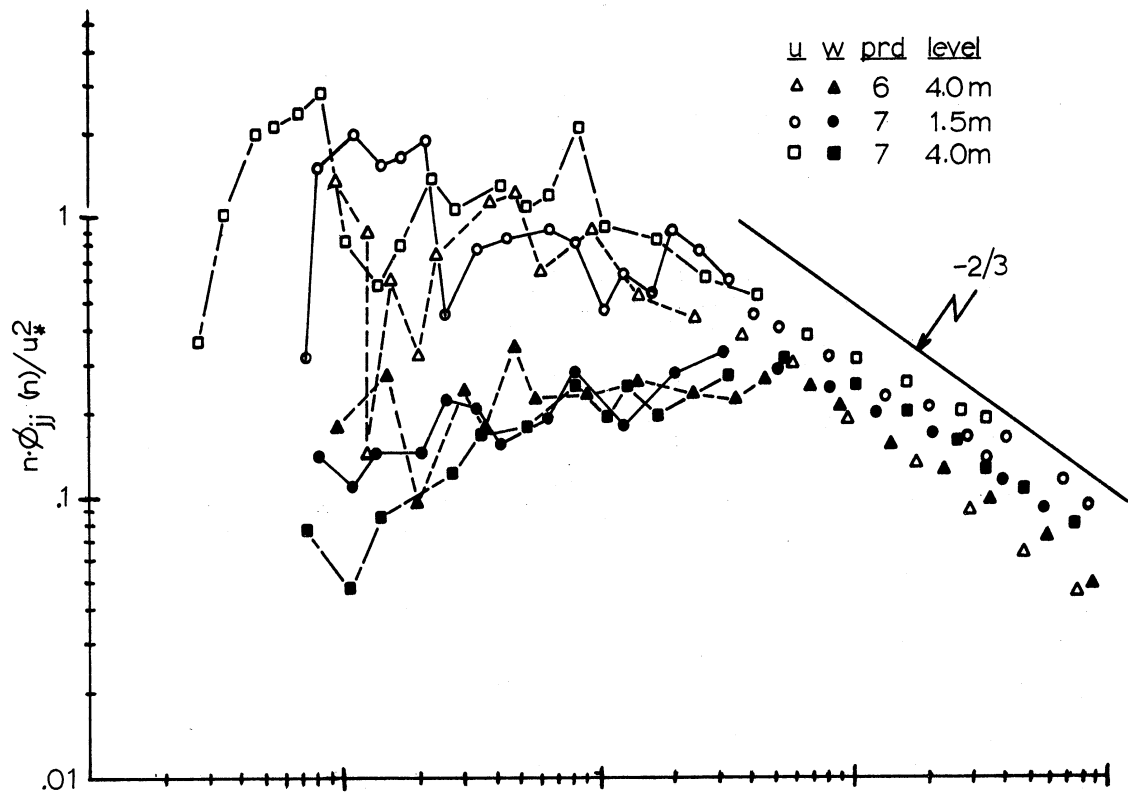


Figure 6.51: Smoothed and normalized velocity spectral results; Periods 6 and 7.

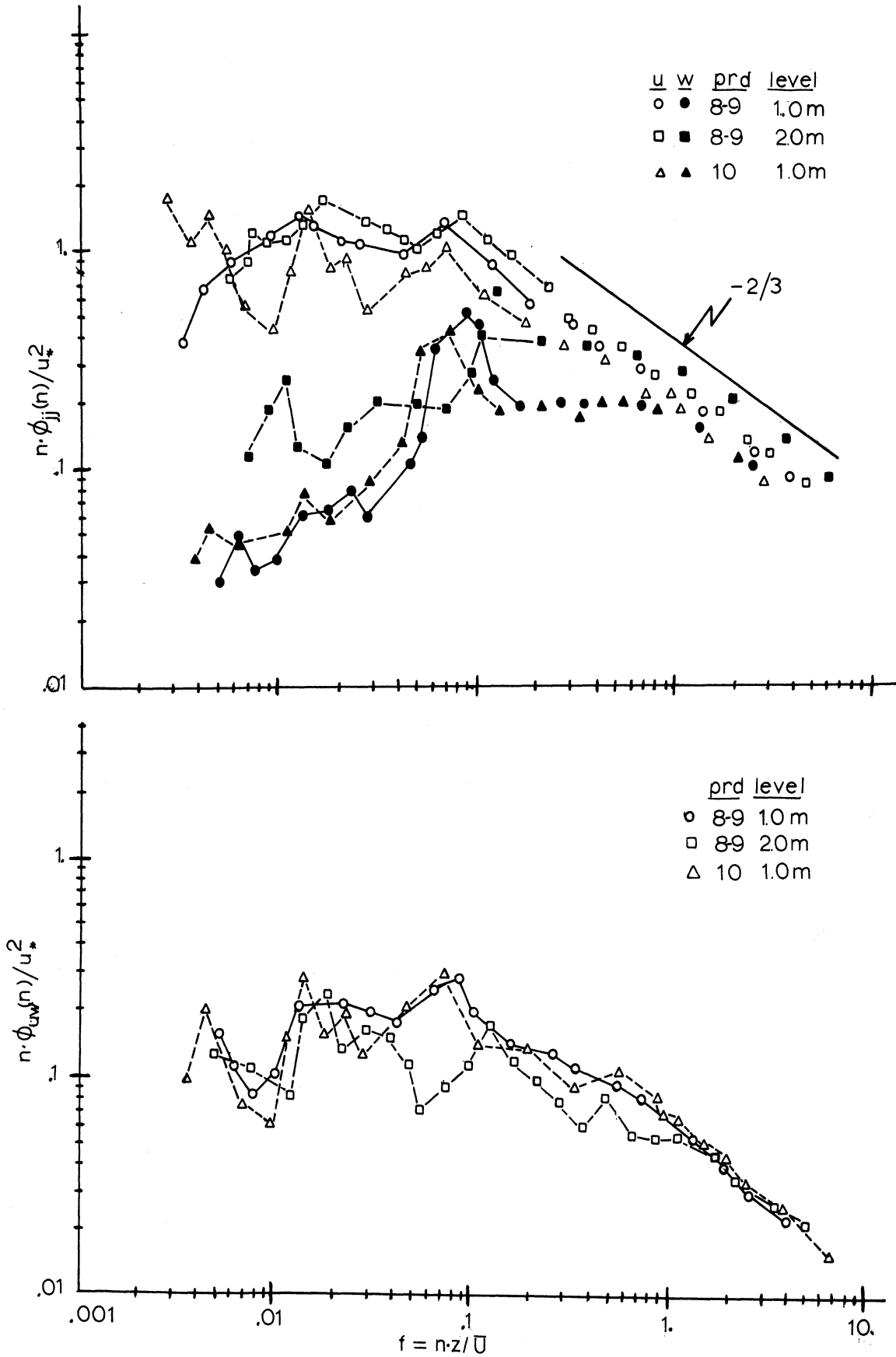


Figure 6.52: Smoothed and normalized velocity spectral results, Periods 8, 9 and 10.

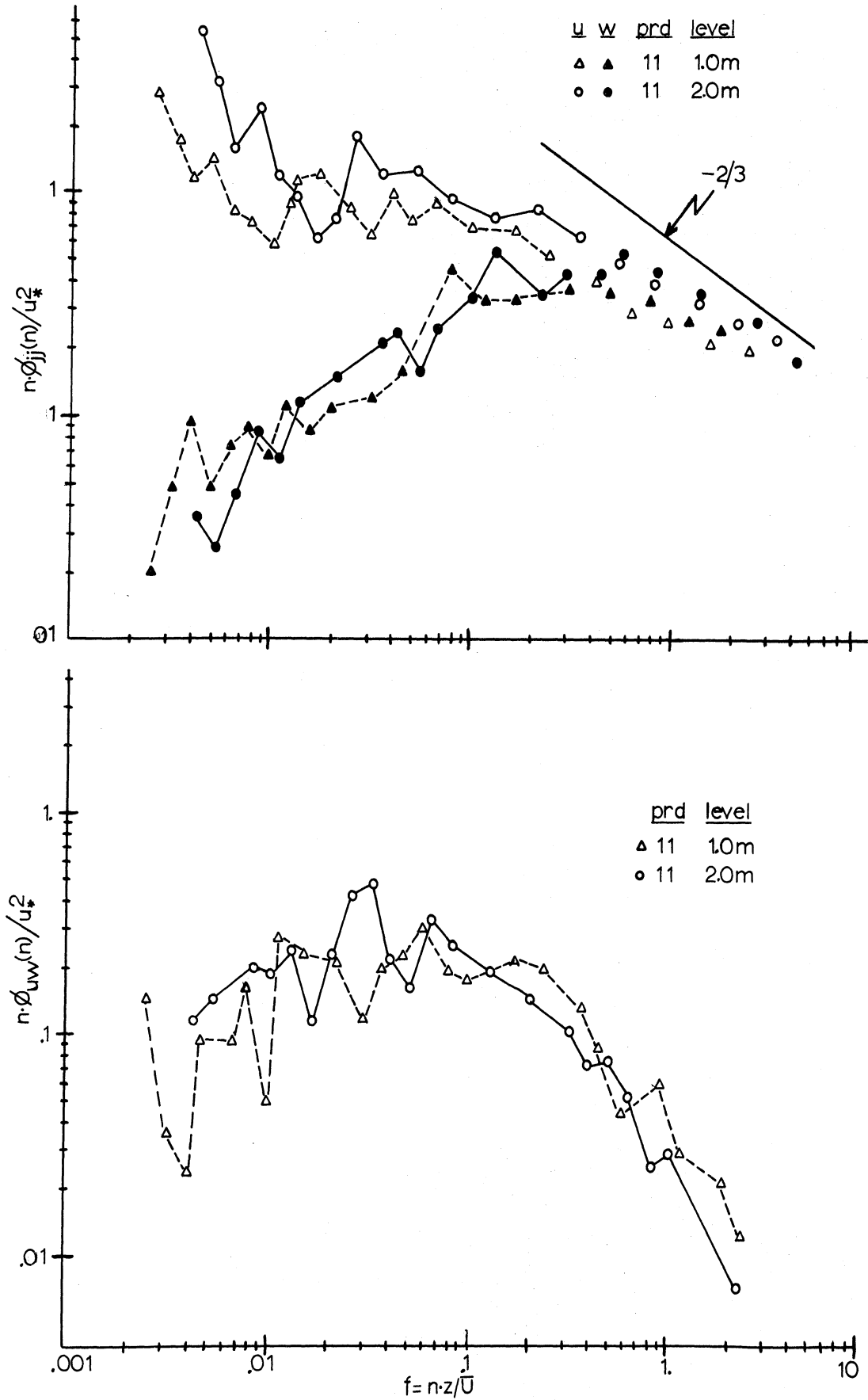


Figure 6.53: Smoothed and normalized velocity spectral results, Period 11.

tuitive if one considers the terms involved; nz/\bar{U} can be written as a wave number (K) times z since K is equal to $2\pi n/\bar{U}$, hence

$$\frac{nz}{\bar{U}} = \frac{Kz}{2\pi} . \quad 6-5$$

The wave number dependence in the new scale accounts for the spatial variations of the fluctuations and shifts the spectra so spatial scales are comparable. However, near the surface, the presence of the boundary limits the energy in low wave numbers. Therefore, spectral maxima, as an example, may not coincide for different heights of measurement, being at higher wave numbers for low measurement levels. Including height, z, as an additional factor, shifts the spectra to account for the influence of the boundary on the scale of turbulence.

Kolmogorov's $-5/3$ power relation (Section 2.1.2) for the inertial subrange corresponds to a $-2/3$ slope in this representation. Other power relations suggested have been a .8 by Miyake et al. (1970) and 1. by Volkov (1969) for the spectral region of the w spectra below its maximum. Suggested, also, have been values for the natural frequency at which the spectral maxima (for u, w and uw) should occur and, as well, the lower limit of the $-2/3$'s region for the u and w spectra. Although energy concentration due to the waves hinder close examination of maxima in the normalized spectra, they are, nevertheless, estimated for 5 of the 6 composite diagrams and are listed in Table 6.4.

TABLE 6.4 Composite Spectral Maxima and Lower Limits of $-2/3$ Slope Regions, (nz/\bar{U})

Composite Figure	Spectral maximum			lower limit $-2/3$	
	u	w	uw	u	w
6.48	*	*	*	*	*
6.49	.01	.3	.08	.5	1.
6.50	.01	.2	.10	.3	1.
6.51	.02	.3	.08	.3	2.
6.52	.02	.2	.04	.2	1.
6.53		.3	.05	.3	1.
MIYAKE et al. ^a	.01	.25	.03	-	2.
VOLKOV ^a	-	.15	-	-	-
BUSCH and PANOFSKY ^b	.02	.32	-	-	.6

*not estimated due to magnitudes of wave induced extrema

a- overwater results

b- overland results

TABLE 6.5 Ratios of ϕ_{ww}/ϕ_{uu} for Individual Levels

Period	Level(m)	ϕ_{ww}/ϕ_{uu}	Level(m)	ϕ_{ww}/ϕ_{uu}
1	1.5	.86	4.0	1.15
2	1.5	1.44	15.0	1.12
3	1.5	1.21	-	-
4	1.5	1.12	4.0	1.59
5	1.5	.90	4.0	.91
6	-	-	4.0	1.27
7	1.5	.81	4.0	.79
8	1.0	.80	2.0	1.39
9	1.0	.91	2.0	1.28
10	1.0	1.18	-	-
11	1.0	1.10	2.0	1.09

Another relation, which has not yet been discussed in this study, is the one between the w and u spectra in isotropic turbulence. Von Karman and Howarth (1938) showed that

$$\phi_{ww}(K) = \frac{1}{2} \left(\phi_{uu}(K) - K \frac{\partial \phi_{uu}(K)}{\partial K} \right). \quad 6-6$$

If inertial subrange turbulence is isotropic, Equation 2-12, Section 2.1.2, page 13, can be substituted into 6-6 and gives

$$\phi_{ww}(K) = \frac{4}{3} \phi_{uu}(K). \quad 6-7$$

Average values of the ratio $\phi_{ww}(n)/\phi_{uu}(n)$ were computed for frequencies where both ϕ_{ww} and ϕ_{uu} exhibited $-2/3$ slopes. These values are given in Table 6.5 for individual levels and periods.

A summary of these results is:

- 1) All u spectra except for those from Periods 1 and 2 appear to follow a $-2/3$ relation for $f = n \cdot z/\bar{U} > .5$ and w spectra for $f > 1$. Values for individual composites appear in Table 6.4.
- 2) Estimated spectral maxima as given in Table 6.4 agree with those reported by other studies.
- 3) For the majority of the results, (12 out of 20) ϕ_{ww}/ϕ_{uu} was larger than 1. The ratios during Periods 8 and 9 at the two meter level were close to the 1.33 value for the inertial subrange and could be associated with the low wind speeds and hence small wave numbers represented by the high frequency results. Although the $4/3$'s relation was not expect-

ed for a frequency range below 10 Hz, the tendency of the energy in the w component to exceed or equal that in the u component at high frequencies indicates successful determination of the u and w components from the X-probe data.

6.5 TURBULENT TRANSPORTS, RELATIVE INTENSITIES AND PROBABILITY DISTRIBUTIONS

Table 6.6 lists values which correspond to the following properties of the turbulent flow:

- 1) Momentum flux (= shear stress per unit area) given in terms of the reference velocity, $u_* = (-\overline{uw})^{\frac{1}{2}}$, from hot-wire, u_* , bivane anemometer, $u_*(B)$, and wind profile estimates, $u_*(P)$;
- 2) Heat flux given in terms of $\overline{wT'}$ where w was that measured by the hot-wire and T' from the high response "cold wire" system;
- 3) Drag Coefficient, C_{10} , a factor of proportionality commonly used to relate the stress to the mean wind speed at 10 meters, $C_{10} = (u_*/\overline{U}_{10})^2$;
- 4) z/L , buoyant production of turbulent kinetic energy;
- 5) Relative intensities of fluctuating quantities σ_u/u_* , σ_w/u_* , $\sigma_{T'}/|T_*|$, where u_* is defined above and $T_* = \overline{wT'}/ku_*$ and σ_x = standard deviation of variable x .
- 6) C/u_* , a ratio considered to be representative of the non-dimensional height of the matched layer. C is the phase speed corresponding to wave spectra peaks.

A principal result shown in Table 6.6 is that reference velocities (u_*) obtained from hot-wire measurements always equal or exceed those from the bivane anemometer or from wind profiles. Figure 6.54 is a plot showing profile, $u_*(P)$, versus hot-wire, u_* , estimates along with a solid line for over-

Table 6.6 Estimates of Turbulent Transports, Drag Coefficients, z/L , Relative Intensities and C/u_*

PRD	Date Time	level (meters)	Turbulent Transports			$C_{10} \times 10^{-3}$	z/L	Relative Intensities				
			u_*	$u_*(B)^a$	$u_*(P)$			$\frac{wT'}{cm^3 C}$	σ_u/u_*	σ_w/u_*	σ_T/T_*	C/u_*
1	8-19 1226	1.5	18.7		20.0	- .05	1.2	+0.002	2.51	1.58	10.60	39
2	8-19 1407	4.0	26.9			- .10	2.5	+0.003	1.57	1.20	10.00	25
3	9-24 1724	1.5	23.5			- .77		+0.012	3.26	1.79	.77	31
4	9-24 1755	15.0	28.2						2.22	1.90		25
5	9-26 1100	1.5	22.3	17.0	19.9	1.02	1.0	-0.019	1.93	1.04	.96	27
6	9-26 1324	4.0	22.8	18.5	20.7	.60	.9	-0.010	2.51	1.13	1.45	26
7	9-26 1355	1.5	29.8				1.5		1.99	1.19		20
8	9-27 1120	4.0	33.1	18.0	22.6	2.30	2.5	-0.013	3.06	1.15	1.48	15
9	9-27 1140	4.0	40.3			3.10	3.7	-0.026	2.07	1.22	.96	12
10	9-27 1200	1.0	40.2		16.4	3.75	6.4	-0.031	1.89	1.63	.79	15
11	10-5 1050	1.0	25.4		16.7	3.31	2.2	-0.041	2.62	1.14	.91	23
		4.0	32.8			4.15	3.7	-0.064	2.21	1.23	.64	18
		1.0	23.2		12.1	1.87	3.8	-0.021	2.26	1.09	.94	26
		2.0	25.1	10.5		-1.26	4.5	+0.022	2.05	1.31	1.21	24
		1.0	26.4		12.2	1.97	4.6	-0.013	2.06	1.07	1.12	23
		2.0	26.5	13.0			4.6		3.10	1.65		23
		1.0	26.5	13.2	16.5	2.30	3.3	-0.017	2.12	1.00	.94	25
		1.0	27.2		22.0	-.48	1.5	+0.006	2.41	-1.29	1.32	21
		2.0	22.2	22.0		-.32	1.5	+0.008	2.92	1.48	1.52	21

a - Elder and Soo (1969)

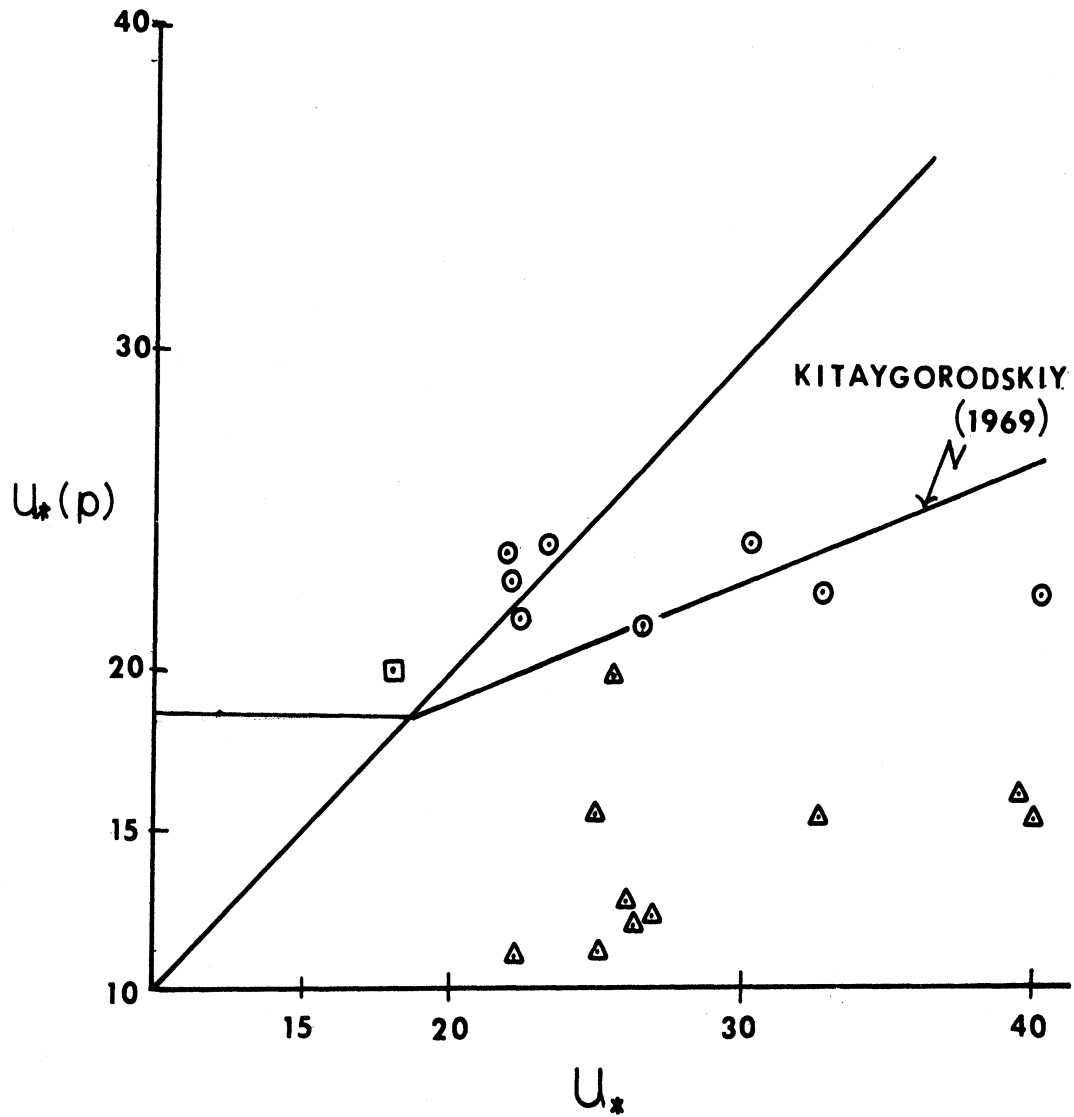


Figure 6.54: Comparison of reference velocity (cm/sec) obtained from profile, $u_*(p)$, estimates and hot wire, $u_* = (-\overline{uw})^{\frac{1}{2}}$, estimates.
 □ Period 1 (1.5 meter), △ case 1, ○ case 2.

water results reported by Kitaygorodskiy (1969).

Data for Case 2 periods agree with those observed by Kitaygorodskiy and the difference between both sets of data (Cases 1 and 2) and profile results may be associated with the bands of enhanced stress near the wave spectra peaks. Case 1 estimates exhibit even greater deviations from profile estimates. The stress for Period 1, 1.5 meter level, is less, as expected, than the profile estimate.

Hot-wire estimates of u_* indicate momentum flux convergence, $\frac{\partial}{\partial z} (-\overline{uw}) \neq 0$, during Periods 1, 2, 4, 5 and 7. During Periods 1 and 2, decreased and enhanced stress at the lower levels and upper levels respectively were clearly evident. During Periods 4, 5 and 7, which had measurements at the same levels (1.5 and 4.0 meters), the lower level u_* value is approximately 80% that at the upper level (Period 4 = 80%, 5 = 81% and 7 = 78%). Similar ratios exist for the $\overline{wT'}$ values and the initial reaction was a scale selection error that would be the same for $\overline{wT'}$ and u_* . However, $\overline{uT'}$ had no similar relation and the cospectra in all cases showed that the upper levels had the greater enhancement due to the waves' influence.

The apparent sensible heat ($\overline{wT'}$) convergence between the 1 and 2 meter levels for Periods 8 and 9 is difficult to account for. It is presumably due to organized motion implied by the large phase shift in the w component during these periods (Section 6.2.4.1, Figure 6.39, page 164). The third dimension could be an important factor in this

phenomenon. \overline{uT} had the same sign (negative) at both levels and was also two times that of \overline{wT} .

Drag coefficients, C_{10} , are larger by a factor of 3 to 4 than those normally reported, 1×10^{-3} , (Weiler and Burling, 1966; Stewart, 1967). However, Seesholtz (1968) reported values ranging from (4 to 7) $\times 10^{-3}$ for observations over natural waves. The consistent occurrence of stress enhancement due to the waves implies that the concept of a drag coefficient in this region is untenable. This is because it relates the stress to the wind speed at an upper level with the assumption that all turbulent transport of momentum is involved in maintaining the wind profile.

Figures 6.55 and 6.56 show relations between the relative intensities of u and w (σ_u/u_* , σ_w/u_*) and z/L and C/u_* respectively. A reason for these considerations is to examine the utility of using C/u_* as a non-dimensional parameter for boundary layer analyses as has been suggested by Kitaygorodskiy (1969) with the relations;

$$\frac{\partial \bar{u}}{\partial z} = \frac{u_*}{kz} \cdot f_1\left(\frac{z}{\lambda}, \frac{C}{u_*}\right) \quad 6-8$$

$$\sigma_u^2 = q \cdot u_*^2 \cdot f_2\left(\frac{z}{\lambda}, \frac{C}{u_*}\right) \quad 6-9$$

for $z \ll z_c$

where λ = wave length

q = constant .

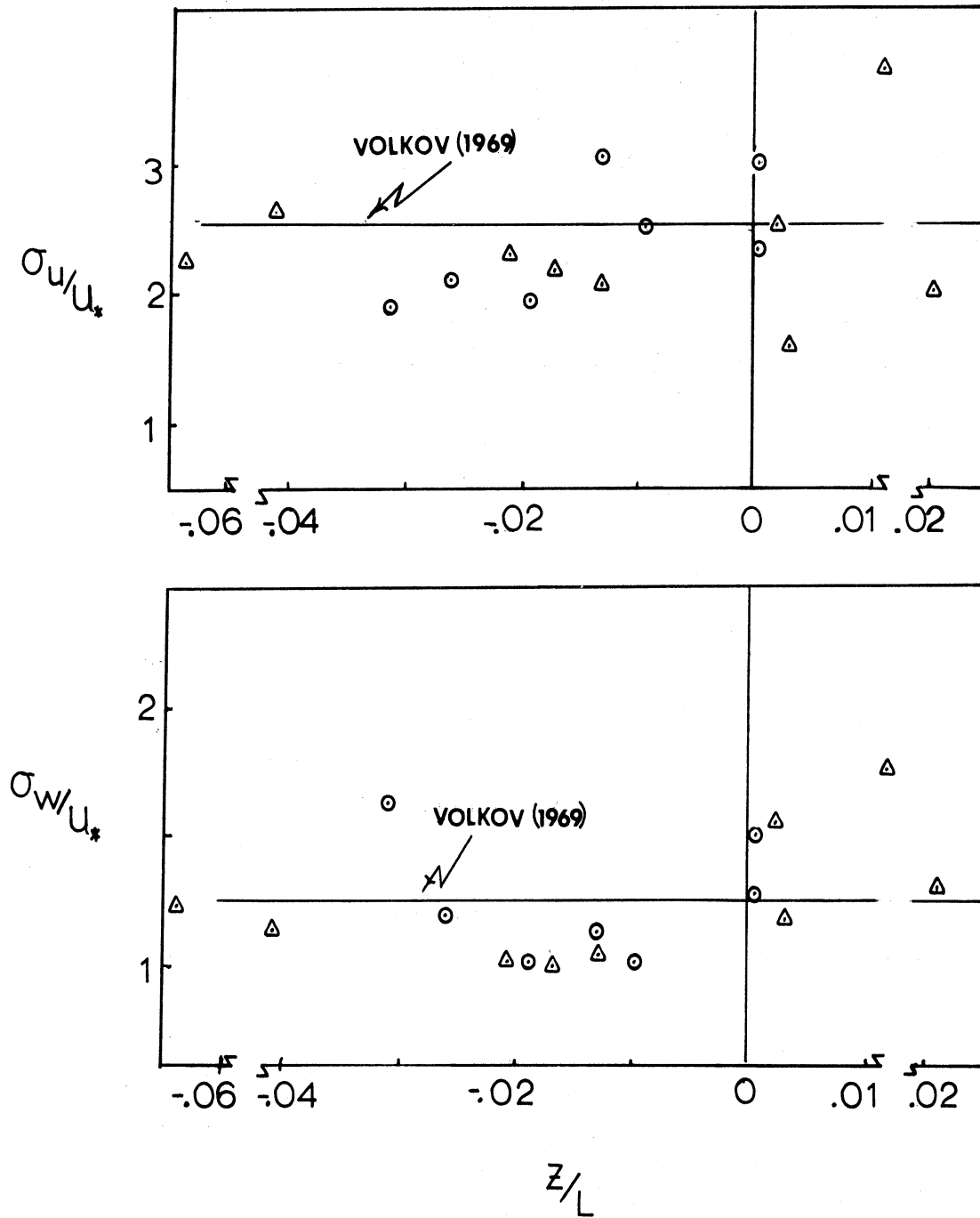


Figure 6.55: Relative intensities of velocity components (σ_u/u_* , σ_w/u_*) versus Z/L ; Δ case 1, \circ case 2.

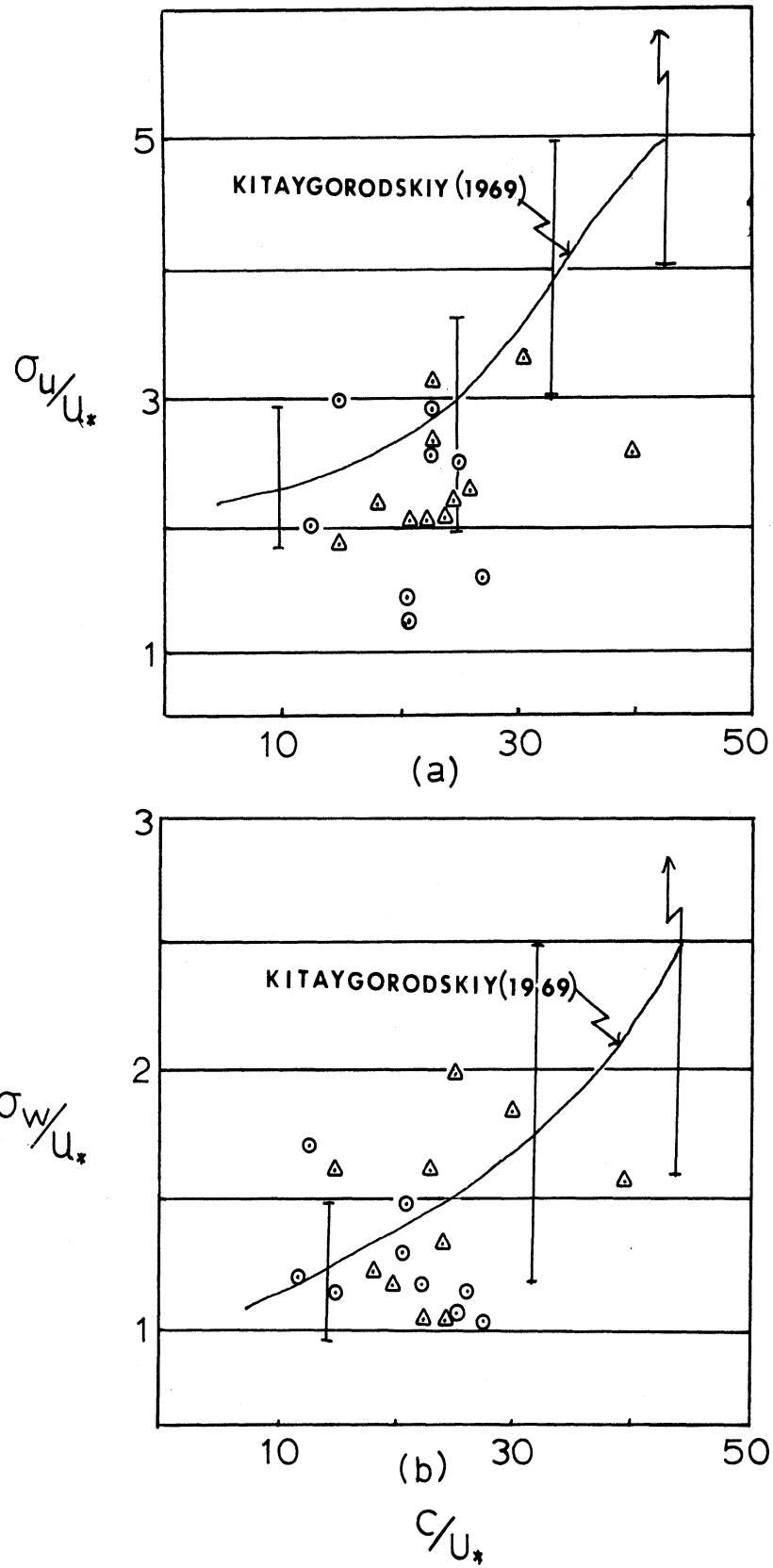


Figure 6.56: Relative intensities of velocity components (σ_u/u_* , σ_w/u_*) versus C/u_* ; Δ case 1, \circ case 2.

His conclusions were that additional measurements are necessary to define the functions f_1 and f_2 .

Figure 6.55 indicates that the relative intensities are not influenced by stability conditions close to the surface. The solid line represents the value expected in near neutral conditions (Volkov, 1969). Figure 6.56 shows that Case 1 values increase with C/u_* in general agreement with results reported (solid line) by Kitaygorodskiy (1969).

Table 6.7 lists skewness and kurtosis values of turbulent fluctuations and of the water surface (η). The skewness of the water surface indicates a near symmetrical distribution during Periods 1, 8 and 10 and has the highest values during Periods 3 and 4, when active wave growth was most evident. Its value is always positive as expected for natural waves which have sharp crests.

Skewness values for u are all negative and for w all positive except for the anomalous 2.0 meter level for Periods 8 and 9. In general, the results are consistent with those expected under unstable conditions which prevailed during most of the observations. During unstable conditions, skewness of u should be negative because convective updrafts would be frequent and would have a deficit of u momentum. The occurrence of the positive value in the skewness of u and also the negative values for w appears to be due to fluctuations in each associated with the waves.

Table 6.7 Skewness and Kurtosis Results

PRD	DATE	LEVEL (m)	Skewness			Kurtosis				
			u	T'	n	u	T'	n		
1	8-19-1226	1.5	-.27	.10	-.45	.04	-.01	.71	.84	-.25
		4.0	-.11	.20	-.37		.37	.78	.27	
2	8-19-1407	1.5	-.13	.32	.37	.12	-.37	.72	.11	-.02
		15.0	-.25	.07			-.14	-.02		
3	9-24-1729	1.5	-.21	.28	.08	.25	-.31	.47	-.33	.24
4	9-24-1755	1.5	-.07	.18	-1.16	.25	-.40	.53	-.53	.06
		4.0	-.35	.14			-.37	.52		
5	9-26-1100	1.5	-.09	.37	.37	.12	-.10	.73	-.28	-.78
		4.0	-.14	.22	.80		-.18	.21	.40	
6	9-26-1324	4.0	-.41	.39	.82	.16	.27	.83	.30	.17
7	9-26-1355	1.5	-.01	.26	.41	.20	.04	.60	-.32	.14
		4.0	-.03	.42	.71		-.03	1.03	-.09	
8	9-27-1120	1.0	-.09	.50	.32	.01	-.28	.74	-.32	.08
		2.0	.03	-.24	.39		-.33	.31	-.42	
9	9-27-1140	1.0	-.25	.41	.34	.10	-.16	.49	-.38	.08
		2.0	-.04	-.17			.33	-.27		
10	9-27-1200	1.0	-.21	.37	.20	.07	-.19	.50	-.28	.15
11	10-5-1650	1.0	-.11	.17	.08	.12	-.48	.35	-.67	-.76
		2.0	-.22	.15	-.19		-.25	.38	-.32	

6.6 TURBULENT ENERGY BALANCE COMPUTATIONS

Three terms of the non-dimensional form of the turbulent energy balance equation (Equation 2-7, Section 2.1.1, page 9) were computed to estimate the fourth, viz., the divergence, ϕ_D . Two of the three terms (ϕ and z/L) were computed from the momentum and heat flux data along with the wind shear, i.e. $\phi = \frac{kz}{u_*} \frac{\partial \bar{U}}{\partial z}$, $z/L = -\frac{g}{T} \frac{\overline{wT}}{u_*^3} kz$. The third term, ϕ_e , was estimated using the power relation (Equation 2-15, page 13) for the inertial subrange.

Assumptions necessary to estimate ϕ_D by this method were that the total turbulent kinetic energy was not changing during the periods and that estimates of the dissipation, ϕ_e , could be obtained from the $-2/3$ power relation for the u component even though all requirements for the inertial subrange were not met.

Results in Section 6.4 indicated that a $-2/3$ power relation existed for u spectra for all periods except Periods 1 and 2. It was assumed that the $-2/3$ slope extended to the inertial subrange, and ϕ_e was estimated for levels and periods which had both temperature fluctuations and wind profile data available. Equation 2-15 was used in the form

$$\phi_e = \left(\frac{n \cdot \phi_{uu}(n)}{.26 \cdot u_*^2} \right)^{3/2} \cdot f \quad 6-10$$

where $f = nz/\bar{U}$.

Table 6.8 lists values of the resulting terms in the turbulent energy balance equation along with values which represent the wave conditions. Values of the divergence

Table 6.8 Results from Energy Balance Computation along with Wave Parameters

Period	Normalized Energy Balance Terms											WAVE PARAMETERS		
	Level(m)	Computed terms					$\phi_b = \phi - z/L - \phi_e$					Case	n_o (Hz)	$(z/\lambda_o) \cdot N$
		ϕ	z/L	ϕ_e	Hot wire	Bivane*								
1	1.5	1.78	.002	3.50	-1.72		1	.21	.015					
	4.0	1.09	.003	1.78	-.69**		1	.21	.041					
2	1.5	1.41	.012	4.40	-3.00**		2	.21	.015					
3	1.5	1.61	-.019	.83	+.80	+1.30	2	.26	.036					
4	1.5	1.31	-.010	1.00	+.32	+.69	2	.26	.030					
5	1.5	.46	-.013	1.00	-.53	-.17	2	.26	.045					
	4.0	.33	-.026	.93	-.57		2	.26	.120					
6	4.0	.20	-.031	.49	-.26		1	.26	.095					
7	1.5	1.19	-.041	.76	+.47		1	.26	.065					
	4.0	.25	-.064	.76	-.45		1	.26	.174					
8	1.0	.81	-.021	.79	+.04	+1.08	1	.26	.033					
	2.0	.39	.022	.65	-.28	+.03	1	.26	.066					
9	1.0	.52	-.013	.56	-.03	+.50	1	.26	.031					
10	1.0	.90	-.017	.44	+.48	+1.48	1	.24	.047					
11	1.0	1.16	.006	1.00	+.15	+.14	2	.26	.063					
	2.0	.85	.008	2.70	-1.86**	-2.24**	2	.26	.125					

*Elder and Soo (1969)

**Not included in Figure 6.58

term computed with stress estimates from the bivane anemometer data are also included for times when the bivane was within .5 meters of the hot-wire anemometers.

Figure 6.57 shows ϕ_{ϵ} in relation to z/L and the solid line represents a theoretical value suggested by Busch and Panofsky (1968). There does not appear to be any distinction between Case 1 and Case 2 estimates. Figure 6.57 shows ϕ_{ϵ} versus the sum of the production terms $(\phi - z/L)$. The solid line represents production equal to dissipation and it is apparent that that was not the general case. Furthermore, it appears that Case 1 results favor production exceeding dissipation.

Figure 6.58 shows the difference, $(\phi - z/L) - \phi_{\epsilon} = \phi_D$, between local production and local dissipation as a function of $(z/\lambda_0) \cdot N$ where N is a factor introduced to account for different wave heights. It is equal to the ratio of the wave heights during Period 6 to those during a given period. Wave height differences were included because Periods 1 and 2 which had the largest wave heights also had the clearest evidence of waves imparting momentum into the airflow.

The points in Figure 6.58 are:

- i) Δ estimates from hot-wire u_* values
- \circ estimates from bivane u_* values
- ii) $\Delta \circ$ estimates for Case 1 observations
- \blacktriangle estimates for Case 2 observations

The line in Figure 6.58 was drawn subjectively by considering those points that coincide with Case 1). It should

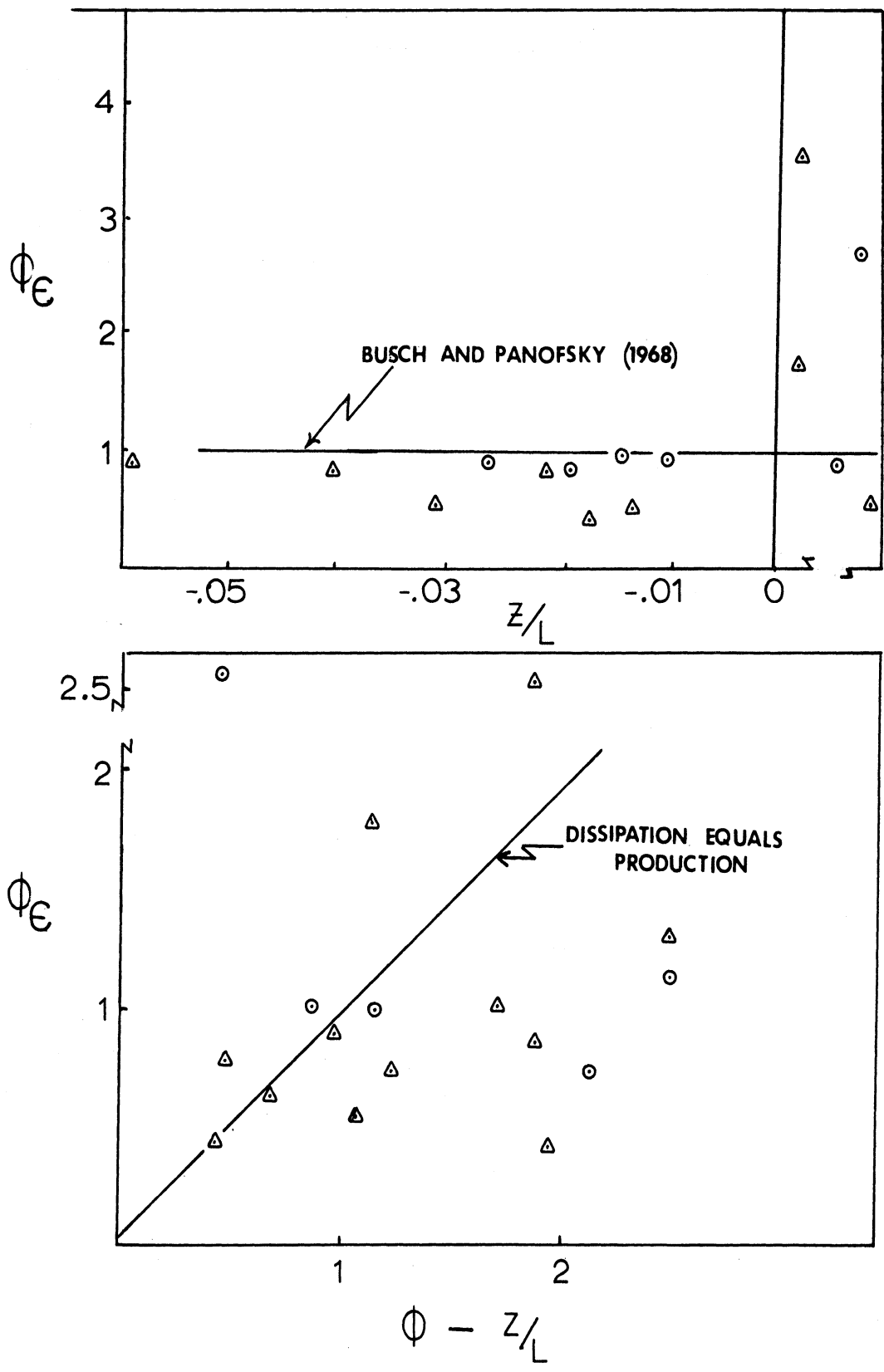


Figure 6.57: Normalized dissipation, ϕ_ϵ , versus Z/L and versus normalized production ($\phi - Z/L$); Δ case 1, \circ case 2.

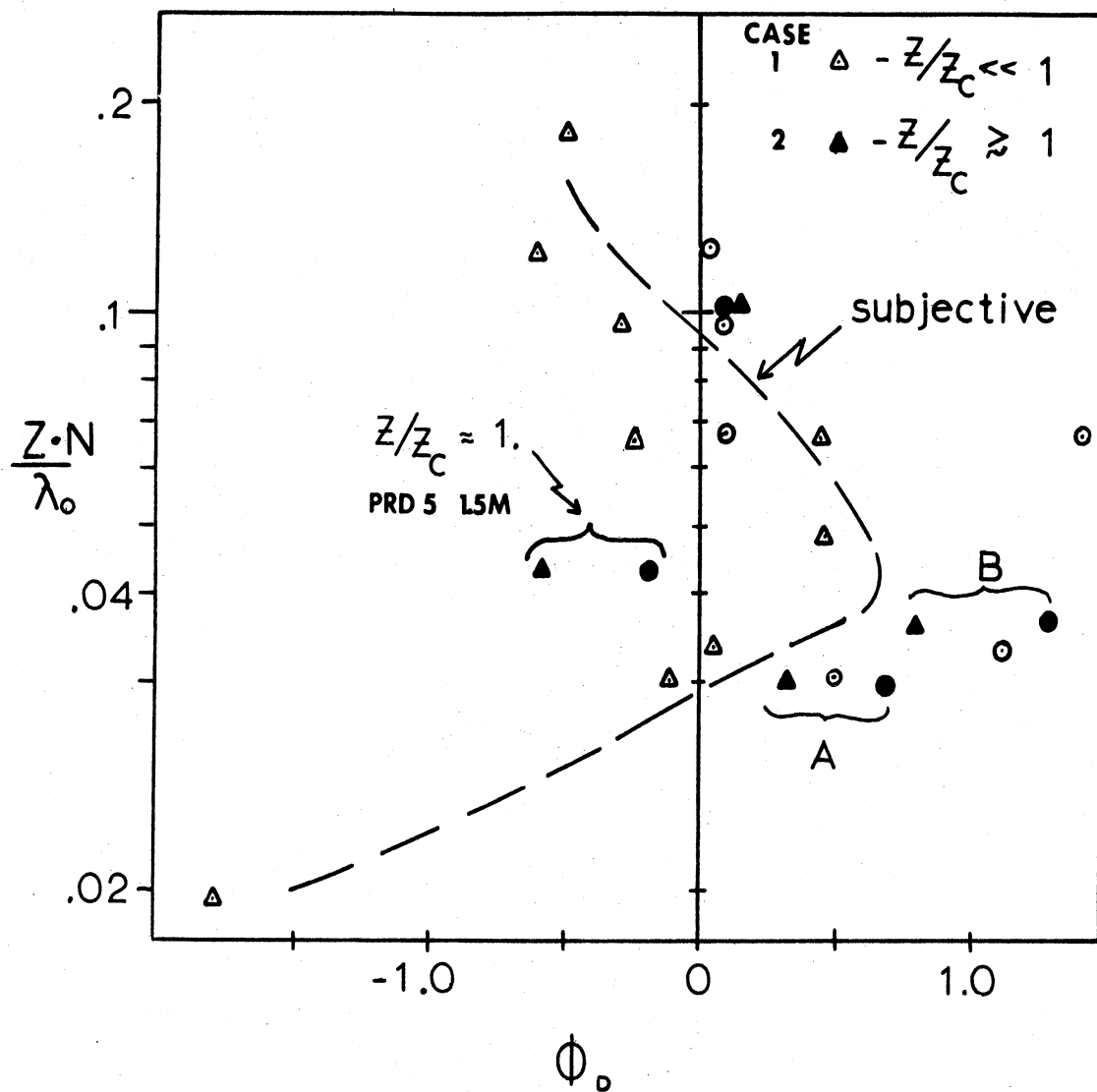


Figure 6.58: Non-dimensional divergence, ϕ_D , as a function of $(Z/\lambda_0) \cdot N$ where λ_0 would be representative of wave length corresponding to wave spectrum peak and N is a linear correction which is inversely proportional to wave height.

be noted that the points labeled A and B were from Period 4 which was a Case 2 period, but phase relationships during Period 4 (Figure 6.16, page 130) reflected those associated with Case 1.

The negative value at the lowest position on the figure is from the 1.5 meter level during Period 1. This is the only estimate included from Periods 1 and 2 because of the uncertainty in ϕ_e due to the failure of the velocity spectra to approach a $-2/3$ slope. However, one would expect a sign change at this level due to the occurrence of positive stress near the wave spectrum peak.

The results shown in Figure 6.58 suggest that there is a relation between the sign of the divergence term, which is normally assumed negligible over land, and $(z/\lambda_0) \cdot N$. In a region above $(z/\lambda_0) \cdot N = .1$ and also near the critical level the divergence term is negative. ($(z/\lambda_0) > .1$ was also associated with the "supplemental maximum".) However, for $.03 < (z/\lambda_0) \cdot N < .1$ the divergence term is positive. These results would indicate the wave length could be an "external parameter" used as a scaling length if one considers for a given height over waves, local production as related to local dissipation of turbulent kinetic energy. Although the evidence is very weak in view of the number of points, the results indicate that the dynamics near the supplemental maximum could be similar to those near the critical level.

7. CONCLUSIONS

The subject of this study is turbulent processes in the layer of air from 1 to 15 meters above water waves. The purpose is to examine, from observations in a natural regime, the nature and extent of the influence of the wave field on the turbulent airflow. Results from the observed data are presented and interpreted in Chapter 6. where it is ascertained that significant fluctuations were observed in the airflow due to the underlying water surface.

Conditions were observed during times when the "critical level" was near the level of measurement and when the "critical level" was effectively at infinity. For the latter case, for the first time in a natural regime, cospectral results of the velocity components showed horizontal momentum being transported upward from the waves.

The following conclusions apply to the nature and extent of the waves' influence and include when applicable, the roles of the critical level and the wave imparted momentum:

1. Fluctuations in the airflow due to the underlying wave surface do not decrease with height as in the manner expected for simple bending of streamlines by the mobile water surface.
2. Spectral bands of energy concentrations associated with the wave-induced fluctuations broaden with increasing height due, apparently, to diffusive properties of turbulence.

3. During times when the critical level is near the level of measurements (and, therefore, near the surface), phase relationships between velocity components and the waves agree with those predicted by analytical theory as described by Lighthill (1962).
4. During times when the critical level is effectively at infinity, the waves are a source of horizontal momentum for the airflow. A "supplemental maximum" in u may occur above $z/\lambda_0 = .1$ where z is the level above the surface and λ_0 is the wave length of the wave spectrum peak.
5. Stress enhancement of 100 to 150% occurs within bands corresponding to the wave spectrum peak. The enhancement is not dependent on whether the critical level is near the measurement levels or effectively at infinity.
6. Wave-induced fluctuations are superimposed, within relatively narrow bands, on the wide frequency scale corresponding to boundary layer turbulence. The superimposed fluctuations do not influence the universal properties of the velocity spectra at high frequencies. Velocity spectra approach a $-2/3$ power law relation and in smoothed spectra have maxima at natural frequencies ($f = nz/\bar{U}$) comparable to those observed in investigations over land.

7. Direct measurements of stress are not constant with height but decrease as the surface is approached and also exceed those estimated from wind profiles by a factor of 2 to 4.
8. Relative intensities (σ_u/u_* , σ_w/u_*) of velocity fluctuations increase with increasing C/u_* , a measure of wind-wave conditions.
9. A scale representing the extent of influence of the waves on the turbulent kinetic energy balance with respect to the importance of the divergence term appears to be $z/\lambda_0 \approx .1$. The divergence term is positive from z/λ_0 equal .03 to .1 for cases when the critical level is effectively at infinity. z is the height above mean water level and λ_0 is the wave length of the spectrum peak.

Conclusions 8 and 9 support relations suggested by Kitaygorodskiy (1969), Equations 6.8 and 6.9, page 204, and indicate that the wave field could be defined with a single parameter, the wave length corresponding to the wave spectrum peak. A layer of fully developed turbulence, for which assumptions over ground could be applied, exists above $z/\lambda_0 = .1$ for conditions when C/u_* is large.

If these results are representative of conditions existing over the oceans, analyses of the boundary layer over a majority of the earth's surface cannot be based on the assumption

that the surface is a rigid boundary. The influence of the waves on the adjacent airflow has been found to be too significant to rely on overland data to describe the boundary layer over waves. Reliable empirical relations giving the flux of momentum as a function of the wind profile and density gradients will have to be formulated from data obtained over the ocean surface itself.

APPENDIX A

DISCUSSION OF HOT-WIRE RELATIONS AND
CONSTANTS REQUIRED FOR INTERPRETATION

A.1 Discussion of Hot-wire Relations

This section describes two separate approaches for obtaining the relation between a fluctuating hot-wire signal and fluctuating velocity components. The final form in both cases is that given by Equation 3.2 , page 51. Both derivations were used in order to provide independent methods for determining calibration constants.

The first derivation employs a general expression relating the hot-wire signal to properties of the air-flow. Investigations leading to this derivation and discussions of its use have been made by Tielman (1967), Sandborn (1967) and Weiler (1966). In the above studies, the measured signal is considered to be a function of the instantaneous velocity, angle of inclination and temperature,

$$E = E(U, \phi, T) \quad A-1$$

Where E = measured voltage

$$U = \text{total instantaneous velocity} \\ = \left[(\bar{U} + u)^2 + v^2 + w^2 \right]^{1/2}$$

ϕ = angle of inclination of wire to mean wind, U ,
(see Figure A.1)

T = temperature.

If the temperature dependence is neglected, the differential form of Equation A-1 is

$$dE = \frac{\partial E}{\partial \bar{U}} dU + \frac{\partial E}{\partial \phi} d\phi . \quad A-2$$

If the mean wind, \bar{U} , is much greater than the turbulent components (u, v and w) and with the substitution $d\phi = w/\bar{U}$

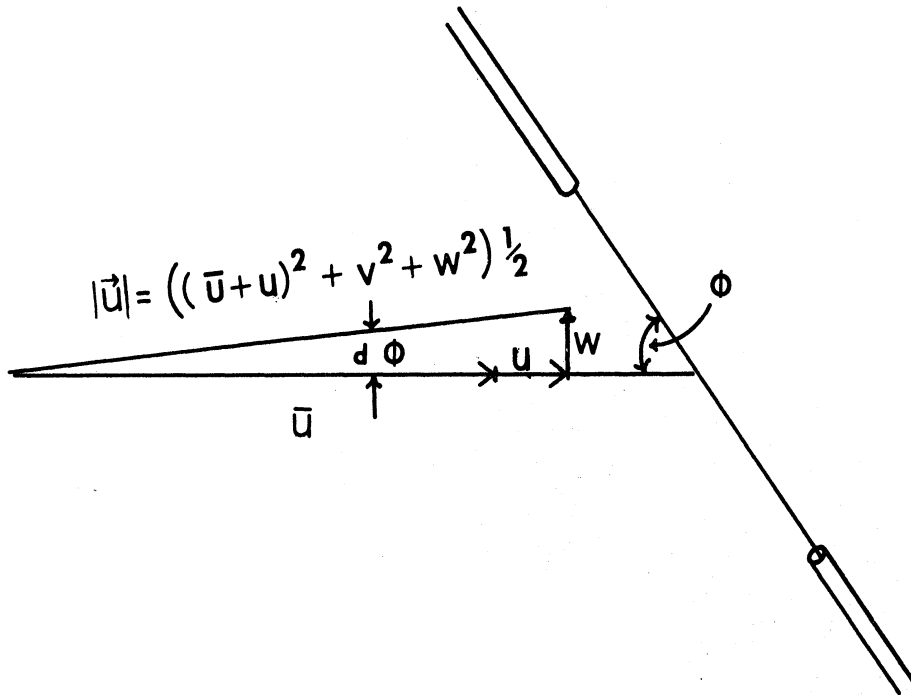


Figure A.1: Flow geometry with respect to yawed hot-wire.

(see Figure A.1) and $du = u$, Equation A-2 can be written

$$dE = e = \frac{\partial E}{\partial U} u + \frac{1}{U} \frac{\partial E}{\partial \phi} w. \quad A-3$$

Furthermore, Arya and Plate (1968) have shown that

$$\frac{1}{U} \frac{\partial E}{\partial \phi} = c \cdot \cot \phi \cdot \frac{\partial E}{\partial U}. \quad A-4$$

Therefore, a relation between hot-wire signal fluctuations (e) and velocity components (u,w) is

$$e = \frac{\partial E}{\partial U} [u + c \cdot w \cdot \cot \phi], \quad A-5$$

where

$\frac{\partial E}{\partial U}$ is a scaling constant (velocity to volts)

c is an empirical constant which corrects for deviations from a perfect cosine response.

Another derivation was formulated by Davies and Fisher (1964). The form of the calibration constant in the resulting equation leads to the use of in situ calibrations. This derivation begins with a generalized form of King's Law,

$$E^2 - E_0^2 = K \cdot U^n \cdot \sin^m \phi, \quad A-6$$

where

U = instantaneous wind

E = measured voltage

E_0 = voltage for $U = 0.0$

K = scaling constant

n and m = empirical indexes.

Differentiating Equation A-6, assuming K remains constant, one gets the following expression for the fluctuating signal in terms of the velocity components,

$$2 \cdot E \cdot dE = K \cdot U^{n-1} \cdot \sin^m \phi (n \cdot dU + m \cdot \cot \phi \cdot d\phi). \quad A-7$$

Substitution of K from Equation A-6, $w/U = d\phi$, $u = du$ and $e = dE$ into Equation A-7, with suitable rearrangement, gives the following expression

$$e = \frac{n}{2 \cdot U} \cdot \left(\frac{E^2 - E_0^2}{E} \right) \cdot \left(u + \frac{m}{n} \cdot w \cdot \cot \phi \right) \quad (a)$$

or

A-8

$$e = n \cdot K' \cdot (u + c \cdot w \cdot \cot \phi), \quad (b)$$

where $K' = \frac{1}{2} \cdot \frac{1}{U} \cdot \left(\frac{E^2 - E_0^2}{E} \right)$ (in situ calibration constant from averaged values over measurement period)

$$c = m/n.$$

Equation A-8b is a general differential expression similar to Equation 3-2, page 51, and also to Equation A-5. In Equation A-5, $\frac{\partial E}{\partial U}$, is comparable to $n \cdot K'$ of Equation A-8b.

A.2 Constants and Calibrations for Hot-Wire Interpretations

In order to interpret hot-wire signals, selections of procedures for determining constants in the expressions of the preceding section have to be made. In general, the constants can be grouped according to what determines their relative values, as follows:

- i) n and m (or $c = \frac{m}{n}$), geometrical features (length to diameter ratio),
- ii) K' or $\frac{\partial E}{\partial U}$, resistance change or contamination of filament.

A.2.1 Empirical Constants m and n or $c = \frac{m}{n}$

Several investigations, Webster (1962), Champagne, et al. (1967), Arya and Plate (1968), performed with considerable accuracy have shown some variation in values of the constants n and m with averages being approximately .5 and .45 respectively for large ratios of length to diameter (such as that used in the present experiment). The n=.5 value is the same as that suggested earlier by King (1914) whereas Collis and Williams (1959) suggest a value of .45 for n. Values of the constants, n and $c = \frac{m}{n}$ were determined during the present study for the purpose of comparison with values suggested by the above investigations. Figure A.2 shows results from tests in a laboratory wind tunnel which indicate that n = .5 (see Equation A-6) is a good selection for filaments used in this study.

The empirical constant c, ($= \frac{m}{n}$), was estimated from Equation A-4 using the following substitutions

$$1) \frac{\partial E}{\partial U} = \frac{n}{2 \cdot U} \left(\frac{E^2 - E_0^2}{E} \right) \text{ (from Equations A-5 and A-8a)}$$

$$2) n = .5$$

$$3) \phi = 45^\circ, \text{ i.e. } \cot \phi = 1$$

The resulting expression is independent of flow rate (U) and is

$$c \approx 4 \cdot \frac{\Delta E}{\Delta \phi} \cdot \left(\frac{E}{E^2 - E_0^2} \right). \quad \text{A-9}$$

Values of ΔE were determined for various rotation angles ($\Delta \phi = 5^\circ$ to 15°) where E was that at $\Delta \phi = 0$. Figure 3.5 shows the

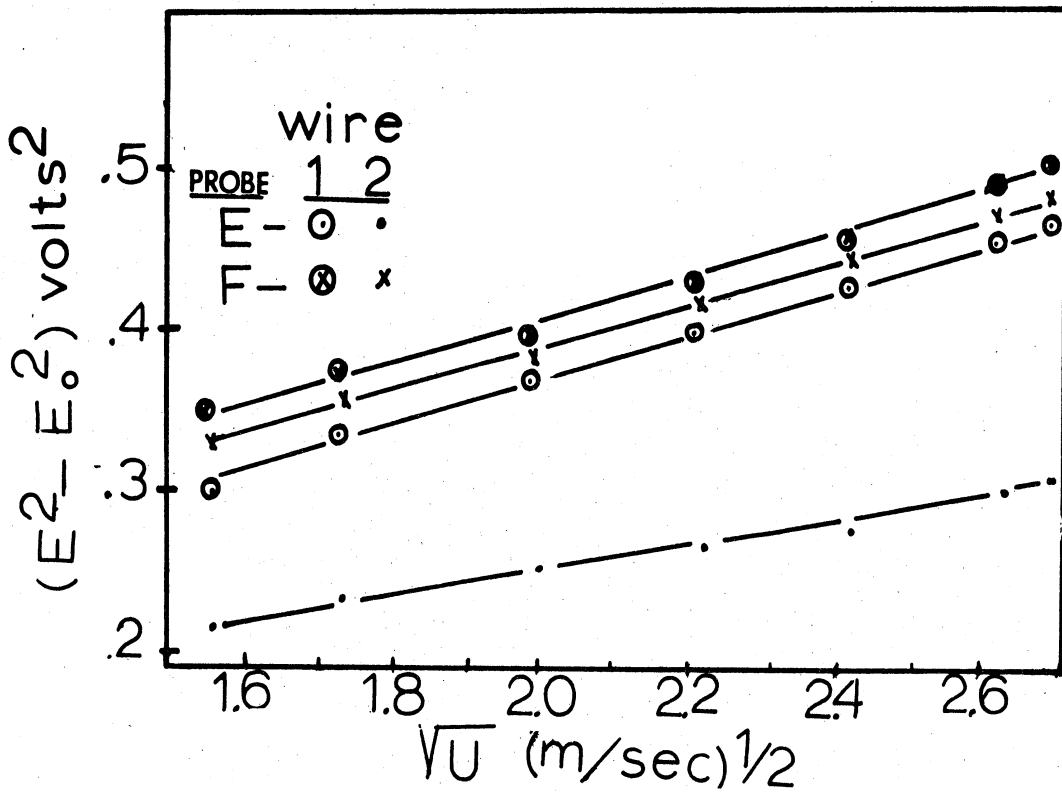


Figure A.2: Calibration curves for hot-wires (Department of Meteorology and Oceanography Wind Tunnel).

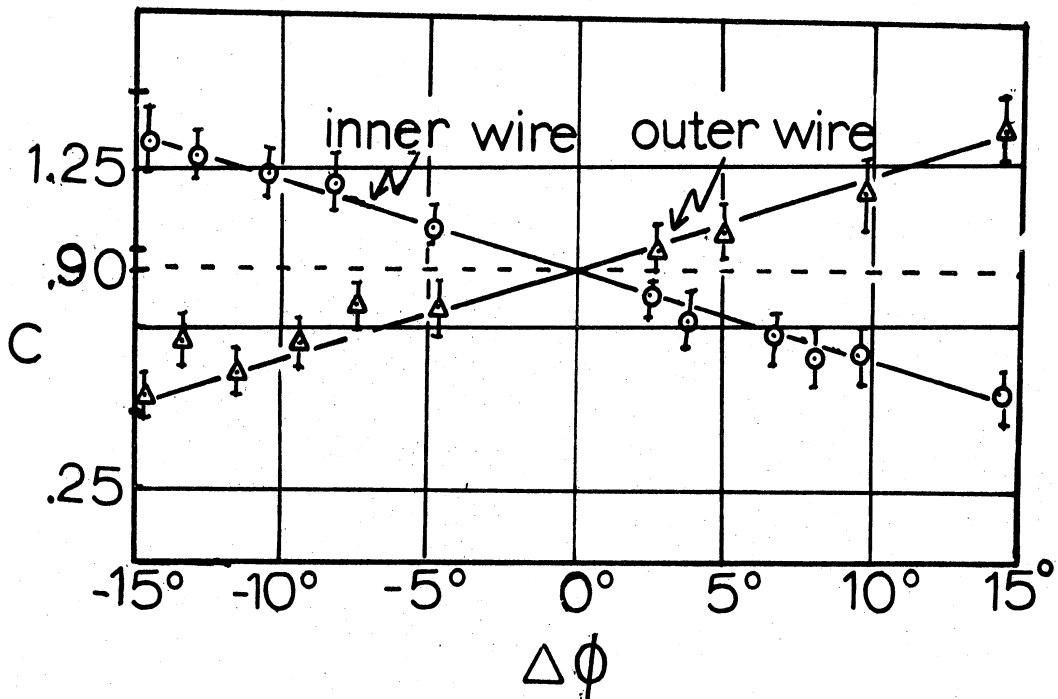


Figure A.3: Composite of several estimates of empirical constant c where lines were drawn to intercept $c = 0.90$ at $\Delta\phi = 0$.

tunnel-calibration unit with the angular scale used to determine $\Delta\phi$.

Estimates shown in Figure A.3 indicate that .90 is a reasonable value for $\Delta\phi = 0$. Figure A.3 represents a composite of six calibration runs and includes 13 filaments. A value of .90 was that suggested by Arya and Plate (1968) and Sanborn (1967) who determined the value with more precise calibration methods than used in this study.

A.2.2 Scaling Constant (K) and the Relative Response of Two Wires (K_1/K_2)

The in situ approach method with cup anemometer data for \bar{U} in the expression $K = (E^2 - E_0^2)/(4\bar{U}E)$, appeared to be the most reliable for obtaining the scaling constant. Experience during wind tunnel calibrations, however, indicated that E_0 could change as much as 20% over a 45 to 60 minute period. For this reason, the relative response (K_1/K_2) of the two wires was selected as an additional useful parameter.

The relative response method, referred to as the $\Delta E_1/\Delta E_2$ method, arises by considering K_1 in the form given by Equation A-5, being

$$K_1 = \frac{\partial E_1}{\partial U} \approx \frac{\Delta E_1}{\Delta U}, \quad i = 1, 2; \text{ for wires 1 and 2.}$$

It is seen that relative response or ratio of the two K_1 's can be given by $\Delta E_1/\Delta E_2$, since

$$\frac{K_1}{K_2} = \frac{\Delta E_1}{\Delta U} \cdot \frac{\Delta U}{\Delta E_2} = \frac{\Delta E_1}{\Delta E_2}. \quad \text{A-10}$$

Values of ΔE_1 ($i = 1,2$) were computed from values of E_1 ($i = 1,2$) averaged over four different time intervals (34, 68, 132 and 273 seconds). Each averaging time provided several values of $\Delta E_1/\Delta E_2$ with the number of values decreasing, of course, as averaging time increased. Mean values of $\Delta E_1/\Delta E_2$ for each averaging time interval appear in Table 3.1 and are listed as columns 1 to 4.

APPENDIX B

DERIVATION OF EQUATIONS TO CORRECT SPECTRAL
ESTIMATES BY AXIS ROTATION AND INFLUENCE OF
ROTATION ON SPECTRAL RESULTS

B.1 Derivation of Equations for Correcting Spectral Estimates by Rotation of Coordinate Axis

Equations 3-7 to 3-14 in Section 3.2.1.5 can be obtained by considering the complex Fourier coefficients which were used to obtain the original spectral estimates. The expressions and algebra are identical to the familiar relations for transformation of two velocity components (u, w) by rotation (θ) except the components (u_n and w_n) are now functions of frequency (or harmonic numbers) instead of time. In the rotated coordinate system, the components u'_n and w'_n are

$$u'_n = u_n \cos\theta + w_n \sin\theta$$

B-1

$$w'_n = -u_n \sin\theta + w_n \cos\theta.$$

The original complex coefficients (u_n, w_n) in terms of real and complex parts are,

$$u_n = a_n - ib_n$$

B-2

$$w_n = c_n - id_n$$

Amplitudes and the cross product for the original system are related to variance ($\phi_{ii}(n)$) and covariance ($\phi_{ij}(n)$) spectral estimates as follows;

$$u_n u_n^* = (a_n^2 + b_n^2) = \phi_{uu}(n) \cdot \left(\frac{2}{T}\right).$$

B-3

¹(*) is used in this appendix to denote the complex conjugate; whereas in Section 3.2.1.5 it is used to denote quadrature spectral estimates.

$$w_n w_n^* = (c_n^2 + d_n^2) = \phi_{ww}(n) \cdot \left(\frac{2}{T}\right) \quad \text{B-4}$$

$$\begin{aligned} u_n w_n^* &= (a_n c_n + b_n d_n) - i(c_n b_n - a_n d_n) \\ &= (\phi_{uw}(n) - i\phi_{uw}^o(n)) \cdot \left(\frac{2}{T}\right) \end{aligned} \quad \text{B-5}$$

where (*) = complex conjugate

T = length of time series

(^o) = quadrature spectral estimates

i = (-1)^{1/2}.

Expressions for the spectral estimates given by Equations B-3 to B-5 are obtained for the new (primed) coordinate system by substituting Equations B-2 into B-1, separating real and imaginary parts and forming products $u_n' u_n'^*$ and $w_n' w_n'^*$ and the cross product $u_n' w_n'^*$. The resulting expressions are;

$$\begin{aligned} u_n' u_n'^* &= (a_n^2 + b_n^2) \cos^2 \theta + (c_n^2 + d_n^2) \sin^2 \theta \\ &\quad + (a_n c_n + b_n d_n) \sin 2\theta \end{aligned} \quad \text{B-6}$$

$$\begin{aligned} w_n' w_n'^* &= (a_n^2 + b_n^2) \sin^2 \theta + (c_n^2 + d_n^2) \cos^2 \theta \\ &\quad - (a_n c_n + b_n d_n) \sin 2\theta \end{aligned} \quad \text{B-7}$$

$$\begin{aligned} u_n' w_n'^* &= \left[(c_n^2 + d_n^2) - (a_n^2 + b_n^2) \right] \sin \frac{2\theta}{2} \\ &\quad + (a_n c_n + b_n d_n) \cos 2\theta - i(c_n b_n - a_n d_n). \end{aligned} \quad \text{B-8}$$

Multiplication of both sides of Equations B-6 to B-8 by T/2 and expressing terms as they appear in Equations B-3 to B-5 gives the following expressions for the new spectral

estimates,

$$\phi'_{uu}(n) = \phi_{uu}(n)\cos^2\theta + \phi_{ww}(n)\sin^2\theta + \phi_{uw}(n)\sin 2\theta \quad \text{B-9}$$

$$\phi'_{ww}(n) = \phi_{uu}(n)\sin^2\theta + \phi_{ww}(n)\cos^2\theta - \phi_{uw}(n)\sin 2\theta \quad \text{B-10}$$

$$\phi'_{uw}(n) = \left[\phi_{ww}(n) - \phi_{uu}(n) \right] \frac{\sin 2\theta}{2} + \phi_{uw}(n)\cos 2\theta - 1 \cdot \phi_{uw}^0(n) \quad \text{B-11}$$

where ϕ'_{jk} = spectral term in new system

ϕ_{jk} = spectral term in original system

ϕ_{jk}^0 = quadrature spectral estimate.

It should be noted that there is no change in the quadrature spectral estimate.

Covariance spectra for a velocity component and a scalar quantity (temperature or wave height) are also changed by a transformation by rotation. Considering the $T_n w_n$ covariance spectrum as an example where w_n' is defined by Equation B-1, one gets

$$T_n w_n'^* = T_n \cdot (-u_n \sin\theta + w_n \cos\theta)^* \quad \text{B-12}$$

Substitution of Equation B-2 for u_n and w_n and the complex form of T_n ,

$$T_n = e_n - i f_n,$$

in Equation B-12 gives

$$T_n \cdot w_n^{*1} = (e_n c_n + f_n d_n) \cos \theta - (f_n a_n - a_n b_n) \sin \theta \\ - 1 \left[(c_n f_n - e_n d_n) \cos \theta - (e_n b_n - a_n f_n) \sin \theta \right] .$$

This yields for the,

cospectrum estimate

$$\phi_{Tw}^i(n) = \phi_{Tw}^o(n) \cos \theta - \phi_{Tu}^o(n) \sin \theta,$$

B-13

quadrature spectrum estimate

$$\phi_{Tw}^o(n) = \phi_{Tw}^o(n) \cos \theta - \phi_{Tu}^o(n) \sin \theta.$$

Equations B-9 to B-11 and ones similar to B-13 were those used for the rotation discussed in Section 3.2.1.5.

B.2 Influence of Rotation on Spectral Results

This section includes examples of the spectral results after various rotation angles for data which were transformed by axis rotation for reasons discussed on page 59. A summary of the influence for the four data sets that required rotations (all 8°) would be;

- 1) Variance spectra changed a negligible amount;
- 2) Cospectra did not change significantly in the spectral region corresponding to the wave-induced stress; and,
- 3) Integrated cospectra increased by a factor of 2 to 6 due to contributions from low frequencies. If low frequency values were initially positive, the rotation erased the positive contributions to the negative integrated value.

Variance spectra, cospectra and cumulative cospectra from Periods 5, 8 and 11 appear in the next 6 figures in the following order¹,

- Figure B.1 and B.2 - Period 5, 4.0 meter level,
- Figure B.3 and B.4 - Period 8, 2.0 meter level,
- Figure B.5 and B.6 - Period 11, 2.0 meter level,

¹Data for Period 9 (2.0 meter level) are not included because the results were nearly identical to those for Period 8.

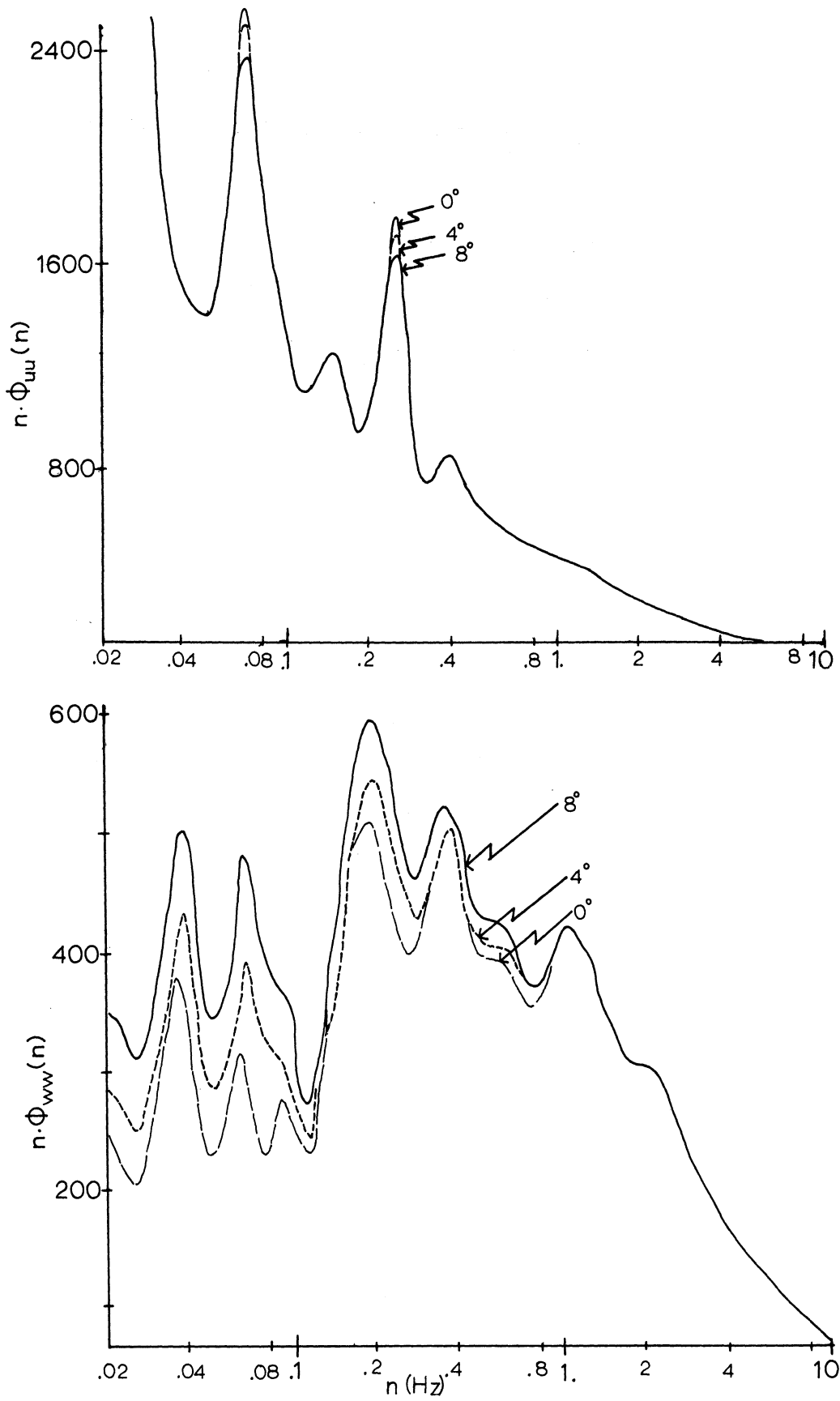


Figure B.1: Variance spectra $(\text{cm/sec})^2$ for 0° , 4° and 8° rotations; Period 5, 4.0 meter level.

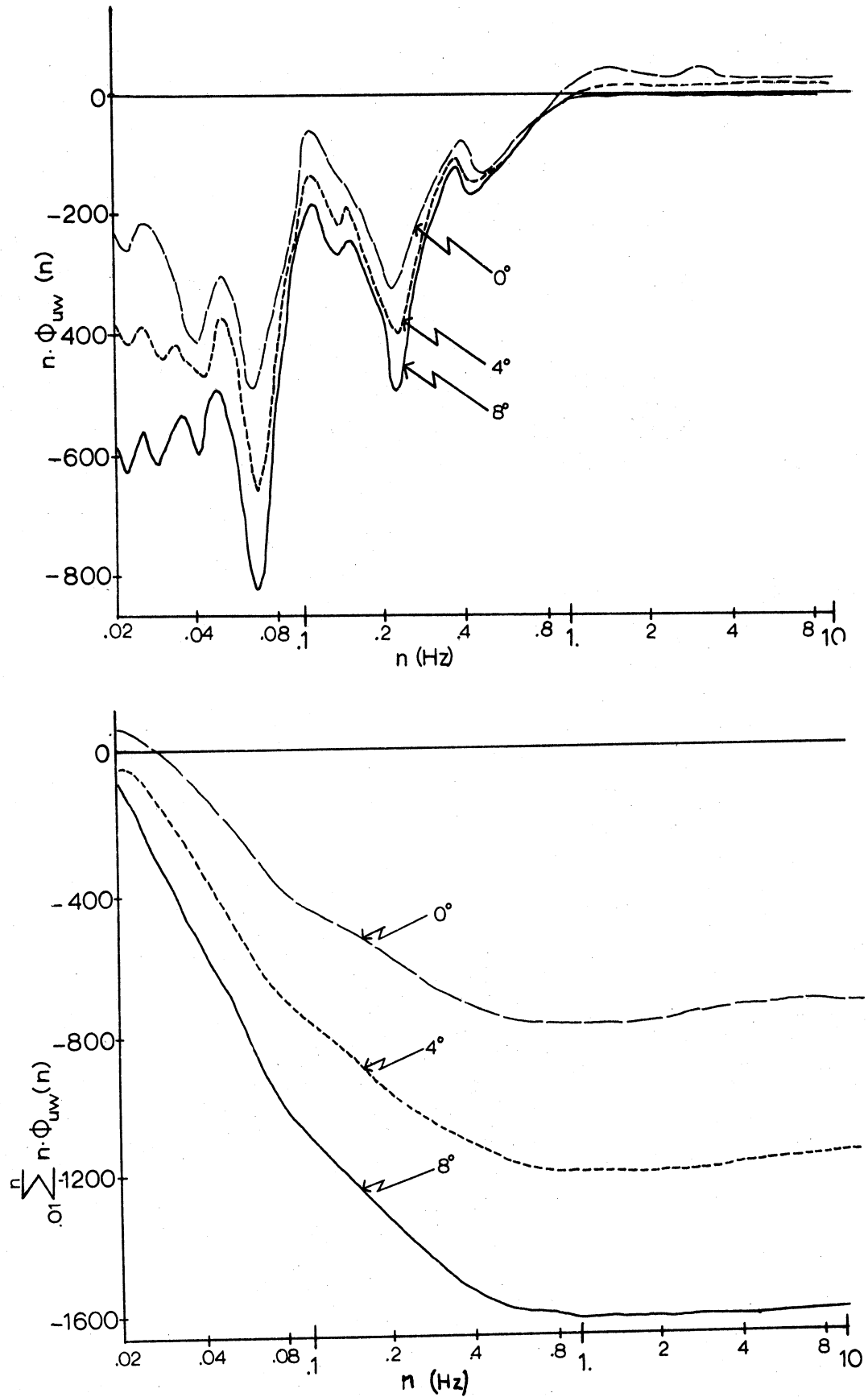


Figure B.2: Cospectra and cumulative cospectra $(\text{cm/sec})^2$ for 0° , 4° and 8° rotations; Period 5, 4.0 meter level.

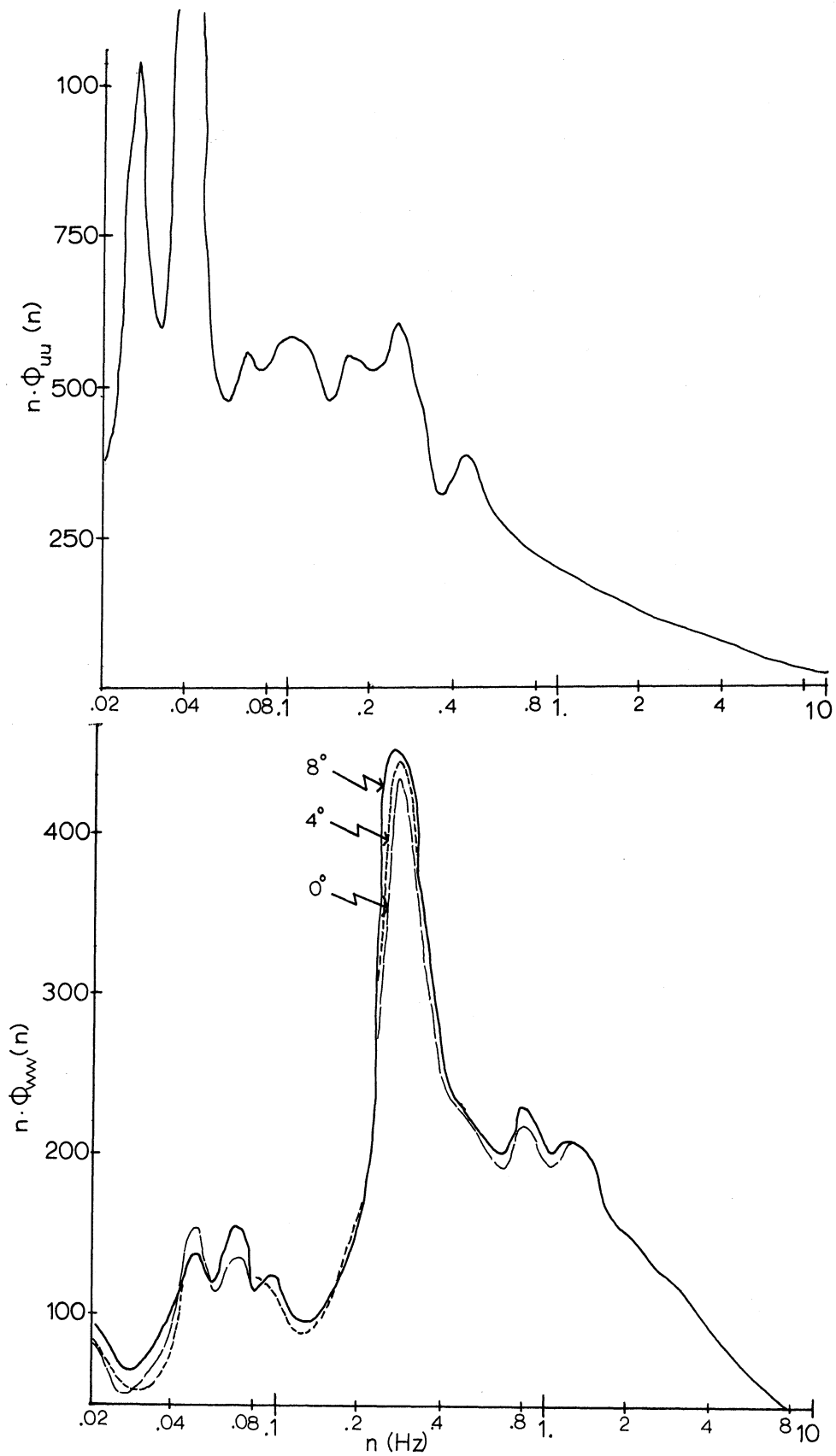


Figure B.3: Variance spectra $(\text{cm/sec})^2$ for 0° , 4° and 8° rotations; Period 8, 2.0 meter level.

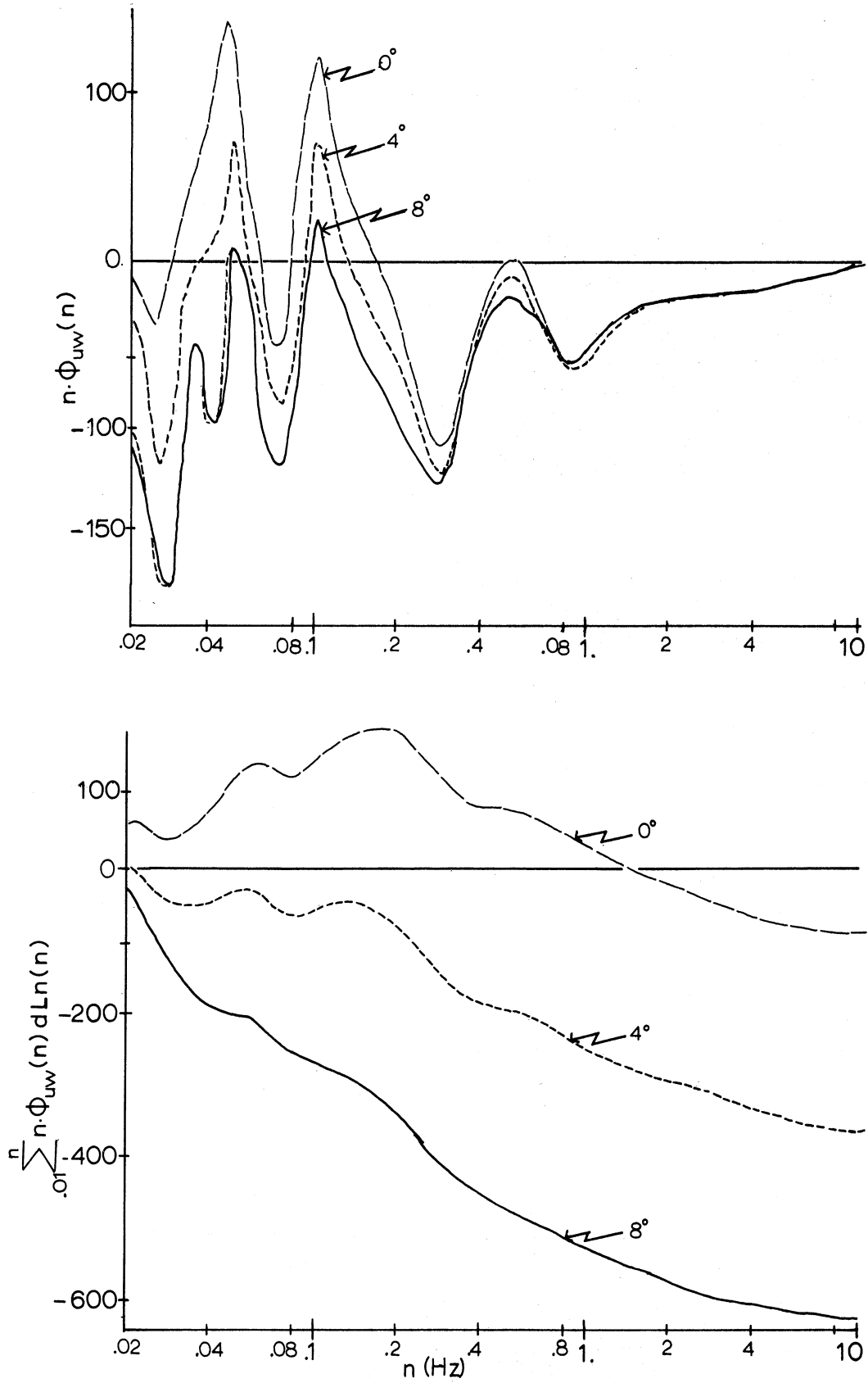


Figure B.4: Cospectra and cumulative cospectra (cm/sec^2) for 0° , 4° and 8° rotations; Period 8, 2.0 meter level.

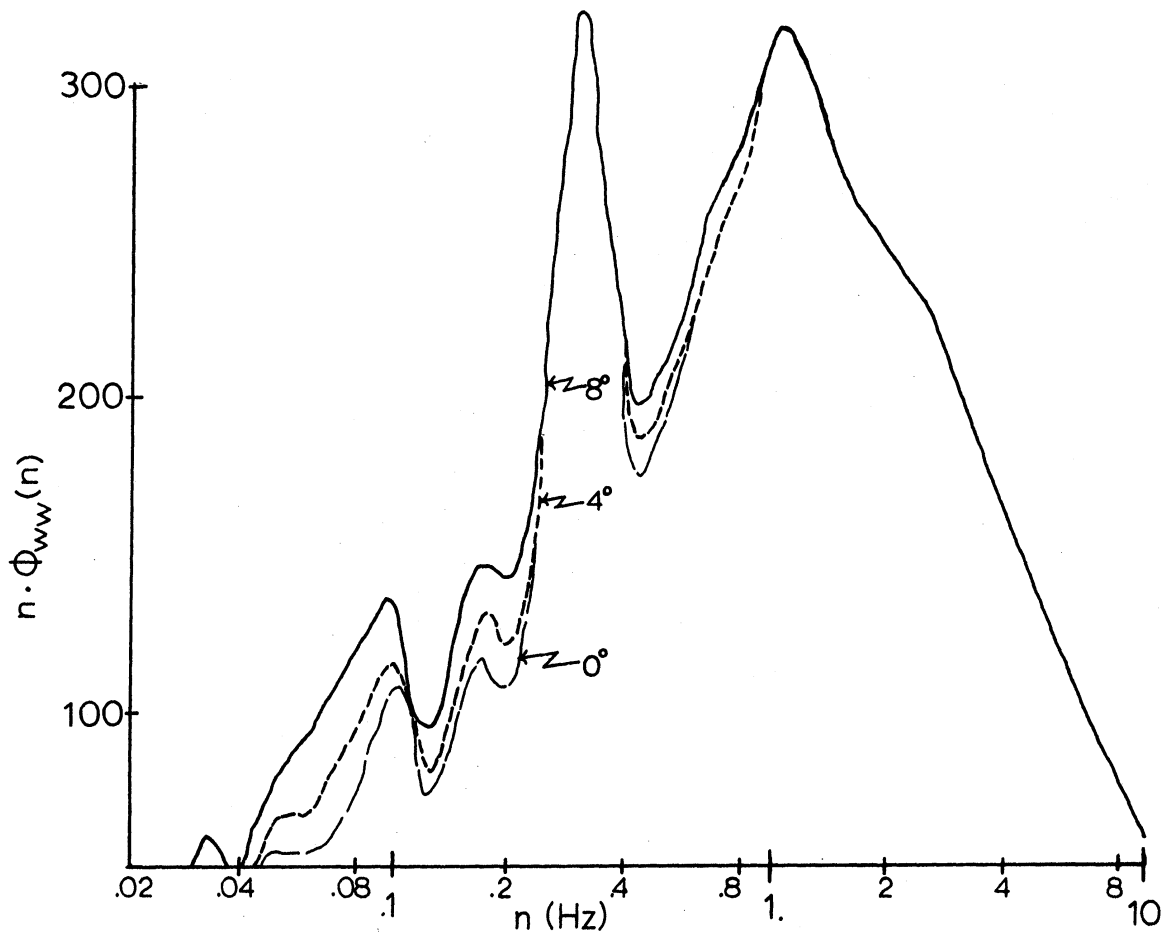
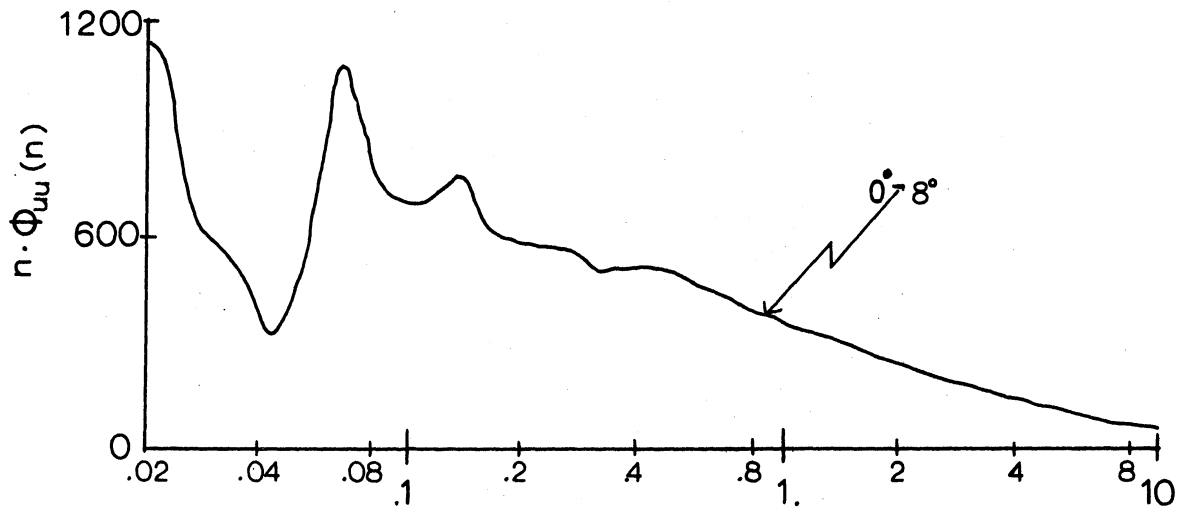


Figure B.5: Variance spectra $(\text{cm/sec})^2$ for 0° , 4° and 8° rotations; Period 11, 2.0 meter level.

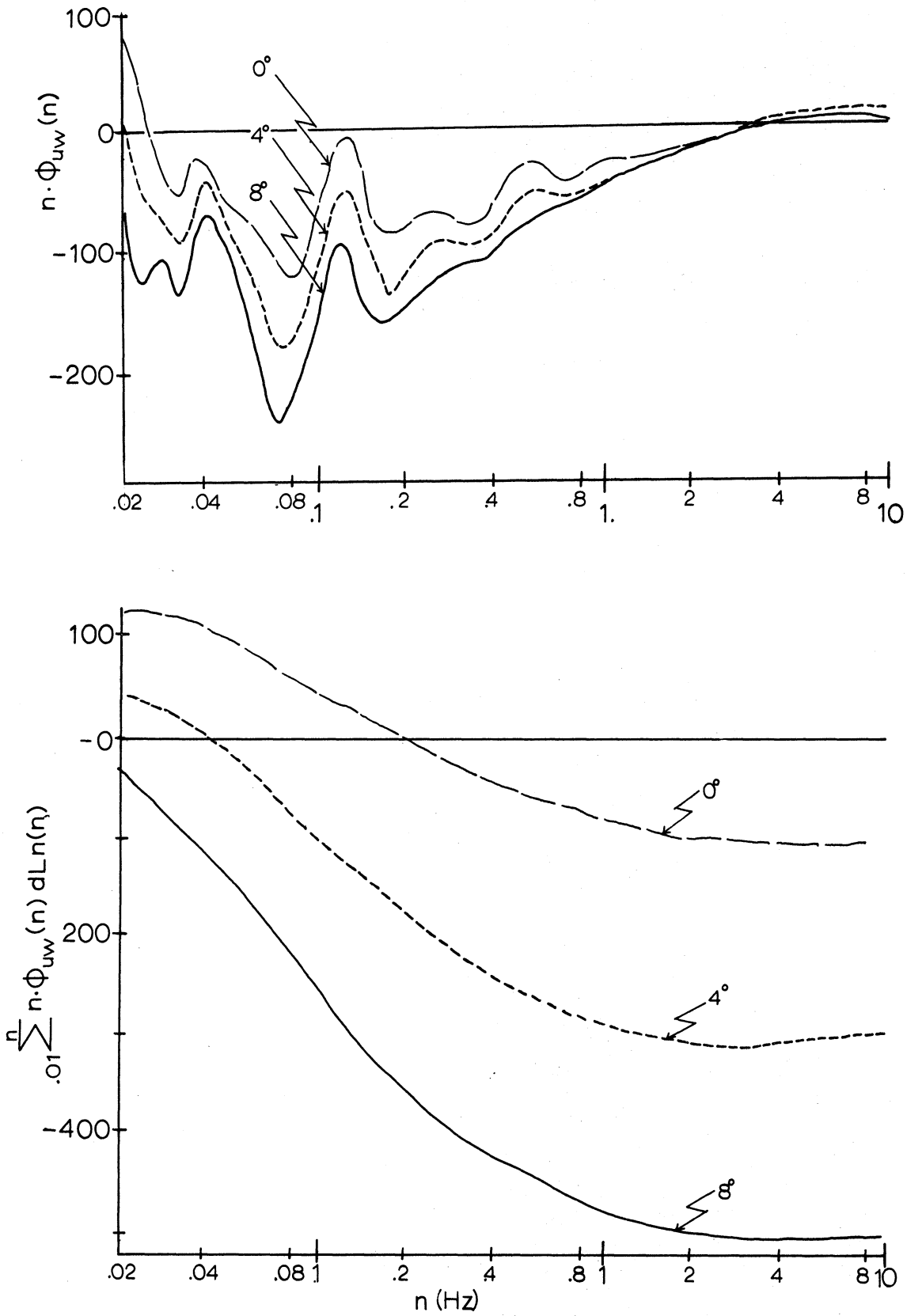


Figure B.6: Cospectra and cumulative cospectra $(\text{cm/sec})^2$ for 0° , 4° and 8° rotations; Period 11, 2.0 meter level.

APPENDIX C

SCHEMATICS OF BRIDGE-AMPLIFIER CIRCUITS
USED IN MEASUREMENTS

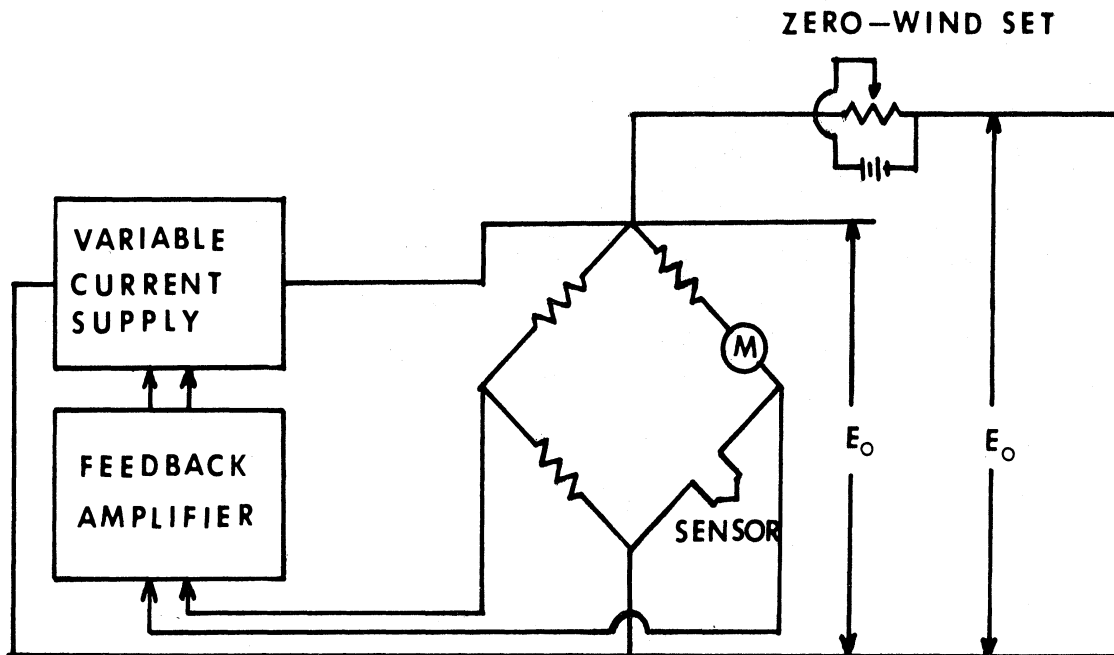
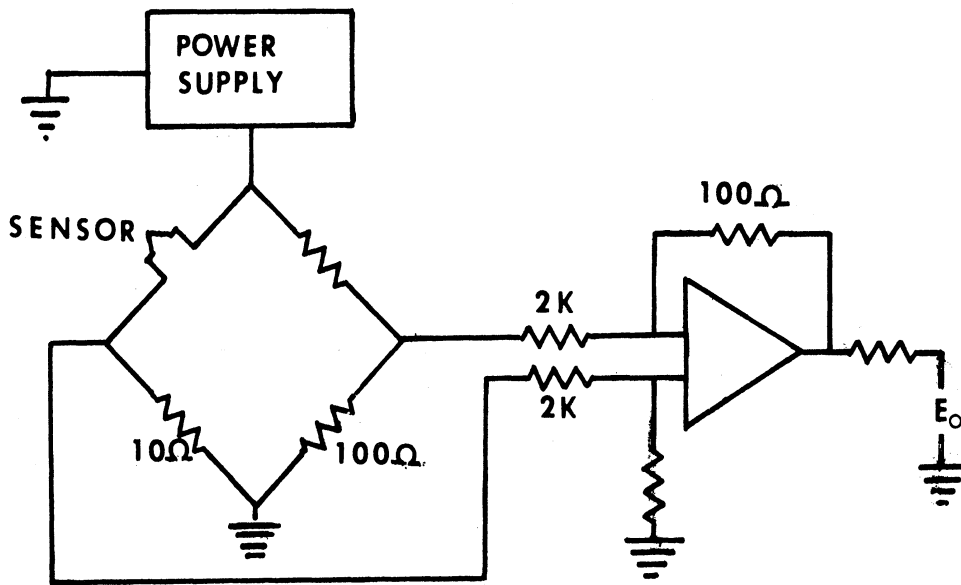


Figure C.1: Hot-wire anemometer bridge-amplifier (constant resistance); Miller, Model M-5.



900-1 BRIDGE-AMPLIFIER

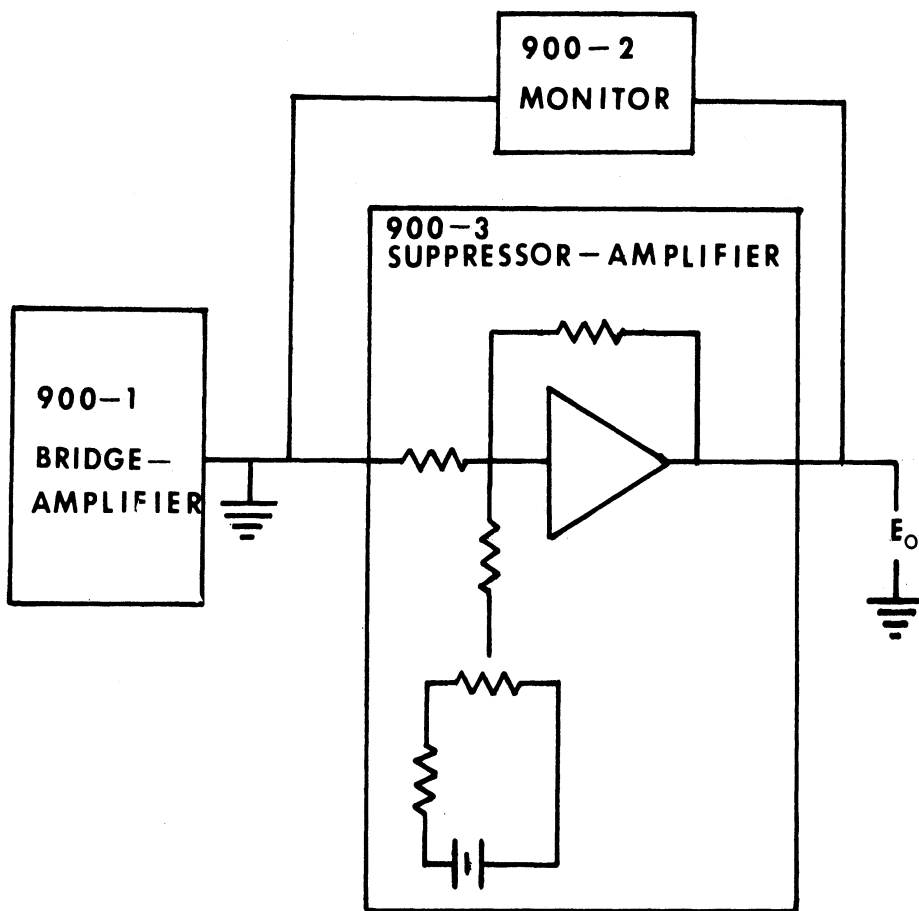


Figure C.2: Temperature system bridge-amplifier (constant current); Flow Corporation System, Series 900.

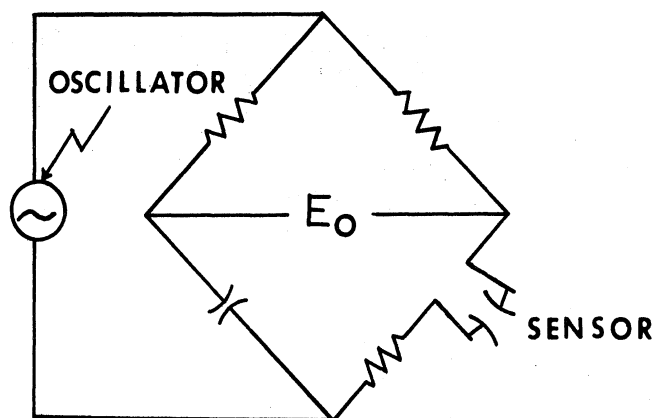


Figure C.3: Typical capacitance bridge showing active oscillator and sensor (wave gauge).

APPENDIX D

COMPUTER PROGRAM FOR AVERAGING OF SPECTRAL VALUES WITH
BANDWIDTH INCREASING LOGARITHMICALLY WITH FREQUENCY

Because experimental objectives may often lead to averaging over local spectral values obtained from harmonic analysis of a single time series, the following discussion and a listing of the subroutine (Fortran IV) used for the logarithmic averaging in this study are given.

D.1 Determining the Averaging Intervals

The interval is, of course, defined by its' first, $n(f)$, and last, $n(L)$, harmonic. The last harmonic for a given interval (i) is related to the first by the following expression,

$$n(L)_i = n(f)_i \cdot \exp (\ln(\text{noin})/(\text{noout}-1)) \quad \text{D-1}$$

where noin = number of original spectral values

noout = number of final spectral values.

A succeeding averaging interval ($i + 1$), $n(f)_{i+1}$, begins one harmonic after the last harmonic in the preceding interval, i.e. $n(f)_{i+1} = n(L)_i + 1$.

D.2 Listing of Subroutine

The internal function FSTEN in statement 0003 determines the base for the logarithmic scale as indicated in Equation D-1. Its' use in statement 0003 is for determining the first endpoint, $n(L)$, and therefore does not coincide with the expression in Equation D-1. Statement 0008 makes the correction, by squaring FSTPNT, so the base indicated by Equation D-1 is that used for determining the averaging interval.

Computations of equivalent degrees of freedom and root mean square values for each averaged value are performed in statements 0012, 0013, 0019, 0020, and 0022-25.

```

0001      SUBROUTINE LOGAVG (DATA,OUT,Y,NOIN,NOOUT,CPS)
          C      SUBROUTINE TO REDUCE THE NUMBER OF POINTS FOR LOG PLOTS
0002      DIMENSION DATA(NOIN),OUT(NOOUT),Y(NOOUT),DF(256),RMS(256),
          ICOUNT(256)
0003      FSTEND (LEN,N)=EXP(ALOG(FLOAT(LEN))/(N+N-2))
0004      NOOUT2=2*NOOUT
0005      NOFST =1
0006      FSTPNT = FSTEND(NOIN,NOOUT)
0007      ENDPNT =FSTPNT
0008      FSTPNT=FSTPNT*FSTPNT
0009      Y(1)=CPS
0010      DO 2 I=2,NOOUT
0011      K=K+1
0012      SUMX=0.0
0013      SUMX2=0.0
0014      NOLAST = ENDPNT
0015      OUT(I-1)=0.0
0016      KK=0
0017      DO 1 J=NOFST,NOLAST
0018      KK=KK+1
0019      SUMX2=DATA(J)*DATA(J)+SUMX2
0020      SUMX=DATA(J)+SUMX
0021      1      OUT(I-1)=OUT(I-1)+DATA(J)
0022      XB2=(SUMX/KK)**2
0023      X2B=SUMX2/KK
0024      COUNT(I-1)=KK
0025      RMS(I-1)=SQRT(X2B-XB2)
0026      IF(X2B.EQ.0.0) GO TO 5
0027      DF(I-1)=(KK*XB2)/X2B
0028      5      IF(NOLAST-NOFST)7,7,6
0029      6      OUT(I-1)=OUT(I-1)/(NOLAST-NOFST+1)
0030      NOFST=NOLAST+1
0031      7      Y(I)=Y(I-1)*FSTPNT
0032      2      ENDPNT=FSTPNT*ENDPNT
0033      OUT(NOOUT)=0.0
0034      DO 3 I=NOFST,NOIN
0035      3      OUT(NOOUT)=OUT(NOOUT)+DATA(I)
0036      IF(NOLAST-NOFST) 9,9,8
0037      8      OUT(NOOUT)=OUT(NOOUT)/(NOIN-NOFST+1)
0038      9      DO 10 I=1,NOOUT
0039      DATA(I)=DF(I)
0040      DATA(I+NOOUT)=RMS(I)
0041      DATA(I+NOOUT2)=COUNT(I)
0042      10      CONTINUE
0043      RETURN
0044      END

```


APPENDIX E

TEMPERATURE SPECTRA AND \overline{wT} COSPECTRA

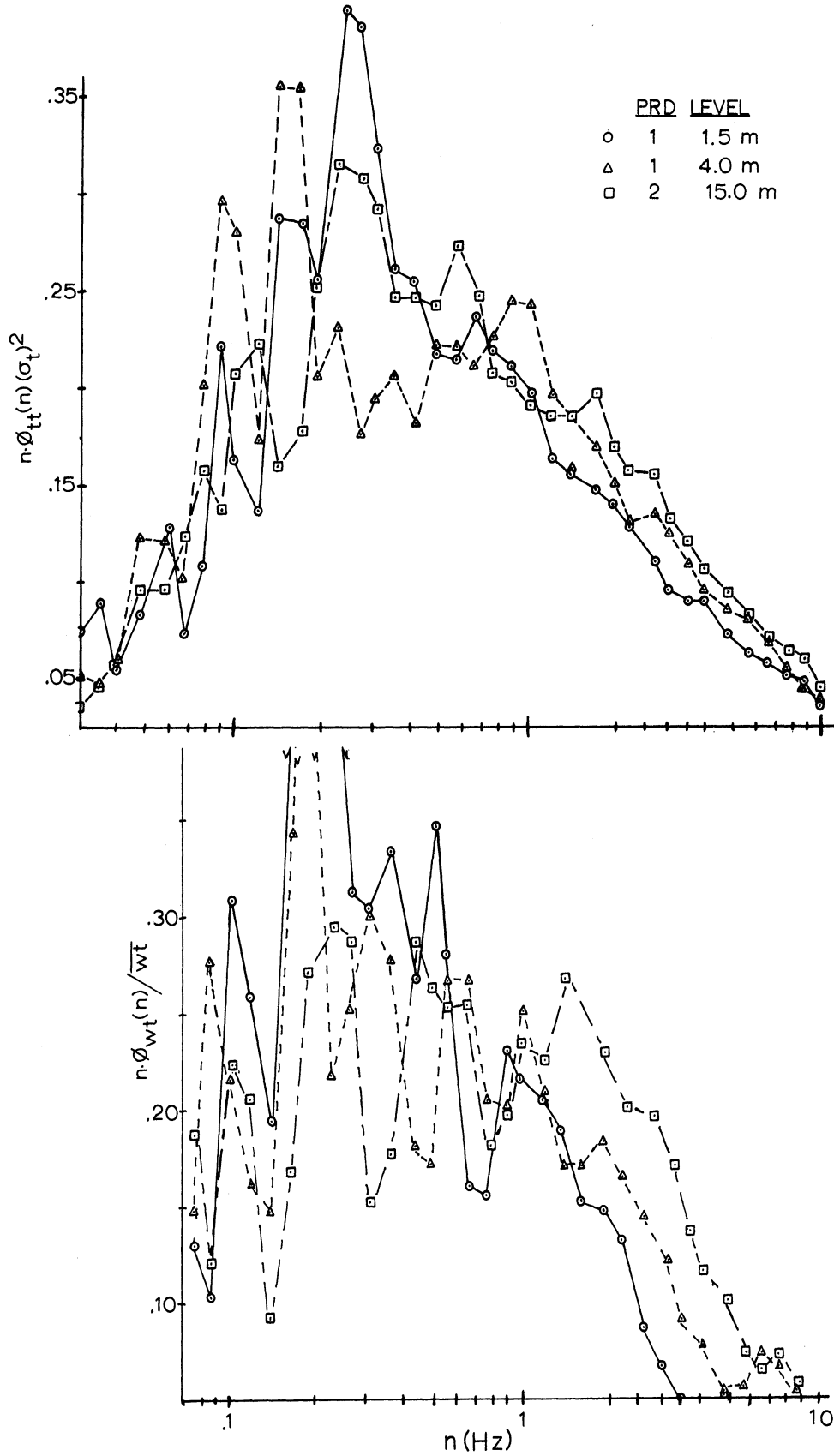


Figure E.1: Normalized temperature (t) spectra and \overline{wt} cospectra for Periods 1 and 2.

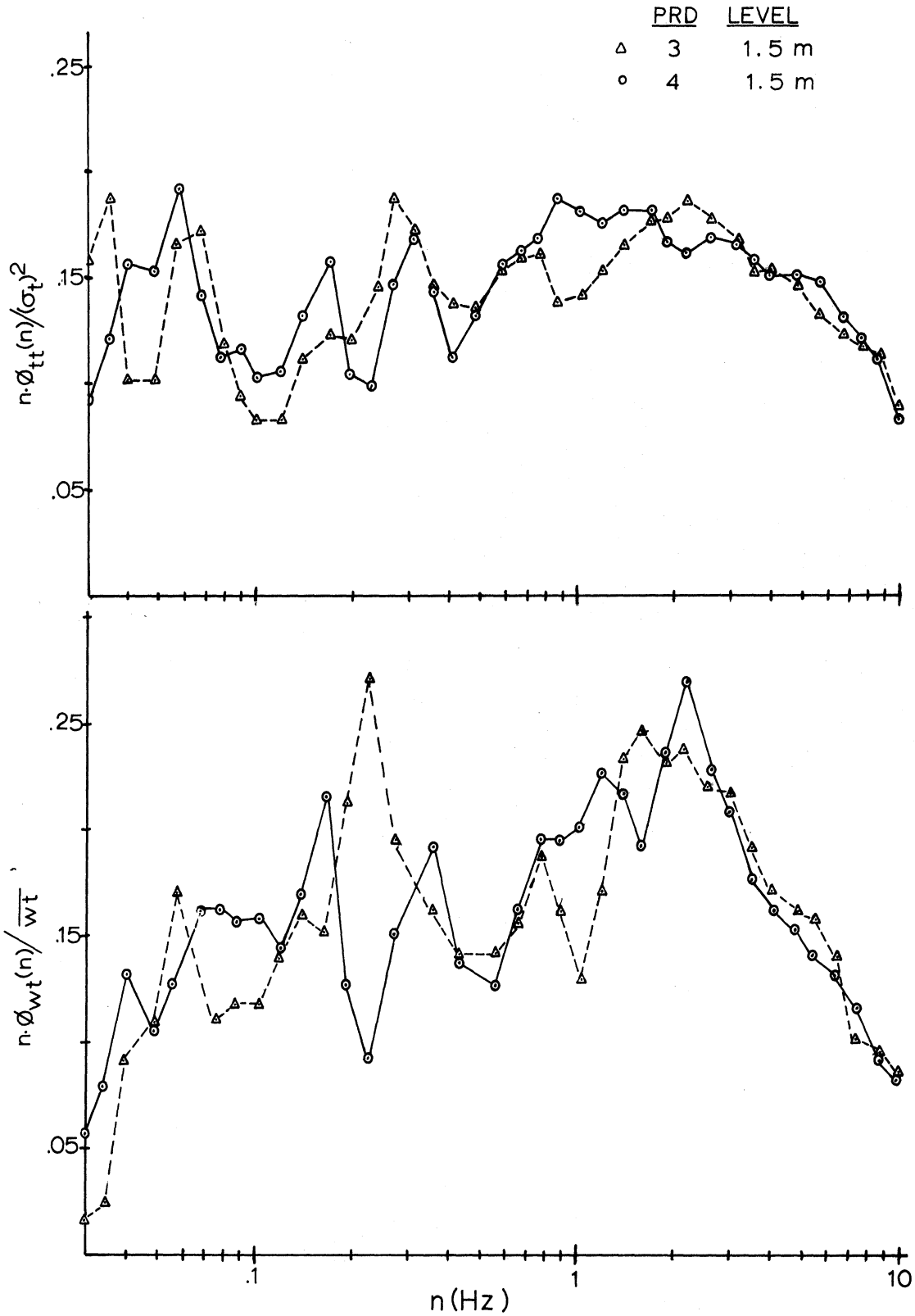


Figure E.2: Normalized temperature (t) spectra and \overline{wt} cospectra for Periods 3 and 4.

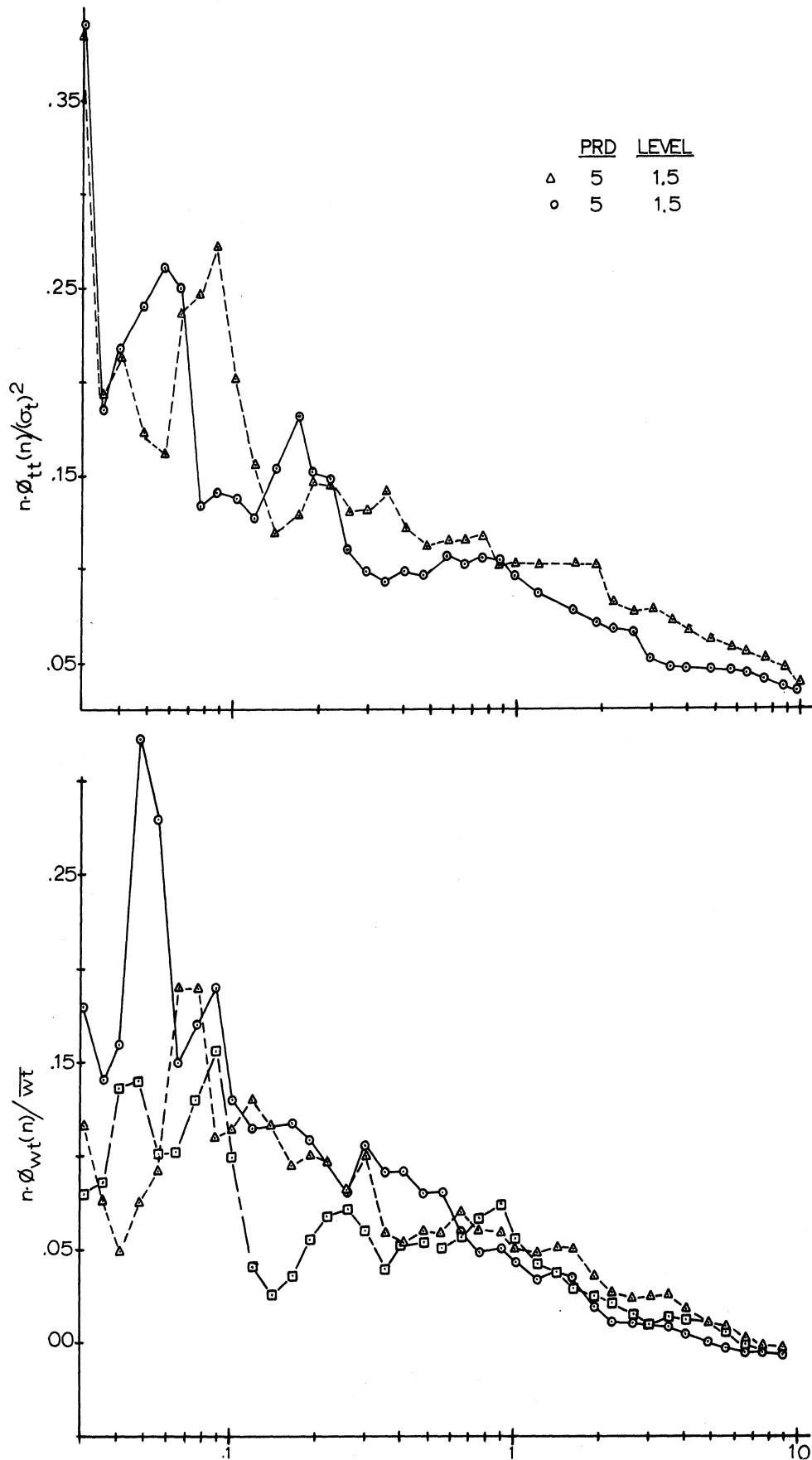


Figure E.3: Normalized temperature (t) spectra and \overline{wt} cospectra for Period 5.

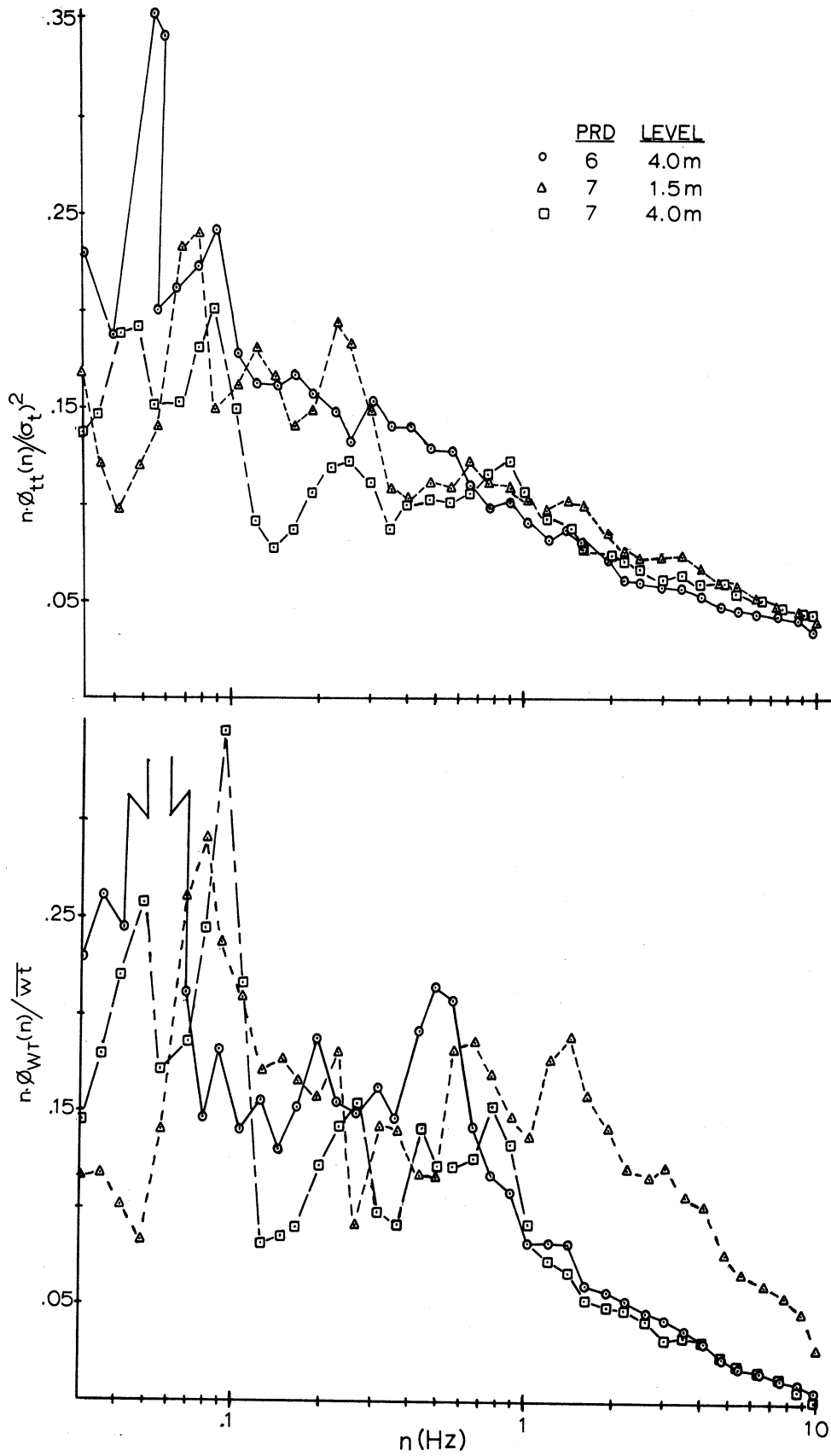


Figure E.4: Normalized temperature (t) spectra and \overline{wt} cospectra for Periods 6 and 7.

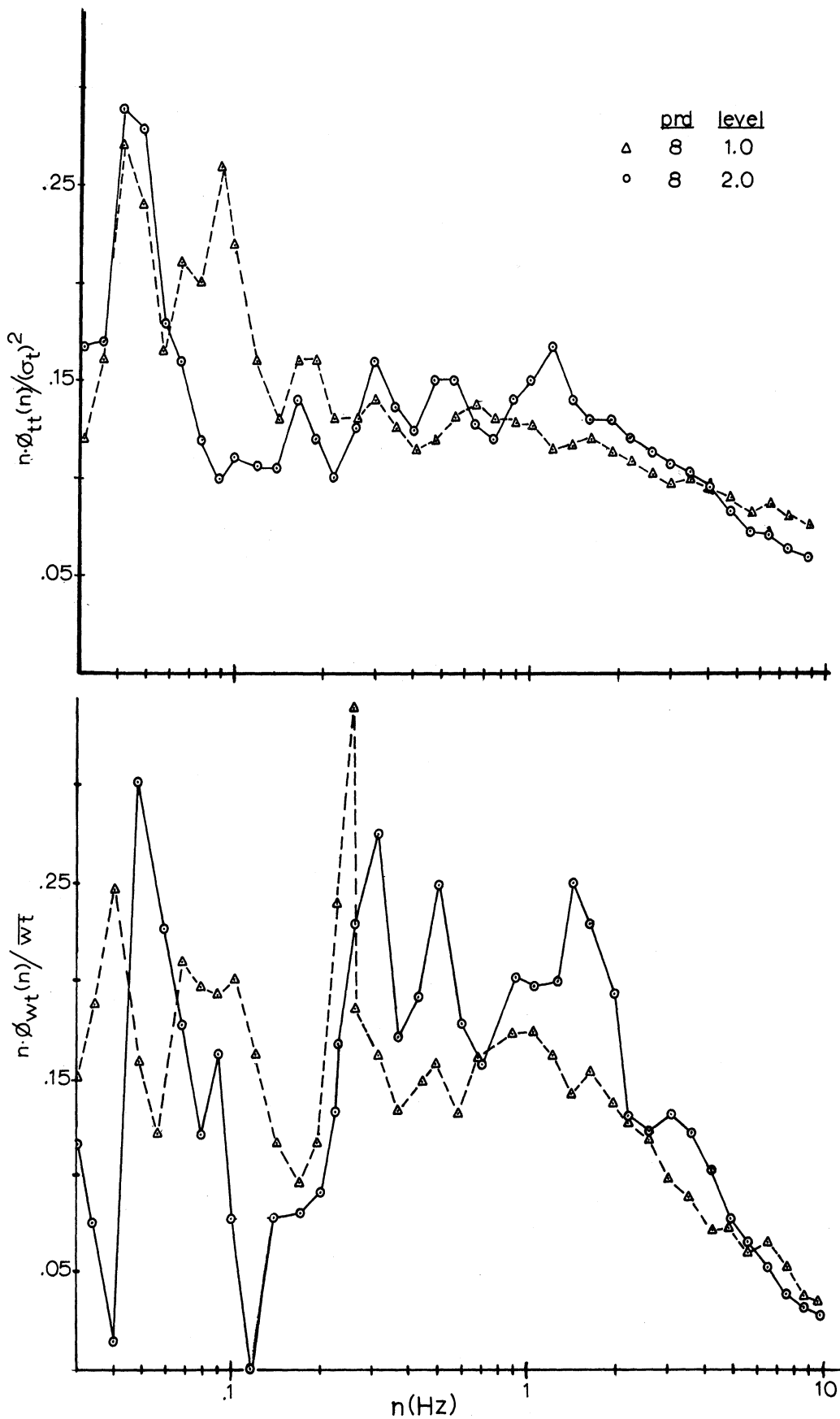


Figure E.5: Normalized temperature (t) spectra and \overline{wt} cospectra for Period 8.

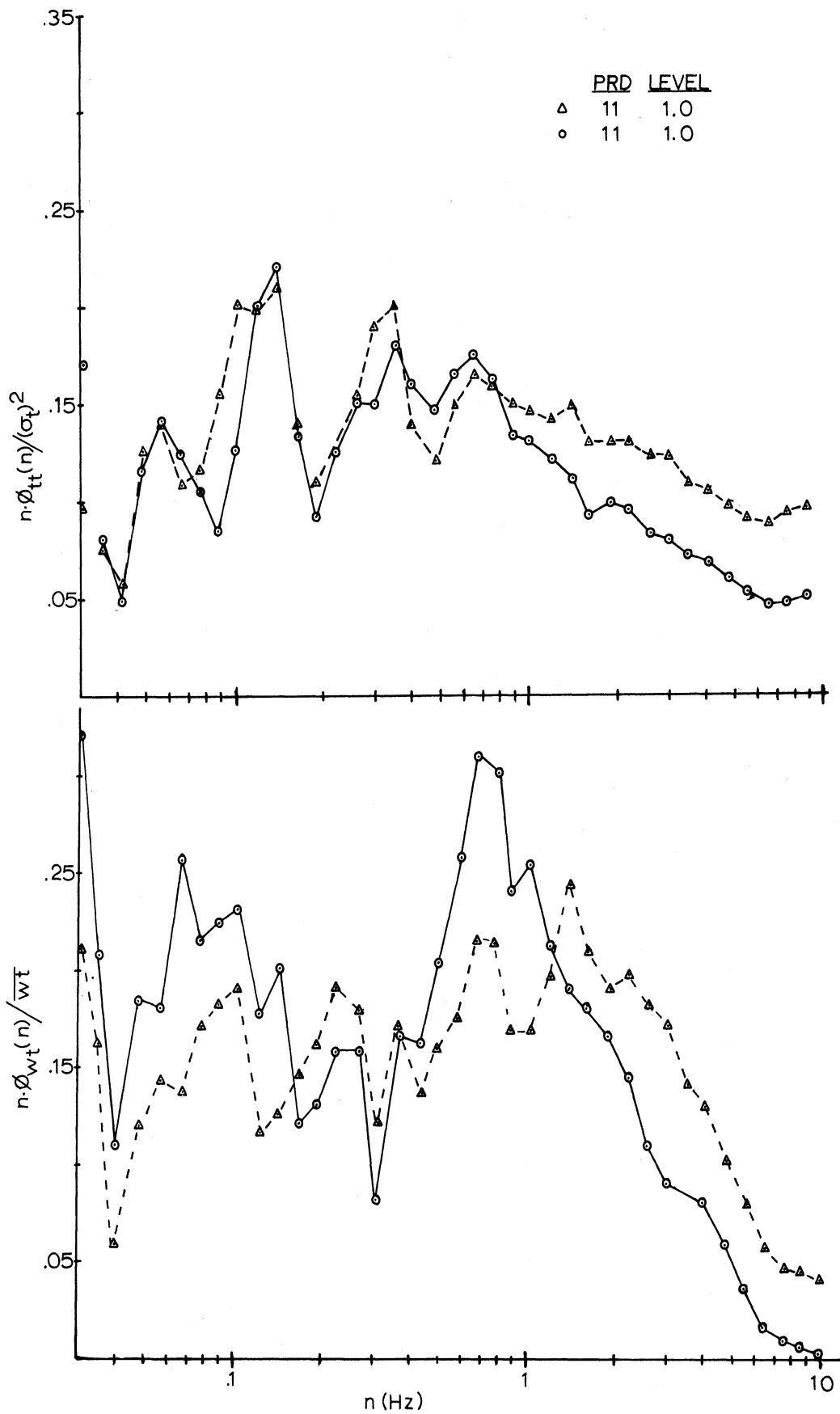


Figure E.6: Normalized temperature (t) spectra and \overline{wt} cospectra for Period 11.

BIBLIOGRAPHY

- Arya, S.P.S. and E.J. Plate, 1968: Hot-wire Measurements of Turbulence in a Thermally Stratified Flow. Research Memorandum No. 11, Fluid Dynamics and Diffusion Laboratory, College of Engineering, Colorado State University, Fort Collins, Colorado, 28 pp.
- Bartlett, M.S., 1950: Periodogram Analysis and Continuous Spectra, Biometrika, 37(1), 1-16.
- Bendat, J.S. and A.G. Piersol, 1966: Measurement and Analysis of Random Data. John Wiley and Sons, New York, 390 pp.
- Blackman, R.B. and J.W. Tukey, 1958: The Measurement of Power Spectra, Dover Publications, Inc., New York, 190 pp.
- Booker, J.R. and F. P. Bretherton, 1967: The Critical Layer for Internal Gravity Waves in a Shear Flow. J. Fluid Mech., 27(3), 513-539.
- Busch, N.E. and H.A. Panofsky, 1968: Recent Spectra of Atmospheric Turbulence. Quart. J. Roy. Met. Soc., 94(400), 132-149.
- Byshev, V.I. and O.A. Kuznetsov, 1969: Structural Characteristics of Atmospheric Turbulence in the Near-water Layer over the Open Sea, IZV., Atmospheric and Oceanic Physics, Academy of Science USSR, 5(6), Eng. Trans. J.D.L. McIntosh, 327-332.
- Champagne, F.H., C.A. Shleicher and O.H. Wehrman, 1967: Turbulence Measurements with Inclined Hot-wires. J. Fluid Mech., 28(1), 153-174.
- Collis, D.C. and M.J. Williams, 1959: Two Dimensional Convection from Heated Wires at Low Reynolds Number. J. Fluid Mech., 6(3), 359-384.
- Cooley, J.W. and J.W. Tukey, 1965: Algorithm for the Machine Calculations of Complex Fourier Series, Math. of Comp., 19(90), 297-301.
- Davies, P.O.A.L. and M.J. Fisher, 1964: Heat Transfer from Electrically Heated Cylinders. Proc. Roy. Soc., A280, 486-527.
- Elder, F.C., 1964: A Facility for Air-Sea Interaction Study on Lake Michigan. Proc. 7th Conf. on Great Lake Res., Great Lakes Res. Div., The University of Michigan, Pub. No. 11, 228-237.

- Elder, F.C., 1965: An Investigation of Atmospheric Turbulent Transfer Processes over Water. Report No. 2, University of Michigan, Office of Research Administration, 67 pp.
- Elder, F.C., 1966: An Investigation of Atmospheric Turbulent Transfer Processes over Water. Report No. 3, University of Michigan, Office of Research Administration, 24 pp.
- Elder, F.C., D.L. Harris and A. Taylor, 1970: Some Evidence of Organized Flow over Natural Waves. Boundary Layer Meteorology, 1(1), 80-87.
- Elder, F.C. and D.J. Portman, 1963: An Investigation of Atmospheric Turbulence Transfer Processes over Water. Report No. 1, University of Michigan, Office of Research Administration, 25 pp.
- Elder, F.C. and H.K. Soo, 1969: Some Wind Stress Measurements over Wave Surfaces, Special Report No. 42, Great Lakes Research Division, University of Michigan, 32 pp.
- Gill, G.C., L.E. Olsson, J. Sela, and M. Suda, 1967: Accuracy of Wind Measurements on Towers and Stacks. Bull. Am. Met. Soc., 48(9), 665-674.
- Goodknight, R.C. and T.L. Russell, 1963: Investigations of the Statistics of Wave Heights. J. Waterways and Harbors Div., Proc. ASCE, 1(89), 29-54.
- Harris, D.L., 1965: Wave Generated Wind. Ph.D. dissertation, Department of Meteorology and Oceanography, University of Michigan, (unpublished manuscript), 58 pp.
- Harris, D.L., 1966: The Wave Driven Wind, J. Atmos. Sci., 23(6), 688-693.
- Harris, Denard; Editor, 1967: Spectral Analysis of Time Series. Proc. of an Advanced Seminar at the University of Wisconsin, 11 papers, John Wiley and Sons, Inc., New York, 319 pp.
- Hewson, E.W. and F.V. Brock, 1967: A Hybrid Analog-Digital Computer for the Atmospheric Sciences, Bull. Am. Met. Soc., 48(9), 692-695.
- Hinze, J.O., 1959: Turbulence, McGraw Hill Book Company, Inc., New York, 586 pp.
- Holub, R.J., 1970: Wind Interference and the Placement of Anemometers and Vanes on Open Faced Towers. Report No. 20, Atmospheric Science Group, College of Engineering, University of Texas, Austin, Texas, 49 pp.

- Jeffreys, H., 1965: Cartesian Tensors. London: Cambridge University Press, 6th Edition, 92 pp.
- Jenkins, G.M., 1962: General Considerations in the Analysis of Spectra. Technometrics, 3(2), 133-166.
- Jenkins, G.M. and D.G. Watts, 1968: Spectral Analysis and its Applications, Holden-Day, San Francisco, 525 pp.
- Karaki, S. and E.Y. Hsu, 1968: An Experimental Investigation of the Structure of a Turbulent Wind over Water Waves. Technical Report No. 68, Department of Civil Engineering, Stanford University, 100 pp.
- King, L.V., 1914: On the Convection of Heat from Small Cylinders in a Stream of Fluid. Phil. Trans. Roy. Soc., London, A214, 373-432.
- Kinsman, B., 1965: Wind-waves, their Generation and Propagation on the Ocean Surface, Englewood Cliffs, N.J. Prentice-Hall, Inc., 676 pp.
- Kitaygorodskiy, S.A., 1969: Small Scale Atmosphere-ocean Interactions, IVZ. Atmospheric and Oceanic Physics, Academy of Sciences USSR, 5(11), Eng. Trans., K. Syers, 641-649.
- Kovaszny, L.S.G., L.T. Miller and B.R. Vasudeva, 1963: A Simple Hot-wire Anemometer. Project Squid Tech. Report, JHU-22P, The Johns Hopkins University, Baltimore, Maryland.
- Kraus, E.B., 1967: Wind Stress along the Sea Surface. Advances in Geophysics, Vol 12, Academic Press, Inc. New York and London, 213-255.
- Lamb, H., 1932: Hydrodynamics, Sixth Edition, Dover Reprint, 738 pp.
- Lighthill, M.J., 1962: Physical Interpretation of the Mathematical Theory of Wave Generation by Wind, J. Fluid Mech., 14(3), 385-398.
- Lumley, J.L. and H.A. Panofsky, 1964: The Structure of Atmospheric Turbulence, John Wiley and Sons, Inc., New York, 231 pp.
- Miles, J.W., 1957: On the Generation of Surface Waves by Shear Flows. J. Fluid Mech., 3(2), 185-204.
- Miles, J.W., 1959: On the Generation of Surface Waves by Shear Flows, Part 2, J. Fluid Mech., 6(4), 568-582.

- Miles, J.W., 1960: On the Generation of Surface Waves by Turbulent Shear Flows, J. Fluid Mech., 7(3), 469-478.
- Miles, J.W., 1965: A Note on the Interaction between Surface Waves and Wind Profiles, J. Fluid Mech., 22(4), 823-827.
- Miles, J.W., 1967: On the Generation of Surface Waves by Shear Flows, Part 5, J. Fluid Mech., 30(1), 163-175.
- Miyake, M., R.W. Stewart and R.W. Burling, 1970: Spectra and Cospectra of Turbulence over Water. Quart. J. R. Met. Soc., 96(407), 138-143.
- Monin, A.S., 1962: Empirical Data on Turbulence in the Surface Layer of the Atmosphere, J. Geophys. Res., 67(8), 3103-3111.
- Oort, A.H. and A. Taylor, 1969: On the Kinetic Energy Spectrum near the Ground. Mon. Wea. Review, 97(9), 623-636.
- Panofsky, H.A. and G.W. Brier, 1958: Some Applications of Statistics to Meteorology. The Pennsylvania State University, University Park, Pa., 224 pp.
- Panofsky, H.A. and R.A. McCormick, 1960: The Spectrum of Vertical Velocity near the Surface. Quart. J. Roy. Met. Soc., 86(370), 495-503.
- Paulson, C.A., 1967: Profiles of Wind Speed, Temperature and Humidity over the Sea. NSF Scientific Report GP-2418, University of Washington, Seattle, Wash., 128 pp.
- Phillips, O.M., 1957: On the Generation of Waves by Turbulent Wind, J. Fluid Mech., 2(5), 417-445.
- Phillips, O.M., 1958: The Equilibrium Range in the Spectrum of Wind Generated Waves. J. Fluid Mech., 4(4), 426-434.
- Phillips, O.M., 1966: The Dynamics of the Upper Oceans. Cambridge Press, Cambridge, England, 261 pp.
- Pond, S., R.W. Stewart and R.W. Burling, 1963: Turbulence Spectra in Wind over Waves. J. Atmos. Sci., 20(4), 319-324.
- Pond, S., S.D. Smith, P.F. Hamblin, and R.W. Burling, 1966: Spectra of Velocity and Temperature Fluctuations in the Atmospheric Boundary Layer over the Sea. J. Atmos. Sci., 23(4), 376-386.
- Powell, S.W., 1965: Methods of Digital Filtering, Aeroballistics Internal Note No. 37-63, George C. Marshall Space Flight Center, Huntsville, Ala., 29 pp.

- Putz, R.R., 1952: Statistical Distribution for Ocean Waves. Trans. Amer. Geophys. Union, 33(5), 685-692.
- Roll, H.V., 1965: Physics of the Marine Atmosphere. Academic Press, New York, 426 pp.
- Sandborn, V.A., 1967: Hot-wire Anemometer Measurements in Large-Scale Boundary Layers. Advances in Hot-wire Anemometry, Melnic and Weske, Edibors, Proc. of Int. Sym. on Hot-wire Anemometry, 102-119.
- Seesholtz, J.R., 1968: A Field Investigation of Air Flow Immediately above Ocean Surface Waves, Massachusetts Institute of Technology, Department of Meteorology Technical Report, 137 pp.
- Shemdin, O.H., 1969: Instantaneous Velocity and Pressure Measurements above Propagating Waves, Technical Report No. 4. Dept. of Coastal and Oceanographic Engineering, College of Engineering, University of Florida, 104 pp.
- Smith, S.D., 1967: Thrust Anemometer Measurements of Wind Velocity Spectra and of Reynolds Stress over a Coastal Inlet. J. Marine Res., 25(3), 239-252.
- Stewart, R.H. II, 1969: Laboratory Studies of the Velocity Field over Deep-Water Waves, Ph.D. dissertation, Department of Oceanography, University of California, San Diego, (unpublished manuscript), 161 pp.
- Stewart, R.W., 1961: The Wave Drag of Wind over Waves, J. Fluid Mech., 10(2), 189-194.
- Stewart, R.W., 1967: Mechanics of the Air-Sea Interface. Physics of Fluids Supplement, 10, S189-S194.
- Stokes, G.G., 1847: On the Theory of Oscillatory Waves. Trans. Cambridge Phil. Soc., 8(5), 441-455.
- Strohbehn, J.W., 1968: Line-of-Sight Wave Propagation through the Turbulent Atmosphere. Proc. of the IEEE. 56(8), 1301-1318.
- Tielman, H.W., 1967: Viscous Region of Turbulent Boundary Layer. Technical Report, Fluid Dynamics and Diffusion Laboratory, College of Engineering, Colorado State University, Fort Collins, Colorado, 197 pp.
- Tukey, J.W., 1967: An Introduction to the Calculation of Numerical Spectrum Analysis. Spectrum Analysis of Time Series, 11 papers, Denard Harris, Editor, John Wiley and Sons, Inc., New York, 24-46.

- Van Atta, C.W. and W.Y. Chen, 1968: Correlation Measurements in Grid Turbulence using Digital Harmonic Analysis. J. Fluid Mech., 34(3), 497-515.
- Von Karman, T. and L. Howarth, 1938: On the Statistical Theory of Isotropic Turbulence, Proc. Roy. Soc. A., (164), 192-215.
- Volkov, Y.A., 1969: The Spectra of Velocity and Temperature Fluctuations in Airflow above the Agitated Sea Surface, IZV. Atmospheric and Oceanic Physics, Academy of Sciences, USSR, 5(12), Eng. Trans. by J. Findlay, 723-731.
- Webster, C.A., 1962: A Note on the Sensitivity to Yaw of a Hot-wire Anemometer, J. Fluid Mech., 13(2), 307-311.
- Weiler, H.S., 1966: Direct Measurements of Stress and Spectra of Turbulence in the Boundary Layer over the Sea. Part I, Ph.D. dissertation, Department of Physics, University of British Columbia, (unpublished manuscript), 87 pp.
- Weiler, H.S. and R.N. Burling, 1967: Direct Measurements of Stress of Spectra of Turbulence in the Boundary Layer over the Sea. J. Atmos. Sci., 24(6), 653-664.
- Welch, P.O., 1967: The Use of Fast Fourier Transfer for the Estimation of Power Spectra: A Method Based on Time Averaging over Short, Modified Periodograms, IEEE Trans. on Audio and Electroacoustics, AU-15(2), 61-64.
- Yefimov, V.V. and A.A. Sizov, 1969: Experimental Study of the Field of Wind Velocity over Waves, IVZ. Atmospheric and Oceanic Sciences, Academy of Sciences, USSR, 5(9), Eng. Trans. A. Peiperl, 530-537.

UNIVERSITY OF MICHIGAN



3 9015 02539 6915